UNIVERSIDAD AUTONOMA DE MADRID

Programa de Doctorado de Biociencias Moleculares

Influence of GRK2 levels in hepatic pathophysiology

Marta Cruces Sande

Madrid, 2018

Memoria presentada por la licenciada

MARTA CRUCES SANDE

para optar al título de

DOCTORA EN BIOCIENCIAS MOLECULARES

(BIOQUÍMICA, BIOLOGÍA MOLECULAR, BIOMEDICINA Y BIOTECNOLOGÍA)

DIRECTORAS DE TESIS:

DRA. CRISTINA MURGA MONTESINOS

DRA. ROCÍO VILA BEDMAR

Este trabajo ha sido realizado en el Departamento de Biología Molecular. Centro de Biología Molecular "Severo Ochoa" (CSIC-UAM)

FACULTAD DE CIENCIAS
UNIVERSIDAD AUTÓNOMA DE MADRID

Departamento de Biología Molecular

CBM Severo Ochoa
CENTRO DE BIOLOGÍA MOLECULAR
CSIC UAM

Este trabajo ha sido realizado en el Centro de Biología Molecular Severo Ochoa (CSIC-UAM) bajo la dirección de la Dra. Cristina Murga Montesinos, Profesora Titular del Departamento de Biología Molecular de la Universidad Autónoma de Madrid y la Dra. Rocío Vila Bedmar Investigadora Postdoctoral de la Universidad Autónoma de Madrid en el laboratorio del Dr. Federico Mayor Menéndez, Catedrático del Departamento de Biología Molecular de la Universidad Autónoma de Madrid. Además, parte de los resultados fueron obtenidos en el Dana-Farber Cancer Institute (DFCI, Havard Medical School, Boston, USA) bajo la dirección del Dr. Pere Puigserver.

La realización de esta Tesis ha sido posible gracias a un Contrato Predoctoral para Formación de Personal Investigador (FPI-UAM) y a fondos de la Fundación Severo Ochoa. La autora también ha recibido una ayuda de movilidad para estancias breves de la UAM.

AKNOLEDGMENTS/ AGRADECIMIENTOS

ABSTRACT/RESUMEN

G protein-coupled receptor kinase 2 (GRK2) phosphorylates and desensitizes G protein coupled-receptors (GPCRs), and plays an important role in the development of both insulin resistance (IR) and obesity in vivo. In this work we further explore the role of GRK2 in these disorders, focusing on the establishment and progression of non-alcoholic fatty liver disease (NAFLD), a disease spectrum related to obesity and IR. We find that hepatic GRK2 protein levels are upregulated in different mouse models of steatosis and, conversely, we demonstrate that the development of NAFLD is prevented in mice with low levels of GRK2 (GRK2+/- mice) upon a high fat diet (HFD). Moreover, using an inducible GRK2 knock-out mouse model we demonstrate that decreasing GRK2 levels during the course of the high-fat feeding reverts the HFD-induced obese and insulin-resistant phenotype. GRK2 downmodulation prevents further body weight gain and fat mass accretion, causes beneficial effects in glucose tolerance and insulin sensitivity and increases the expression of markers of thermogenesis in brown adipose tissue after the HFD. In the liver, tamoxifen-induced GRK2-/- mice are protected from NAFLD, showing less signs of lipid accumulation and inflammation compared to control littermates after the HFD.

We also used a methionine and choline deficient diet (MCD) as a model of non-alcoholic steatohepatitis (NASH) that is independent of fat mass accretion and IR. A blinded anatomopathological analysis revealed that GRK2+/- mice are protected from the development of NASH detected in their WT littermates. GRK2+/- mice show decreased hepatic triglyceride accumulation, inflammation and ER stress responses, while they preserve protective mechanisms against MCD-induced NASH that are lost in WT mice, as indicated by markers of autophagy or mitochondrial biogenesis and fusion.

Interestingly, GRK2 protein and mRNA levels are upregulated in human liver biopsies from simple steatosis and NASH patients when compared to normal liver samples. Moreover, GRK2 overexpression is per se able to increase palmitic acid-induced steatosis in human hepatoma cells, thus establishing not only a parallelism but rather a cause-effect relationship between the expression levels of this kinase and lipid accumulation.

Conversely, fasting, which induces a state of physiological hepatic steatosis, provokes a similar degree of lipid deposition in livers of WT and GRK2+/- mice, together with a marked decrease in hepatic GRK2 levels in both genotypes. However, GRK2+/- mice display higher levels of fasting serum fatty acids and glucose. Remarkably, glucagon-induced glucose production and mRNA expression of the gluconeogenic enzyme PEPCK are enhanced in mouse primary hepatocytes with silenced GRK2 demonstrating that this kinase can regulate glucagon actions in these cells.

In sum, our results suggest that GRK2 acts as a central integrative node able to regulate different intracellular routes that control metabolic responses in vivo due to its unique ability to both directly modulate the insulin receptor cascade as well as key GPCRs related to metabolism (such as the glucagon receptor). These results consolidate GRK2 as a prospective therapeutic target for a potential clinical intervention in diseases with a metabolic component such as IR, obesity and NAFLD.

La proteína GRK2 es una quinasa clásicamente conocida por su función en la desensibilización de receptores acoplados a proteínas G (GPCR). Sin embargo, se ha descrito que GRK2 desempeña un papel importante en el desarrollo de resistencia a la insulina (IR) y obesidad *in vivo*. En este trabajo, se analiza el papel de GRK2 en estas situaciones patológicas centrándonos específicamente en la enfermedad de hígado graso no alcohólica (NAFLD), una condición estrechamente relacionada con obesidad e IR. Así, encontramos que los niveles proteicos de GRK2 se incrementan en el hígado en diferentes modelos murinos de esta patología y demostramos que los ratones con niveles reducidos de GRK2 (animales GRK2 +/-) están protegidos frente al desarrollo de NAFLD inducida por una dieta alta en grasa (HFD). Además, mostramos que una reducción genética inducible en los niveles de GRK2 no sólo previene sino que revierte el desarrollo de obesidad, IR y NAFLD. Los ratones Tam-GRK2-/- (inducidos por tamoxifeno) en los que se reducen los niveles de la quinasa cuando los animales ya han desarrollado un fenotipo obeso y resistente a la insulina por la dieta dejan de ganar peso a pesar de continuar con la HFD, tienen menor acumulación de grasa y una mayor expresión de marcadores de termogénesis en el tejido adiposo marrón. Además, estos animales Tam-GRK2-/- no desarrollan NAFLD tras la HFD mostrando una menor acumulación de lípidos y menos marcadores de inflamación en el hígado en comparación con animales control.

Por otro lado, se utilizó una dieta deficiente en metionina y colina (MCD) como modelo de esteatohepatitis no alcohólica (NASH) independiente de obesidad e IR. Un análisis anatomopatológico ciego reveló que los ratones GRK2+/- están protegidos frente al desarrollo de NASH, al contrario que los animales silvestres (WT) que sí desarrollan esta patología tras la MCD. En ratones GRK2+/-, la MCD causa menor acumulación de triglicéridos, inflamación y estrés de retículo en el hígado comparado con animales WT. Además, estos animales GRK2 +/- conservan mecanismos de protección frente a NASH que se pierden en ratones WT, como indican los marcadores de autofagia o de biogénesis y fusión mitocondrial.

Los niveles de proteína y mRNA de GRK2 se encuentran aumentados en biopsias hepáticas de pacientes diagnosticados con esteatosis simple o NASH en comparación con individuos con histología hepática normal. Además, la sobreexpresión de GRK2 en una línea de células hepáticas humanas provoca *per se* una mayor esteatosis inducida por ácido palmítico estableciendo así no sólo un paralelismo sino una relación causa-efecto entre los niveles de GRK2 y la acumulación de lípidos intracelulares en hepatocitos.

El ayuno, que induce un estado de esteatosis hepática fisiológica, provoca la acumulación de grasa en hígado además de una importante reducción en los niveles de GRK2 en la misma medida en ratones WT y GRK2+/-. Los ratones GRK2 +/- tienen niveles más altos de ácidos grasos libres circulantes así como de glucosa en ayunas. El silenciamiento de GRK2 en hepatocitos primarios de ratón provoca una mayor producción de glucosa a partir de piruvato y un aumento en la expresión de la enzima gluconeogénica PEPCK inducidas por glucagón, lo que demuestra que GRK2 puede regular las acciones del glucagón.

Nuestros resultados identifican a GRK2 como un nodo señalizador al ser capaz de regular tanto la cascada de la insulina como GPCRs importantes para el control del metabolismo como el receptor de glucagón. Nuestros resultados consolidan esta quinasa como una posible diana terapéutica para una posible intervención clínica en enfermedades con un componente metabólico como IR, obesidad y NAFLD.

INDEX

INDEX

ABBREVIATIONS

AC: Adenilyl cyclase
AMPK: AMP-activated protein kinase
ApoB: Apolipoprotein B
AR: Adrenergic receptor
AUC: Area under the curve
BAT: Brown adipose tissue
ChREBP: Carbohydrate-responsive element-binding protein
CD: Control diet
CD36: Cluster of differentiation 36
CPT: Carnitine palmitoyltransferase
CREB: cAMP response element-binding protein
CNS: Central nervous system
CVD: Cardiovascular disease
DAG: Diacylglycerol
DNL: *De novo* lipogenesis
eiF2α: Eukaryotic translation initiation factor 2A
ER: Endoplasmic reticulum
ERK: Extracellular signal–regulated kinases
eWAT: Epididymal white adipose tissue
FA: Fatty acid
FAS: Fatty acid synthase
FAO: Fatty acid oxidation
FAT: Fatty acid transporter
FFA: Free fatty acids
FGF21: Fibroblast growth factor 21
FOXO: Forkhead box O
FxR: farnesoid X receptor
G6P: Glucose 6-phosphate
GAPDH: Glyceraldehyde-3-phosphate dehydrogenase
GLUT: Glucose transporter
GCGR: Glucagon receptor
GPCR: G protein-coupled receptor
GSK3: Glycogen synthase kinase 3
GRK: G protein-coupled receptor kinase
GTT: Glucose tolerance test
HCC: hepatocellular carcinoma
hCLS: hepatic “crown-like structures”
HCS: hepatic stellate cells
HFD: High fat diet
IGFR: Insulin growth factor receptor
IκBα: Inhibitor of kappa B
iNOS: Inducible nitric oxide synthase
IP3: Inositol trisphosphate
IR: Insulin resistance
IRS: Insulin receptor substrate
ITT: Insulin tolerance test

JNK: c-Jun NH(2)-terminal kinase
LC3: Microtubule-associated protein 1A/1B-light chain 3
LPS: Lipopolysaccharide
LXR: liver X receptor
MAPK: Mitogen-activated protein kinase
MRC1: Mannose receptor type C 1
MCD: methionine and choline deficient diet
MEK: MAPK/ERK kinase
MKK: Mitogen-activated protein kinase kinase
mTORC1: Mammalian target of rapamycin complex 1
NAFLD: Non-alcoholic fatty liver disease
NAS: NAFLD activity score
NASH: Non-alcoholic steatohepatitis
NEFA: Non-esterified fatty acids
NF-κB: Nuclear factor kappa-light-chain-enhancer of activated B cells
OPA 1: Dynamin-like 120 kDa protein or Optic atrophy 1
PDK1: 3-Phosphoinositide-dependent protein kinase-1
PEPCK: phosphoenolpyruvate carboxykinase
PGC-1: Peroxisome proliferator-activated receptor gamma coactivator 1
PIP2: Phosphatidylinositol 4,5-bisphosphate
PIP3: Phosphatidylinositol 3,4,5 trisphosphate
PKA: Protein kinase A
PKC: Protein kinase C
PLC: Phospholipase C
PNS: peripheral nervous system
PPAR: Peroxisome proliferator-activated receptor
PTT: Pyruvate tolerance test
ROS: Reactive oxygen species
RTK: receptor tyrosine kinase
SD: Standard diet
SNS: Sympathetic nervous system
SREBP1c: Sterol regulatory element-binding protein 1c
T2D: Type 2 diabetes mellitus
Tam: Tamoxifen
TFAM: Mitochondrial transcription factor A
TNFα: Tumor necrosis factor alpha
UCP1: Uncoupling protein 1
UPR: Unfolded protein response
VLDL: Very low density lipoproteins
WAT: White adipose tissue

INTRODUCTION

1. Regulation and dysregulation of glucose and lipid homeostasis: the liver as an orchestrating organ

A continuous supply of glucose is necessary to ensure proper function and survival of all organs, especially the brain. Plasma glucose levels are thus maintained in a narrow range controlled mainly by the liver and the skeletal muscle as well as the pancreas as key organ involved in glucose homeostasis. The balance between the utilization and production of glucose is primarily maintained by two opposing hormones produced by the pancreas, insulin and glucagon. In the fed state and in response to an elevation in plasma glucose and amino acids, insulin is released from the beta cells of the islets of Langerhans and activates glucose uptake in different organs (with the lion´s share of the withdrawal occurring in the skeletal muscle). Insulin also inhibits glucose output primarily by its actions in the liver. During fasting or exercise, plasma glucose falls and glucagon is secreted by pancreatic α cells and the levels of glucose are determined principally by the glucose output from the liver (Saltiel 2016).

Not only glucose but also lipid homeostasis is finely controlled in the organism. Lipids represent an important fuel for cells and are also key components of the cell structure. At the same time, lipids and lipid-derived metabolites (particularly diacylglycerol or DAG and ceramides) can mediate deleterious effects in cells in a process called lipotoxicity (Cusi 2012). Moreover, fatty acids (FA), lipids and lipid-derived metabolites are currently considered signaling molecules (see BOX 1 in Section 1.c). Thus, the control of lipid metabolism is also of great importance for whole body homeostasis.

The liver is a key metabolic organ in charge of regulating the correct handling of glucose and lipids. This response is mainly orchestrated by the insulin/glucagon ratio as well as by the substrate availability (Samuel and Shulman 2016). Moreover, multiple hormones, cytokines and other bioactive molecules released from different tissues (adipokines, myokines, etc) as well as the central nervous system (CNS), the peripheral nervous system (PNS) and, in particular, the sympathetic nervous system (SNS) (Nonogaki 2000; Lowell and Spiegelman 2000; Li et al. 2009) can regulate lipidic and glycemic homeostasis.

1.A. Insulin signaling

Insulin is a major physiological anabolic hormone, promoting the synthesis and storage of glucose, lipids, and proteins and inhibiting their degradation and release back into the circulation. Insulin acts by binding to the insulin receptor, a tyrosine kinase receptor found in insulin-target tissues (Saltiel 2016). Mechanistically, insulin binding stimulates tyrosine auto-phosphorylation in the insulin receptor β subunits which activates its kinase activity and recruits and phosphorylates members of a family of adaptor proteins called insulin receptor substrates 1–6 (IRS1–6) (Taniguchi, Emanuelli, and Kahn 2006)

or, alternatively, heterotrimeric Gαq proteins (Imamura et al. 1999) leading in both cases to the regulation of glucose uptake and cellular metabolism. IRS proteins act as scaffolds coupling insulin receptor stimulation to downstream effectors, recruiting and activating various SH2 domain-containing proteins, such as phosphatidylinositol 3-kinase (PI3K). The activation of PI3K produces PIP3 (phosphoinositide-3,4,5-trisphosphate) by phosphorylation of PIP2 (phosphoinositide-3,4-bisphosphate) which recruits PDK1 and AKT to the plasma membrane. AKT is activated via phosphorylation at T308 by PDK1 and at S473 by mTORC2, classically termed as PDK2 (Boucher, Kleinridders, and Kahn 2014) .AKT phosphorylates many cellular proteins, triggering the metabolic and transcriptional reprogramming of the cell (White 2003). Many AKT substrates that directly control metabolic steps have been identified, such as glycogen synthase kinase 3 (GSK3), the transcription factor Forkhead box O (FOXO), the phosphodiesterase PDE3B, and TBC1D1 or TBC1D4/AS160 (Boucher, Kleinridders, and Kahn 2014). The last two proteins are Rab GTPase-activating proteins that play an important role in insulin-stimulated translocation to the plasma membrane of the glucose transporter GLUT4 (Sakamoto and Holman 2008). Additionally, AKT phosphorylation can activate mTORC1, which in turn activates p70-S6K1 promoting the serine phosphorylation of IRS1 thus reducing its stability and providing an auto-regulatory negative feedback loop (Harrington, Findlay, and Lamb 2005).

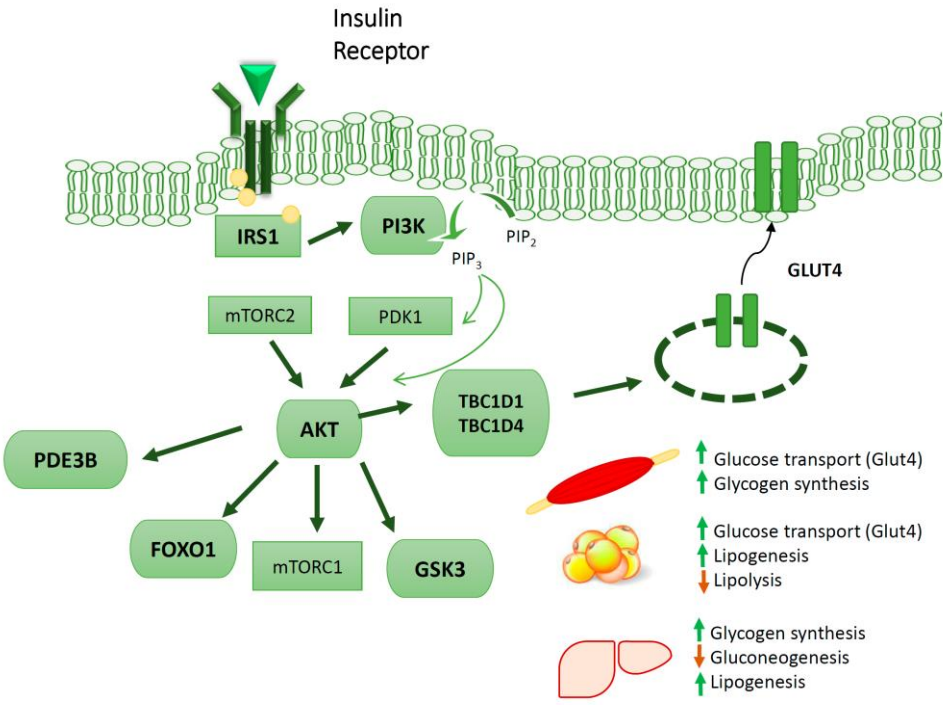

Figure I1. Schematic overview of insulin signaling and its metabolic consequences in insulin-target tissues. Insulin activation of the insulin receptor recruits IRS to activate the PI3K/AKT pathway, that exerts different effects depending on the tissue (See text for details).

The specific molecular mechanisms and anabolic consequences elicited by the activation of the insulin signaling cascade on three insulin-target tissues with important metabolic relevance (liver, muscle and adipose tissues) are herein described and summarized in Figure I1.

- In the **liver**, insulin exerts its effects on glucose handling chiefly by suppressing hepatic glucose production. Insulin directly causes inactivation of GSK3β (Cross et al. 1995), which enables the activation of glycogen synthase thus stimulating the storage of glucose as glycogen, and also inhibits glycogen breakdown or glycogenolysis. Moreover, *de novo* synthesis of glucose (gluconeogenesis) is blocked by insulin through direct and indirect effects. Insulin induces the phosphorylation and nuclear exclusion of FOXO1, which, when in the nucleus, drives the expression of key enzymes involved gluconeogenesis (Gross 2008 Oncogene). Also, insulin decreases PGC-1α (peroxisome proliferator-activated receptor-γ-coactivator-1α) transcriptional activity and blocks CREB complex formation thus inhibiting gluconeogenic gene expression (Hatting et al. 2018). At the same time, insulin decreases the availability of gluconeogenic substrates by suppressing white adipose tissue (WAT) lipolysis (see below). Insulin also increases liver lipid content regulating its synthesis, oxidation and export (described in detail in section 1.C). Briefly, insulin increases *de novo* synthesis of FA (*de novo* lipogenesis or DNL) enhancing the transcription of genes encoding lipogenic enzymes while, simultaneously, turns off the oxidation of FA in the mitochondria (β-oxidation) through direct and indirect effects (Leavens and Birnbaum 2011). The increase in DNL, together with the inhibition of FA oxidation causes the accumulation of FA that can be esterified into triglycerides (TG) and eventually exported in very low density lipoproteins (VLDLs) for storage and utilization by peripheral tissues. Insulin also acutely decreases VLDL secretion (Sparks and Sparks 2010).
- In **muscle**, insulin-induced glucose uptake accounts for the majority of the postprandial glucose clearance from the blood (DeFronzo and Tripathy 2009). AKT activation leads to increased muscle glucose uptake (Sakamoto and Holman 2008) via phosphorylation and inactivation of two Rab-GTPase-activating proteins, TBC1D4 (or AS160) and TBC1D1, which, in their active forms, restrain GLUT4 translocation (Roach et al. 2007; Kane et al. 2002). Moreover, insulin action in the muscle also stimulates glucose storage in the form of glycogen (Shulman et al. 1990).
- In **WAT**, glucose uptake is largely insulin-dependent and is regulated by pathways similar to those in skeletal muscle. However the role of WAT in glucose uptake is relatively minor in the organism, accounting for only 5%–10% of whole body glucose disposal (Virtanen et al. 2002; Ng et al. 2012). Insulin inhibits lipolysis in WAT, what has been demonstrated to regulate hepatic glucose output as it reduces glycerol delivery to the liver that serves as a gluconeogenic substrate. In fact, it is nowadays believed that the ability of insulin to acutely regulate hepatic gluconeogenesis occurs mostly by an indirect mechanism through inhibition of WAT lipolysis even when hepatic insulin signaling may establish the transcriptional tone of gluconeogenic enzymes and determine the gluconeogenic capacity of the liver

(Samuel and Shulman 2016). Insulin also stimulates glucose uptake in **brown adipose tissue (BAT)** (Klein et al. 2002; Inokuma et al. 2005) and this tissue has been suggested to play a more important role in glucose disposal compared to WAT (Orava et al. 2011). Insulin regulates metabolism in both brown and white adipocytes, but the role of both tissues in energy storage and utilization is quite different. Unlike WAT, BAT accumulates lipids not as an energy store but rather as a source of FA to be oxidized in mitochondria when thermogenesis is activated (Cannon and Nedergaard 2004).

1.B. Glucagon signaling

In the fasted state glucose and insulin levels are low and glucagon is secreted from α cells in the pancreas. Glucagon, together with glucocorticoids and adrenergic mediators such as adrenaline or noradrenaline and the growth hormone are called "insulin counterregulatory hormones". This means that their role is to increase the glycemia principally upon fasting or in response to a dangerous/life-threatening event. FA and glycerol released from WAT during fasting can also regulate glucose levels (see Box 1). Additionally, glucose-sensing neurons in the hypothalamus further control responses to glycemic changes. Among these systems, glucagon plays a central role in the response to hypoglycemia and efficiently opposes insulin effects (Quesada et al. 2008).

Glucagon acts through the glucagon receptor (GCGR), a member of the G protein-coupled receptor (GPCR) superfamily, that is, a type of receptors of seven transmembrane domains coupled to GTP-binding heterotrimeric G proteins. The GCRG binds to a Gαs type of G protein that leads to the activation of adenylate cyclase (AC), cyclic-AMP production and protein kinase A (PKA) activation. Alternatively, this receptor can also activate the phospholipase C/inositol phosphate pathway via Gαq proteins, resulting in calcium release from intracellular stores (Figure I2). In addition to the canonical pathways, glucagon can act through AMPK-, p38 MAPK-, PPARα-, Foxa2-, and FGF21-dependent mechanisms. The GCGR in the liver is highly selective for glucagon, but exhibits a modest affinity for glucagon-like peptides (GLP) (Quesada et al. 2008).

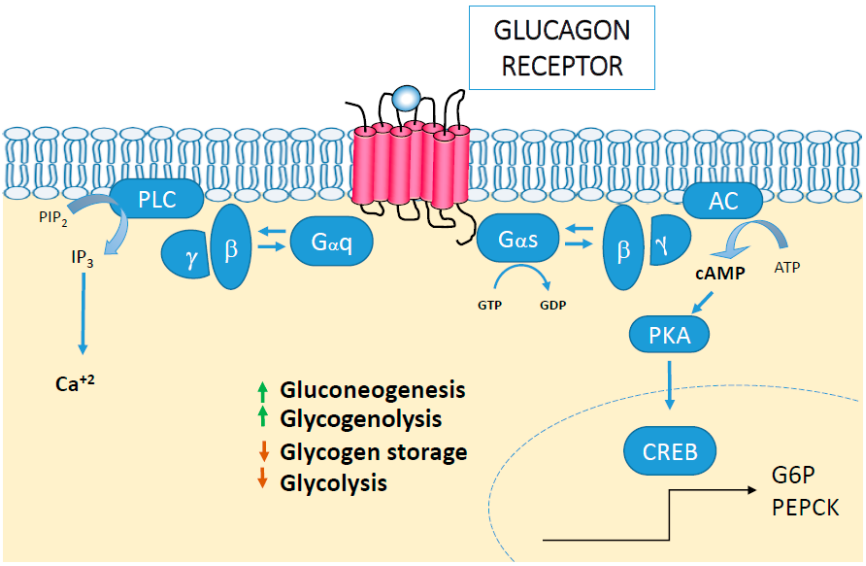

Figure I2. Schematic summary of the glucagon receptor pathway. GCGR activation leads to activation of Gαs and, alternatively, Gαq, to activate intracellular cascades (See text for details).

The liver is the main site of action of glucagon, where it stimulates *de novo* synthesis of glucose or gluconeogenesis from non-carbohydrate carbon substrates such as lactate, pyruvate, glycerol, and glucogenic amino acids. Glucagon also increases the breakdown of glycogen to glucose (glycogenolysis) altogether increasing hepatic glucose output while it blocks glucose storage as glycogen (glycogenesis) and also glucose catabolism (glycolysis). Its main action on the liver is mediated by the activation of AC and the PKA pathway to regulate gluconeogenesis mainly by the up-regulation of key enzymes such as glucose-6-phosphatase (G6P) and phosphoenolpyruvate carboxykinase (PEPCK) through the activation of the cAMP response element-binding protein (CREB) and PGC-1α (Herzig et al. 2001; Yoon et al. 2001). Glucagon also affects glycogen metabolism phosphorylating and inactivating glycogen synthase while it phosphorylates and activates glycogen phosphorylase (Band and Jones 1980; Ciudad et al. 1984; Westergaard et al. 1999). Thus, the net effect in liver glucose handling is opposed to that of insulin (Figure I3).

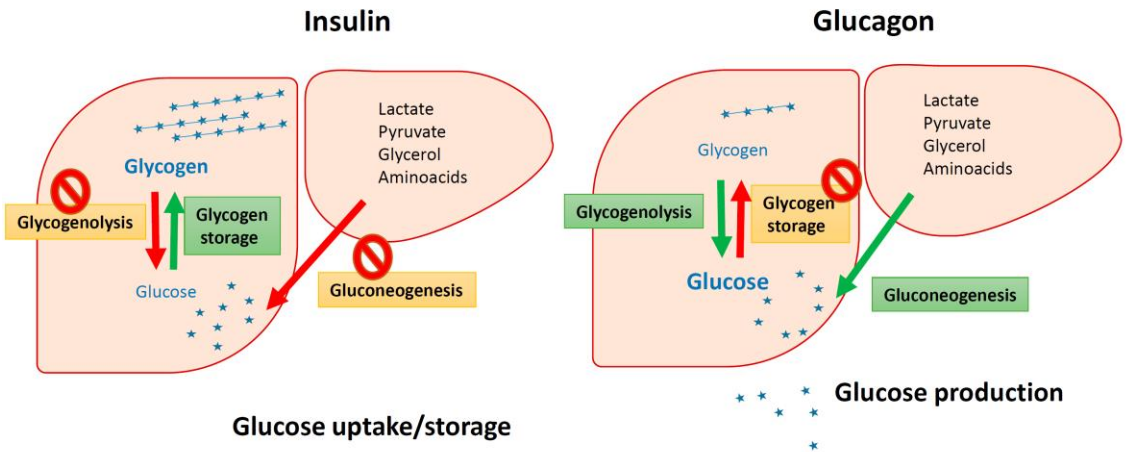

Figure I3. Opposing effects of insulin and glucagon in hepatic glucose handling. The net effect of insulin and glucagon in glucose homeostasis and their role (positive in green and negative in red) in glycogen storage, glycogen lysis and gluconeogenesis are shown.

Beyond glucose homeostasis, glucagon reduces VLDL release from the liver, decreases plasma lipids and cholesterol levels and stimulates FA oxidation in the liver at the same time that reduces hepatic triacylglycerol synthesis (Eaton 1973; Longuet et al. 2008; Habegger et al. 2010). In adipose tissue, glucagon stimulates hormone-sensitive lipase (HSL) to promote lipolysis (Perea et al. 1995; Slavin, Ong, and Kern 1994). Moreover, glucagon also stimulates energy expenditure both in rats and humans and glucagon infusion results in increased oxygen consumption (Keller 1979; Nair 1987). Although *in vitro* studies suggest that this effect is mediated by BAT (Joel 1966), it has been suggested that the increase in energy expenditure might be independent of BAT activation (Salem et al. 2016). Therefore, besides the role in glycemia, glucagon has both catabolic and thermogenic actions.

In sum, glucagon modulates multiple responses in several tissues besides the liver, including BAT or WAT as previously mentioned, but also pancreas, heart, kidney or the CNS. In pancreas, glucagon exerts an inhibitory effect on insulin secretion (Song et al. 2014). This effect in particular, when added to the previously described biological actions of glucagon, defines its counter-balancing role relative to the actions of insulin.

BOX 1: FA and the control of gluconeogenesis

As previously cited, lipids can serve as signaling molecules. In fact, specific receptors for FA have been described, many of them members of the GPCR superfamily. FA stimulate insulin secretion from pancreatic islets suppressing gluconeogenesis in the liver (Wyne 2003; Boden 2005). Nevertheless, FA can positively regulate hepatic gluconeogenesis in several ways: i) serving as a source of substrates and energy, ii) directly modulating the transcription of key gluconeogenic genes as PEPCK and PGC-1α in a process involving p38 MAPK (Collins et al. 2006) and iii) dampening insulin-induced suppression of gluconeogenesis through desensitization of insulin signaling upon exposure to FA. Summing up, the net effect of FA in glucose homeostasis would be the elevation of hepatic glucose output (Bevilacqua et al. 1987; Oakes et al. 1997).

1.C. Hepatic lipid handling

Hepatic lipid content depends on several factors: i) FA uptake, ii) *de novo* lipogenesis iii) FA oxidation, iv) autophagy and v) secretion of VLDLs. These processes and their mechanisms of control are described below and summarized in Figure I4.

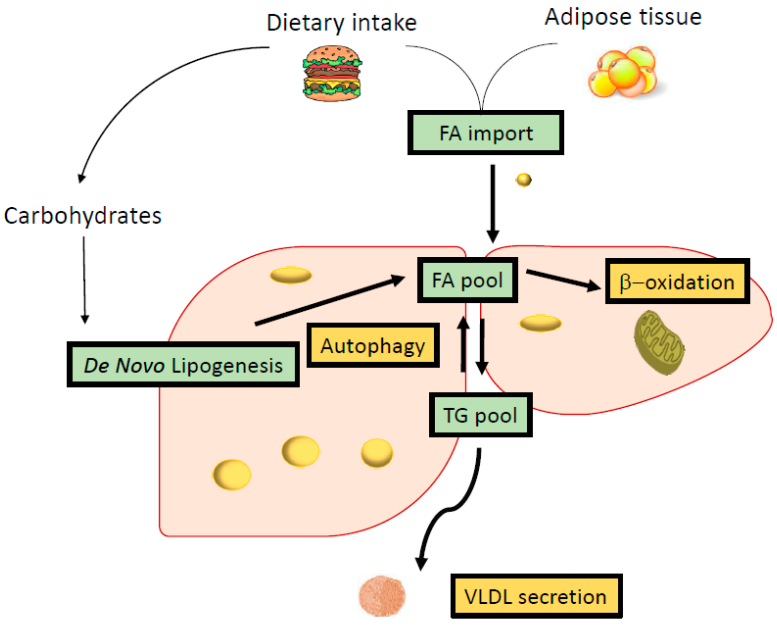

Figure I4. Overview of the main processes regulating hepatic lipid handling. Hepatocytes can uptake FA from the bloodstream or synthesize them via DNL. These FA can then be oxidized in the mitochondria or stored as TG that can be at the same time exported in VLDLs or catabolized through autophagy.

I. FA uptake

In the absorptive state, dietary TG are transported in the circulation as chylomicrons which degradation releases FA that enter the liver. In the fasting state, FA are derived from lipolysis in adipose tissue and incorporated into the liver (Berlanga et al. 2014). FA release from adipose tissue is promoted by catecholamines (that activate β-adenergic receptors or β-AR), natriuretic peptides and glucagon, and usually repressed by insulin. The entrance of FA into the liver depends on the concentration of FA outside and inside the cell and on the hepatocellular capacity for FA uptake. This capacity relies on the number and activity of transporter proteins in the sinusoidal plasma membrane of the hepatocyte since FA are taken up in a facilitated fashion rather than by passive processes (Berk 2008). This facilitated transport depends on protein-mediated mechanisms involving a number of FA transporters, of which cluster of differentiation 36 (FAT/CD36) is the best characterized. Its role is to facilitate the uptake and intracellular trafficking of FA and its function is largely dependent on its translocation from intracellular depots to the plasma membrane. Insulin and the transcription factor FOXO1, among others, induce FAT/CD36 translocation and thus enhance FA uptake (Miquilena-Colina et al. 2011). The expression of CD36 is regulated in the liver by transcription factors such as PPARγ, liver X receptor (LXR) and pregnane X receptor (Zhou et al. 2008).

II. FA synthesis

In addition to incorporating circulating FA, hepatocytes synthesize FA from dietary carbohydrate via DNL. The rate of DNL is regulated primarily at the transcriptional level by several nuclear transcription factors as LXR, sterol regulatory element-binding protein 1c (SREBP1c), carbohydrate-responsive element-binding protein (ChREBP), and farnesoid X receptor (FxR). Postprandially, activation of lipogenesis is achieved by a rise in plasma glucose and insulin levels and their respective activation of ChREBP and SREBP1c (Kawano and Cohen 2013). Thus, glucose serves both as substrate and as an activator of DNL. Glucagon has an inhibitory effect on SREBP1c transcription thus decreasing its downstream lipogenic target enzymes (Ferre and Foufelle 2010; Wang et al. 2016). Moreover, activation of AMP-activated protein kinase (AMPK) by low AMP:ATP ratio during fasting inhibits SREBP1c-mediated transcription of lipogenic genes (Yap, Craddock, and Yang 2011; Li et al. 2011).

III. FA oxidation

Oxidation of FA to acetyl-CoA occurs within the mitochondria, peroxisomes, and the endoplasmic reticulum (ER). In general, short-, medium-, and long-chain FA are oxidized within mitochondria (β-oxidation), while toxic, very long-chain FAs are oxidized within peroxisomes. In the fed state, FA oxidation is inhibited and DNL promoted, allowing for storage and distribution of lipids. DNL inhibits β–oxidation in the mitochondria through the accumulation of malonyl-CoA that directly inhibits

carnitine palmitoyltransferase-1 (CPT1), a transporter that shuttles FA into the mitochondria what represents the rate- limiting step of FA β-oxidation (Ruderman, Saha, and Kraegen 2003). Simultaneously, insulin turns off β-oxidation through its inhibition of PGC-1α, a master regulator of FA oxidation (Lin, Handschin, and Spiegelman 2005). PPARα is also involved in the regulation of FA oxidation, acting in tissues with highly oxidative function such as muscle, BAT and liver to increase the expression of a set of enzymes required for FA oxidation, including CPT1. In fact, the effect of glucagon in hepatic FA metabolism is also mediated by PPARα (Longuet et al. 2008). Fasting or long-term starvation triggers a PPARα-dependent response to activate the catabolism of lipids as an energy supply. Similarly, in response to reduced blood glucose concentration, glucagon-mediated signaling augments cAMP concentrations, which activate the transcription factor CREB. This increases the expression of genes involved in lipid catabolism activating at the same time fasting and glucagon activate AMPK that ultimately lowers malonyl-CoA levels further promoting FA oxidation in the mitochondria (Kimball, Siegfried, and Jefferson 2004; Foster 2012).

Mitochondria are highly dynamic organelles that can change in overall mass (mitochondrial biogenesis) and shape (fusion and fission events) upon dietary challenges (Chan 2006). The transcription factor PGC-1α also regulates mitochondrial biogenesis, that is: increased mitochondrial genome duplication combined with increased protein mass involving the mitochondrial transcription factor A (TFAM) (Ventura-Clapier, Garnier, and Veksler 2008). In this line, PGC-1α can also regulate mitochondrial fission and fusion to maintain mitochondrial homeostasis (Valero 2014; Peng et al. 2017). Mitochondrial fusion requires the action of fusion proteins dynamin-like 120 kDa protein or OPA-1 at the inner mitochondrial membrane and mitofusins (1 and 2) at the outer mitochondrial membrane promoting the fusion of membranes of juxtaposed mitochondria. Fusion also contributes to increased respiration and mitochondrial metabolism likely by promoting increased diffusion of intermediate metabolites and reducing agents (Boland, Chourasia, and Macleod 2013).

Mitochondrial dynamics and biogenesis are tightly regulated in different tissues including the liver to efficiently adapt metabolic changes to the energy requirements of the organism. For instance, upon dietary challenge mitochondrial biogenesis and fusion events would be activated to restore the energetic balance in the cell. Defects in this mitochondrial processes are related with different diseases such as T2D or cancer (Boland, Chourasia, and Macleod 2013; Lee et al. 2014; Begriche et al. 2006; Zorzano, Liesa, and Palacin 2009).

IV. Autophagy

Autophagy is a process that consists of a series of molecular reactions that result in the degradation of intracellular components in lysosomes and contributes to efficient quality control of organelles and cytosolic proteins in hepatocytes. Moreover, autophagy plays an important role in the efficient

utilization of energetic resources and helps maintain a positive energy balance in the liver through: 1) breakdown of intracellular stores of macromolecules that can be utilized as cellular fuel; 2) control of key regulatory enzymes of cellular metabolism; and 3) preservation of mitochondrial homeostasis by efficient organelle turnover (Schneider and Cuervo 2014).

Autophagy is particularly important in highly metabolically active organs such as the liver, in which periods of starvation as short as 4 hours are enough to induce maximal activation of autophagy (Deter, Baudhuin, and De Duve 1967). Activation of liver macroautophagy during starvation is promoted by the increase in circulating glucagon and the concomitant decrease in circulating levels of insulin and amino acids, both potent inhibitors of hepatic macroautophagy (Deter, Baudhuin, and De Duve 1967; Mortimore and Mondon 1970; Mortimore and Schworer 1977). Also, epinephrine and norepinephrine can activate autophagy (Farah et al. 2014; Kondomerkos et al. 2005). At the molecular level, the mTORC1 pathway is the canonical negative regulator of autophagy and AMPK acts as the principal positive regulator inhibiting the mTORC1 pathway (Alers et al. 2012).

Autophagy might contribute to the maintenance of the energetic balance in the liver through catabolism of glycogen, a major hepatic energy store (Kotoulas, Kalamidas, and Kondomerkos 2006). Moreover, autophagy can directly regulate the intracellular level of lipids by removing lipid droplets that are then transformed into FA through a type of autophagy known as lipophagy (Singh et al. 2009; Liu and Czaja 2013). In fact, pharmacological or genetic activation of autophagy decreases lipid content in hepatocytes, while its inhibition increases TG accumulation (Ueno and Komatsu 2017; Mao et al. 2016).

V. VLDL secretion

Excess FA are re-esterified to TG that can be stored or exported as VLDL for storage and utilization by peripheral tissues. Regulation of hepatic VLDL production involves an interplay between systemic FA availability, and hormonal and nutritional factors (Nielsen and Karpe 2012). While insulin stimulates lipogenesis and thus increases lipid substrates for VLDL particles, it also acutely decreases VLDL secretion (Sparks and Sparks 2010). VLDL assembly requires the presence of both hepatic lipids and apolipoprotein B (apoB) substrates, and insulin likely functions by reducing the latter. Moreover, insulin inhibits the transcription of the gene Mtp, probably via AKT-mediated phosphorylation and deactivation of FOXO1 ((Kamagate et al. 2008). Reduction in Mtp activity would reduce transfer of TG to nascent apoB, which could result in smaller particles formed and less TG secreted. On the other hand, glucagon maintains a long-term inhibitory effect on assembly and secretion of VLDL in primary cultures of rat hepatocytes (Bjornsson et al. 1994) and was found to decrease VLDL-TG in a range of species (Habegger et al. 2010; Wang et al. 2016).

1.D. Insulin resistance and obesity

In healthy individuals all the aforementioned metabolic processes are coordinated to maintain homeostasis, however, in some pathological conditions these processes are altered and the homeostasis is lost. Insulin resistance (IR) is a pathological condition in which cells fail to respond to the actions of insulin. Obesity, a pathological condition in which there is an excessive accumulation of body fat, is commonly associated to IR and contributes to a diversity of pathological effects, including IR. The metabolic syndrome is a common metabolic disorder that results from the increasing prevalence of obesity. The metabolic syndrome is a condition characterized by the co-existence of at least three of the five following medical conditions: hypertension, IR or fasting hyperglycemia, dyslipidemia (reduced high-density lipoprotein cholesterol or elevated TG levels) and increased waist circumference (as an indicator of obesity) (Eckel, Grundy, and Zimmet 2005). The metabolic syndrome increases the risk of suffering pathologies including cardiovascular disease, non-alcoholic fatty liver disease (NAFLD), and type 2 diabetes (T2D) (Figure I5).

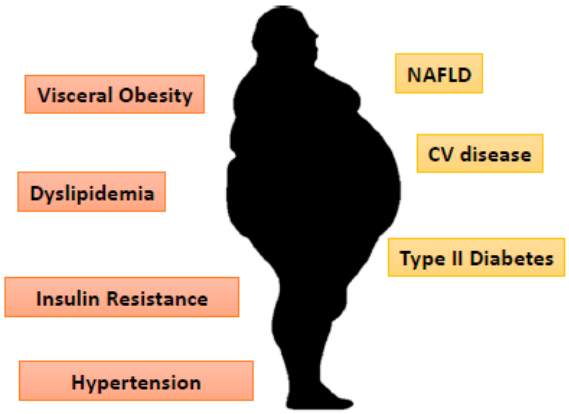

Figure I5. The metabolic syndrome encompasses different conditions (in orange boxes) that may include: dyslipidemia, visceral obesity, IR and hypertension. Metabolic syndrome patients are more prone to suffer different complications (in yellow boxes) as cardiovascular diseases, NAFLD, T2D or cancer, among others.

Besides a condition in which there is an excess in the accumulation of adipose tissue in the body, obesity is now considered a chronic state of low-intensity inflammation in which the increase in proinflammatory and decrease in anti-inflammatory factors influences glucose homeostasis and decreases insulin sensitivity in peripheral tissues (Olefsky and Glass 2010). Defining the precise mechanisms of IR in peripheral tissues is difficult while vital for the development of new and more effective therapies for T2D. As so happens during obesity, inflammation is a key feature underlying IR. TNFα and other proinflammatory cytokines activate mitogen-activated protein kinases (MAPK) (Tanti et al. 2012) interfering with insulin signaling. In this regard, the activity of IκB-kinase β (IKKβ) and c-Jun NH(2)-terminal kinase (JNK), both activated by TNFα, is elevated in different tissues during obesity, and several studies in mice have established the importance of these kinases in the development of IR (Tanti et al. 2012; Hirosumi et al. 2002). At the molecular level, one mechanism by which these kinases impair insulin signaling is the phosphorylation of IRS proteins on inhibitory serine sites, either directly or indirectly (Hirosumi et al. 2002). On the same line, activation of the mTORC1 node by TNFα (Gao et al.

2003) is known to negatively feedback on IRS1 via S6K, thus decreasing insulin sensitivity. On the other hand, the innate immune system is activated in response to threatened homeostasis triggering at the same time different reactions such as the acute-phase response, mediated primarily by interleukin-6 (IL-6), that has been related to IR and adiposity (Leinonen et al. 2003). Additionally, the innate immune system can be activated by metabolic signals in the course of obesity, such as increased circulating free FA. These may be recognized by receptors involved in the immune response, and lead to stimulation of inflammatory signaling cascades including IκBα kinase/nuclear factor-κB (IKK/NF-κB) or ER-stress-induced unfolded protein response (UPR) to finally interfere with insulin signaling (Ringseis et al. 2015).

Emerging data are pointing at ER stress as an important player in the pathophysiology of obesity, IR and T2D (Ozcan et al. 2004). In obesity the capacity of the ER is surpassed, thus leading to the accumulation of misfolded/unfolded proteins and triggering ER stress. Accordingly, interventions that suppress ER stress can improve diabetes and associated comorbidities (Ozcan et al. 2006). Moreover, accumulation of lipid metabolites, such as DAG or ceramides, has also been related to the pathogenesis of IR. Thereby, an increase in intracellular DAG content due to an imbalance between FA delivery and intracellular FA oxidation and storage, would lead to activation of new protein kinase C (PKC) isoforms that may in turn inhibit insulin action in liver and skeletal muscle (Erion and Shulman 2010; Samuel and Shulman 2012).

Additionally, several studies have demonstrated that hyperinsulinemia, hyperlipidemia, mitochondrial dysfunction and oxidative stress routes lead to attenuated insulin signaling and decreased cellular responsiveness to insulin (Samuel and Shulman 2012; Ye 2013). Hyperglucagonemia is also present in most forms of diabetes. This is because glucagon secretion is inhibited by insulin, but in the face of IR (such as during T2D) or a complete absence of endogenous insulin (in type 1 diabetes), this inhibition does not take place effectively and these high levels of glucagon could be contributing to the hyperglycemia during IR. Due to the hyperglycemic and insulin-suppressing effects of glucagon, the GCGR has historically been a prime target for pharmacological suppression rather than activation. However, as described in the section 1.b, glucagon has both catabolic and thermogenic actions in addition to its effects on glucose homeostasis. For this reasons, GCGR agonism would also be an attractive target for obese and T2D individuals except for the undesirable hyperglycemic effect. Thus, drugs have been developed to take advantage of the catabolic and thermogenic effects of glucagon receptor activation and weaken the stimulation of gluconeogenesis and glycogenolysis, an these drugs have demonstrated beneficial effects against obesity in mice (Pocai et al. 2009; Sanchez-Garrido et al. 2017).

2. Non-Alcoholic Fatty Liver Disease (NAFLD)

Obesity and IR are the key pathogenic factors associated with NAFLD, an extremely prevalent chronic liver disease worldwide, affecting about one quarter of adults in the developed countries (Younossi et al. 2018). The accumulation of TG in the liver in the absence of excessive alcohol consumption is the hallmark of NAFLD. This hepatic TG accumulation is caused by the dysregulation of the processes controlling liver lipid content (described in section 1.c). The imbalance between lipid input and output can be due to: 1) an increase in FA uptake derived from the circulation due to increased lipolysis from adipose tissue and/or from the diet; 2) an increase in DNL; 3) a decrease in FA mitochondrial oxidation; 4) a decrease in TG hepatic secretion of VLDLs.

NAFLD refers to a variety of different hepatic pathological conditions ranging from simple steatosis to Non-Alcoholic Steatohepatitis or NASH, in which there is inflammation and varying degrees of fibrosis, that may ultimately lead to cirrhosis, end-stage liver failure and hepatocellular carcinoma (HCC) (Figure I6). Most cases of simple steatosis rarely progress to advanced liver disease, but NASH has the potential of proceeding to more advanced stages of the disease (Malaguarnera et al. 2009).

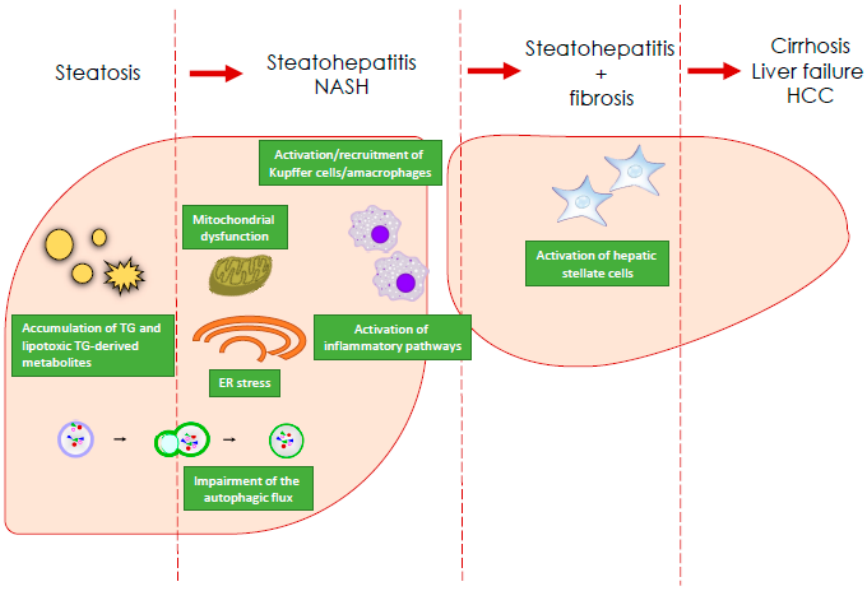

Figure I6. Main steps associated with the pathogenesis and progression of NAFLD. Simple steatosis can lead to NASH and more advanced liver disease through the activation of different mechanisms (See text for details).

The "two-hit" theory explaining the progression of this disease postulates that the "first hit" would consist of the accumulation of excessive hepatic fat owing to IR. This step is often present in metabolic syndrome patients, and, although it is not sufficient to cause NASH, it is enough to predispose the liver to chronic inflammation (Malaguarnera et al. 2009). The "second hit" would correspond to factors such as oxidative stress and the presence of reactive oxygen species (ROS), gut-derived LPS, soluble mediators synthesized both from cells of the immune system and from cells of the adipose tissue (Malaguarnera et al. 2009), and also to the activation of hepatic stellate cells (leading to collagen

deposition and the potential for cirrhosis) (Chiang, Pritchard, and Nagy 2011). However, this theory is now obsolete and has been substituted by the "multiple hit" one. The "multiple hit" hypothesis considers multiple insults acting together on genetically predisposed subjects to induce NAFLD and provides a more accurate explanation of NAFLD pathogenesis (Buzzetti, Pinzani, and Tsochatzis 2016). Such hits include IR, hormones secreted from the adipose tissue, nutritional factors, effects from gut microbiota and genetic and epigenetic factors.

2.A. Role of insulin resistance and inflammation in the development of NAFLD

In the insulin-resistant individual, insulin fails to impair lypolisis, so TG (FA and glycerol) are released from WAT to the bloodsteam. The liver can act as a buffer for these FA overload, and thus FA are prone to enter the liver and be reesterified into TG. This, together with the increased FA influx coming from the diet, leads to increased lipid accumulation in the liver. Moreover, in rodents with fatty liver, FA intake is further facilitated by enhanced expression of hepatic FAT/CD36 probably as a consequence of the upregulation of PPARγ (Inoue et al. 2005). Increased FAT/CD36 levels have also been related with NAFLD in humans (Miquilena-Colina et al. 2011; Bechmann et al. 2010). Also, the glycerol derived from the TG of the insulin-resistant WAT serve as a substrate for hepatic glucose production. In the insulin-resistant liver, insulin fails to block gluconeogenesis and glycogen breakdown. These effects, together whith the increased availability of glycerol, increases hepatic glucose output what contributes to the hyperglycemia found in insulin-resistant patients. Moreover, glucose serves as a substrate of DNL and also promotes the transcription of lipogenic genes through the activation of the transcription factor ChREBP. Consequently, an hyperglycemic state aggravates lipid accumulation. In the pathogenesis of T2D, there is a long-standing paradox regarding a selective IR in the liver (Brown and Goldstein 2008): in the insulin-resistant liver, insulin fails to suppress hepatic glucose production while it still potentiates DNL. There are several theories trying to identify branch points that may exist in the insulin signaling cascade able to separate insulin effects into final independent actions regarding gluconeogenesis (involving FOXO1) and DNL (controlled by SREBP1c). mTORC1 has been proposed as one such branch point, as it is required for insulin-dependent SREBP1c induction but not for PEPCK transcriptional repression (Li, Brown, and Goldstein 2010). However, other theories suggest that TG synthesis is mostly regulated by substrate influx into the liver independently of changes in hepatic insulin signaling (Leavens and Birnbaum 2011). Regardless of the etiology, the fact is that the final activation of DNL in the insulin-resistant liver plays a substantial role in the pathogenesis of NAFLD, accounting for 26% of accumulated hepatic TG in human subjects while it is almost absent in lean individuals (Donnelly et al. 2005).

Evidence also suggests that TG accumulation exacerbates hepatic IR and increases systemic levels of insulin-antagonizing cytokines. The development of NAFLD may thus predispose towards or exacerbate IR in patients, potentially leading to a vicious cycle of increased hepatic TG accumulation that in turn would worsen IR. Furthermore, the metabolic changes that accompany T2D have also been implicated as pathogenic factors for progressive NASH (Smith and Adams 2011). It is well described that the accumulation of TG-derived toxic lipid metabolites and the release of cytokines due to the activation of intracellular inflammatory pathways promote the activation and the infiltration of macrophages in liver tissue. Macrophages can change from an M1 or "classically activated" state that secretes large amounts of pro-inflammatory cytokines *vs* an M2 or "alternatively activated" phenotype with anti-inflammatory actions. Macrophages play a key role in adipocyte dysfunction, adipose tissue IR, release of FFAs into the circulation, and ectopic fat deposition in the liver (McArdle et al. 2013; Cusi 2012). Kupffer cells are the liver counterpart of adipose tissue macrophages that play a significant role in NAFLD, as demonstrated by the fact that experimental depletion of these cells prevents hepatic steatosis in different mice models of NAFLD/NASH (Tosello-Trampont et al. 2012; Rivera et al. 2007; Lanthier et al. 2010).

Once a steatotic and inflammatory state has been established in the liver, the next step in the progression of NASH would be the appearance of fibrosis through the activation of hepatic stellate cells (HCS), the fibroblasts within the liver, and the deposition of collagen fibers. The appearance of fibrosis in addition to NASH represents a much worse prognosis (Kim et al. 2013; Ekstedt et al. 2015).

2.B. Additional mechanisms involved in the pathogenesis of NAFLD

As already mentioned, alterations in insulin signaling caused by hepatic and systemic IR constitute key pathogenic factor in the onset and progression of NAFLD and inflammation plays a central role both in IR and in the development and progression of NAFLD (Asrih and Jornayvaz 2013). However, a variety of cellular responses not directly related to IR or inflammation such as ER-stress, autophagy defects and mitochondrial dysfunction also contribute to the pathogenesis of NAFLD.

Lipid accumulation in the fatty liver disturbs the function of the ER in the hepatocytes, thereby generating chronic ER stress that interferes with the normal cellular function (Baiceanu et al. 2016). Interestingly, ER stress activates the cleavage of SREBP-1c independently of insulin, thus being able to stimulate lipogenesis even in an insulin-resistant liver. Accordingly, alleviating ER stress in obese rodents markedly improves both hepatic steatosis and insulin sensitivity (Ferre and Foufelle 2010). Upon ER stress, various protecting mechanisms (namely, ER-associated degradation, UPR and autophagy) are activated. However, they are unable to shutdown ER stress in the context of the fatty liver. Of note, promoting autophagy improves NAFLD (Lin et al. 2013) and also prevents ER stress in lipid-overloaded human hepatocytes (Gonzalez-Rodriguez et al. 2014). However, the lipotoxicity observed in NAFLD

provokes a blockade of liver autophagy that causes the impairment of the autophagic flux. This impairment represents a key feature of NASH (Gonzalez-Rodriguez et al. 2014; Fukuo et al. 2014).

Mitochondrial dysfunction may also play a crucial role in the genesis of NASH, since mitochondria are involved in FA oxidation, lipid peroxidation, cytokine release, cell death and are the most important source of cellular ROS (Jezek and Hlavata 2005; Begriche et al. 2006). Actually, alterations in mitochondrial biogenesis or mitochondrial dynamics have been suggested to be important contributors in the progression of NAFLD (Nassir and Ibdah 2014). Interestingly, in patients with NASH, liver mitochondria show ultrastructural abnormalities and impaired function (Caldwell et al. 1999; Sanyal et al. 2001).

Reduced GCGR content in the plasma membrane of the hepatocytes and hepatic glucagon resistance is also associated with the development of fatty liver (Charbonneau, Unson, and Lavoie 2007; Charbonneau, Couturier, et al. 2005; Charbonneau, Melancon, et al. 2005). Conversely, administration of exogenous glucagon reduces liver TG content and prevents the development of fatty liver in dairy cows (Nafikov et al. 2006; Bobe et al. 2003; Bobe et al. 2007). In mice, the treatment with a GLP1/glucagon receptor dual agonist is able to improve NASH (Valdecantos et al. 2017).

2.C. Models in NAFLD and NASH preclinical research

The use of animal models has proven to be a useful tool to provide insight into the development of NAFLD and progression of NASH (Sanches et al. 2015). However, research in this field has been hampered by the lack of an animal model that can fully recapitulate the human disease phenotype in a consistent and timely manner. Due to the number of factors that are associated with the progression of NAFLD and its as yet unclear pathogenesis, rodent models must be carefully chosen to answer the research question. We can distinguish between two different NAFLD mice models, genetic and dietary ones. In the first group we can highlight the leptin-deficient and the leptin receptor-deficient mutant mice as models of obesity, IR and NAFLD. Feeding mice with a High Fat Diet (HFD) also induces an IR (especially in long-term feeding) and an obese state including hepatic steatosis that could be accompanied with different signs of inflammation. HFD feeding is the most widely used model (Kraegen et al. 1986; Storlien et al. 1986). Alternatively, the methionine and choline deficient diet (MCD) that induces NASH independently of the development of obesity and IR can be used as a model of non-obese NASH (Rinella et al. 2008). In Table I1 we summarize the characteristics of these models.

Model		Description	Obesity	IR	Steatosis	Hepatocyte ballooning	Inflammation	Fibrosis	Disease phenotype
Genetic	Ob/ob mice	Leptin deficient	Yes	Yes	Yes	Yes	No	No	NAFLD
	Db/db mice	Leptin receptor deficient	Yes	Yes	Yes	Yes	No	No	NAFLD
Dieatary	HFD	Short term	Yes	Mild	Yes	Uncommon	No	No	NAFLD
		Long term	Yes	Yes	Yes	Yes	Minimal	Minimal	NASH (mild)
	MCD	Methionine and choline deficient	No	No	Yes	Yes	Yes	Minimal	NASH

Table I1. Main characteristics of different models for the study of NAFLD.

The principal characteristics of the MCD as a model of non-obese NASH and the main differences between this and the HFD model as a model of obese fatty liver are depicted below.

The MCD model is based on the fact that methionine and choline are essential for the export of lipids in VLDL rapidly leading to NASH. Moreover, the lack of methionine reduces glutathione synthesis and impairs the antioxidant defense against free radical attack. In addition to the methionine and choline deficiency, this diet contains a high quantity of sucrose (10% fat, 40% sucrose), what further promotes lipid accumulation. Also, MCD-fed mice present an acquired defect in mitochondrial β-oxidation (Anstee and Goldin 2006). Mice fed an MCD exhibit lipid accumulation with increased activation, migration, adhesion, and accumulation of liver macrophages promoting proinflammatory cytokine secretion and activation of inflammatory pathways (Yu et al. 2006; McCuskey et al. 2004). Although these proinflammatory mechanisms are similar to human NASH, and the MCD promotes real liver damage, MCD does not perfectly mimic the pathogenesis of human NASH. The main difference is the accompanying phenotype that in the human pathology as well as in the HFD model, is an obese an insulin-resistant state, while MCD-fed mice are cachectic and not overtly insulin-resistant (Rinella and Green 2004). TG and cholesterol levels are also reduced in this model what contrasts with obese patients with NAFLD/NASH and HFD-fed mice. Other discrepancies in the metabolic profile of the MCD diet are reduced levels of insulin, glucose, and leptin, which are opposite to the effects of human NASH. However, it is a widely used model because it mirrors several features of human NASH in a very short time, since overt NASH is detected after 4 weeks and the prolongation of the diet up to 10 weeks elicits the appearance of fibrosis (Itagaki et al. 2013).

De novo lipogenesis is another mechanism differentially affected in the MCD model *vs.* the HFD model and the human disease. As previously mentioned, DNL contributes to the increased hepatic TG accumulation in the insulin-resistant context. However, this process has been found to be

downregulated in MCD-fed mice even when it might play a role in the onset of the pathology in this dietary model (Rizki et al. 2006).

Because of the strong link between NAFLD and metabolic syndrome, the HFD model is one of the most used models for the study of this disease. In these models, the animals are fed a HFD in which 45–75% of the caloric intake comes from fat. In the majority of the HFD models, the degree of liver injury is not severe compared with the MCD model. However, the HFD can recapitulate the detrimental eating habits of the Western diet and mimic the etiology of NAFLD/NASH in terms of metabolic parameters (Hebbard and George 2011).

A totally different approach to study hepatic lipid accumulation in a physiological condition is fasting-induced steatosis, a non-obese, non-pathological hepatic steatosis model. Under fasting conditions, glucose and insulin fall and the inhibitory effect of insulin on WAT lipolysis is reduced. FA are released into the bloodstream and used as fuel in liver, heart and skeletal muscle. In the liver, FA oxidation is enhanced and ketone bodies are generated, which represent the main energy source for the brain in the absence of glucose (Kersten et al. 1999). However, when the influx of FA exceeds the oxidative capacity of the liver FA are re-esterified into TG for intracellular storage (Guan et al. 2009; Nishikawa et al. 2008), this occurring in the absence of inflammation or fibrosis (Mustonen et al. 2013; Mustonen et al. 2012; Xu et al. 2013). Thus, after 6-24 hours of food deprivation, mice accumulate TG in the liver resulting in fasting-induced fatty liver (Lin et al. 2005; Guan et al. 2009).

Finally, steatosis can be studied in cell culture models that are summarized in BOX 2.

BOX 2: *In situ* models of steatosis.

Primary human hepatocytes are considered to be the “gold standard” cellular model for studying hepatic fatty acid and glucose metabolism; however, they come with limitations such as availability of cells, donor variability, inability to proliferate, and a short life span (Nikolaou et al. 2016). Therefore, a variety of human hepatoma cell lines have been generated to investigate human hepatocyte metabolism and function, including the HepG2 and Huh7 cell lines. Experimental strategies have been developed to understand how hepatocytes respond to lipid overload. These *in situ* assays induce FA accumulation in human hepatocyte lines 18–24 h after incubation in the presence of high lipid concentrations, usually complexed to albumins such as bovine serum albumin (BSA) (Alsabeeh et al. 2018). This allows us to mimic the physiological ratio between bound and unbound FA in humans (Richieri and Kleinfeld 1995; Boden 2005).

3. G protein-coupled receptor kinase 2 (GRK2)

G protein-coupled receptor kinase 2 (GRK2) is a Ser/Thr kinase classically known for its role in the regulation of GPCRs (G-protein coupled receptors). More precisely, GRK2 mediates the homologous desensitization of GPCRs such as β-AR among others. When stimulated, GPCRs activate GRK2 which then phosphorylates serine and threonine residues at the intracellular tail of the receptor, thus promoting β-arrestin recruitment and the uncoupling of GPCRs and G proteins. These events finally lead to internalization of the receptor thus abrogating further G protein-dependent signal propagation while initiating in certain tissues other signaling events (Bologna et al. 2017; Mayor, Penela, and Ruiz-Gomez 1998; Gurevich et al. 2012). Besides such canonical role in GPCR modulation, GRK2 is also able to phosphorylate a variety of non-GPCR substrates and to dynamically interact with other important signal transduction partners in a kinase activity-independent manner (Penela et al. 2010; Watari, Nakaya, and Kurose 2014). The implication of GRK2 in regulating different GPCRs controlling metabolism, its function as a negative regulator of the insulin signaling cascade and its role in mitochondria as well as in regulating other important kinases as p38 MAPK and ERK are described herein .

3.A. GRK2 in the regulation of GPCRs involved in metabolic regulation

Regarding its canonical role, GRK2 have been described to desensitize different GPCRs important for metabolic regulation, such as β-AR or the GCGR, although the latter only in HEK293 (Krilov et al. 2011). The SNS controls a variety of responses of the body to different stresses acting through adrenergic receptors such as the β-AR. Among this responses, we can highlight the adrenergic lipolytic response in the adipose tissues and also the expression of uncoupling protein 1 (UCP1) in BAT increasing its thermogenic capacity. Interestingly, increasing energy expenditure (EE) is regarded as a possible alternative for the treatment of the metabolic syndrome. BAT is the natural target for increasing EE since it is the main organ involved in heat production *via* non-shivering adaptive thermogenesis, an energy-dissipating process key to maintaining body temperature (Cannon and Nedergaard 2004). It has been demonstrated that GRK2 negatively regulates EE *in vivo* and the overexpression of GRK2 in mature brown adipocytes impairs β3-agonist and norepinephrine-stimulated lipolysis (Vila-Bedmar et al. 2012). In the liver, β-adrenergic signaling mediates the increase in glycogenolisis and gluconeogenesis. However, the GCRG is the main GPCR involved in glucose output in the liver and, in HEK293, the amount of GCRG in the plasma membrane was reduced by GRK2 overexpression (Krilov et al. 2011).

3.B. GRK2 in insulin signaling and other non-canonical functions

Several lines of evidence suggest that GRK2 levels play a relevant role in insulin signaling and IR (Mayor et al. 2018; Lucas et al. 2015; Ciccarelli, Cipolletta, and Iaccarino 2012). First, certain GPCRs can transmodulate insulin pathway signals and this crosstalk can be regulated by GRK2 levels (Cipolletta et al. 2009). Second, GRK2 has been recently found by our and other groups to act as an inhibitor of insulin-mediated glucose transport and insulin signaling by interacting with:

- Gαq/11, via direct binding of the RH domain of GRK2 to Gαq proteins, in a process that is independent of GRK2 kinase activity (Usui et al. 2005).

- IRS1, either by physical association and sequestration (Garcia-Guerra et al. 2010) or by directly phosphorylating it at Ser307 (Ciccarelli et al. 2011) (Figure I7).

Moreover, work from our group has shown that altered GRK2 levels markedly modify insulin-mediated signaling in cultured adipocytes, myocytes and brown adipicytes (Vila-Bedmar et al. 2012; Garcia-Guerra et al. 2010).

Additionally, *in vitro* results in mouse liver FL83B cells demonstrated that GRK2 deficiency increases basal and insulin-stimulated glycogen synthesis via a post-insulin receptor signaling mechanism probably involving GSK3α, and that GRK2 may contribute to reduced insulin receptor expression and function during chronic insulin treatment (Shahid and Hussain 2007).

Interestingly, Sprague-Dawley rats fed a HFD for two weeks presented increased hepatic GRK2 at the plasma membrane (Charbonneau, Unson, and Lavoie 2007). In the same line, our group has shown that GRK2 levels are augmented in different animal models of IR, as well as in insulin-resistant human adipocytes and in peripheral blood cells from metabolic syndrome patients. In contrast, hemizygous GRK2 mice (GRK2+/-) show enhanced insulin sensitivity and do not develop IR upon aging, TNFα influsion or HFD feeding. Furthermore, reduced GRK2 levels induce a lean phenotype and decrease age- or HFD-related adiposity (Garcia-Guerra et al. 2010).

For all these reasons, GRK2 is emerging as a potentially important regulator of metabolism due to its unique capability to regulate both important GPCRs and the insulin cascade (Figure I7).

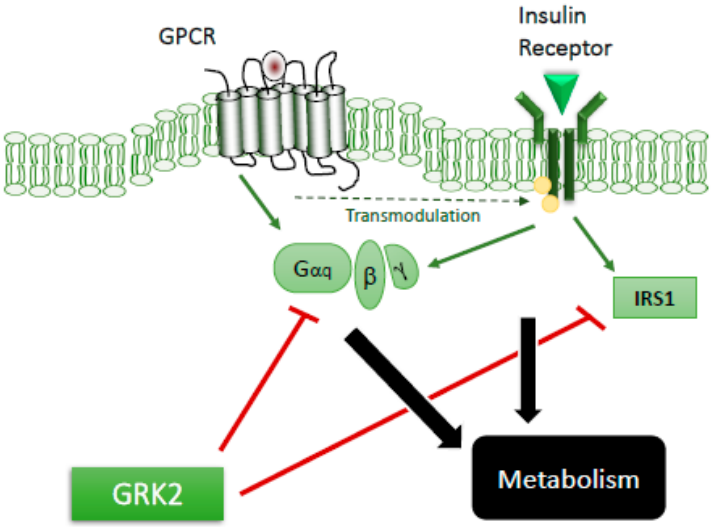

Figure I7. GRK2 as a signaling hub controlling both GPCRs and the insulin receptor pathway. Insulin binds its receptor, recruiting IRS to activate the PI3K/AKT pathway, or, alternatively, heterotrimeric Gq proteins (G protein). GRK2 can bind to Gq or to IRS, impairing downstream insulin signals. Moreover, GRK2 can regulate different GPCRs, some of them able to modulate insulin signaling ("transmodulation").

Moreover, GRK2 has been described to localize and accumulate in the mitochondria in different cell lines and contexts to regulate diverse mitochondrial processes. However, the role of GRK2 in mitochondria in terms of ATP synthesis is controversial and both positive and negative effects have been suggested (Sato et al. 2015; Sorriento et al. 2014). Moreover, GRK2 has been reported to negatively regulate FA oxidation in cardiomyocyte mitochondria (Sato et al. 2015).

Finally, GRK2 can also to interact and regulate p38 MAPK and ERK, members of the MAPK family. MAPK signaling cascades transduce a variety of extracellular signals following activation of GPCRs, receptors tyrosine kinase (RTKs) or insulin growth factor receptor (IGFR) (Mohan et al. 2017) and can modulate different cellular responses (some mentioned throughout this Introduction). GRK2 phosphorylates p38α MAPK at Thr123 and interferes with the ability of p38 MAPK to bind to one of its upstream activators (MKK6) preventing p38 activation (Peregrin et al. 2006). Also, GRK2 can inhibit MEK (ERK kinase) resulting in reduced ERK activation (Jurado-Pueyo et al. 2008; Jimenez-Sainz et al. 2006).

To sum up, GRK2 can control key GPCRs involved in metabolism and insulin, apart from MAPK signaling and possibly mitochondrial processes. These results identify GRK2 as a very interesting signaling hub in the field of metabolism that deserves a more extensive characterization, particularly regarding its potential role in hepatic physiopathological conditions related to IR, NAFLD and glucose homeostasis that have not been addressed so far.

OBJECTIVES

In the recent years, GRK2 has emerged as a signaling hub with a very complex interactome. GRK2 has the singular potential to regulate metabolism playing key roles in the control of both important GPCRs, i.e. β-adrenergic receptors or the glucagon receptor, and insulin-modulated intracellular cascades, as well as interacting with many other important proteins. Even when previous studies revealed that GRK2 downmodulation prevents insulin resistance *in vitro* as well as *in vivo* during aging- and HFD-induced adiposity, the effect of lowering GRK2 levels in NAFLD, a very common condition among obese and insulin resistant patients, had not been evaluated before. Consequently, the general objective of this work was to study the levels of GRK2 in NAFLD both in humans and preclinical settings, and to analyze the impact of altering them on the development of fatty liver, both dependent or independent of obesity, in mice. Moreover, we sought to validate GRK2 downmodulation as a feasible intervention to tackle obesity, insulin resistance and NAFLD. Finally, we wanted to assess the role of GRK2, if any, in the adaptation to fasting, another context in which the liver has an orchestrating function controlling glucose and lipid homeostasis.

Specific objectives:

1. Analyze hepatic GRK2 levels in mice suffering from HFD-induced NAFLD, exploring the impact of GRK2 dosage in the onset or progression of the disease upon short- and long-term high fat feeding.
2. Investigate if genetically lowering GRK2 levels during a HFD in already insulin-resistant and obese mice would reverse the phenotype, including:
    i. Insulin sensitivity, glucose tolerance and obesity
    ii. The presence of NAFLD comprising steatosis and inflammation signs
3. Monitor hepatic GRK2 levels in MCD-induced non-obese NASH. Explore the impact of low GRK2 levels in the development of the disease and in different underlying processes as well as diverse protective mechanisms.
4. Examine the levels of GRK2 in human liver biopsies from simple steatosis and NASH patients.
5. Study the influence of GRK2 levels on intracellular lipid accumulation in an *in vitro* model of steatosis.
6. Elucidate the influence of GRK2 dosage on the physiological adaptation to fasting regarding steatosis and glucagon-mediated responses.

MATERIALS AND METHODS

MATERIALS

Buffers and solutions

Buffer	Composition	Comments
Hypotonic lysis buffer	20 mM Tris-HCl pH 7.5 1 mM EDTA 1 mM EGTA 5 mM NaF	
PBS (1x)	137 mM NaCl (0.8% w/v) 2.7 mM KCl (0.02% w/v) 10 mM Na_2HPO4 (0.144% w/v) 1.75 mM KH_2PO4 (0.024% w/v) pH 7.4	autoclaved
Oil red O cell staning stock solution (for cells)	0.7 g Oil Red O 200 ml Isopropanol	Stir O/N, filter through a 0.2 µm filter and store at 4ºC
Oil red O tissue staning stock solution (for tissues)	0.5 g Oil Red O 60 ml Triethyl-phosphate 40 ml H20	
Ponceau staining solution	0.2% Ponceau-S in 3.0% TCA	
Protease/phosphatase Inhibitor Cocktail:	0.1 µM PMSF 1 µM Benzamidin 16 µg/µl Aprotinin 350 µM Na_3VO_4 10 µg/ml STI 10 µg/ml Bacitracin	
Protein sample buffer 4x	200 mM Tris pH 6.8 40% (v/v) glycerol 0.15% (w/v) bromophenol blue 4% (w/v) SDS 5% (v/v) β-Mercaptoethanol	
RIPA buffer (1x)	Tris-HCl 20 mM pH 7.5 150 mM NaCl 1% Triton-X100 0.1% SDS 0.5% sodium deoxycholate	Stir with heat to dissolve. Store at 4°C for 3 months maximum. Add fresh protease inhibitor cocktail before each use
Resolving Polyacrylamide gel (6-15%)	Acrylamide/N,N'methylenbisacrylamide 30:0.8 (w/v) 0.375 M Tris-HCl pH 8.9 0.1% SDS	
Running buffer(10x)	0.25 M Tris base 2.0 M Glycine 1% SDS	
Stacking Polyacrylamide gel (4%)	Acrylamide/N,N'methylenbisacrylamide 30:0.8 (w/v) 0.25 M Tris-HCl pH 6.8 0.1% SDS	
TAE buffer (1x)	40 mM Tris-acetate pH 7.6 1 mM EDTA	Autoclaved
TBS (10x)	0.1 M Tris base pH 7.4 1.5 M NaCl	
Transfer buffer (10x)	0.2 M Tris base 1.5 M glycine 20% methanol (v/v)	

Primary hepatocytes cell culture media

Media	Composition	Comments
Attachment Media	DMEM/F12 20 mM HEPES pH 7.4 0.05% $NaHCO_3$ 5 mM glucose 10% FBS 5 mg/ml BSA 100 U/ml penicillin, 100 µg/ml streptomycin and 50 µg/ml gentamicin	Filter through a 0.2 µm filter
Plating Media	DMEM High Glucose Sodium Pyruvate 2 mM Penicillin/Streptomycin 2% Fetal Bovine Serum 10% Dexamethasone 1 µM Insulin 0.1 µM	Filter through a 0.2 µm filter
Maintenance Media	DMEM High Glucose Sodium Pyruvate 2 mM Penicillin/Streptomycin 2% Fetal Bovine Serum 10% Dexamethasone 0.1 µM Insulin 1 nM	Filter through a 0.2 µm filter
Glucose Production Media Lactate/Pyruvate	Glucose-free Medium Powder (SIGMA) 8,3g/L FA free BSA 2% Penicillin/Streptomycin 2% $NaHCO_3$ 3.7g/L L-Glutamine 4 mM Sodium Pyruvate 2 mM Sodium Lactate 20 mM	Adjust pH=7.2 Filter through a 0.2 µm filter

Name	Company
DMEM High Glucose HyClone ™	GE Healthcare
Phenol-Red free Glucose-free DMEM Medium Powder	SIGMA

Reagents

Name	Company
4% Paraformaldehyde (PFA) in PBS	Santa Cruz
Bluing	ThermoScientific
DNA dye as loading buffer 6X EZ-VISION®	Amresco
DAB	Vector Laboratories
DAPI	Merck
DPX mountant for histology	Sigma
Elite ABC kit	Vector Laboratories
Hematoxylin	ThermoScientific
Histoclear	Conda
Tamoxifen	Sigma
Sodium Pyruvate	Merck
Insulin Actrapid®	Novo Nordisk
Glucose	Merck
Propranolol	Sigma-Aldrich
Palmitic Acid	Sigma-Aldrich
BSA	Roche
BSA fatty acids free	US Biologicals
Oil Red O	Sigma
Tissue-Tek OCT	Sakura
Sucrose	Merck
Triethyl phosphate	Aldrich
Glucagon	Sigma-Aldrich
Forskolin	Santa Cruz
Sodium lactate	Sigma-Aldrich
Sodium pyruvate	Sigma-Aldrich

Oligonucleotides for qPCR

All oligonucleotides were purchased from Sigma-Aldrich or Invitrogen.

Gene name		Sequence
36b4 (human)	*Forward* *Reverse*	5´-CAGGCGTCCTCGTGGAAGTGAC- 3´ 5´-CCAGGTCGCCCTGTCTTCCCT-3´
actb	*Forward* *Reverse*	5´-CTAAGGCCAACCGTGAAAAG-3´ 5´-ACCAGAGGCATACAGGGACA-3´
adrbk1	*Forward* *Reverse*	5´-CATGCACAATCGCTTTGTAGTC-3´ 5´ -GGTCCGAGATTCTCACATGG-3´
Adrbk1 (human)	*Forward* *Reverse*	5´-GGCAGATGGTCTTCTTGCAG-3´ 5´-CCTCATCGAAGGAGCCAATG-3´
cd36	*Forward* *Reverse*	5´-GGCCAAGCTATTGCGACAT-3’ 5´-CAGATCCGAACACAGCGTAGA-3’

emr1 (F4/80)	*Forward* *Reverse*	5′-AGTACGATGTGGGGCTTTTG-3′ 5′-CCCCATCTGTACATCCCACT-3′
fasn	*Forward* *Reverse*	5′-GCTGCTGTTGGAAGTCAGC-3′ 5′-AGTGTTCGTTCCTCGGAGTG-3′
g6pc	*Forward* *Reverse*	5′- CTTAAAGAGACTGTGGGCATCA-3′ 5′- GCGTTGTCCAAACAGAATCC-3′
gapdh	*Forward* *Reverse*	5′-CTGCACCACCAACTGCTTAGC-3′ 5′-GGTCATGAGCCCTTCCACAAT-3′
mcr1 (CD206)	*Forward* *Reverse*	5′-CCACAGCATTGAGGAGTTTG-3′ 5′-ACAGCTCATCATTTGGCTCA-3′
nos (iNOS)	*Forward* *Reverse*	5′-TGAACTTGAGCGAGGAGCA-3′ 5′-TTCATGATAACGTTTCTGGCTCT-3′
pck1	*Forward* *Reverse*	5′-GGAGTACCCATTGAGGGTATCAT -3′ 5′- GCTGAGGGCTTCATAGACAAG -3′
pparg	*Forward* *Reverse*	5′-TGCTGTTATGGGTGAAACTCTG-3′ 5′-TCTGTGTCAACCATGGTAATTTCT-3′
ppargc1a	*Forward* *Reverse*	5′- CCCTTCTTTGCCATTGAATC -3′ 5′- AATGTTAGGAAAGTTTAGCATCTGG -3′
srebf1	*Forward* *Reverse*	5′-CGTCTGCACGCCCTAGG-3′ 5′-CTGGAGCATGTCTTCAAATGTG-3′
pck1	*Forward* *Reverse*	5′-GGAGTACCCATTGAGGGTATCAT-3′ 5′-GCTGAGGGCTTCATAGACAAG -3′
tfam	*Forward* *Reverse*	5′-CGCATCCCCTCGTCTATCAG-3′ 5′-AACTCATAGGTTTCTTTGGATAGCTACC-3′
tnf	*Forward* *Reverse*	5′-TCTTCTCATTCCTGCTTGTGG-3′ 5′-GGTCTGGGCCATAGAACTGA-3′
ywhaz	*Forward* *Reverse*	5′- TTACTTGGCCGAGGTTGCT-3′ 5′-TGCTGTGACTGGTCCACAAT-3′

Oligonucleotides for Genotyping

Primer Name	**Oligonucleotide sequence**
Cre1	5′ – GCGGTCTGGCAGTAAAAACTATC – 3′
Cre2	5′ – GTGAAACAGCATTGCTGTCACTT – 3′
Cre Pos Control Forward	5′ – CTAGGCCACAGAATTGAAAGATCT – 3′
Cre Pos Control Reverse	5′ – GTAGGTGGAAATTCTAGCATCATCC – 3′
GT-2	5′ – TGAGGCTCAGGGATACCTGTCAT – 3′
GT-4	5′ – GTTAGCTCAGGCCAACAAGCC – 3′
GT-5	5′ – CAGGCATTCCTGCTGGACTAG – 3′
GRK2 BK3	5′ – GACTTCTGCCTGAACCATCTG – 3′
GRK2 BK6	5′ – TCTGACAAATCTCCTCAATGTAT – 3′
GRK2 PGK1	5′ – TGGATGTGGAATGTGTGCGAG – 3′

Primary Antibodies

Antibody	Company	Reference	Dilution
β-Actin	Sigma-Aldrich	A5441	WB: 1/5000
β-Arrestins 1/2	Made in our laboratory (Penela et al. 2001)		WB: 1/1000
AMPKα	Cell Signaling	2532	WB: 1/1000
Phospho-AMPKα Thr 172	Cell Signaling	2535	WB: 1/1000
CD36	Novus Biologicals	NB400-144	WB: 1/1000
eiF2α	Cell Signaling	9722	WB: 1/1000
Phospho-eiF2α Ser51	Cell Signaling	9721	WB: 1/1000
ERK 1	Santa Cruz Biotechnology	sc-93	WB: 1/1000
ERK 2	Santa Cruz Biotechnology	sc-154	WB: 1/1000
Phospho-ERK1/2 Thr202/Tyr204	Cell Signaling	9101	WB: 1/2000
F4/80 (clon BM8)	abcam	ab16911	IHC: 1/200
FAS	BD Biosciences	610962	WB: 1/3000
GAPDH	abcam	ab8245	WB: 1/1000
GRK2	Santa Cruz Biotechnology	sc-562	WB: 1/1000
GRK2 (“PF2”)	Made in our laboratory(Nogues et al. 2016)		IHC: 1/200
Hadha	Abcam	Ab54477	WB: 1/1000
JNK 1/2	Cell Signaling	9252	WB: 1/1000
Phospho-JNK1/2 Thr184/Tyr 185	Cell Signaling	9251	WB: 1/1000
LC3 I/II	Novus Biologicals	NB100-2220	WB: 1/1000
Mitofusin 2	Abnova	H00009927-M03	WB: 1/1000
OPA- 1	BD Biosciences	612606	WB: 1/1000
p38α MAPK	Cell Signaling	9218	WB: 1/1000
Phospho-p38α MAPK Thr180/Tyr182	Cell Signaling	9215	WB: 1/1000
p62	Progen	GP62-C	WB: 1/1000
PPARγ	Santa Cruz Biotechnology	sc-7196	WB: 1/1000
S6	Cell Signaling	2217	WB: 1/1000
Phospho-S6 Ser240/244	Cell Signaling	2215	WB: 1/1000
STAT3	Santa Cruz Biotechnology	sc-482	WB: 1/1000
Phospho-STAT3 Tyr705	Cell Signaling	9145	WB: 1/1000

Tubulin	Sigma-Aldrich	T4026	WB: 1/2000
UCP-1	Made in Jan Kopecký´s laboratory (Baumruk et al. 1999)		WB: 1/1000

Secondary antibodies

Name, Antigen	Company	Dilution
IRDyeTM 680 TL, donkey anti-mouse IgG, conjugated to infra-red dyes	LI-COR	WB:1/25000
IRDyeTM 800 CW, donkey anti-mouse IgG, conjugated to infra-red dyes		
IRDyeTM 680 TL, goat anti-rabbit IgG, conjugated to infra-red dyes		
IRDyeTM 800 CW, goat anti-rabbit IgG, conjugated to infra-red dyes		
IRDyeTM 680 TL, donkey anti-guinea pig IgG, conjugated to infra-red dyes		
IRDyeTM 800 CW, donkey anti- guinea pig IgG, conjugated to infra-red dyes		
IRDyeTM 680 TL, donkey anti-mouse IgG, conjugated to infra-red dyes		
IRDyeTM 800 CW, donkey anti-goat IgG, conjugated to infra-red dyes		
Soluble rabbit peroxidase-anti-mouse IgG	Nordic Immunology	WB: 1/50000
Soluble mouse peroxidase-anti-rabbit IgG		
Soluble mouse peroxidase-anti-goat IgG		
Biotin-conjugated donkey anti-rabbit IgG	Jackson Immnunoresearch	IHC: 1/4000
Biotin-conjugated donkey anti-rat IgG		

METHODS

Animal Protocols

Animals were maintained at a room temperature of 22 ± 2 °C on a 12:12 light–dark cycle (lights on at 08:00 am) with a relative humidity of 50 ± 10% and under pathogen-free conditions in the animal facility of Centro de Biología Molecular Severo Ochoa unless otherwise stated. Mice had free access to food and water. Mice were euthanized using CO_2 and weighted. Tissues were surgically removed, washed, dried and immediately weighted. Then cut in several pieces and either frozen in liquid nitrogen or fixed in 4% paraformaldehyde (PFA). Other procedures are specified for each animal protocol.

Db/db mice

db/db and *db/+* control mice in the C57BL/KsJ genetic background were purchased from Charles River Laboratories (Charles River, Barcelona, Spain) and maintained in the animal facility of Instituto de Investigaciones Biomédicas Alberto Sols.

GRK2+/-

Hemizygous-GRK2 (GRK2 +/-) mice were generated on the C57BL/6 background as described (Mohamed Jaber et al. Proc Natl Acad Sci, 1996). Experiments were performed on GRK2 +/- mice and control wild-type (WT) mice (C57BL/6J, The Jackson Laboratory, Bar Harbor, ME, USA). Animals were genotyped by

PCR on genomic DNA using reported oligonucleotides (see GRK2 BK3, BK6 and PGK1 in the Materials section) following the conditions specified in the Genotyping section.

12 weeks and 30 weeks-long high fat diet (HFD) feeding model

GRK2+/- and WT mice were fed *ad libitum* either a normal chow diet (providing 13% of total calories from fat, 67% from carbohydrate and 20% from protein; 2014S Rodent Maintenance Diet, Teklad, Harlan, Barcelona, Spain) or a high fat diet (HFD, providing 45% of total calories from fat, 35% from carbohydrate and 20% from protein, Rodent Diet D12451, Research Diets, New Brunswick, NJ, USA) for 12 or 30 weeks. High fat feeding period started 6 weeks after birth in the 12 weeks-HFD experiment and at 8 weeks of age for the long-term feeding protocol. Body weight was measured before and after the high fat feeding period.

Methionine and choline-deficient diet (MCD) model

For the MCD experimental model, 14 weeks old GRK2+/- and WT mice were fed either an MCD (TD.90262 E1553-94, ENVIGO) or the corresponding choline and methionine-sufficient control diet (CD, TD.90262 E15654-04, ENVIGO) for 4 weeks (unless otherwise stated). In the fourth week of MCD/CD feeding GTT, ITT and PTT were performed. Body weight was measured at the end of the experiment.

Fasting experiments

3-4 months old WT and GRK2+/- mice were either fasted for 14, 24 or 48 hours or sacrificed in the fed state for controls. Blood was drawn at the different fed/fasting conditions, glucose levels were measured and a sample was collected for future analysis. Body weight was measured before and after the fasting period. Besides the liver, eWAT was also surgically removed and snap frozen in liquid nitrogen.

Tam-GRK2−/− and Tam-GRK2+/+ mice

We used a transgenic mice strain (B6.Cg-Tg(CAG-cre/Esr1) 5Amc/J maintained on the C57BL/6J background, The Jackson Laboratory) overexpressing a Cre recombinase protein fused to a mutant estrogen receptor ligand-binding domain under the control of the chicken beta actin promoter/enhancer coupled to the cytomegalovirus (CMV) immediate-early enhancer. We crossed these mice with homozygous loxP-GRK2-loxP (GRK2fl/fl) mice (kindly donated by Dr. Marc Caron, Duke University, USA) and Cre+/−GRK2fl/− offsprings were backcrossed with GRK2fl/fl mice to obtain mice carrying both floxed GRK2 alleles and either none (Cre−/−GRK2fl/fl) or a single CreER allele (Cre+/−GRK2fl/fl) (Figure MM1). Recombination was induced by an intraperitoneal injection of tamoxifen (Tam) (Sigma-Aldrich, 2 mg/mouse, in saline containing 9% ethanol and 51% sunflower oil) for 5 consecutive days, what causes the translocation of Cre recombinase to the nucleus.

Genotyping of these mice required two PCRs to check for floxed alleles of GRK2 and Cre presence. Cre was genotyped by PCR using specific primers (see Cre1, Cre2, Cre pos Control Forward and Cre pos Control Reverse from the Materials section) and floxed alleles of GRK2 were checked using specific primers (see GT-2, GT-4 and GT-5 in the Materials section). Floxed alleles of GRK2 were amplified in a 400 bp DNA fragment, while WT GRK2 resulted in a 300 bp fragment amplification.

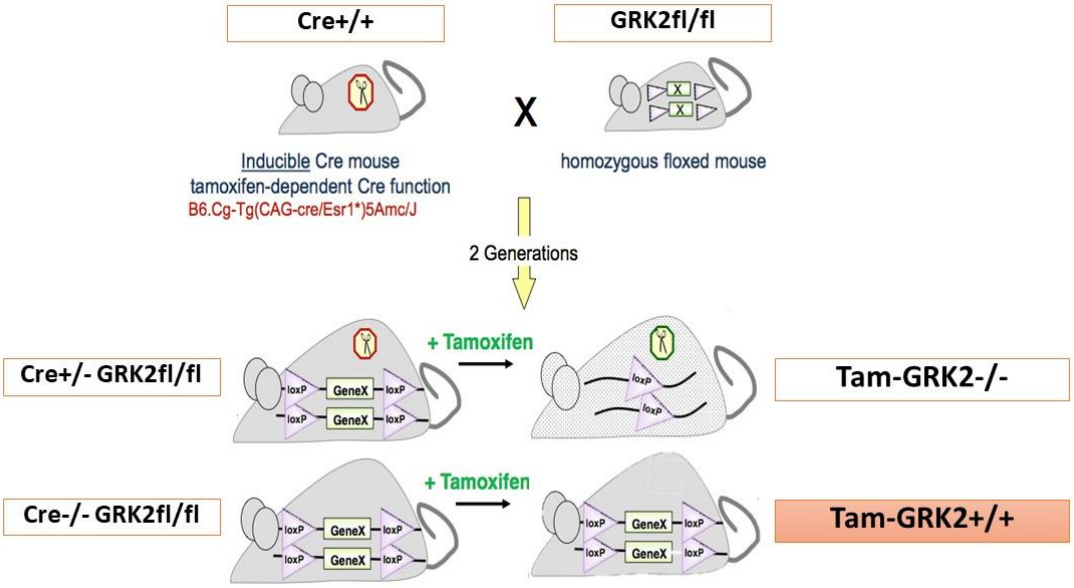

Figure MM1. Schematic summary of the generation of Tam-GRK2-/- mice (Adapted from The Jackson Laboratory).

Insulin resistance-reversion model (8 weeks HFD+Tam+5 weeks HFD)

At 8 weeks of age, mice continued on a standard diet (SD) (2018S Harlan-Teklad, 12% calories from fat) or were fed a HFD (providing 51% of total calories from fat, 26% from carbohydrate and 23% from protein Sniff E 15126-34) during 8 weeks. At this time point, glucose tolerance tests (GTTs) and insulin tolerance tests (ITTs) were performed to confirm insulin resistance had been developed. HFD-fed mice were then injected with tamoxifen (Tam) and maintained on the HFD for 5 more weeks. Body weight and food intake were measured weekly. At the end of the HFD, GTT and ITT were repeated. Liver, BAT and eWAT were removed and a piece of tissue was stored at -80ºC and another was fixed in 4% PFA for further examination.

Animal Experimentation Ethics

The different transgenic mouse models used in this study were housed and bred following all established regulatory standards, and all the experiments were performed in accordance with guidelines of the European Convention for the Protection of Vertebrate Animals used for Experimental

and Other Scientific Purposes (Directive 86/609/EEC) and with the authorization of the Bioethical Committee of the Universidad Autónoma de Madrid and the Local Government (PROEX-048- 15, PROEX-339-14 and PROEX-304-14). The animal research facility of the Centro de Biología Molecular "Severo Ochoa" has the appropriate license to hold and use animals for scientific research (ES280790000180).

Metabolic assays and treatments

For an acute β-adrenergic blockade, mice were injected with propranolol (Sigma-Aldrich, 5mg/Kg body weight) one hour prior to performing the GTT. For a chronic treatment, after the 5 days of tamoxifen injections, propranolol was administered in drinking water 0.1 mg/ml to a final dosage of ≈0.6 mg of propranolol per mice per day, as each mouse drinks an average of 6 ml/day (Bachmanov et al. 2002).
To study acute insulin signaling, 10 minutes before sacrifice mice were intraperitoneally injected with either vehicle (NaCl 0.9%) or insulin (1 IU/Kg body weight). Glucose tolerance test (GTT), insulin tolerance test (ITT) and pyruvate tolerance test (PTT) were performed to evaluate glucose homeostasis and insulin sensitivity. Glucose (2g/kg body weight dissolved in 0.9% NaCl) or sodium pyruvate (1.5 g/kg body weight dissolved in 0.9% NaCl) were administered intraperitoneally after an overnight fasting and glucose concentration was determined in tail blood samples using an automatic analyzer (One Touch Ultra, LifeScan) before and 30, 60 and 120 minutes after the injection. For the ITT, animals were fasted for 4 hours and insulin (0.8 U/kg body weight dissolved in 0.9% NaCl) was administered as an intraperitoneal injectionly. Glycaemia was measured before and 15, 30 and 60 minutes after the injection. The assessment of the metabolic profile in humans and mice is briefly explained in BOX 3.

For the analysis of biochemical parameters, blood was allowed to clot after collection by leaving it undisturbed at room temperature for 30 minutes. The clot was removed by centrifugation at 1,000–2,000 x g for 10 minutes in a refrigerated centrifuge leaving the serum as the resulting supernatant. Serum triglyceride and non-esterified fatty acids (NEFA) were measured using enzymatic methods (Serum Triglyceride Determination Kit, Sigma-Aldrich and NEFA-HR kit, Wako Chemicals, respectively).

BOX 3: Assessing the metabolic profile.

Several metabolic parameters can be analyzed in order to characterize the IR phenotype. Obviously, body weight, body mass index (BMI kg/m^2) as well as waist and hip circumference are non-invasive and the most used methods to diagnose obesity and predict its severity. Moreover, the fasting glycemia or insulinemia are already increased in the prediabetic state and are commonly analyzed in humans, as is the lipoprotein profile. Glucose tolerance test (GTT) can be used to explore the response to a glucose overload. In humans, the oral GTT is commonly used but in mice intraperitoneal GTT is more widely utilized since it more finely establishes glucose tolerance. Also, intraperitoneal insulin tolerance test (ITT) can be performed in mice to study whole body insulin sensitivity. Finally, we can assess the response to insulin in particular tissues analyzing the insulin-induced AKT phosphorylation in tissue lysates after an acute insulin bolus.

Insulin and glucagon concentration were measured by ELISA (Mercodia).

Genotyping

Extraction of genomic DNA from mice tails was carried out using the Wizard® SV Genomic DNA Purification System. A fragment of mouse tail (0.5-1 cm) was cut and preserved at -20ºC until the DNA extraction starts. The first step is digestion of the samples in a mixture of Nuclei Lysis Buffer and EDTA pH 8.0 (90mM) supplemented with RNase A (73 µg/ml) and Proteinase K (1.45 mg/ml). Each tail is digested in 275 µl of the previous buffer mixture in 1.5 ml Eppendorf tubes in a rocking thermoblock at 55ºC overnight. The following day, Lysis Buffer (250 µl) is added at each tube, mixed well and then transferred to one of the provided columns. The columns containing the tissue lysates were centrifuged at 14000 rpm for 3 minutes and the buffer remaining in the collecting tube was then discarded. The same process was repeated four times using Wash Buffer (650 µl) followed by DNA elution in Nuclease-free Water (100-200 µl).

Amplification of DNA was evaluated by PCR in the GeneAmp PCR 9700 system (Applied Biosystems) using the primers described in the "Materials" section. The following PCR protocols were used:

For GRK2+/- and WT animals:

	94ºC	5 min
40 cycles	94ºC	40 sec
	60ºC	40 sec
	72ºC	1 min 30sec
	72ºC	10 min
	4ºC	∞

For the genotyping of Cre:

	94ºC	3 min
40 cycles	94ºC	30 sec
	51,7ºC	1 min
	72ºC	1 min
	72ºC	2 min
	4ºC	∞

For the genotyping of GRK2 floxed mice:

	94ºC	5 min
40 cycles	94ºC	30 seg
	60ºC	30 seg
	72ºC	30 seg
	72ºC	10 min
	4ºC	∞

The products of amplification with the DNA dye as loading buffer 6X (EZ-VISION®) were subjected to electrophoresis on a 2-3.5% agarose gel in TAE and the resulting bands were detected using ultraviolet light.

Western-Blot

Lysis

Approximately 50 mg of frozen tissue was homogenized in 500 □l of hypotonic lysis buffer using metal beads in a Tissue Lyser (Qiagen) with 2 pulses of 2 min each at 30 Hz. To prepare cellular lysates, cells were detached from the culture plate using a plastic scraper and 100-300 µl of ice-cold RIPA lysis buffer with protease/phosphatase inhibitors, transferred to a 1.5 ml tube and incubated in a rocker (250 rpm) for 1 hour. The lysates (from tissue or cells) were centrifuged for 15 minutes at 4°C in a microfuge at 15000 rpm. The cleared lysates were transferred to fresh pre-cooled 1.5 ml eppendorf tubes and stored at -80 °C for further analysis.

Determination of protein concentration

Protein concentration in cellular lysates was determined using the DC Protein Assay Reagents A, B and S (Bio-Rad). 1 µl of cellular lysates were mixed on a 96-well plate with 25 µl of solution obtained by the combination of 20 µl DC Protein Assay Reagents S and 1 ml of Reagent S'. Afterwards, 200 µl of Reagent B was added and the solution was incubated 10 minutes at room temperature. Absorbance at 750 nm was measured on a Biorad iMark microplate Reader. Protein concentration was determined by comparing to the absorbance of a set of standard samples of BSA of known concentrations

Electrophoresis, transfer and detection

The volume of lysates containing 30-50 µg of protein was transferred to new 1.5 ml tubes with the corresponding amount of protein sample buffer. The samples were boiled for 5 min and resolved by SDS-PAGE on a 6-15% Acrylamide/N,N'methylen-bisacrylamide gel. After electrophoresis, proteins were transferred to a 0.45 mm nitrocellulose membrane (BioRad) using a wet blotting apparatus (BioRad). The efficiency of transference and the equivalent loading was always evaluated by staining the membrane with Ponceau staining solution. Ponceau was washed out with TBS-tween 0.1% and the membranes were blocked for 1 hour in 5% BSA-TBS at room temperature. Membranes were incubated with the primary antibodies diluted in 3% BSA-TBS overnight at 4°C (see Materials for antibodies dilutions). The following day, the blots were washed three times for 10 minutes in TBS-Tween 0.1% followed by incubation with the secondary antibodies 1 hour at room temperature (see Materials for antibodies dilutions). After extensive washing with TBS-Tween, immunoreactive bands were visualized using enhanced chemiluminescence (ECL; Amersham Biosciences) or the Odissey Infrared Imaging System (Li-Cor Biosciences) and AGFA films. Films were scanned with a GS-700 Imaging Densitometer and analyzed with Quantity One Software (Bio-Rad). Alternatively, in the case of fluorescent secondary antibodies, the Odyssey Infrared Imaging System (Li-Cor Biosciencies) was used. Bands were quantified by laser densitometry with a Biorad GS-700 scanner or using the software included in the Odyssey Infrared Imaging System.

qPCR analysis

mRNA purification and analysis of concentration, purity and integrity

For mRNA purification, a portion of tissue extracted directly from mice was put into RNA Later Solution (Ambion), that prevents the degradation of mRNA, kept at 4ºC overnight and stored at -80ºC. Approximately 50 mg of frozen tissue was homogenized using metal beads in a Tissue Lyser (Qiagen) and mRNA was extracted using the RNeasy Mini Kit (Qiagen) following the instructions provided by the supplier. Cultured hepatocytes were resuspended directly in TRIzol reagent (Invitrogen) and mRNA was extracted using RNeasy Mini Kit (Qiagen) for further mRNA analysis.

mRNA was quantified in a Nanodrop One spectrophotometer (Thermo Fisher Scientific), the 260/280 and 260/230 ratio values were anaylzed and discarded if they were far from a ratio of 2, which corresponds to pure RNA relative to protein contamination or to co-purified contaminants respectively. RNA Integrity was checked with the Agilent 2100 Bioanalyzer.

Retrotranscription reaction

RT reactions were performed using the iScript cDNA Synthesis kit (Biorad) following manufacturer´s instructions. Briefly, 1000 ng of total RNA from each sample were combined with 5 µl of master mix (includes all necessary reagents among which a mixture of random primers and oligo-dT for priming). The reaction volume was completed up to 20 µl with DNAse/RNAse free distilled water (Gibco). Thermal conditions consisted of the following steps: 5´ x 25 °C; 20´ x 46 °C and 1 ´x 95 °C.

qPCR reaction

qPCR reactions were performed in hard-Shell® 384-Well PCR Plates White Well Clear shell (Bio-Rad) in 10 µl final volume (4 µl of sample + 6 µl of mastermix and primers). Primers used were self-designed or designed by the Genomic Facility (see Materials section) and obtained from Sigma or Invitrogen.

- Samples: - Non template control (NTC): 0 µl sample + 4 µl H2O.
- Control points and efficiency curve points: a control point per triplicate (from a 5 ng pool cDNA samples) was made for all the genes of interest, in order to check the correct annealing of the primers.
- Unknown Samples: 0.1 µl (5 ng cDNA) + 3.9 µl H2O.
- Primers and mastermix: 1 µl of primer mix (5 µM of each primer) + 5 µl Sso Fast EvaGreen Supermix (Biorad) which includes Sso7d-fusion® DNA Polymerase, dNTPs and the rest of reagents needed to perform the PCR. Retrotranscription mixture was set up manually. The rest of the reactions were set up robotically, with an Eppendorf pipetting robot (epMotion 5075).

qPCR measures were performed in a CFX384 Real Time System C1000 Thermal Cycler (BioRad). Thermal conditions consisted of the following steps: 30´´x 95 ºC + (5´´x 95ºC and 5´´x 60 ºC) x 40. We also included

a melting curve from 60 ºC to 95 °C (0.5 ºC/s) at the end of the program to verify the specificity of the PCR. Fluorescence was acquired during both the 60ºC and melting steps.

The assay specificity was confirmed because all of the designs showed a unique melting peak, which indicate that the primers are amplifying the adequate products. In order to discard a potential contamination of reagents and/or primer-dimer artifacts, a NTC reaction was carried out using all the reagents except the sample. Technical triplicates were performed in order to correct pipetting errors in plate loading.

Suitable reference genes for normalization of gene expression data for mRNA can be evaluated by Cq stability and variability testing, using the GenNorm (Vandesompele et al. 2002) and Normfinder (Andersen, Jensen, and Orntoft 2004) algorithms in GenEx v. 5.4.4. The expression of one selected reference gene or the geometric mean of the stably expressed and commonly used reference genes was used as reference index. Valid Prime Kit (Tataa Biocenter) was used as control for genomic background. qPCRs and statistical analysis of the data were performed using GenEx software (MultiD Analyses AB).

Liver triglyceride content determination

A piece of approximately 50 mg of frozen tissue was lysed in 1 ml of isopropyl alcohol using Tissue Lyser (Qiagen) metal beads for 2 pulses of 1 min each at 30 Hz and centrifuged at 2000 g for 10 min at 4ºC. The amount of triglycerides in the supernatant was measured with Serum Triglyceride Determination Kit (Sigma-Aldrich).

Histochemistry

Samples were fixed in 4% PFA overnight and then changed to 50% and then 70% ethanol in PBS for 24 hours each and embedded in paraffin wax (formalin-fixed paraffin-embedded, FFPE). For the OCT frozen blocks, after PFA fixation the tissues were transferred to 20% and 30% sucrose in PBS for 24 hours each and OCT blocks were prepared in dry ice.

Hematoxylin and eosin (H&E) staining

Liver or BAT sections (5 µm) were de-paraffinized by 15-minute incubation at 65ºC followed by submersion 3 times in Histoclear for 3 minutes and re-hydration in three changes in 100% ethanol, followed by 95, 70 and 50% ethanol and distilled water. Then they were stained in Mayer hematoxylin solution for 3 to 5 minutes and gently washed in water. Then they were dipped 15 times in 4% acetic acid, washed and immersed in Bluing reagent for 1 minute and washed. For the eosin counterstaning, slides were rinsed in 95% ethanol and dehydrated through 95% ethanol, two changes of absolute alcohol of 5 minutes each. Finally, slides were cleared twice in histoclear for 5 and 10 minutes respectively and mounted with DPX mounting medium (Sigma).

Masson´s trichrome

Liver sections (5 µm) were de-paraffinized and re-hydrated as described for the H&E protocol. Then, slides were re-fixed in Bouin's solution for 1 hour at 56ºC to improve staining quality and rinsed with running tap water for 5-10 minutes to remove the yellow color. Next, the tissues were stained in Weigert's iron hematoxylin working solution for 10 minutes, rinsed in running warm tap water for 10 minutes and washed in distilled water. Afterwards, slides were stained in Biebrich scarlet-acid fuchsin solution for 10-15 minutes, washed in distilled water and differentiated in phosphomolybdic-phosphotungstic acid solution for 10-15 minutes or until collagen is not red. Sections were transferred directly (without rinse) to aniline blue solution and stained for 5-10 minutes, rinsed briefly in distilled water, differentiated in 1% acetic acid solution for 2-5 minutes and washed in distilled water. Slides were dehydrated very quickly through 95% ethanol, absolute ethanol, cleared in xylene and mounted.

F4/80

For immunohistochemical detection of the F4/80 macrophage marker and quantification of hepatic "crown-like structures" (hCLS) Liver tissue sections were de-paraffinized and rehydrated, and quenching of the endogenous peroxidase was carried out in 3% H_2O_2 in PBS for 15 minutes. Sections were then incubated with blocking solution (5% donkey serum in PBS) for one hour. The anti-F4/80 antibody dilution (1/200) was prepared in blocking solution and the incubation was carried out in a humidity chamber overnight at 4ºC. The following day, sections were washed three times with PBS. Donkey anti-rat secondary antibody conjugated with peroxidase was also diluted 1/4000 in PBS and incubated for one hour. Sections were washed three times with PBS and the peroxidase signal was amplified using the ABC Kit (Vector Laboratories) for 30 minutes. After washing, tissue sections were developed with 3,3'-Diaminobenzidine (DAB) under the microscope. Finally, tissue sections were counterstained with hematoxylin and dehydrated with increasing concentrations of ethanol and Histoclear. Mounting the sections on cover slides was performed with DPX (Sigma).

The absence of the primary antibody was used as negative control. The presence of macrophages (F4/80 stained area) as well as the fat-free tissue area were determined using image analysis software (ImageJ). Three to five different high-power fields from each section were analyzed per animal. The number of hCLS in the whole area of each F4/80-stained section was quantified and expressed as the mean number/mm^2.

GRK2

Immunohistochemistry of paraffin sections of formalin-fixed human liver samples for the detection of GRK2 using the anti-GRK2 PF2 antibody (Nogues et al. 2016) was performed as described (Martinez-Chantar et al. 2006). Human liver tissue sections were de-paraffinized and rehydrated prior to staining

and then samples were unmasked with Tris pH 10 for 20 minutes at 97ºC and were incubated overnight at 4ºC with a 1/750 dilution of the primary antibody. Detection was performed with VECTOR VIP substrate (purple). A negative control in the absence of the primary antibody was used. The presence of GRK2-stained area was determined using Cell Profiler software (http://cellprofiler.org/). Five representative 40x magnification fields from each section were analyzed per animal. Images were taken with a Zeiss Axioimager microscope.

Oil red O (ORO)

ORO in tissue

OCT frozen blocks of liver tissue were cut in 10 µm-thick slices. The frozen slices were allowed to equilibrate at RT for 5 to 10 minutes and stained with Oil red O for 30 minutes in the dark. Oil Red O working solution was prepared mixing 6 parts of Oil Red O stock solution (for tissues) (See Buffers Table) and 4 parts of distilled water and filtered through a pleated filter paper. Slides were mounted on 10% glycerol in PBS-DAPI (5ng/µl) to visualize the nucleus as described (Koopman, Schaart, and Hesselink 2001) and coverslips edges were sealed with nail polish.

All sections were examined using a Fluorescence Resonance Energy Transfer (FRET) equipment coupled to an inverted Axiovert200 (Zeiss) microscope in the Confocal Microscopy Facility in the CBMSO. Oil red O-stained sections were examined in epifluorescence using a DsRed (500–650 nm) and DAPI (359-371 nm) excitation filter.

ORO in cells

To quantify the intracellular lipid accumulation, Huh7 cells seeded in 6-well dishes were washed in PBS, fixed in 4% PFA for 20 minutes, and then permeabilized with 60% isopropyl alcohol before allowing drying at RT. The cells were covered with 1 mL of Oil Red O working solution for 30 minutes. Oil Red O working solution was prepared mixing 6 parts of Oil Red O cell staining stock solution for cells (See Buffers Table) and 4 parts of distilled water, the mixture was let sit at RT for 20 min and then filtered through a 0.2 µm filter. The stain was washed with water several times. Representative microscopic images were obtained on an Olympus IX51 microscope.

To quantify the intracellular lipid content, the stained dishes were dried at RT and lipids were extracted with isopropyl alcohol. Oil Red O staining was quantified by measuring the absorbance of the extract at 520 nm and normalized to protein content (Bio-Rad DC protein assay).

Cell culture

Isolation and culture of primary murine hepatocytes and Kupffer cells

Hepatocytes were isolated from male C57BL6/J mice by perfusion through the inferior cava vein with Hank's balanced salt solution (HBSS) (Gibco), 1 mM HEPES pH 7.4, 0.2 mM EGTA and William's E medium (Sigma-Aldrich) with 0.8 mg/ml collagenase type 1 (Worthington Biochemical Corporation) (Benveniste et al. 1988). After filtering through a cell strainer (100 µm) and centrifugation at 70 g at 4 °C for 5 min, cells were resuspended in the culture attachment medium (see Primary Hepatocytes Culture Media in the Material section), and purified by density gradient centrifugation using an isotonic solution of Percoll (GE Healthcare Bio-Sciences AB). After 2 washes, cells were plated in attachment medium in 6-well dishes for subsequent studies.

For Kupffer cells isolation, the supernatant from the first centrifugation of the hepatocyte isolation protocol was collected and centrifuged twice at 50 g for 5 min to discard the pellet with remaining hepatocytes, as described previously (Pardo et al. 2015). Briefly, the resulting supernatant was centrifuged at 500 g for 5 min at 4 °C and the pellet containing the Kupffer cells was resuspended in the culture attachment medium. Cells were mixed by inversion with 50% Percoll and centrifuged at 1059 g for 30 min without brake at room temperature. Finally, the cell pellet was washed with PBS, centrifuged twice at 500 g for 10 min at 4 °C to wash out the residual Percoll solution and plated on dishes in attachment cultured medium with 10% FBS.

Glucose production in primary hepatocytes

For the glucose production assays, primary hepatocytes were isolated from 8- to 12-week-old male C57BL6/J mice similarly as described but platted using platting medium (see Primary hepatocytes media in Materials). Sixteen hours after isolation, the medium was changed to maintenance medium (see Primary hepatocytes media in Materials). At this point, cells were infected with 10 M.O.I. of adenovirus carrying the sequence of bovine GRK2 (Ad-GRK2) or an adenovirus control (Ad-GFP) or with adenovirus carrying a silencing construct for mouse GRK2 (shGRK2) or human GRK2 as a non-silencing control (shC) for 4-5 hours. The medium was replaced every day and 72 hours post-infection the experiment was performed. Plates were incubated with 200 nM glucagon (Sigma-Aldrich) for 4 h in glucose-free medium (phenol-red/glucose free DMEM, 0.2% BSA) with 2mM sodium pyruvate and 20mM sodium lactate as gluconeogenic substrates. The glucose level in the medium was measured using a glucose assay kit from Eton Biosience by adding 50 µL of assay buffer to 50 µL of medium followed by 15 min incubation at 37ºC to quantify the absorbance at 490 nm.

Huh7 cell culture, infection and treatments

The human hepatocellular carcinoma cell line Huh-7 was kindly provided by Dr. Á.M. Valverde and maintained in Dulbecco's modified Eagle's medium (DMEM) supplemented with 10% FBS, as previously described (Akazawa et al. 2010). For modulating GRK2 levels, cells were infected with 100 M.O.I. of an adenovirus carrying the sequence of bovine GRK2, an sh-GRK2 construct for human GRK2 or a control adenovirus previously described (Nogues et al. 2016). Medium was replaced after 16 hours of infection.

To induce intracellular lipid accumulation in Huh7 cells, palmitic acid (PA) was dissolved to a 160 mM concentration in isopropyl alcohol and added to DMEM containing 1% fatty acid free BSA to obtain a physiological ratio between bound and unbound FA in the media (Richieri and Kleinfeld 1995) and a final concentration of 500 µM PA, similar to the fasting total FFA plasma concentrations observed in humans with NASH (de Almeida et al. 2002).

Huh7 cells were plated in 6-well dishes and infected with the aforementioned adenovirus. 24 hours after infection cells were incubated for 24 h with palmitic acid-BSA complexes, using fatty acid-free BSA as a control. Intracellular lipid accumulation was determined by ORO staining (see above).

Human Samples

Cohort 1: Liver samples come from 27 well-characterized obese NAFLD patients subjected to bariatric surgery in Valdecilla Hospital (Santander, Spain). In this cohort of obese patients 4 presented normal liver histology (NL), 11 simple steatosis (SS) and 12 NASH. Inclusion criteria for NAFLD patients were based on an alcohol intake lower than 20 g/day, the presence of biopsy-proven steatosis with/without necroinflammation and/or fibrosis, and no evidence of hepatitis B and/or C virus (HBV and/or HCV, respectively) infection, inborn errors of metabolism, Wilson´s disease, autoimmune hepatitis or cholestatic liver disease. Healthy human liver samples from non-obese organ-transplant donors, whose liver biopsies showed no lesions, were used as controls (n=5).

Cohort 2: Liver samples come from 41 patients with a clinical diagnosis of NAFLD (31 SS and 11 NASH) who underwent a liver biopsy by a percutaneous route during programmed cholecystectomy in Santa Cristina Hospital (Madrid, Spain). Inclusion criteria for NAFLD patients were based on the absence of alcohol intake (<20 g/day), the presence of biopsy-proven steatosis with/without necroinflammation and/or fibrosis, and no evidence of HBV, HCV, and human immunodeficiency virus (HIV) infections. Patients with other causes of chronic liver disease or those receiving potentially hepatotoxic drugs were excluded. We further studied 34 patients to whom a liver biopsy was taken during programmed laparoscopic cholecystectomy and were diagnosed of histologically NL. All the NL patients had normal fasting glucose, cholesterol and TG, normal serum ALT levels, and negative anti-HBV, anti-HCV, and anti-

HIV tests. In addition, NL patients drank less than 20 g of alcohol per day and none used potentially hepatotoxic drugs.

Both studies were performed in agreement with the Declaration of Helsinki, and with local and national laws. The Institution´s Human Ethics Committee approved the study procedures, and written informed consent was obtained from all patients before inclusion in the study.

H&E and Masson´s trichrome-stained paraffin-embedded liver biopsy sections were examined and interpreted by an expert hepatopathologist. Hepatic histopathological analysis was performed as described above, and according to the scoring system of Kleiner et al. (Kleiner et al. 2005). Biopsies without steatosis and with or without few inflammatory cells or ballooned hepatocytes were considered as normal liver (NL). Simple steatosis (SS) was defined as the presence of at least 5% of steatotic hepatocytes with or without mild lobular or portal inflammation but in the absence of features of hepatocellular injury (ballooning, apoptosis or necrosis) and significant fibrosis. On the other hand, minimal criteria for the histological diagnosis of definite NASH included the combined presence of grade 1 steatosis, hepatocellular injury and lobular inflammation with or without fibrosis (Bedossa et al. 2012).

Data analysis

All data are expressed as mean values ± SEM and for each figure the number of experiments/ animals/ human samples is specified in the figure legend. Normal distribution was determined using a Shapiro-Wilk normality test prior to statistical analysis. Whenever normality test was positive, statistical significance was analyzed by using unpaired Student's t test or one- or two-way repeated measures ANOVA followed by Bonferroni's post hoc test as appropriate for each set of data. When the normality test was not positive, or when significant differences were found between variances (determined by Bartletts' or by F-test of equality of variances), statistical significance was analyzed using Mann-Whitney test, unpaired t test with Welch's correction or Kruskal Wallis followed by Dunn's Multiple Comparison Test as appropriate for each set of data. Differences were considered statistically significant when P values were below 0.05.

The qPCR data analysis was performed by the Genomics and NGS Core Facility at the Centro de Biología Molecular Severo Ochoa (CBMSO, CSIC-UAM) as mentioned in the previous section.

RESULTS

PART 1: Metabolic syndrome and hepatic steatosis: GRK2 in disease

1.1.- Role of GRK2 in the metabolic syndrome: NAFLD

A. Effect of GRK2 downmodulation in short- and long-term HFD

Reduced GRK2 levels prevents the development of NAFLD in mice fed a HFD for 12 weeks

C57BL/6 mice fed a HFD develop obesity, IR and NAFLD (Hebbard and George 2011). In this context, published data from our laboratory have already confirmed that GRK2+/- mice are protected against HFD-induced obesity and IR (Garcia-Guerra et al. 2010). Moreover, this study also shows that GRK2+/- mice display enhanced insulin signaling within the liver, despite the HFD feeding. However, a deeper study of the liver and the development of NAFLD was not performed.

Given the close relationship between hepatic IR and NAFLD we sought to further evaluate the contribution of GRK2 to NAFLD development *in vivo*, comparing the effect of 12 weeks of HFD feeding specifically in the livers of GRK2+/- and WT mice (Figure 1A). In the first place, we confirmed that the body weight increase triggered by the 12 weeks of HFD was lower in GRK2+/- mice than in WT littermates (Figure 1B), as previously reported (Garcia-Guerra et al. 2010). As expected, hepatic steatosis was detected in HFD-fed WT mice as evidenced by increased liver weight (Figure 1C) and by histological analysis using hematoxylin and eosin as well as Oil Red O staining (Figure 1D). Nevertheless, HFD did not induce a significant increase in liver weight in GRK2+/- mice whose livers weighed significantly less than those of WT mice and showed no histological signs of hepatic steatosis after the HFD (Figure 1C,D). Moreover, HFD induced a 2-fold increase in liver TG in WT mice while GRK2+/- mice were protected against HFD-induced liver TG accumulation (Figure 1E).

Western blotting revealed that GRK2 protein levels were increased in the liver of WT mice after 12 weeks of HFD. In contrast, this was not observed in GRK2+/- mice where GRK2 levels remained unaltered after the HFD (Figure 1F) as previously reported (Garcia-Guerra et al. 2010).

These data indicate that the expression of GRK2 is increased under HFD feeding in association with NAFLD in WT mice, and that this increase might play a fundamental role in NAFLD development since mice with reduced levels of GRK2 are protected from short-term (12 weeks) HFD-induced NAFLD.

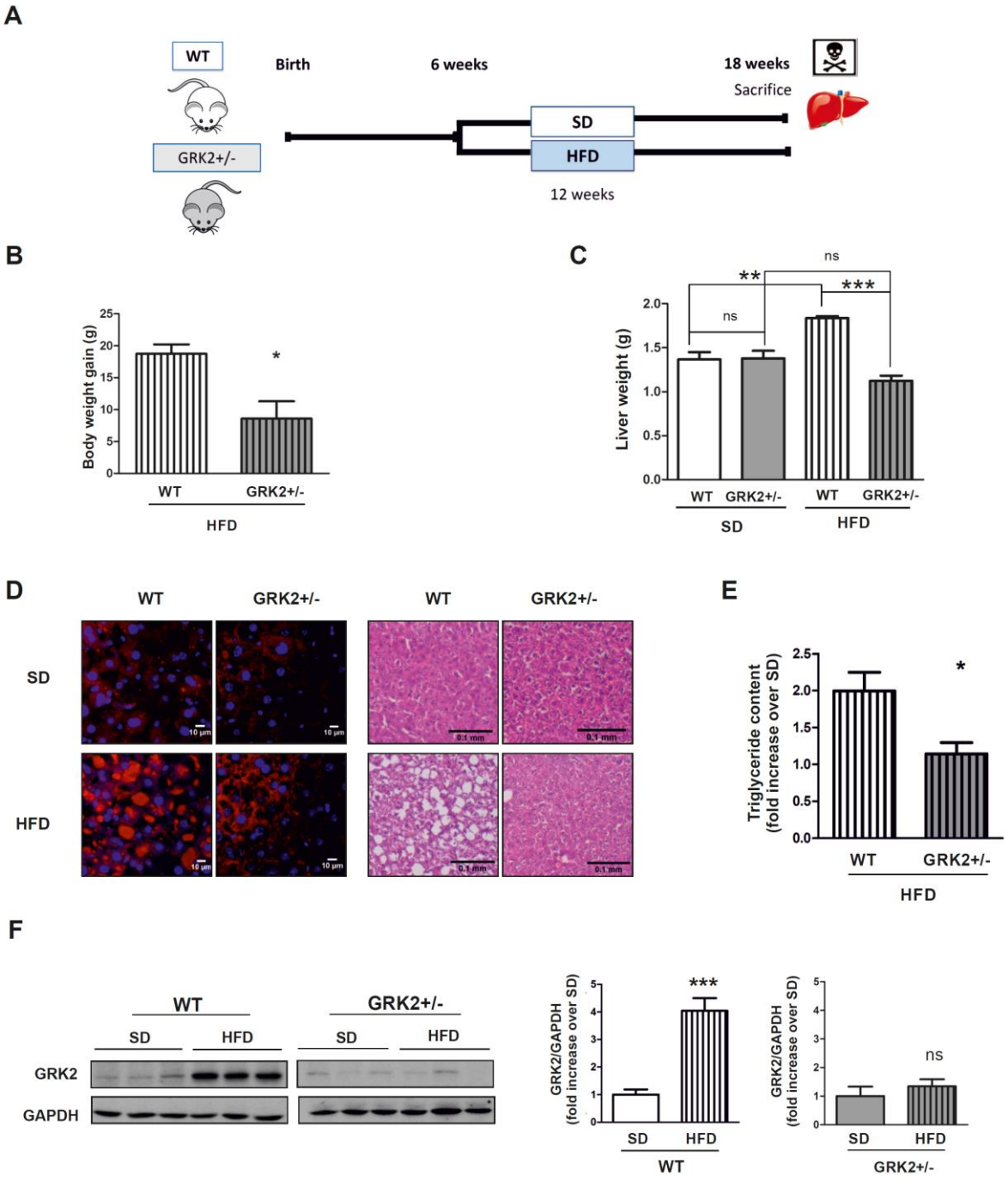

Figure 1. After 12 weeks of HFD, GRK2 hemizygous mice are protected from NAFLD and the associated increase in hepatic GRK2 levels. (A) Outline of the experimental design: 6 weeks old WT and GRK2+/- mice were fed with a (standard diet) SD or a High Fat Diet (HFD) for 12 weeks. **(B)** Body weight gain of HFD-fed animals over SD-fed mice after the high fat feeding. **(C)** Liver weight of WT and GRK2+/- mice after SD or HFD feeding. **(D)** Representative photomicrographs of liver sections from SD and HFD-fed animals stained with Oil Red O and H&E (magnification ×40; scale bar 10 µm and ×10; scale bar 0.1 mm, respectively). **(E)** Extracted hepatic triglycerides (TG) expressed as equivalent triolein concentration (mg/ml) normalized by mg of tissue. The increase in TG content caused by the HFD (expressed as fold over SD-fed mice) mice is shown. **(F)** WB analysis of liver lysates using antibodies against GRK2 and GAPDH. Densitometric analysis results are expressed as fold change over SD-fed mice. Representative immunoblots are shown (Result obtained with the help of Irene Herranz). Data are means ± SEM of 4-6 animals per group. Statistical significance was analyzed by unpaired t-test (B,E,F) or one-way ANOVA followed by Bonferroni´s post-test (C). *P < 0.05; **P < 0.01; ***P<0.005.

GRK2+/- mice protection against HFD-induced NAFLD is not preserved in a long-time high fat feeding period

We next sought up to investigate if the protective effect of GRK2 dowmodulation against HFD-induced metabolic alterations, including NAFLD, was preserved in a chronic exposure to the HFD. Two months after birth WT and GRK2+/- mice were fed either a SD or a HFD for 30 weeks (Figure 2A). An important feature to take into account in this new experimental setting is that in the long-term HFD feeding model mice had reached the adulthood when they started the high fat feeding (9-10 months-old at sacrifice) while in the previous short-term model mice were still young (4–5 months old).

After the long-term HFD feeding, mice from both genotypes gained more than 15 grams of weight, although GRK2+/- mice gained significantly less weight than WT mice during the HFD feeding period (Figure 2B). Regarding systemic IR, previous data from our lab had shown that 9-10 months-old GRK2+/- mice were more sensitive to insulin than their WT littermates not only when fed a standard diet (Garcia-Guerra et al. 2010) but also when fed a HFD (Lucas et al. 2016). These results indicate that GRK2+/- animals are modestly protected against long-term HFD-induced weight gain and are able to maintain insulin sensitivity compared to WT littermates even after a 30 week-long HFD feeding (Lucas et al. 2016). However, it is worth mentioning that we cannot state that GRK2+/- mice are protected against obesity or IR, but rather that they are less affected by the long-term high fat-feeding deleterious effects in whole body metabolic homeostasis compared with WT mice.

Regarding the liver, we found an increase in liver weight of WT and GRK2+/- mice after the HFD, even if this increase was statistically significant only in WT mice, both reaching a similar final liver weight after the 30 weeks of HFD (Figure 2C). Accordingly, the high fat feeding induced equivalent lipid accumulation in the tissue, as observed by histological staining (Figure 2D) and by the quantification of the increase in hepatic TG content (Figure 2E). Interestingly, hepatic protein levels of GRK2 were increased both in WT and GRK2+/- mice after the long-term HFD (Figure 2F).

These results indicate that, after 30 weeks of HFD, hepatic GRK2 levels increase in GRK2+/- mice, in contrast to the short-term HFD experiment, and that, in this scenario, GRK2+/- mice are no longer protected against HFD-induced steatosis. Thus, these data suggest that the degree of protection conferred by the low levels of GRK2 found in the liver of GRK2+/- mice after 12 weeks of HFD, disappears once these levels surpass a certain threshold, what seems to be the situation in the liver of GRK2+/- mice after 30 weeks of HFD.

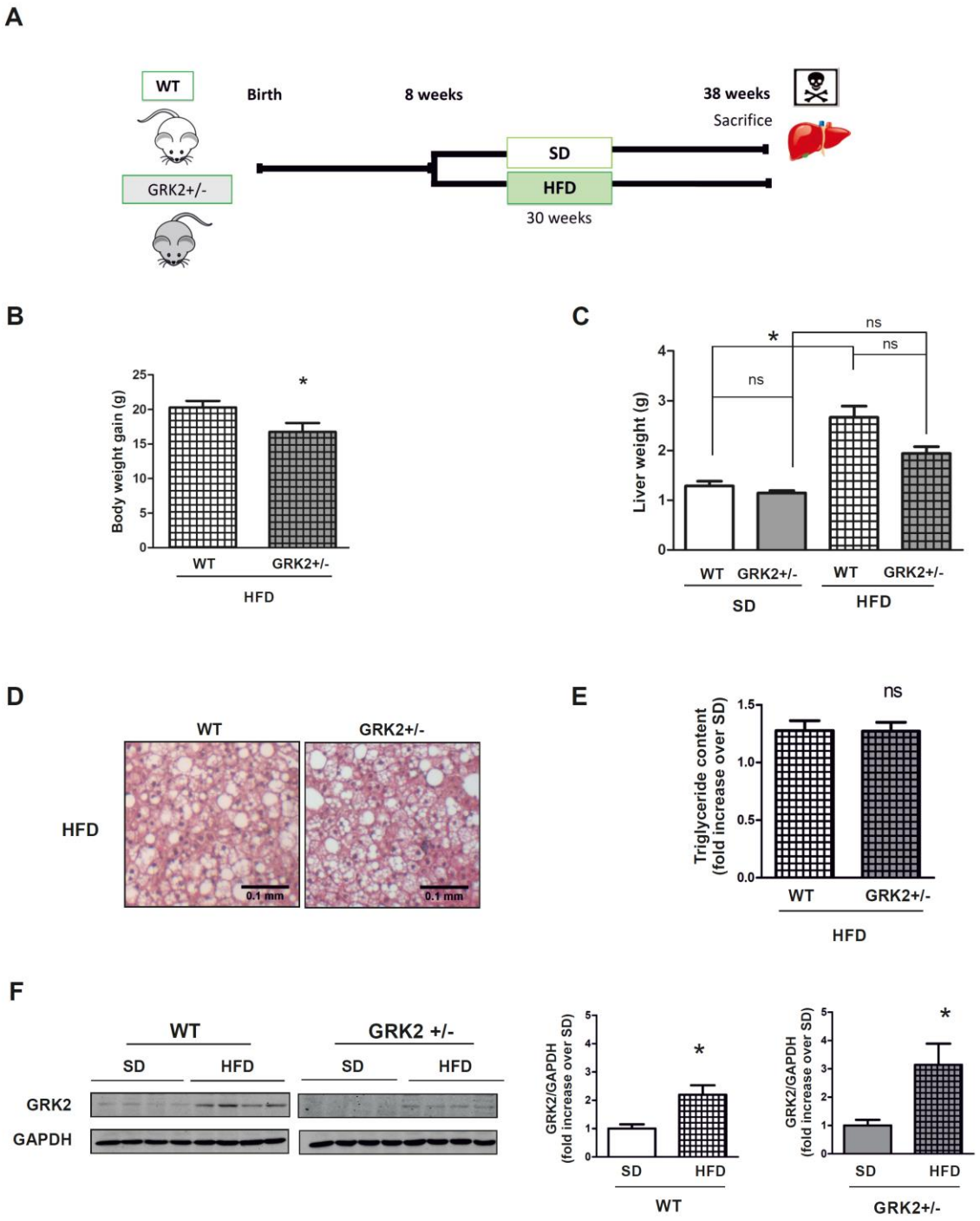

Figure 2. Long-term high fat feeding induces an increase in GRK2 levels and lipid accumulation in the liver both in WT and GRK2+/- mice. (A) Diagram of the experimental protocol: 8 weeks-old WT and GRK2+/- mice were fed either a SD or a HFD for 30 weeks. **(B)** Body weight gain of HFD-fed animals over SD-fed mice after the high fat feeding. **(C)** Liver weight of WT and GRK2+/- mice after SD or HFD feeding. **(D)** Representative photomicrographs of liver sections of animals fed a HFD stained with H&E (magnification 10x; scale bar 0.1mm). **(C)** TG content in the liver expressed as triolein equivalents (mg/ml) and normalized to mg of tissue analyzed. The increase in TG caused by the HFD compared to the corresponding SD-fed controls is shown**. (F)** WB analysis of liver lysates using antibodies against GRK2 and GAPDH. Densitometric analysis results are expressed as fold change over SD-fed mice. Representative immunoblots are shown. (Result obtained with the help of Irene Herranz). Data are means ± SEM of 4-6 animals per group. Statistical significance was analyzed by unpaired t-test or Mann-Whitney (B,E,F), depending on the normality of the distribution of the data, or one-way ANOVA followed by Bonferroni´s post-test (C). *P < 0.05.

B. Effect of tamoxifen-induced GRK2 downmodulation during a HFD

As already mentioned, GRK2+/- mice are protected from the development of IR and obesity (Garcia-Guerra et al. 2010) and also from the development of NAFLD induced by 12 weeks of high fat feeding (see Results 1.1.a). These findings raised the question of whether GRK2 downmodulation or inactivation would be able to not only protect, but also to revert an already established insulin-resistant phenotype, including the manifestation of NAFLD. Given the fact that the role of GRK2 depends not only on its kinase activity but also on scaffolding interactions (Penela et al. 2010), we decided to use a genetic approach to decrease GRK2 levels once the HFD-induced insulin-resistant phenotype had been established.

Characterization of the model: Mice develop an insulin-resistant phenotype after 8 weeks of HFD

Eight weeks-old Cre-/-GRK2fl/fl animals, used as controls, and Cre+/-GRK2fl/fl mice, that will undergo GRK2 deletion upon tamoxifen (Tam) treatment (Tam-GRK2−/− animals), were transferred to a HFD or continued on a SD for 8 weeks (Figure 3A). At this point, we confirmed the establishment of the insulin-resistant phenotype. We evaluated body weight, fasting glucose concentrations and the onset of systemic IR in the animals fed a HFD compared with their SD-fed littermates. We confirmed that upon 8 weeks of HFD, mice showed increased body weight (Figure 3B) and hyperglycemia in fasting conditions (Figure 3C), a well-known sign of prediabetes. Intraperitoneal ITT revealed that HFD-fed animals were insulin-resistant (Figure 3D). These results confirmed that the insulin-resistant phenotype was already achieved after 8 weeks of HFD, and, moreover, that the presence of Cre did not have any effect in the absence of Tam injection, as we could not detect any differences between genotypes (Cre-/- and Cre+/- both with floxed GRK2) in the parameters analyzed. Moreover, we confirmed that 8 weeks of HFD feeding caused hepatic steatosis compared with SD-fed mice (Figure 3E).

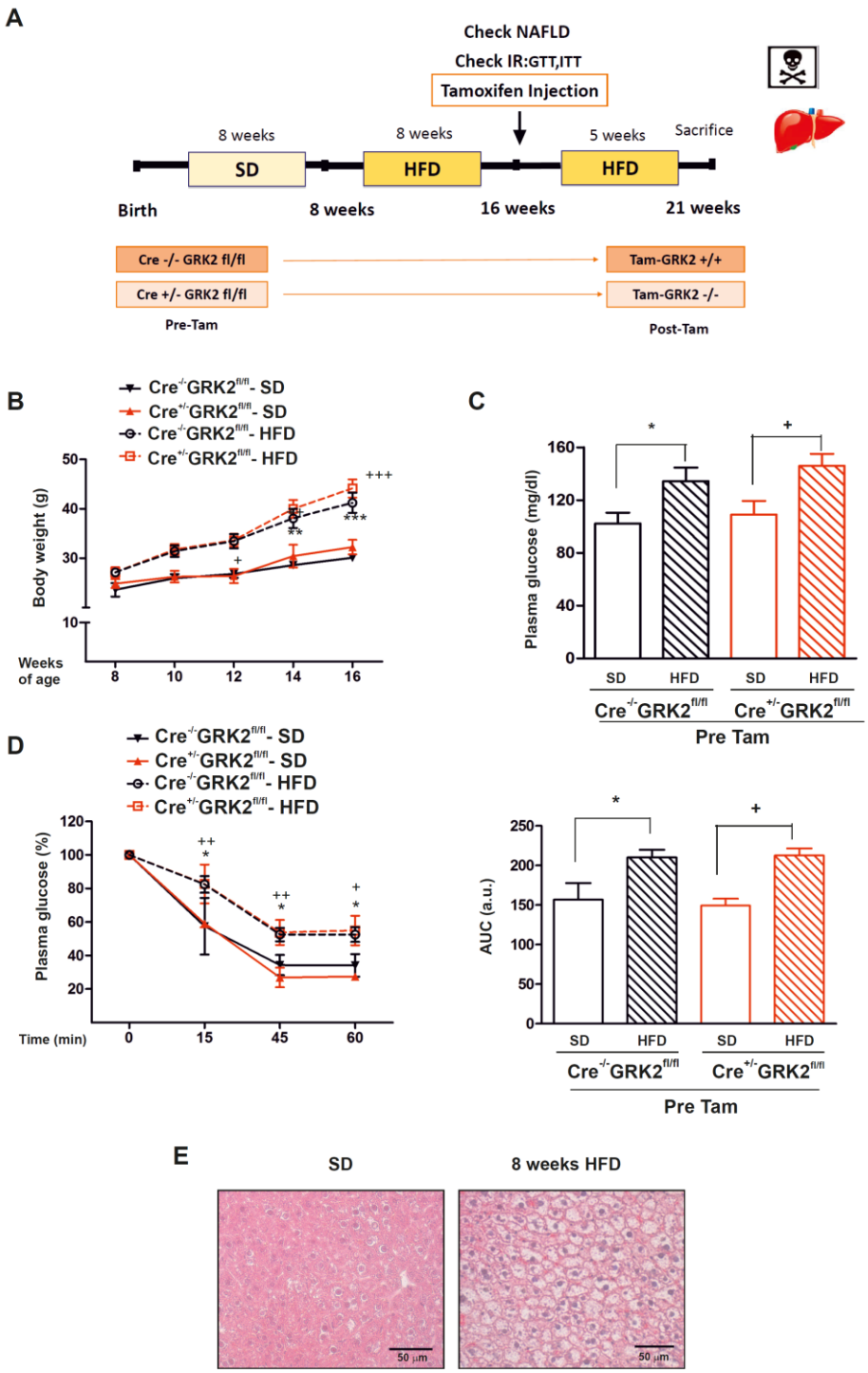

Figure 3. Eight weeks of HFD induce an obese and insulin-resistant phenotype in mice, including the development of NAFLD. (A) Outline of the experimental protocol: 8 weeks after birth, mice were initiated on a HFD and the establishment of IR and obesity was confirmed 8 weeks later; in this moment, a group of mice was to confirm the presence of NAFLD, and the bulk of mice were injected with tamoxifen, and maintained on HFD for 5 more weeks before sacrifice (totalling 13 weeks of HFD and shown in the following figures). Pre-Tam or Post-Tam, previous to or after tamoxifen injection respectively. **(B)** Body weight progression during 8 weeks of SD or HFD before tamoxifen treatment for the indicated mouse genotypes. **(C)** Circulating glucose concentrations after 8 weeks of HFD or SD after an overnight fasting. **(D)** Intraperitoneal ITTs after 8 weeks of SD (solid lines) or HFD (dotted lines), before tamoxifen administration and corresponding area under the curve (AUC). **(E)** Representative photomicrographs of H&E-stained liver sections showing unstained areas of lipid accumulation after 8 weeks of HFD (magnification 20x, scale bar 50 µm). Results are means ± SEM of 6-7 mice per group. Statistical analysis was performed by two-way repeated measures ANOVA (B, D) or one-way ANOVA (C and AUC in D) followed by Bonferroni's post hoc test. *P < 0.05, **P < 0.01, ***P<0.005 compared to HFD-fed Cre-/-GRK2fl/fl mice. +P < 0.05, ++P < 0.01, +++P<0.005 compared to HFD-fed Cre+/-GRK2fl/fl mice.

Tam-induced GRK2 deletion during a HFD prevents further body weight gain and restores glucose tolerance and global insulin sensitivity

Once the establishment of diet-induced IR and obesity was confirmed, mice were injected with Tam and maintained on a HFD for 5 more weeks thus having received a HFD for 13 weeks at the end of the protocol (see Figure 3A). Five days after Tam injection, the Cre-ER that has entered the nucleus can excise the floxed genes (see more details of the model in Methods). In fact, we confirmed this GRK2 downregulation by WB in different tissues including skeletal muscle, BAT, eWAT and liver (Figure 4). From this moment on, control Cre-/- GRK2fl/fl mice will be referred to as Tam-GRK2+/+ mice and Cre+/- GRK2 fl/fl mice as Tam-GRK2-/- mice, since, in these mice, Cre-mediated recombination would take place in every tissue allowing for GRK2 deletion.

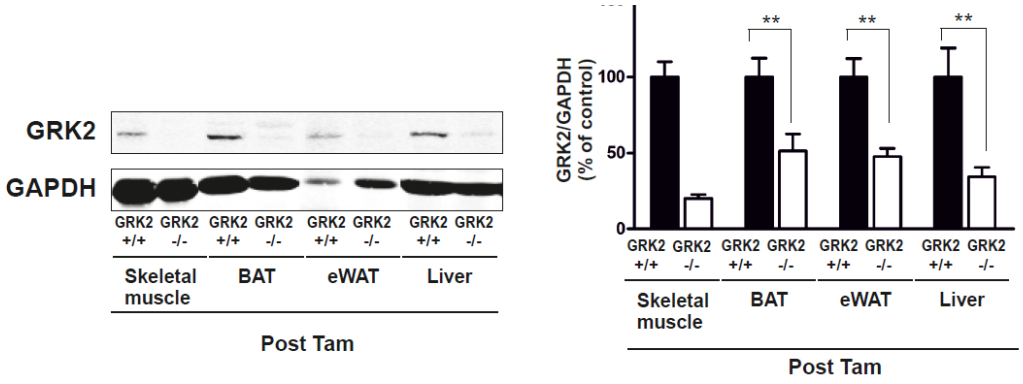

Figure 4. Tamoxifen injection in Cre+/- GRK2fl/fl mice induces GRK2 depletion in different tissues. Lysates of different tissues including skeletal muscle, brown adipose tissue (BAT), epididymal white adipose tissue (eWAT) and liver were analyzed by WB with antibodies against GRK2 and GAPDH. Densitometric analysis results are expressed percent change from control (Cre-/- GRK2fl/fl) mice and representative immunoblots are shown. Results are means ± SEM of 6-7 mice per group. Statistical analysis was performed by unpaired t-test. **P < 0.01.

Regarding body weight evolution, the administration of Tam for 5 days caused a transient decrease in body weight in both groups of mice, as reported (Owen et al. 2013). However, control mice (Tam-GRK2+/+) continued gaining weight after Tam administration throughout the 5 additional weeks of HFD, whereas further body weight gain was prevented in Tam-GRK2-/- mice (Figure 5A) without differences in food intake (Figure 5B).

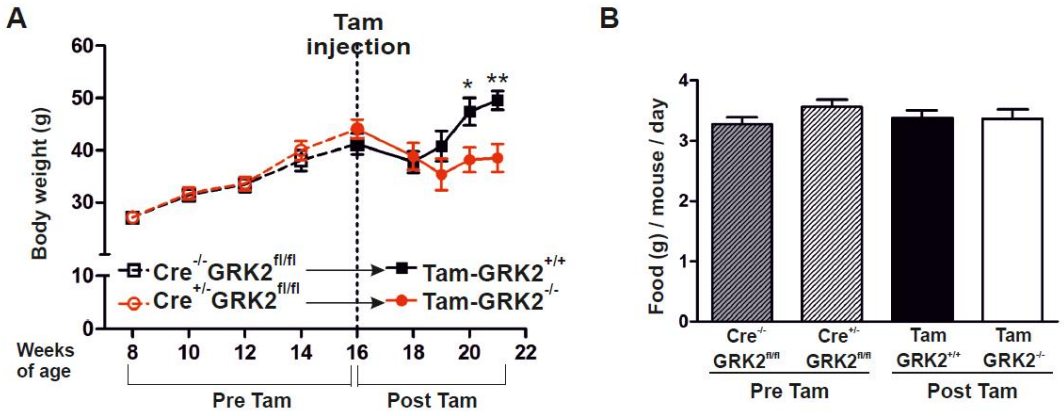

Figure 5. Tamoxifen-induced GRK2 ablation prevents diet-induced obesity without differences in food intake compared to controls. Mice were fed a HFD for 8 weeks, injected with tamoxifen and maintained for 5 more weeks on the HFD. **(A)** Body weight evolution (expressed in g) during the 13 weeks of high fat feeding (dotted lines, Pre-Tam; solid lines, Post-Tam). **(B)** Daily food intake expressed in grams per mouse per day. Results are means ± SEM of 6-7 mice per group. Statistical analysis was performed by two-way repeated measures ANOVA (A) or one-way ANOVA (B) followed by Bonferroni's post hoc test. *P < 0.05, **P < 0.01.

Glucose tolerance and IR were again checked by GTT and ITT respectively, after 5 additional weeks of HFD from Tam injection. Tam-GRK2+/+ mice showed a significant deterioration in glucose tolerance, indicating a progressive intensification of IR during these 5 more weeks of HFD (Figure 6A). In contrast, Tam-GRK2-/- mice showed improved glucose homeostasis compared to their pre-Tam state (Figure 6B) suggesting that the previously observed glucose intolerance was reversed by GRK2 downmodulation. Accordingly, the area under the curve (AUC) was significantly increased by the prolongation of the high fat feeding in control mice (Pre-Tam vs Post-Tam Cre-/- GRK2fl/fl mice) while the AUC was not only not increased but instead reduced in Tam-GRK2-/- mice (Pre-Tam vs Post-Tam Cre+/- GRK2fl/fl mice). Furthermore, at the end of the experiment (Post-Tam) the AUC was significantly reduced in Tam-GRK2-/- mice compared to Cre-/- GRK2fl/fl controls (Figure 6C).

Consistent with the GTT results, insulin sensitivity was diminished in control Tam-GRK2+/+ mice during the course of the high fat feeding period as revealed by de ITT (Figure 6D), whereas Tam-GRK2-/- mice showed significantly enhanced insulin sensitivity after Tam-induced GRK2 deletion compared to their situation prior to Tam injection (Figure 6E). Also, the AUC of the ITT curve was significantly smaller in Tam-GRK2-/- than in Tam-GRK2+/+ mice after the 13 weeks of HFD (Figure 6F). These results also indicate that the improved glucose homeostasis in TamGRK2-/- mice could be attributed to enhanced global insulin sensitivity. In addition, GRK2 deletion induced reduced fasting plasma glucose concentrations in the face of high fat feeding compared with control mice without increasing insulinemia (Figure 6G), indicating that Tam-GRK2-/- mice were protected against the hyperglycemia and hyperinsulinemia characteristic of insulin-resistant and pre-diabetic states.

Taken together, these results demonstrated that GRK2 depletion in HFD-induced insulin-resistant conditions improved whole-body glucose homeostasis, enhanced insulin sensitivity and impaired HFD-induced body weight gain.

The improvement in glucose tolerance after a HFD induced by GRK2 deletion does not rely on increased β-adrenergic signaling

Given that the SNS modulates energy homeostasis mainly through the adrenergic pathway (Nonogaki 2000; Lowell and Spiegelman 2000), we cannot rule out that the canonical role of GRK2 in the desensitization of β-ARs could be responsible for the differences in glucose homeostasis between controls and Tam-GRK2-/- animals . In order to analyze the influence of the adrenergic system on the observed integrated phenotype, we treated control and GRK2-depleted mice with propranolol, a β1- and β2-adrenergic antagonist following two different drug administration protocols (Figure 7A). First, after 13 weeks of HFD, animals were treated with propranolol one hour before performing the GTT, to acutely block β-AR (Figure 7B). Second, animals were chronically treated with propranolol starting right after Tam injections, thus abrogating the adrenergic input from the moment when GRK2 levels were decreased, and a GTT was performed after the 5 additional weeks of HFD (Figure 7C). In both experiments, the GTT curves and the corresponding AUC showed that propranolol-treated Tam-GRK2-/- animals maintained better glucose tolerance compared with propranolol-treated control mice after the 13 weeks of HFD (Figure 7B,C).

These data suggest that propranolol treatment cannot abrogate the improvement in glucose tolerance obtained upon GRK2 depletion, that prevails even under conditions of adrenergic blockade. This demonstrates that GRK2 loss can influence glucose handling independently of its effects on the control of adrenergic stimulation.

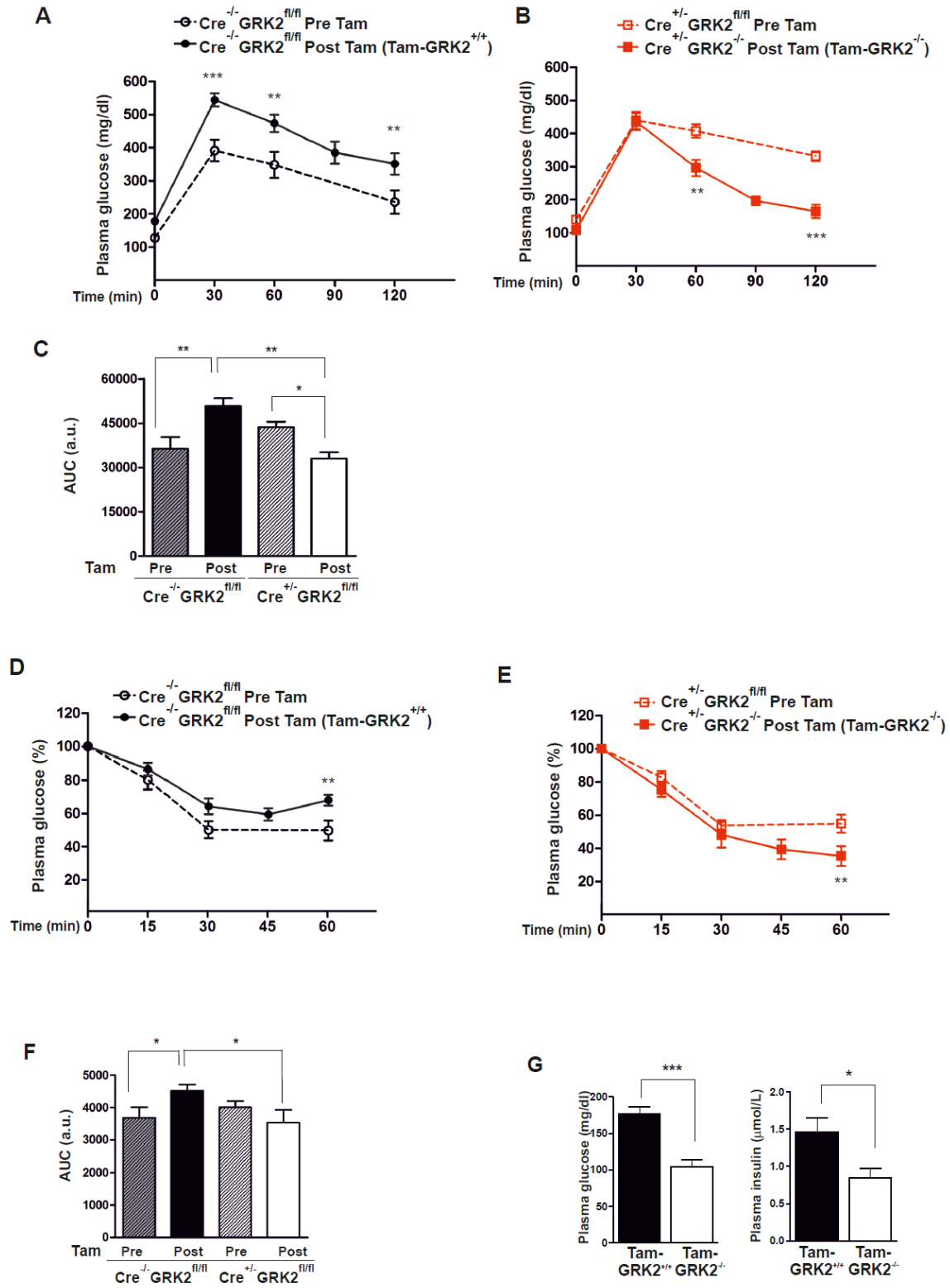

Figure 6. GRK2 downmodulation in the course of a HFD reverses insulin resistance and glucose intolerance. **(A and B)** Intraperitoneal glucose tolerance tests (GTTs) were performed either at 8 weeks of HFD (Pre-Tam, dotted lines) or 5 weeks after tamoxifen injection, following a total of 13 weeks of HFD (Post-Tam, solid lines) in control (Cre-/-GRK2fl/fl) mice (A, black), and Cre+/-GRK2fl/fl mice (B, red). **(C)** GTT area under the curve (AUC) of data in (A) and (B). **(D and E)** Insulin tolerance tests (ITTs) were performed in mice described for the GTTs. **(F)** ITT area under the curve of data in (D) and (E). **(G)** Concentrations of fasting glucose and insulin levels from HFD-fed control (Cre-/-GRK2fl/fl) and Tam-GRK2-/- mice. Results are means ± SEM of 7-8 mice per group. Statistical analysis was performed by two-way repeated measures ANOVA or one-way ANOVA (C,F) followed by Bonferroni's *post hoc* test (A,B,D,E) or by unpaired two-tailed t test (G). *P < 0.05; **P < 0.01; ***P<0.005.

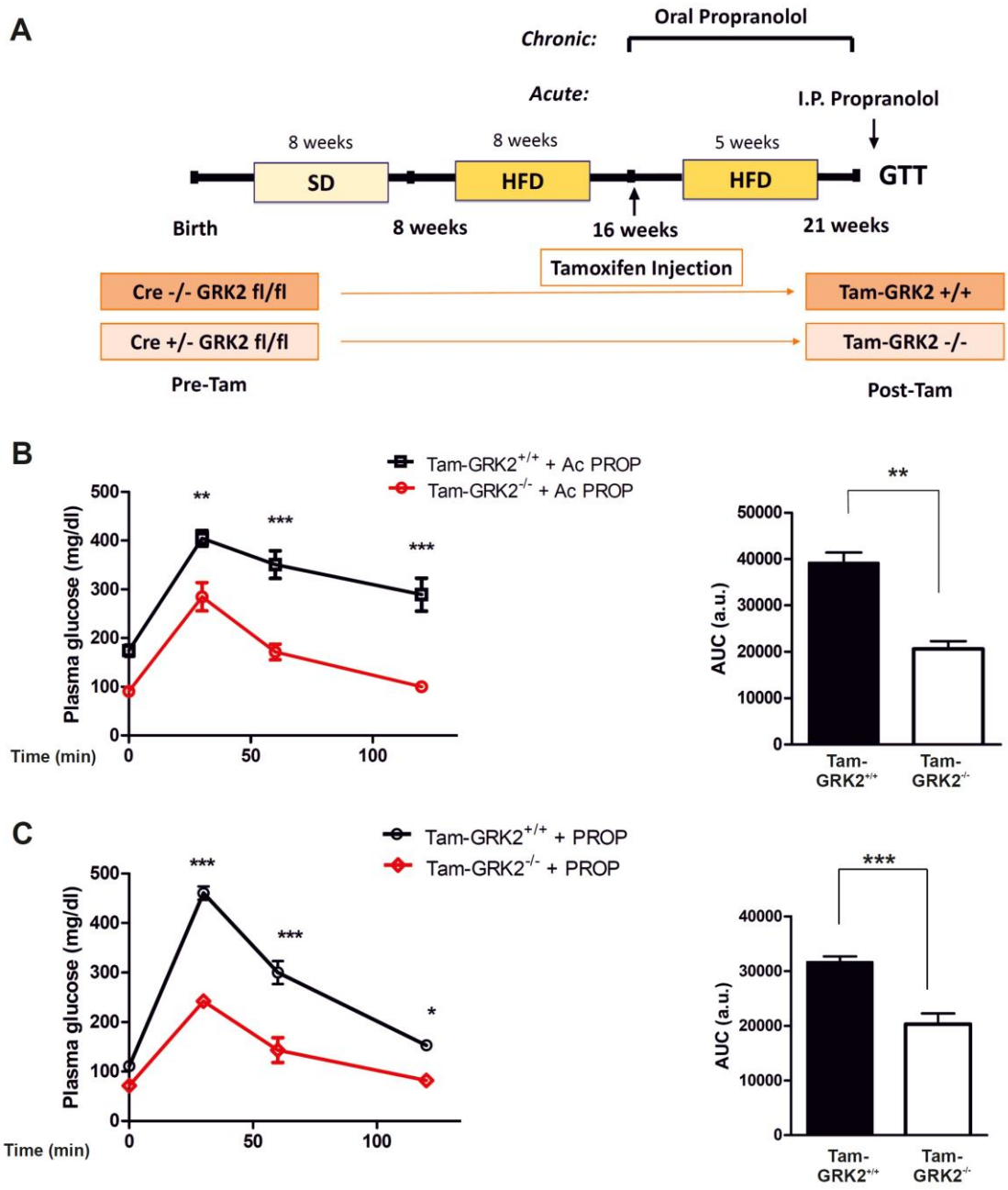

Figure 7. Glucose tolerance in Tam-GRK2-/- mice is preserved under β-adrenergic blockade. (A) Schematic summary of the protocol: propranolol was administered to mice acutely 1 hour before performing the GTTs at the end of the 13 weeks of HFD or chronically in drinking water for the last 5 weeks of HFD. **(B and C)** Intraperitoneal GTTs were performed in mice treated or not with propranolol right before the GTTs **(B)** or chronically from the tamoxifen injection **(C)**. GTT area under the curve (AUC). Results are means ± SEM of 4-6 mice per group. Statistical analysis was performed by two-way repeated measures ANOVA followed by Bonferroni's *post hoc* test. *P < 0.05. **P < 0.01; ***P<0.005.

GRK2 depletion enhances insulin-induced phosphorylation of AKT in the liver

Consistent with the increased glucose tolerance and enhanced insulin sensitivity in Tam-GRK2-/- mice, GRK2 ablation during the HFD also restored insulin-induced phosphorylation of AKT at Ser473 in the skeletal muscle, the major site for insulin-induced glucose disposal (Figure 8A). Moreover, insulin-induced AKT phosphorylation was also enhanced in Tam-GRK2-/- mice in the liver (Figure 8B), a key metabolic regulatory organ in which insulin signals to shut down hepatic glucose production. These data indicate that GRK2 depletion in Tam-treated mice plays a relevant role in the preservation of insulin sensitivity in the analyzed tissues, and this insulin sensitization can explain the improved glucose homeostasis caused by reducing GRK2 abundance during a HFD.

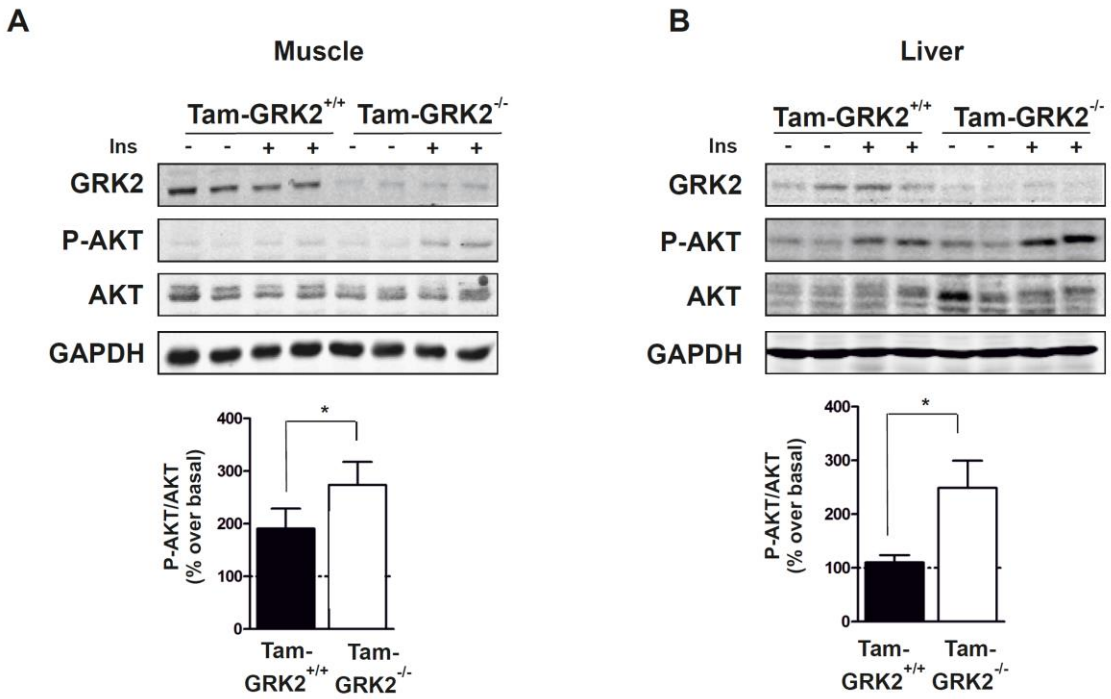

Figure 8. GRK2 loss during a HFD enhances insulin signaling in insulin-sensitive tissues. (A and B) Following the 13 weeks of HFD, control and Tam-GRK2-/- mice were treated with either vehicle or insulin 10 minutes before sacrifice and tissue lysates from muscle **(A)**, and liver **(B)** were subjected to WB analysis with antibodies against GRK2, total and phosphorylated AKT (pSer473), and GAPDH. Densitometric analysis results are expressed as % of stimulation over vehicle-treated mice (basal). Representative immunoblots are shown. Results are means ± SEM of 7-8 mice per genotype, 3-4 mice per treatment. Statistical significance was analyzed by unpaired two-tailed t test. *P < 0.05.

GRK2 deletion during HFD feeding protects against the development of NAFLD

Chronic exposure of mice to HFD induces ectopic lipid accumulation, leading to different pathological responses as IR in some tissues as the liver. In particular, ectopic lipid accumulation in the liver could lead to NAFLD. In our model, we observed that after 13 weeks of HFD the liver weight of Tam-GRK2-/- mice was significantly lower compared to control mice (Figure 9A). This could be indicative of decreased lipid accumulation. Accordingly, histological analysis of H&E-stained tissue revealed a clear hepatic

steatosis in HFD-fed control mice. In contrast, fat accumulation was not detectable in HFD-fed Tam-GRK2-/- mice, that preserved unaltered hepatic tissue structure (Figure 9B).

Besides excessive exogenous lipid supply, the increased hepatic *de novo* lipogenesis characteristic of this disease further increases lipid content and this steatosis can trigger tissue inflammation (see Introduction). Both protein and mRNA levels of the lipogenic transcription factor PPARγ were decreased in the liver of Tam-GRK2-/- mice compared with controls. In line with this observation, we found reduced protein and mRNA expression of the lipogenic enzyme FAS (Figure 9C,D). These results would be coherent with the macroscopic observations, since increased expression of PPARγ and FAS is linked with fatty liver (Kohjima et al. 2007; Inoue et al. 2005). Conversely, reduced mRNA and protein abundance for FAS and PPARγ, suggest a decreased lipogenesis in the liver of Tam-GRK2-/- mice could be taking place (Figure 9C,D).

Since 8 weeks of HFD has been revealed as a period long enough to induce hepatic steatosis (See Figure 4E), we can conclude that lowering GRK2 abundance during a HFD is able to revert hepatic steatosis, possibly, but maybe not exclusively, by cutting off the increase in genes promoting lipogenesis that takes place during the HFD and that is linked with fatty liver.

Decreased expression of pro-inflammatory markers in the liver of Tam-GRK2-/- mice

The inflammatory activation of macrophages and Kupffer cells has been implicated in both obesity-induced IR and fatty liver disease in parallel with the activation of stress- and inflammation-related kinases (Smith and Adams 2011). To analyze the amount of these cells infiltrating hepatic tissue after the HFD, we quantified the area of each section that was positive for the immunostaining against F4/80, a macrophage and Kupffer cell marker (Figure 10A), and normalized it for the fat-free tissue area. We found no differences between controls and Tam-GRK2-/- mice in this parameter (Figure 10B). In parallel, the mRNA expression of *emr1* (encoding for F4/80) was comparable between HFD-fed control and Tam-GRK2-/-mice (Figure 10C). However, in HFD-fed control animals, macrophages frequently aggregated to surround hepatocytes with large intracellular lipid droplets (see arrows in Figure 10A), which are known as hepatic-crown like structures (hCLS). These arrangements have been described to be increased in the liver of NAFLD/NASH patients and are considered an indicator of the presence of pro-inflammatory macrophages (Cinti et al. 2005; Itoh et al. 2013). Notably, HFD-fed Tam-GRK2-/- mice showed a more scattered distribution of their macrophages, with almost absent numbers of hCLS (Figure 10D). In accordance, the mRNA levels encoding for the inflammatory cytokine TNFα (*tnf*) were reduced in these mice as were those encoding for the M1 pro-inflamatory marker iNOS (*nos2*) in the absence of differences in the *mrc1* anti-inflammatory M2 marker (Figure 10E). In addition, the ratio of M2 (anti-inflammatory, *mrc1*-expressing) to M1 macrophages (pro-inflammatory, *nos2* expressing) was significantly increased in Tam-GRK2-/- mice (Figure 10F).

Taken together, these results indicate that, while control mice present M1 infiltrates and proinflammatory cytokines in the liver upon 13 weeks of HFD, GRK2 downmodulation after eighth weeks of HFD avoids the presence of these signs, suggesting that Tam-GRK2-/- mice are protected from hepatic inflammation.

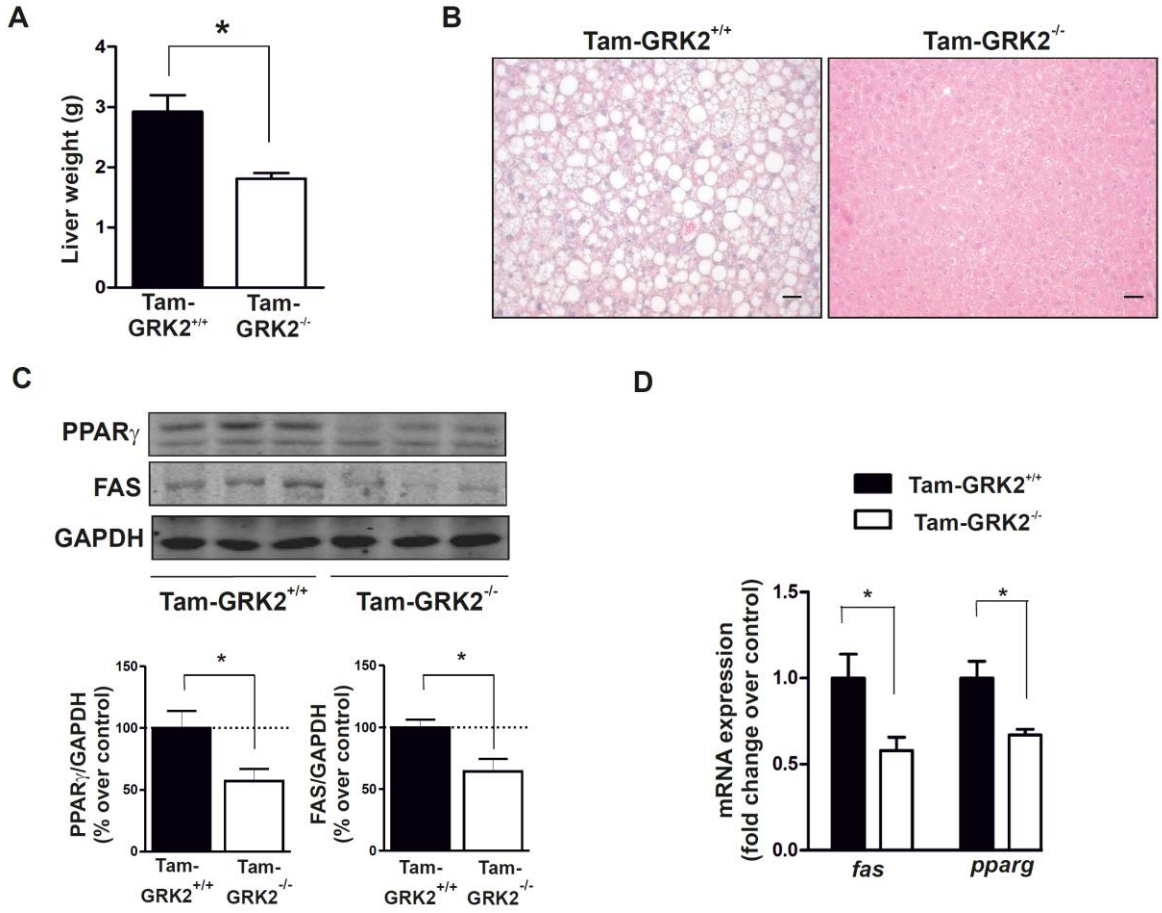

Figure 9. Tamoxifen-induced GRK2 loss protects against the development of fatty liver. (A) Liver weight in control (Cre-/-GRK2fl/fl) and Tam-GRK2-/- mice after 13 weeks of HFD. **(B)** Representative images of H&E-stained liver sections from HFD-fed control and Tam-GRK2-/- mice (magnification 10x; scale bar 50 µm). **(C)** Densitometric analysis of WB of liver lysates from HFD-fed control and Tam-GRK2-/-. Representative immunoblots and are shown for PPARγ, FAS and GAPDH. **(D)** qPCR of mRNAs encoding PPARγ (*pparg*) and FAS (*fasn*). Results were normalized against *ywhaz* and *gapdh* mRNAs. Data in (B,C,D) are means ± SEM of 7-8 mice per genotype. Statistical significance was analyzed by unpaired two-tailed t test. *P <0.05.

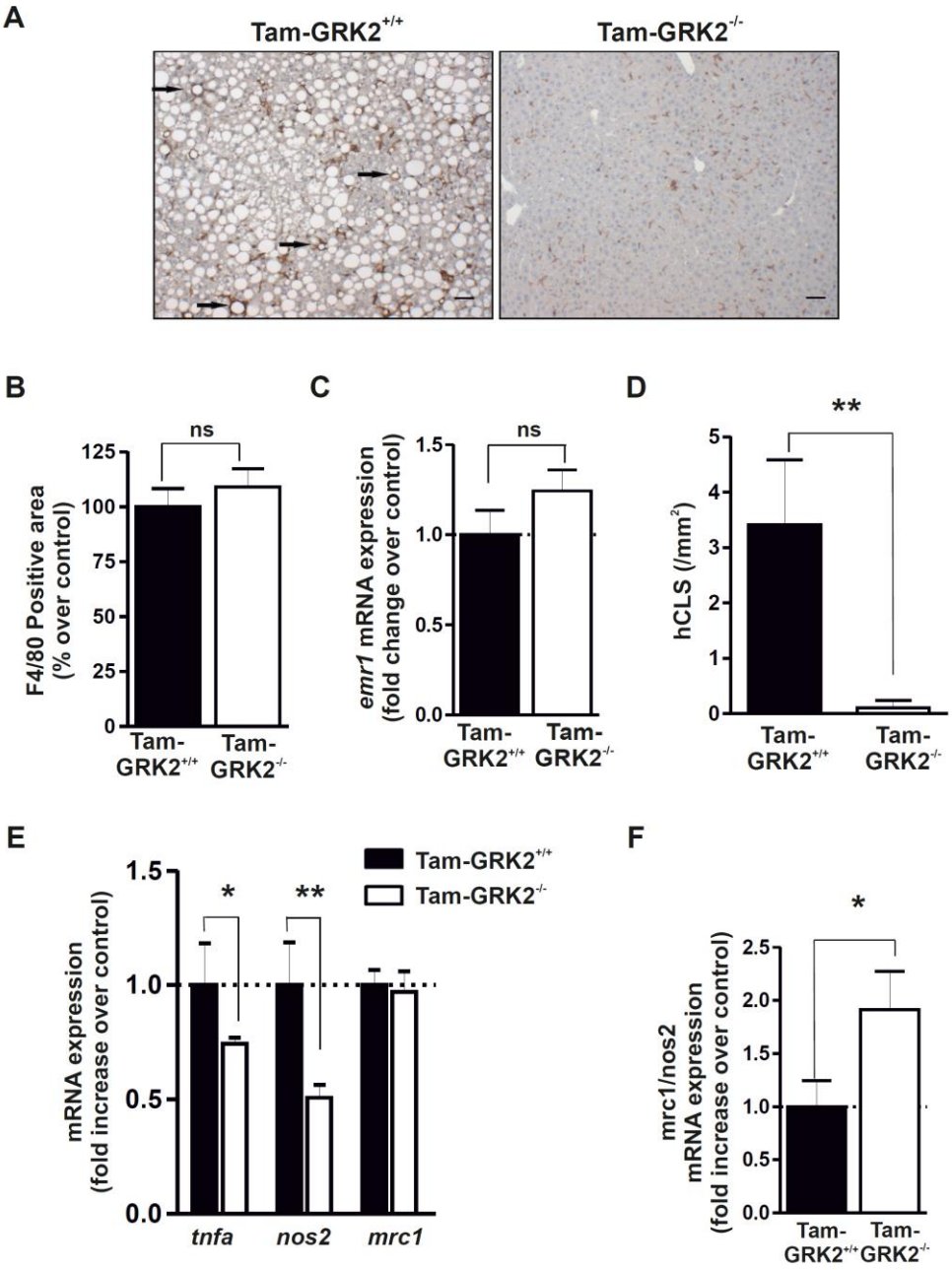

Figure 10. The protection against hepatic lipid accumulation found in Tam-GRK2-/- mice is associated with decreased tissue inflammation. **(A)** Immunohistochemical analysis of liver sections stained with F4/80 antibody and counterstained with hematoxylin. Representative photomicrographs are shown (magnification 10x; scale bar 50 µm) and characteristic macrophage arrangements known as hepatic crown-like structures (hCLS) are indicated by arrows. **(B)** Positively-stained area was quantified using Image J Software in at least four different randomly chosen fields per mouse, in 4-5 mice per genotype. **(C)** qPCR was used to measure the hepatic expression of the F4/80-encoding mRNA (*emr1*) using *ywhaz* and *gapdh* to normalize results. **(D)** Quantification of hCLS within liver sections stained with F4/80 from control and Tam-GRK2-/- mice (> 4 mice per genotype). **(E)** qPCR of *tnf*, *mcr1* and *nos2* mRNAs normalized using *ywhaz* and *gapdh*. **(F)** Normalized mRNA expression levels of mannose receptor C type 1 (*mrc1*), and inducible nitric oxide synthase (*nos2*) was used to calculate the ratio between M2 and M1-polarized macrophage markers (expressed over values of control Tam-GRK2+/+ mice). Values are represented as fold change over control mice and are means ± SEM of 6 mice per genotype. Statistical significance was analyzed by unpaired two-tailed t test or Mann-Whitney test, depending on the normality of the distribution of the data. *P <0.05;**P<0.01.

GRK2 ablation increases FA release from eWAT and BAT function

In accordance with the lower body weight, Tam-GRK2-/- mice had reduced eWAT mass (Figure 11A). Also, greater levels of serum NEFA were detected in Tam-GRK2-/- mice upon fasting (Figure 11B). These results suggest that these mice preserved the fasting-induced lipolytic response in the adipose tissue in the face of a HFD, a reaction that is impaired in control mice and can be a sign of the catecholamine-resistance characteristic of the metabolic syndrome (Reynisdottir et al. 1994).

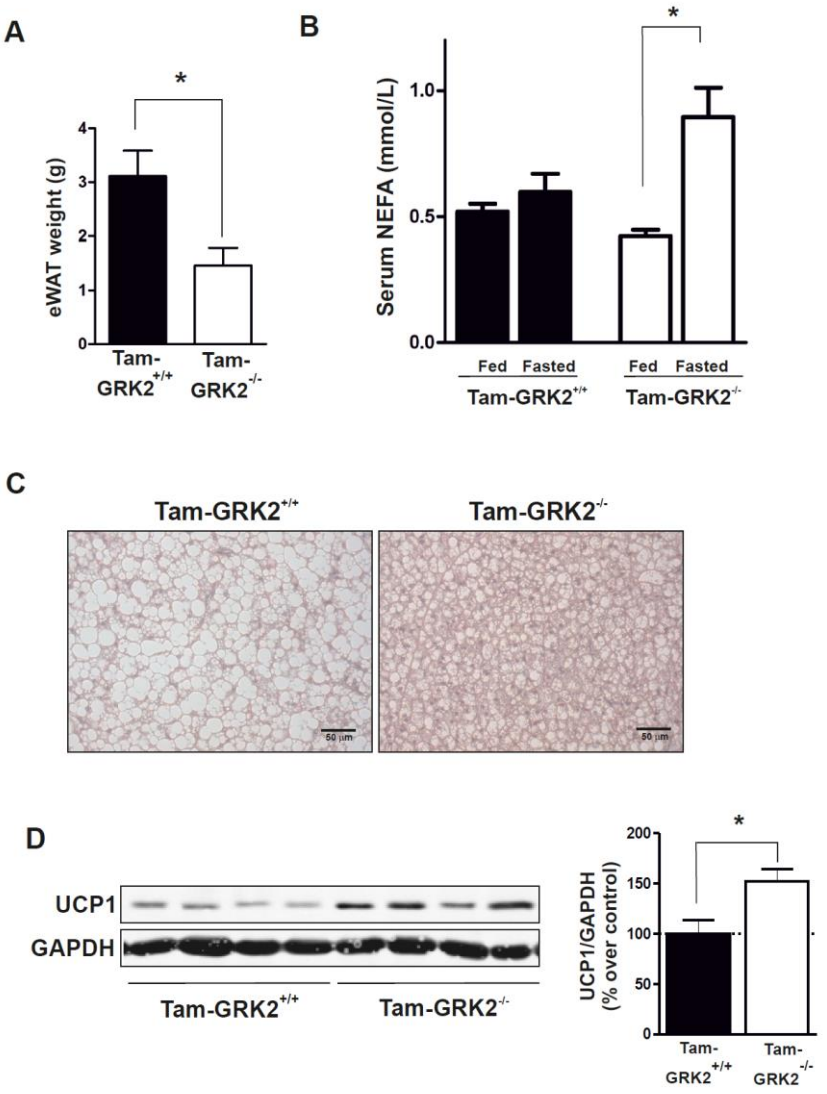

Figure 11. Tamoxifen-induced GRK2 depletion reduces epididymal adipose mass and augments the expression of fatty acid oxidation and thermogenic markers. (A) eWAT weight in control (Tam-GRK2+/+) and Tam-GRK2-/- mice at the end of the 13-weeks HFD. **(B)** Circulating non-esterified fatty acid (NEFA) serum concentrations in HFD-fed controls and Tam-GRK2-/- mice either fed or fasted for 16 hours. **(C)** Representative photomicrographs of BAT sections from control (Tam-GRK2+/+) and Tam-GRK2-/- mice after the HFD stained with H&E (scale bar, 50 µm). **(D)** Densitometric analysis of BAT lysates immunoblotted for UCP1 normalized with GAPDH. Representative immunoblots and are shown. Data are represented as means ± SEM of 7-8 (A,D) or 4-5 (B) mice per genotype. Statistical significance was analyzed by unpaired two-tailed t test (A,D) or Kruskal Wallis followed by Dunn's Multiple Comparison Test (B) .*P < 0.05.

By contributing to whole-body FA oxidation and energy expenditure, BAT regulates fat content (Cypess and Kahn 2010). Increased BAT function could be a possible explanation for the withdrawal of the excess circulating FA in Tam-GRK2-/- mice so that they do not end up accumulating in ectopic tissues as the liver. In fact, BAT of HFD-fed Tam-GRK2-/- mice showed smaller adipocytes, what is indicative of increased BAT function (Figure 11C). Interestingly, Tam-GRK2-/- mice had augmented protein abundance of UCP1 in BAT (Figure 11D), a mitochondrial protein that plays an essential role in the thermogenic capacity of this tissue (Cannon and Nedergaard 2004). These data suggest that an

increased BAT function may exist in Tam-GRK2-/- mice after HFD feeding that might explain the absence of lipotoxicity observed in these animals despite the increase in fasting-induced plasmatic FA levels.

C. Hepatic GRK2 protein levels in a genetic model of obesity

In the aforementioned models the obese and insulin-resistant phenotype was driven by an increase in the intake of calories coming from fat. Thus, we sought to determine if the rise of GRK2 protein levels in these models was caused by the HFD itself or if it was linked with the fatty liver *per se*. In the latter case it would be observed also in a genetic model of obesity. To address this issue, we obtained livers from both *db/db* mice (a genetic model of obesity and T2D) and control *db/+* littermates as well as primary hepatocytes isolated from both *db/+* and *db/db* mice. We observed enhanced GRK2 protein expression in the liver and hepatocytes of *db/db* mice compared to controls (Figure 12), thus suggesting that the increase in GRK2 levels is maintained in obesity- and/or T2D-associated NAFLD independently of the diet.

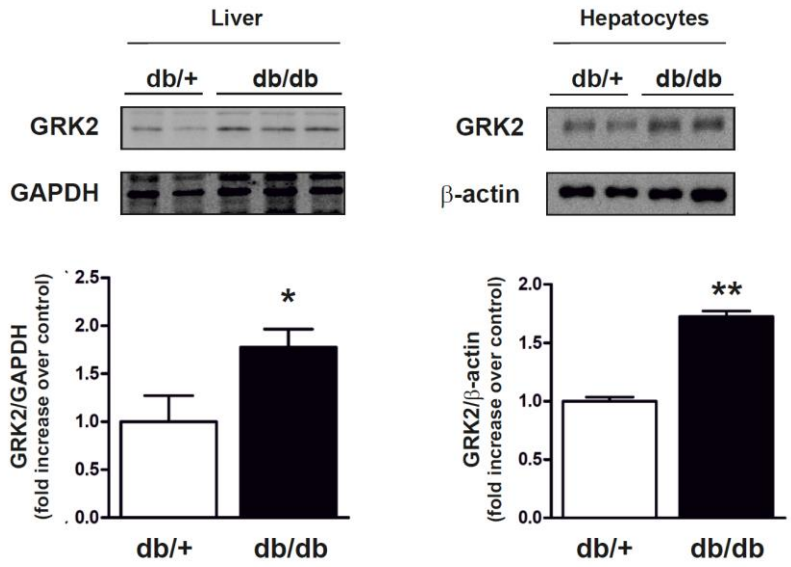

Figure 12. GRK2 protein levels are increased in the liver in a genetic model of obesity and T2D. Whole liver or primary hepatocytes isolated from db/+ (control) and db/db mice were subjected to WB and probed with antibodies against GRK2 and GAPDH or β-actin as loading control. Densitometric analysis and representative immunoblots and are shown. (In collaboration with Dr. Á.M. Valverde lab). Statistical significance was analyzed by unpaired t-test. Data are means ± SEM of 2-3 animals per group. *P < 0.05;**P < 0.01.

1.2- Impact of changes in GRK2 levels in non-obese NASH

So far, we have established that GRK2 heterozygous mice are protected from the development of HFD-induced IR and obesity, and that the genetically-induced downregulation of GRK2 is able to revert these conditions once they were already established (Garcia-Guerra et al. 2010; Vila-Bedmar et al. 2015). Notably, mice with reduced levels of GRK2 are also protected against HFD-induced increase in hepatic lipid content and inflammation, that is, they are protected from NAFLD after 12-13 weeks of HFD. However, whether this outcome is a consequence of the overall phenotype of GRK2+/- and Tam-GRK2-/- mice (which includes decreased body weight gain and adiposity) or, alternatively, GRK2 dosage has an impact in the establishment/development of NAFLD independently of obesity remained to be addressed. To answer this question, we took advantage of the methionine and choline-deficient diet (MCD) mice model, one of the best established preclinical models of NASH that is independent of IR and triggers weight loss rather than weight gain (Reid and Eksteen 2015; Rinella and Green 2004). This fact allows for an analysis of the contribution of GRK2 to NASH independently of its effects on adiposity and IR.

Glucose homeostasis is less affected by the MCD in GRK2+/- mice

WT and GRK2+/- mice were fed either an MCD or a methionine and choline-sufficient equivalent control diet (CD) for 4 weeks (Figure 13A). The weight loss induced by MCD was equivalent in both genotypes, resulting in a similar body weight at the end of the MCD feeding period (Figure 13B). In order to examine some features regarding the metabolic status of these animals, different tests were performed at the end of the feeding period. Remarkably, MCD fed animals displayed decreased glucose levels during the GTT, although GRK2+/- mice were slightly less affected by the MCD (Figure 13C), in the absence of differences in systemic insulin sensitivity, as indicated by the results of the ITT (Figure 13D). We also performed a pyruvate tolerance test (PTT) in which a pyruvate bolus is injected serving as a gluconeogenic substrate. This evokes an increase in blood glucose levels that can be measured as an indicator of the gluconeogenic capacity of the liver. This ability was deteriorated by the MCD feeding, but was slightly preserved in GRK2+/- mice compared to WT (Figure 13E).

These results suggest a slightly better preservation of hepatic glycemic handling in GRK2+/- mice in the face of an MCD challenge in the absence of differences in insulin sensitivity.

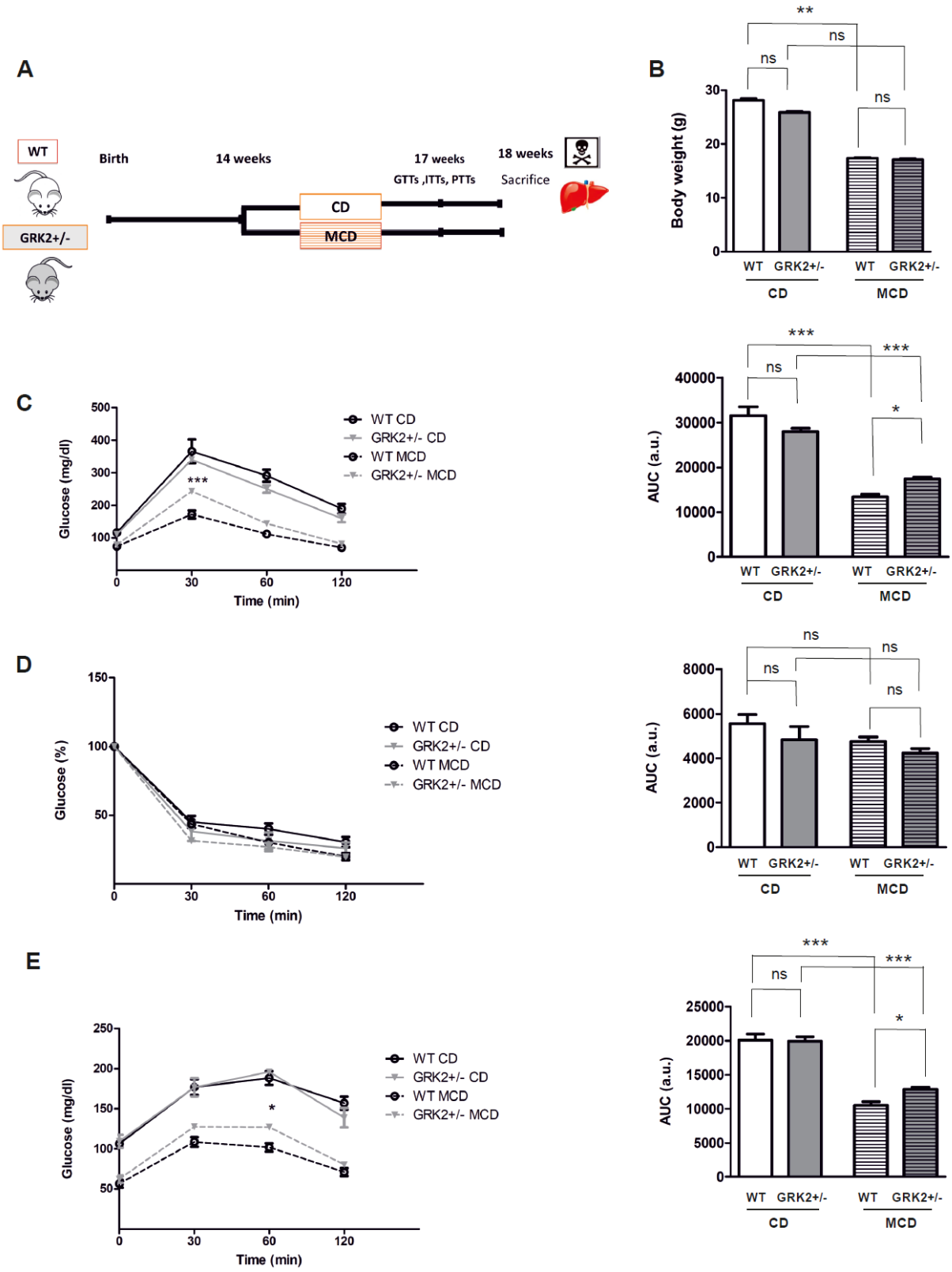

Figure 13. Global effects of MCD feeding in WT and GRK2+/- mice. (A) Outline of the experimental design. 14 weeks after birth, mice of both genotypes (WT and GRK2+/-) were fed either a control diet (CD) or a methionine and choline-deficient diet (MCD) for 4 weeks. **(B)** Mice were weighted at the end of the 4 week-long CD or MCD. **(C)** Intraperitoneal glucose tolerance tests (GTTs) **(D)** insulin tolerance tests (ITTs) and **(E)** pyruvate tolerance tests (PTTs) were performed and areas under the curves (AUC) are represented next to each graph (C, D, E). Data are means ± SEM of 4-7 animals per group. Circles, WT mice; inverted triangle, GRK2+/- mice; solid lines, CD-fed animals; dotted lines, MCD-fed mice. Statistical significance was analyzed by two-way ANOVA or one-way ANOVA (B) followed by Bonferroni´s post-test.*P<0.05; **P < 0.01; ***P < 0.005.

MCD feeding increases GRK2 levels in the liver of WT mice

Notably, we found that GRK2 protein was markedly upregulated in whole liver lysates of WT mice after 4 weeks of MCD to a similar extent to the increase found after a HFD, whereas this rise did not occur in GRK2+/- mice (Figure 14A). This increase occurs specifically in hepatocytes as demonstrated by WB quantification of GRK2 protein levels in lysates from primary cultured hepatocytes or Kupffer cells isolated from WT mice fed either a CD or an MCD (Figure 14B*).* Moreover, this upregulation correlates with a tendency to increased mRNA levels of GRK2 gene (*adrbk1*) in WT MCD hepatocytes compared with CD (Figure 14C).

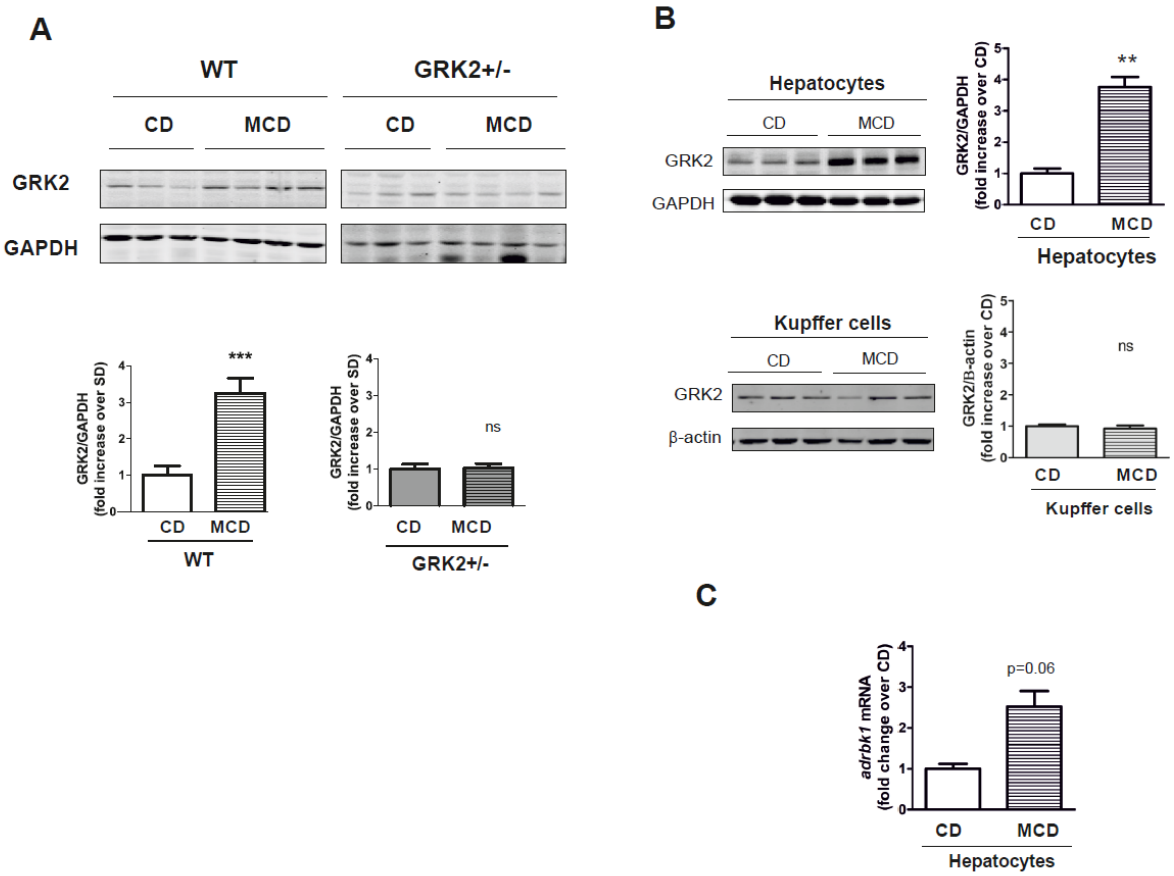

Figure 14. In MCD-induced NASH, GRK2 protein levels are increased in the liver of WT, but not of GRK2+/- mice, and this rise is detected in hepatocytes but not in Kupffer cells. (A) GRK2 protein levels were detected by WB in whole liver lysates from WT and GRK2+/- mice fed a CD or an MCD for 4 weeks. **(B)** Primary hepatocytes or Kupffer cells were isolated from WT mice fed either CD or MCD. Lysates were immunoblotted for GRK2 and normalized by GAPDH or β-actin loading controls. Densitometric analysis and representative immunoblots are shown. **(C)** qPCR analysis of the levels of *adrbk1* (GRK2) normalized with *gapdh* from mRNA extracted from primary hepatocytes from CD and MCD-fed WT mice. Data are means ± SEM of 4-7 (A), 3-4 (B) or 2-3 (C) animals per group. Statistical significance was analyzed by unpaired t-test or Mann-Whitney test, depending on the normal distribution of the data. **P < 0.01; ***P<0.005. (In collaboration with Dr. Á.M. Valverde lab).

GRK2 downmodulation protects mice from non-obese NASH

As expected, feeding mice an MCD caused an increase in the liver-to-body weight ratio (Figure 15A). However, this indicator of steatosis was significantly lower in GRK2+/- mice (Figure 15A). Coherently, decreased lipid deposition was found upon histological examination in the livers from GRK2+/- compared to WT MCD-fed mice (Figure 15B). Concomitantly, the fold- increase in liver TG content caused by the MCD was significantly less pronounced in GRK2 +/- mice (Figure 15C). This partial protection against hepatic steatosis observed in GRK2+/- mice does not seem to be due to decreased circulating levels of TG or NEFA since no significant differences in these parameters were detected between MCD-fed WT and GRK2+/- mice (Figure 15D).

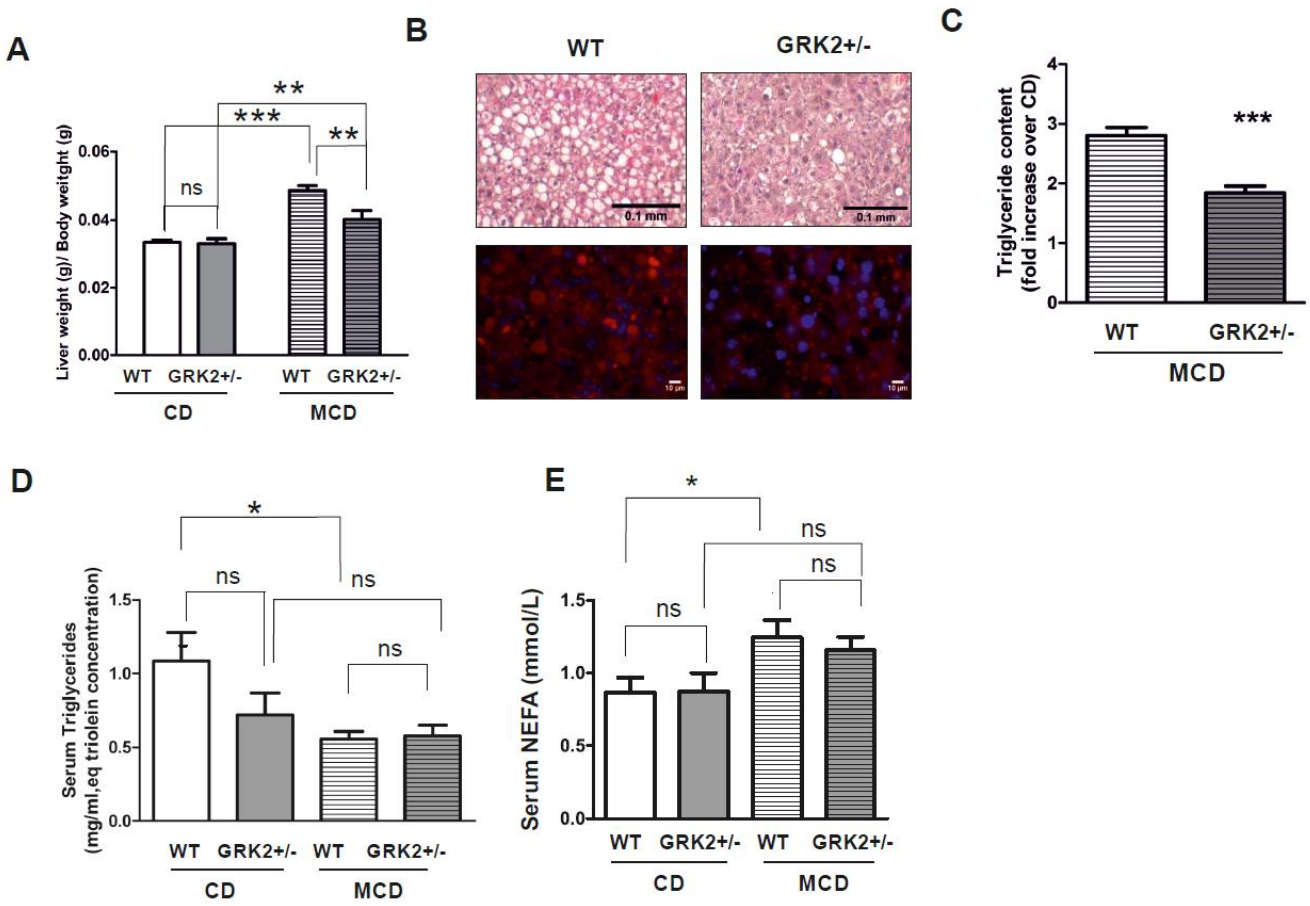

Figure 15. GRK2 downmodulation limits hepatic lipid accumulation in the face of an MCD intervention in the absence of differences in TG or NEFA from serum. (A) Liver-to-body weight ratio of WT and GRK2+/- mice after 4 weeks of CD or MCD. **(B)** Representative photomicrographs of liver sections from MCD-fed WT and GRK2+/- mice stained with H&E (maginification ×10; scale bar 0.1 mm) and Oil Red O (magnification ×40; scale bar 10 μm). **(C)** Hepatic TG expressed as equivalent triolein concentration (mg/ml) per weight of tissue sample (mg). The increase in TG content in the liver caused by the MCD (as fold over CD values) is shown. **(D and E)** TG (D) and NEFA levels (E) in serum samples collected at the end of the experiment after overnight fasting. Data are means ± SEM of 4-7 animals per group. Statistical significance was analyzed by unpaired t-test (C) or one-way ANOVA followed by Bonferroni´s post-test (A,D,E). *P < 0.05; **P < 0.01; ***P<0.005.

In addition to steatosis, inflammation is one major feature of NASH. In this regard, we found significantly higher mRNA levels of the pro-inflammatory cytokine TNFα in WT compared to GRK2+/- animals after the MCD feeding (Figure 16A). We also analyzed the presence of macrophages/Kupffer cells in the liver using F4/80 immunohistochemical staining (Figure 16B). Quantification of the overall immunostained area (normalized by that of fat-free tissue) showed that MCD feeding increased the area with F4/80-positive staining and that GRK2+/- mice had lower macrophage infiltration induced by the MCD with a close to significant difference relative to WT mice (Figure 16C). Moreover, MCD feeding induced the stimulation of inflammatory pathways such as STAT3 or JNK1 in the liver of WT mice, while in GRK2+/- mice this activation was not observed (Figure 16D).

Taken together, these results suggest that GRK2 downmodulation restrains lipid accumulation in the face of an MCD, and limits the activation of different biochemical pathways related to the inflammatory state typical of NASH.

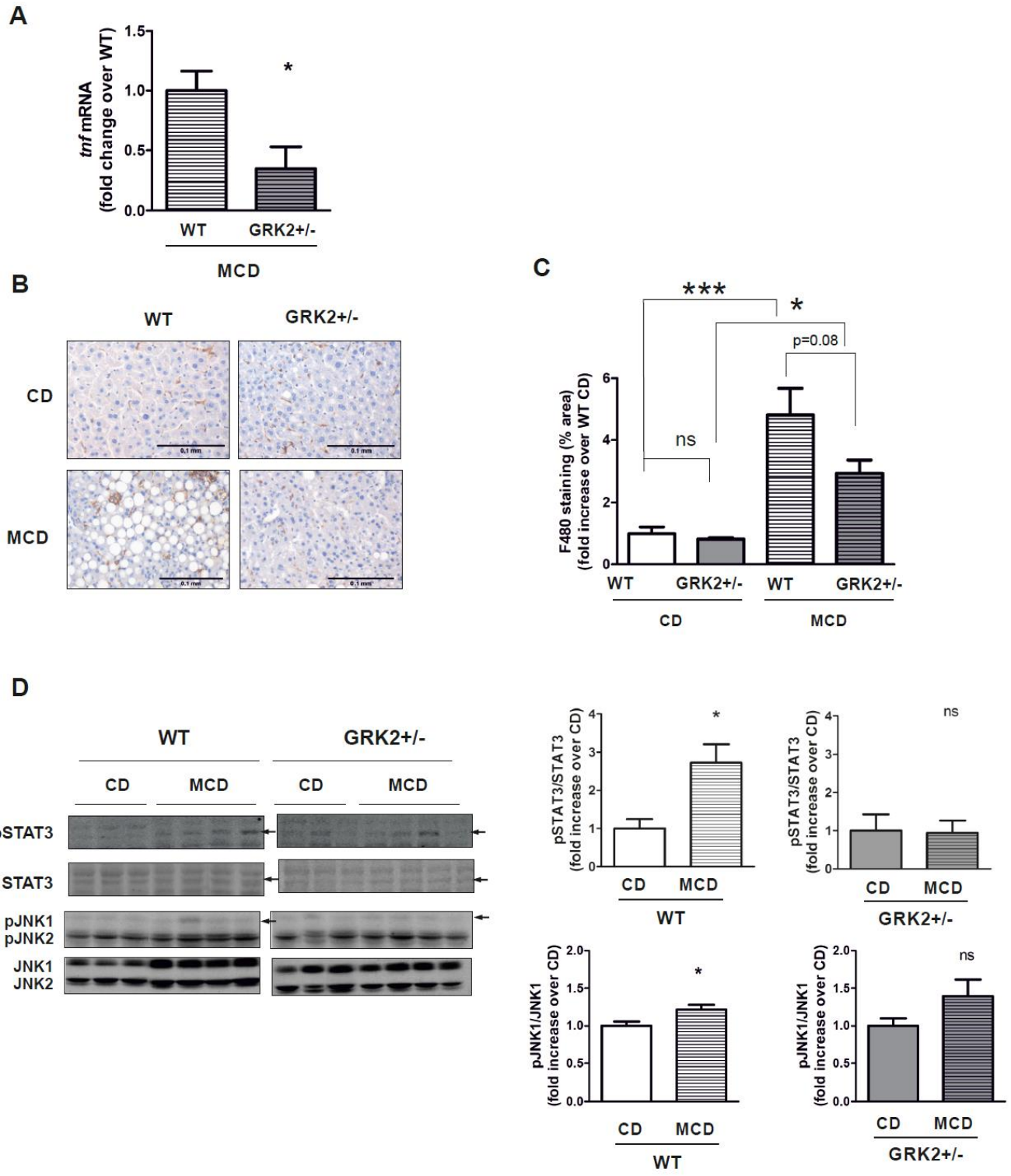

Figure 16. GRK2+/- mice exhibit less hepatic inflammation than WT mice after 4 weeks of MCD feeding. (A) qPCR values of hepatic mRNA expression of *tnf* normalized with *actb* and *ywhaz*. **(B)** Representative immunohistochemistry photomicrographs of liver sections stained for the F4/80 macrophage marker and counterstained with hematoxylin (magnification ×20; scale bar 0.1 mm). **(C)** Positively stained area was quantified using Image J Software and normalized by fat-free tissue area. **(D)** Densitometric analysis of WB of liver lysates from CD- and MCD-fed WT and GRK2+/- using antibodies against the phosphorylated and total form of STAT3 (pTyr705) and JNK1/2 (pThr183/pTyr185). Corresponding bands are marked with arrows in the representative immunoblots shown. Data are means ± SEM of 4-7 animals per group. Statistical significance was analyzed by unpaired t-test (A, D) or one-way ANOVA followed by Bonferroni´s post-test (C). *P < 0.05; ***P<0.005.

GRK2+/- mice are protected from the development of the histopathological signs of NASH

Liver samples from both WT and GRK2+/- mice fed or not an MCD were subjected to a blinded anatomopathological examination in order to assign a NAFLD activity score (NAS) (Kleiner et al. 2005). WT and GRK2+/- mice fed a CD displayed non-pathological liver histology (Table in Figure 17). After the MCD feeding, WT mice developed histological features of NASH with a significantly higher NAS with respect to CD mice including increased steatosis, inflammation and hepatocyte ballooning. Conversely, GRK2+/- mice fed an MCD had significantly lower NAS than their MCD fed-WT littermates, including decreased steatosis and inflammation as well as absence of hepatocyte ballooning, being thus diagnosed with simple steatosis (not NASH) (Figure 17). These results further confirm the previous observations allowing us to corroborate that GRK2+/- mice are protected from MCD-induced NASH.

Diet and genotype		Steatosis	Inflammation	Ballooning	NAS	Diagnosis
CD	WT	0	0	0	**0**	**Normal liver**
	GRK2+/-	0.5±0.3	0.25±0.29	0	**0.75±0.55**	**Not NASH (simple steatosis)**
MCD	WT	$3^{\#\#\#}$	$1^{\#\#\#}$	0.29±0.20	**$4.29\pm0.20^{\#\#\#}$**	**Borderline NASH**
	GRK2+/-	$1.8\pm0.22^{***\#\#}$	0.4±0.27	0	**$2.2\pm0.42^{*\#}$**	**Not NASH (simple steatosis)**

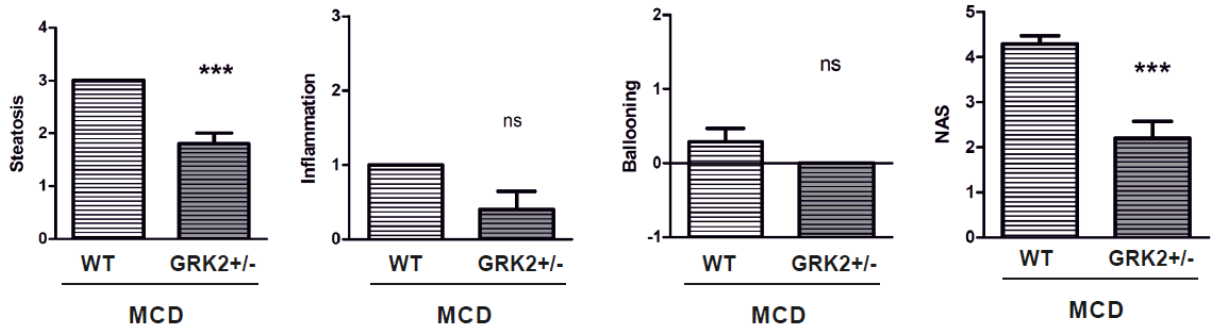

Figure 17. Histopathological analysis shows that GRK2+/- mice are protected against the development of MCD-induced NASH. Table and histograms show the individual scores for steatosis, lobular inflammation and ballooning as well as the integrated NAS value as assessed by two blinded and independent anatomopathological examinations of liver sections from WT and GRK2+/- mice fed either CD or MCD. Statistical significance was analyzed by unpaired t-test or Mann-Whitney test, depending on the normality of the data. Asterisks depict differences between WT and GRK2+/- mice and hashtags between CD and MCD. *P<0.05 WT vs GRK2+/-, #P<0.05 CD vs MCD, n=4-7 per group. (Anatomopathological examination by Dr. Carmelo García-Monzón lab).

Additionally, the deposition of collagen fibers in the hepatic tissue was checked using Masson´s Trichrome staining and the absence of blue staining in the samples made us conclude that mice had not reached the fibrotic stage after 4 weeks of MCD feeding (Figure 18), as previously reported (Itagaki et al. 2013).

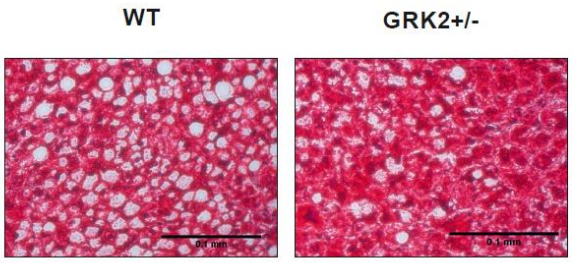

Figure 18. Four weeks of MCD feeding do not trigger hepatic fibrosis. Liver sections from WT and GRK2+/- MCD-fed mice were stained with Masson´s Trichrome staining. Representative images from 4-7 liver samples per group are shown (magnification 20x; scale bar 0.1 mm).

MCD differentially affects cellular processes implicated in the development of NASH in WT and GRK2+/- mice

We next sought to characterize certain pathophysiological mechanisms known to be involved in the development of MCD-induced NASH such as ER stress, FA metabolism, mitochondrial biogenesis and mitochondrial dynamics and autophagy.

Increased phosphorylation of eiF2α in response to the MCD, a well-documented sign of ER stress, was observed in the liver of WT but not of GRK2+/- mice. In addition, the inactivation of both hepatic ERK1/2 and p38 MAPK , described to be related with ER stress (Aghazadeh and Yazdanparast 2010; Kujiraoka et al. 2013; Lee et al. 2011), was detected in MCD-fed WT controls compared with CD fed mice but not in MCD-fed GRK2+/- animals (Figure 19). These results point out that low levels of GRK2 are able to protect mice from MCD-induced ER stress.

Regarding lipid metabolism, we found that the expression of PPARγ, a key transcription factor for the expression of lipogenic genes in the liver, was markedly increased in WT but not in GRK2+/- mice upon MCD feeding (Figure 20A). No differences were detected in mRNA levels of *pparg* between MCD-fed WT and GRK2+/- mice (Figure 20B), suggesting a post-transcriptional mechanism controling PPARγ abundance in these mice. The increase in PPARγ might affect its targets, such as CD36, a transmembrane protein involved in the FA influx. In fact, the levels of CD36 protein were increased after MCD feeding to a much lesser extent in GRK2+/- compared to WT mice, in parallel with PPARγ protein levels (Figure 20A). Accordingly, mRNA expression of CD36 was significantly lower in GRK2+/- mice (Figure 20B). On the other hand, FAS, the enzyme that catalyzes the last step of *de novo* lipogenesis, was decreased both in WT and GRK2+/- mice upon MCD feeding (Figure 20A). This result is in line with the absence of differences after the MCD in the mRNA levels of *srb1f* gene that encodes for SREBP1c, the main transcription factor regulating FAS expression (Figure 20B).

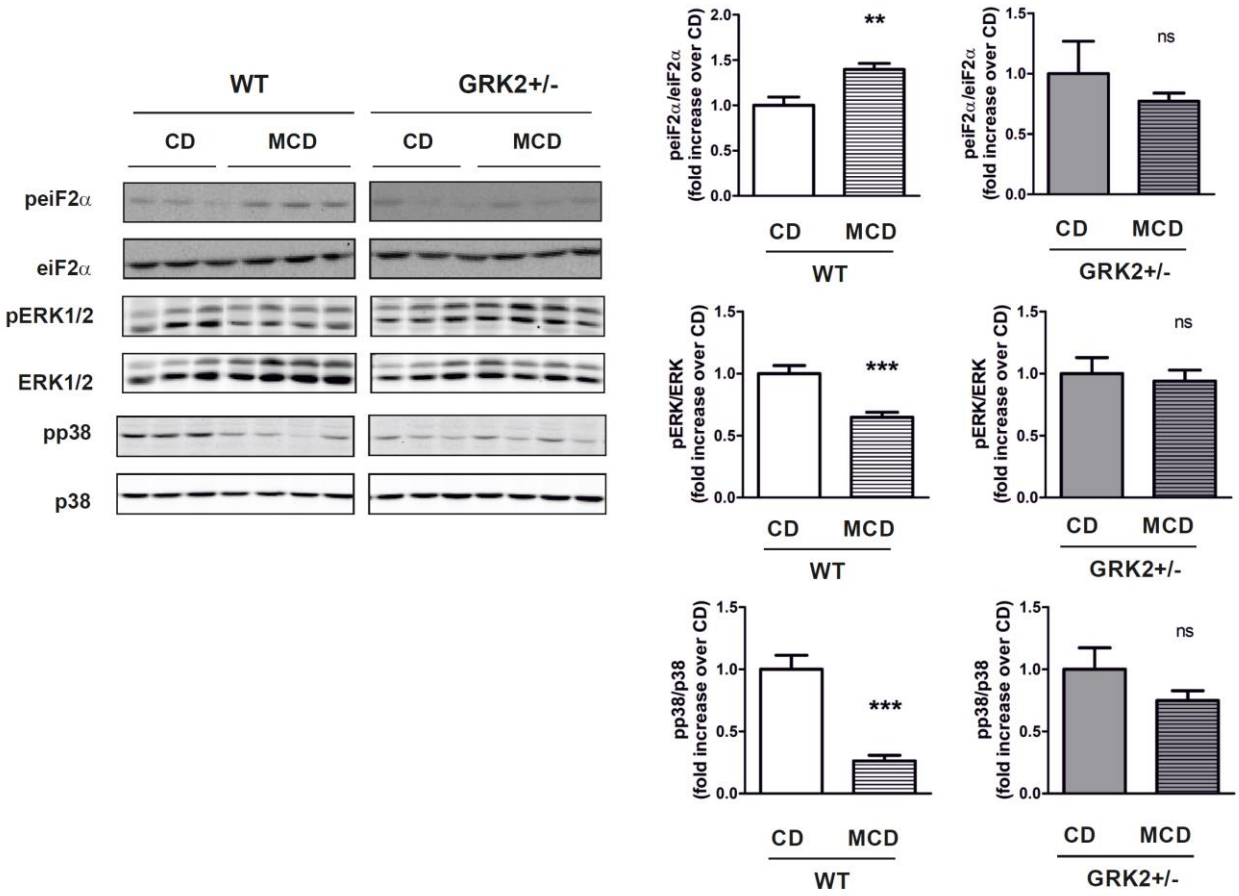

Figure 19. The ER stress response triggered by the MCD challenge in WT mice is not observed in GRK2+/- animals. Densitometric analysis after WB of liver lysates from CD and MCD-fed WT and GRK2+/- mice using phosphorylated and total eiF2α (pSer51), ERK1/2 (pThr202/pTyr204) and p38α MAPK (pThr180/pTyr182). Representative immunoblots are also shown. Data are means ± SEM of 4-7 animals per group. Statistical significance was analyzed by unpaired t-test or Mann-Whitney test, depending on the normal distribution of the data. **P < 0.01; ***P<0.005.

In light of these results, we can conclude that GRK2+/- mice preserve low PPARγ expression upon MCD what could be responsible for the reduced protein and mRNA expression of CD36 relative to WT, limiting the FA transport into the hepatocytes in GRK2+/- mice in the absence of differences in DNL, which is downregulated compared to CD fed mice, consistent with previous reports (Rizki et al. 2006; Rinella et al. 2008).

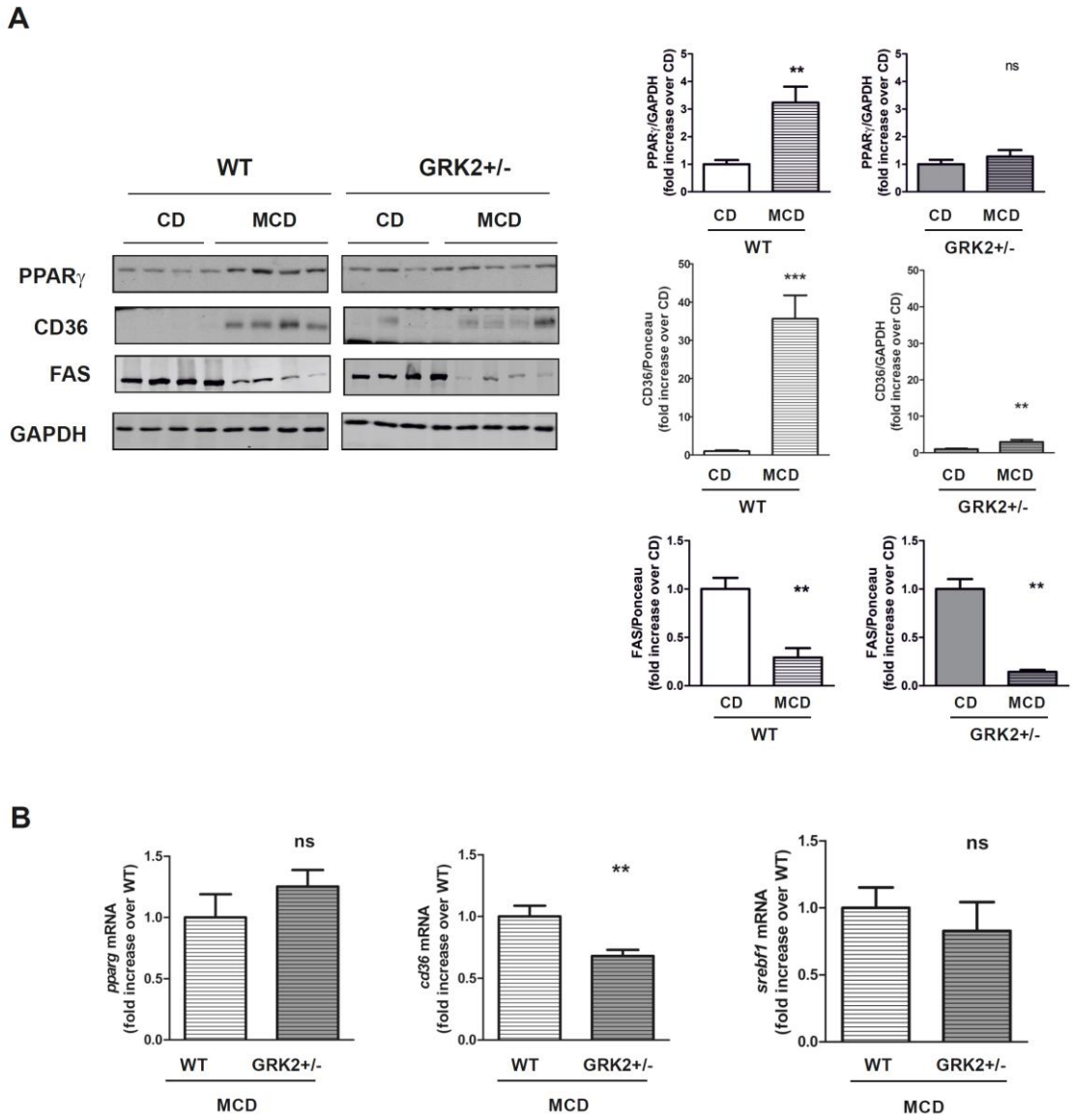

Figure 20. Lipid metabolism markers are differentially altered in MCD-fed WT and GRK2+/- mice. (A) Densitometric analysis of WB from liver lysates using antibodies against PPARγ, CD36, FAS and GAPDH as loading control. Representative immunoblots and densitometric analysis are shown. **(B)** qPCR of hepatic mRNA expression of *pparg, cd36* and *srebf1* normalized with *actb* in MCD-fed WT and GRK2+/- mice. Data are means ± SEM of 4-7 (A) or 7-8 (B) animals per group. Statistical significance was analyzed by unpaired t-test or Mann-Whitney test, depending on the normal distribution of the data. *P < 0.05; **P < 0.01; ***P<0.005.

We also monitored the mRNA levels of *ppagc1a* (PGC-1α), the master regulator of mitochondrial biogenesis, and of its target gene mitochondrial transcription factor A (*tfam)*, key regulator of this process, and they were significantly higher in MCD-fed GRK2+/- compared to WT mice (Figure 21A). Moreover, we analyzed the protein levels of OPA 1 and mitofusin 2, two markers of mitochondrial fusion, a process related with mitochondrial biogenesis and with a critical role in alleviating hepatic FA accumulation (Galloway et al. 2014). Interestingly, the expression of these proteins was significantly reduced after MCD in WT but did not change in GRK2+/- mice (Figure 21B). However, the levels of

Hadha, a subunit of the β-oxidation enzyme mitochondrial trifunctional protein (MTP), were not changed by the MCD neither in WT nor in GRK2+/- mice (Figure 21B). Hence, GRK2+/- livers show higher levels of markers related to mitochondrial biogenesis and mitochondrial fusion in the absence of changes in β-oxidation enzymes.

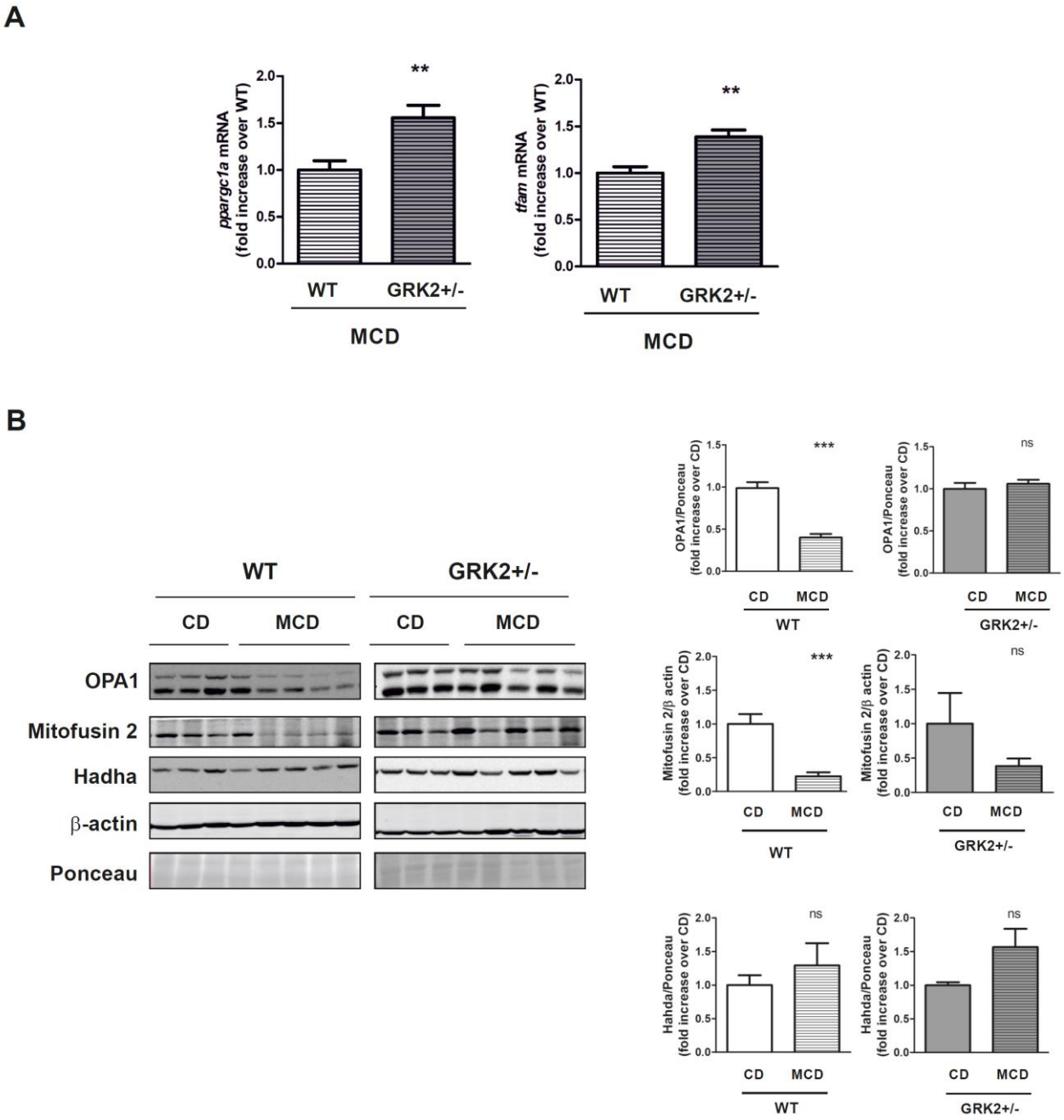

Figure 21. Mitochondrial biogenesis and fusion markers are decreased in MCD-fed WT, but not in GRK2+/- mice. (A) qPCR of hepatic mRNA expression of *ppagc1a* and *tfam* normalized with *actb*. **(B)** Protein levels of OPA1, mitofusin 2, Hadha and β-actin in liver lysates from CD and MCD-fed WT and GRK2+/- mice were analyzed by WB. Densitometric values are shown together with representative immunoblots. Data are means ± SEM of 7-8 (A) or 4-7 (B) animals per group. Statistical significance was analyzed by unpaired t-test or Mann-Whitney test, depending on the normal distribution of the data. *P < 0.05; **P < 0.01; ***P<0.005.

Finally, the impairment of the autophagic flux is another key event in the development of NASH (Gonzalez-Rodriguez et al. 2014) and leads to the accumulation of the p62/SQSTM1 protein, an autophagy substrate that is used as a reporter of autophagy activity. We observed the accumulation of p62 in the liver of MCD-fed WT mice but not in GRK2+/- animals suggesting preserved autophagy in the face of MCD, as also demonstrated by the effective conversion of LC3 I to LC3 II (Figure 22A). In agreement with these results, the stimulation status of two well-established regulatory pathways of autophagy was also differentially altered after the MCD in GRK2+/- livers: AMPK phosphorylation was slightly enhanced and that of S6, a readout of the mTORC1 autophagy-inhibitory pathway, was reduced in the liver of GRK2+/- compared to WT mice (Figure 22B), consistent with a better preservation of autophagy in these mice.

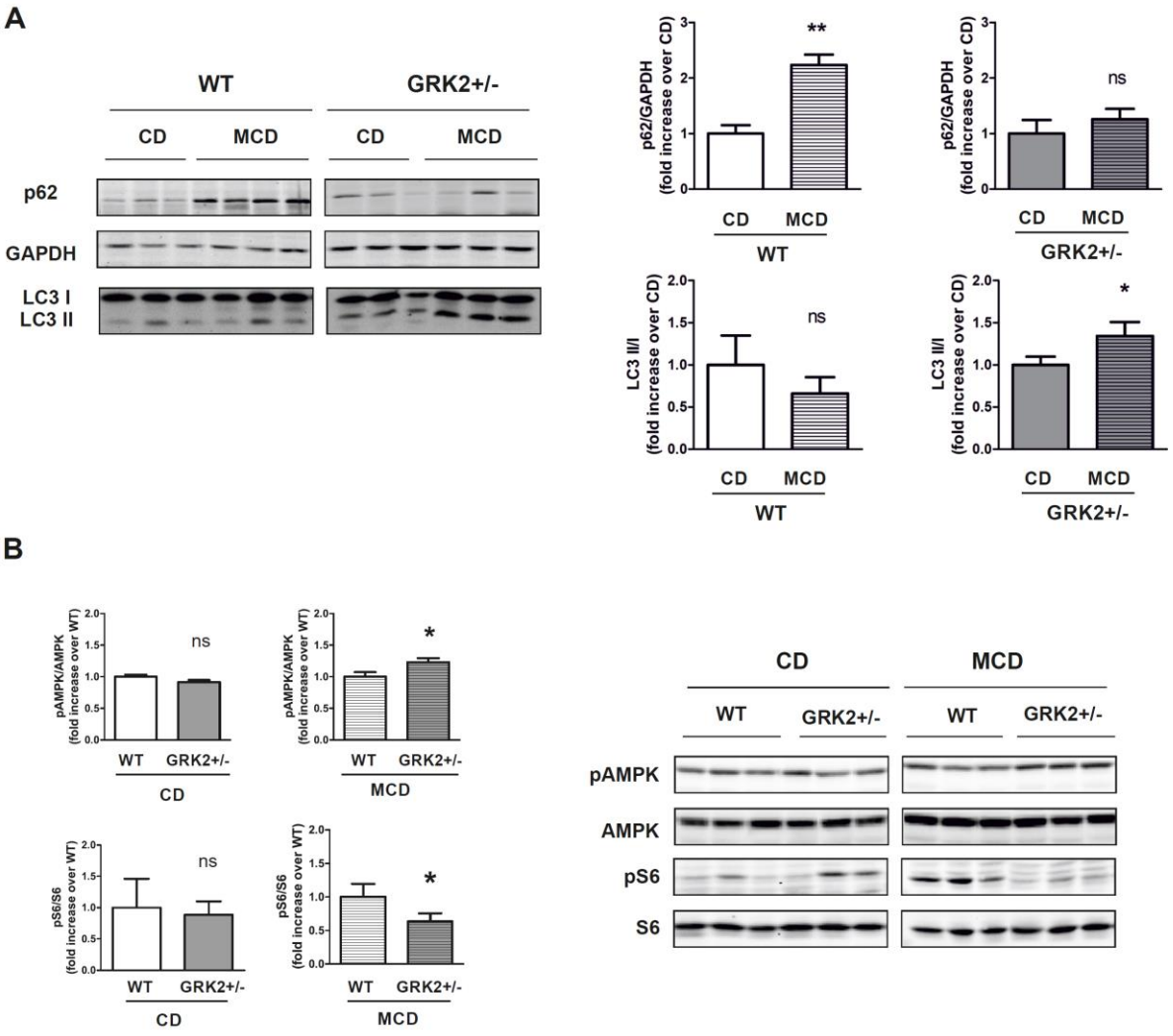

Figure 22. Autophagy is better preserved in the liver of GRK2+/- mice in the face of MCD-induced NASH. (A and B) Protein levels of p62, GAPDH and LC3 I/II (A) and phosphorylated and total AMPKα (pThr172) and S6 (pSer240/244) (B) were analyzed by WB. Densitometric values are shown together with representative immunoblots. Data are means ± SEM of 4-7 animals per group. Results are expressed as fold increase over CD (A) or WT (B). Statistical significance was analyzed by unpaired t-test or Mann-Whitney test, depending on the normal distribution of the data. *P < 0.05; **P < 0.01.

GRK2+/- mice have increased gluconeogenic response after an MCD

An increased hepatic gluconeogenic capacity could be considered as a protective mechanism of the liver against NASH. In fact, treatment with a glucagon receptor/GLP1 receptor dual agonist effectively reduce NASH in mice fed an MCD (Valdecantos et al. 2017). Along this line and consistently with the increased expression of PGC-1α in GRK2+/- mice after the MCD (Figure 21A), we found increased mRNA levels of its target gene *pck1*, that encodes for the gluconeogenic enzyme PEPCK, in GRK2+/- livers (Figure 23A). This enhanced expression was detected in the absence of significant differences in glucagon levels, the main inducer of *pck1* expression, between genotypes (Figure 29B). These results are in line with the results from the PTT (see Figure 13E) and suggest improved gluconeogenic response in GRK2+/- mice in the face of an MCD even when the rise in glucagon levels is similar to that seen in WT animals. These preserved gluconeogenic capacity could further contribute to the protection against MCD-induced NASH detected in GRK2+/- mice.

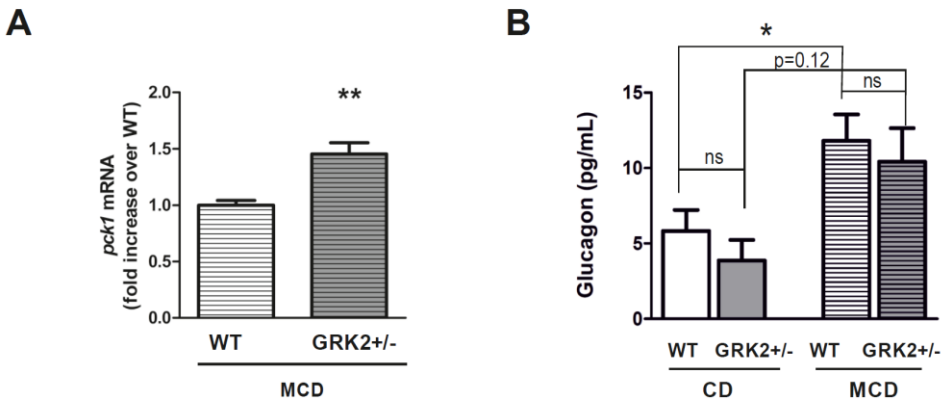

Figure 23. Increased hepatic *pck1* in MCD-treated GRK2+/- mice livers compared to WT. (A) qPCR expression levels of mRNAs encoding PEPCK (*pck1*) normalized with *actb* in hepatic mRNAs from MCD-fed WT and GRK2+/- mice sacrificed after an overnight fasting. **(B)** Glucagon values in serum from WT and GRK2+/- mice fed either CD or MCD for 4 weeks after an overnight fasting. Data are means ± SEM of 7-8 (A) or 5 4-7 (B) individuals per group. Statistical significance was analyzed by unpaired t-test. *P < 0.05; **P < 0.01.

GRK2 regulation may be an early event during MCD-induced NASH

In the MCD-based NASH model, some of the differences observed between WT and GRK2+/- mice were detectable with an early onset after only two weeks of MCD feeding. In particular, liver-to-body weight ratio was significantly lower in GRK2+/- mice compared to WT mice already at this time point (Figure 24A). Importantly, hepatic GRK2 levels were found to be significantly upregulated in mice fed an MCD for only two weeks (Figure 24B). However, and contrary to the data obtained after 4 weeks of MCD, autophagy markers indicate that this process could be increased in WT mice compared with GRK2+/- mice after two weeks of MCD as demonstrated by the lower levels of p62 and the higher LC3 II-to-LC3 I ratio found in WT livers at this time point (Figure 24C). Altogether, these preliminary data indicate that the increase of GRK2 is an early event during the MCD-induced NASH process, and that GRK2+/- mice show an early protection against hepatic steatosis even when autophagy is higher in WT mice at this time point.

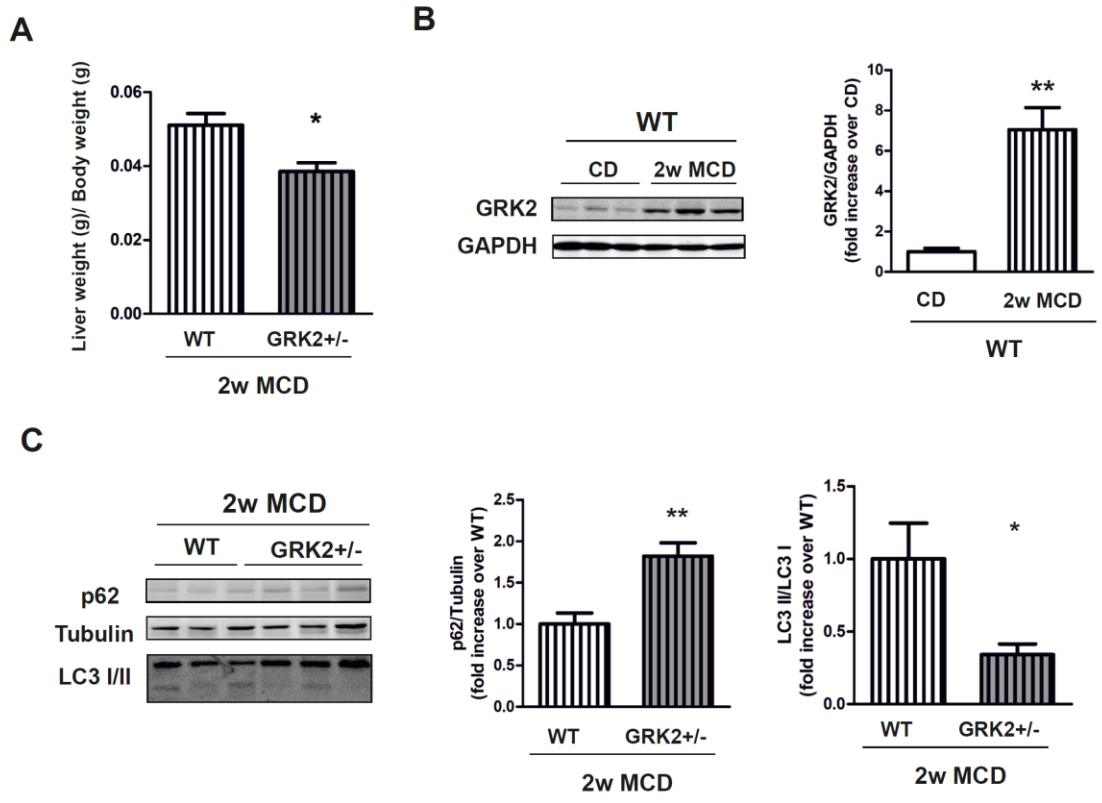

Figure 24. GRK2+/- mice show lower liver weight but reduced autophagy in the liver after two weeks of MCD. 14 weeks-old WT and GRK2+/- mice were fed an MCD for two weeks. **(A)** Liver-to-body weight ratios for MCD-fed mice. **(B)** Densitometric quantification of WB analysis of liver lysates from WT mice fed a CD or a MCD for 2 weeks probed with GRK2 and GAPDH. Representative blots are also shown. **(C)** Same as in (B) using antibodies against p62, tubulin and LC3 II/I. Data are means ± SEM of 4 individuals per group. Statistical significance was analyzed by unpaired t-test. *P < 0.05; **P < 0.01.

1.3.- GRK2 in human steatosis and NASH.

GRK2 is overexpressed in human steatotic livers compared to control

In order to investigate if GRK2 overexpression also occurs during human NAFLD we used two different cohorts of patients from different hospitals (See details in Methods Section) and also different approaches to quantify GRK2 protein and mRNA levels in human biopsies.

We used a cohort of 41 patients with a clinical diagnosis of simple steatosis (SS) or NASH and 31 patients with histologically normal liver (NL). Among SS and NL individuals there are lean (BMI<25) and overweight and obese patients (BMI>25) while all NASH patients had a BMI above 25. We analyzed GRK2 protein levels by WB in biopsies from patients with an BMI bellow 25 (lean patients) and found an upregulation in SS biopsies compared to NL ones (Figure 25A). Moreover, when analyzing the rest of the cohort, the upregulation of GRK2 levels was also observed (Figure 25B). Finally, we found increased GRK2 protein levels in the biopsies from NASH patients compared to NL ones (Figure 25C). Furthermore, we extracted mRNA from the liver biopsies from the aforementioned cohort and found increased GRK2 levels (*Adrbk1*) in both SS and NASH biopsies compared to NL (Figure 25D).

We used a second cohort of 23 obese patients with SS or NASH and also lean (5) and obese (4) NL controls and we analyzed GRK2 protein levels in the biopsies by immunohistochemistry. Quantification of GRK2 positive-stained area showed a statistically significant increase both in SS and NASH liver biopsies compared to lean NL but not to obese NL ones (Figure 25E), this last group showing a high variability in GRK2 staining.

Moreover, hepatic GRK2 levels correlate with histological features of NAFLD patients. Using the first cohort of patients we were able to establish that the mRNA levels of GRK2 in the biopsies correlated with the NAS (r=0.32, p=0.006) and steatosis degree (r= 0.26, p=0.02) of each sample. Moreover, in the second cohort of patients we also observed positive correlations between the percentage of GRK2-positive stained area and the NAS of each sample (r=0.38, p=0.08) or the degree of steatosis (r=0.49, p=0.02).

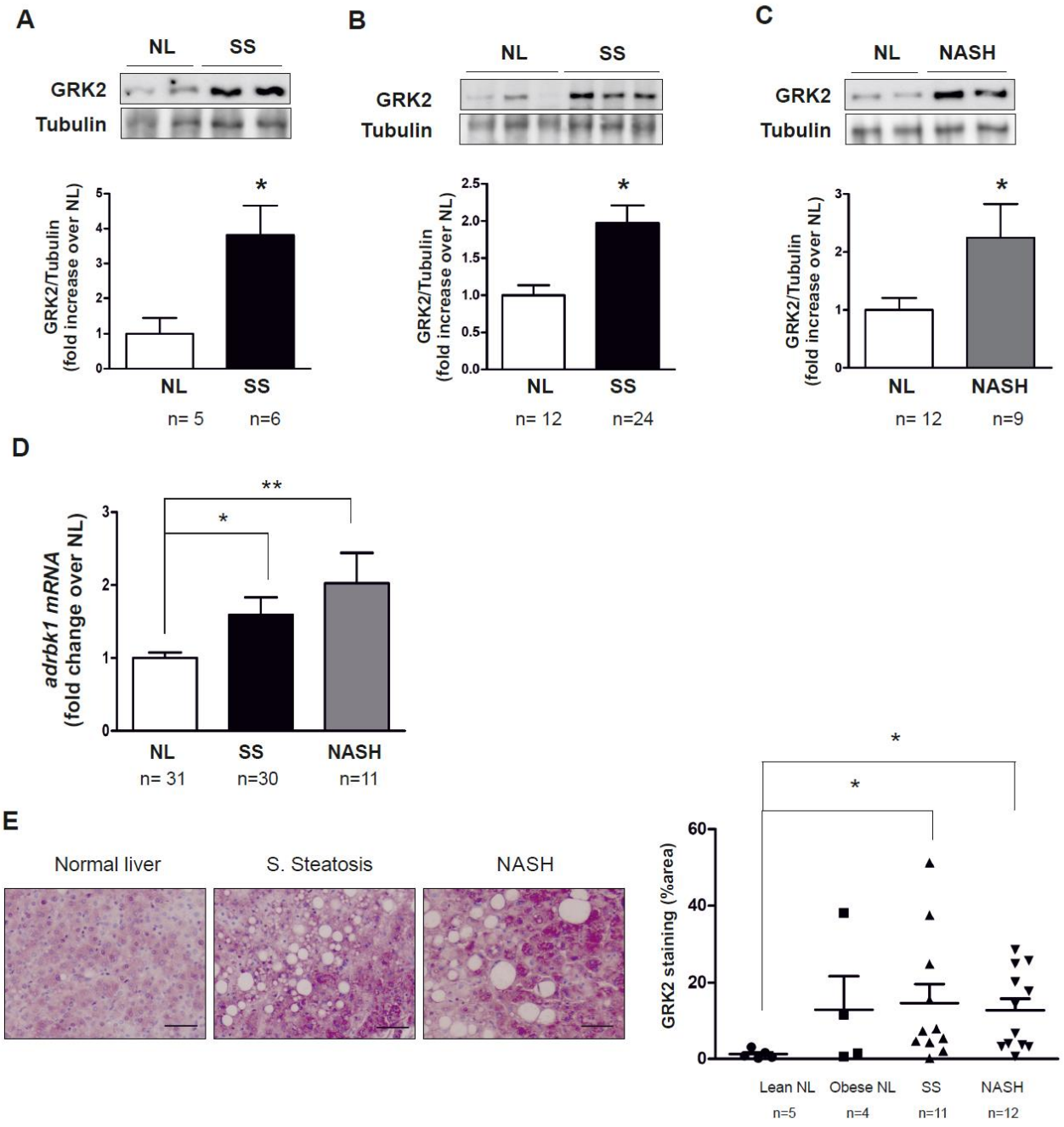

Figure 25. GRK2 levels are upregulated in biopsies of NAFLD patients. (A to C) Liver biopsies from individuals with histologically normal liver (NL) or patients with simple steatosis (SS) either lean (A) or obese (B) and from obese patients with NASH or NL (C) were subjected to WB and probed with antibodies against GRK2 and tubulin. Densitometric analysis and representative immunoblots are shown. **(D)** qPCR was used to study the levels of mRNA expression of *Adrbk1* in biopsies from the same cohort as in A,B and C. Results were normalized with *36b4*. **(E)** Immunohistochemistry of GRK2 was performed in liver biopsies of obese patients with SS and NASH and of obese and lean patients with NL. GRK2-stained area was quantified. Representative photomicrographs are shown (magnification ×40; scale bar 50 μm). A to D biopsies belong to the "Cohort 1" and E to "Cohort 2" described in the Methods section. Data are means ± SEM of the specified individuals per group. Statistical significance was analyzed by unpaired t-test or Mann-Whitney test, depending on the normal distribution of the data (A to C) or one-way ANOVA followed by Dunn´s post-test (D and E). *P < 0.05; **P < 0.01. (In collaboration with Dr. C García-Monzón and Dr. ML Martínez-Chantar labs).

GRK2 upregulation enhances lipid accumulation and induces FAS expression in lipid-overloaded human hepatic cells

The results described above demonstrate that GRK2 levels correlate with the presence of NAFLD/NASH, and that preventing the increase in GRK2 protein levels, as occurs in GRK2+/- mice, is able to impair NAFLD/NASH development. In order to establish a direct cause-effect relationship between GRK2 upregulation and lipid accumulation we set up *in situ* experiments in the human hepatoma cell line (Huh7), widely used as a model to study human hepatocyte metabolism and function (Nikolaou et al. 2016).

We overexpressed (Ad-GRK2) or silenced (sh-GRK2) GRK2 in Huh7 cells using adeno-associated viral vectors or a control virus and subjected these cells to a palmitic acid (PA)-induced steatosis protocol. Cells were treated for 24 hours with 500 μM of PA complexed with BSA, thus obtaining a physiological ratio between bound and unbound FA in the media (Richieri and Kleinfeld 1995) and a PA concentration similar to the fasting total FFA plasma concentrations observed in humans with NASH (de Almeida et al. 2002). The infection effectively increased (Ad-GRK2) or decreased (sh-GRK2) GRK2 levels in Huh7 cells (see Figure 26B). Lipid accumulation was induced with the 24-hour PA treatment as demonstrated by an increase in Oil Red O staining in the representative micrographs in all the conditions (Figure 26A). Interestingly, this increase was greater in GRK2-overexpressing cells as demonstrated by the quantification of the increase of Oil Red O in the eluate. However, we did not find differences in lipid accumulation when silencing GRK2 in Huh7 cells compared with the control (Figure 26A).

Apart from exogenous lipid accumulation, we wanted to detect whether changes in GRK2 levels would influence endogenous lipid production by DNL. Thus, we analyzed by WB the levels of FAS and detected increased protein levels of this protein in GRK2-overexpressing Huh7 cells compared with control cells, being more obvious when the cells are exposed to PA, while FAS levels remained unaffected by GRK2 silencing (Figure 26B).

These findings demonstrate that GRK2 overexpression is able *per se* to increase PA-induced intracellular lipid accumulation by means of enhanced exogenous lipid accretion as well as augmented endogenous DNL, while GRK2 silencing does not affect these processes in Huh7 cells. Moreover, these data establish a cause-effect relationship between GRK2 levels and intracellular lipid accumulation in hepatoma cells.

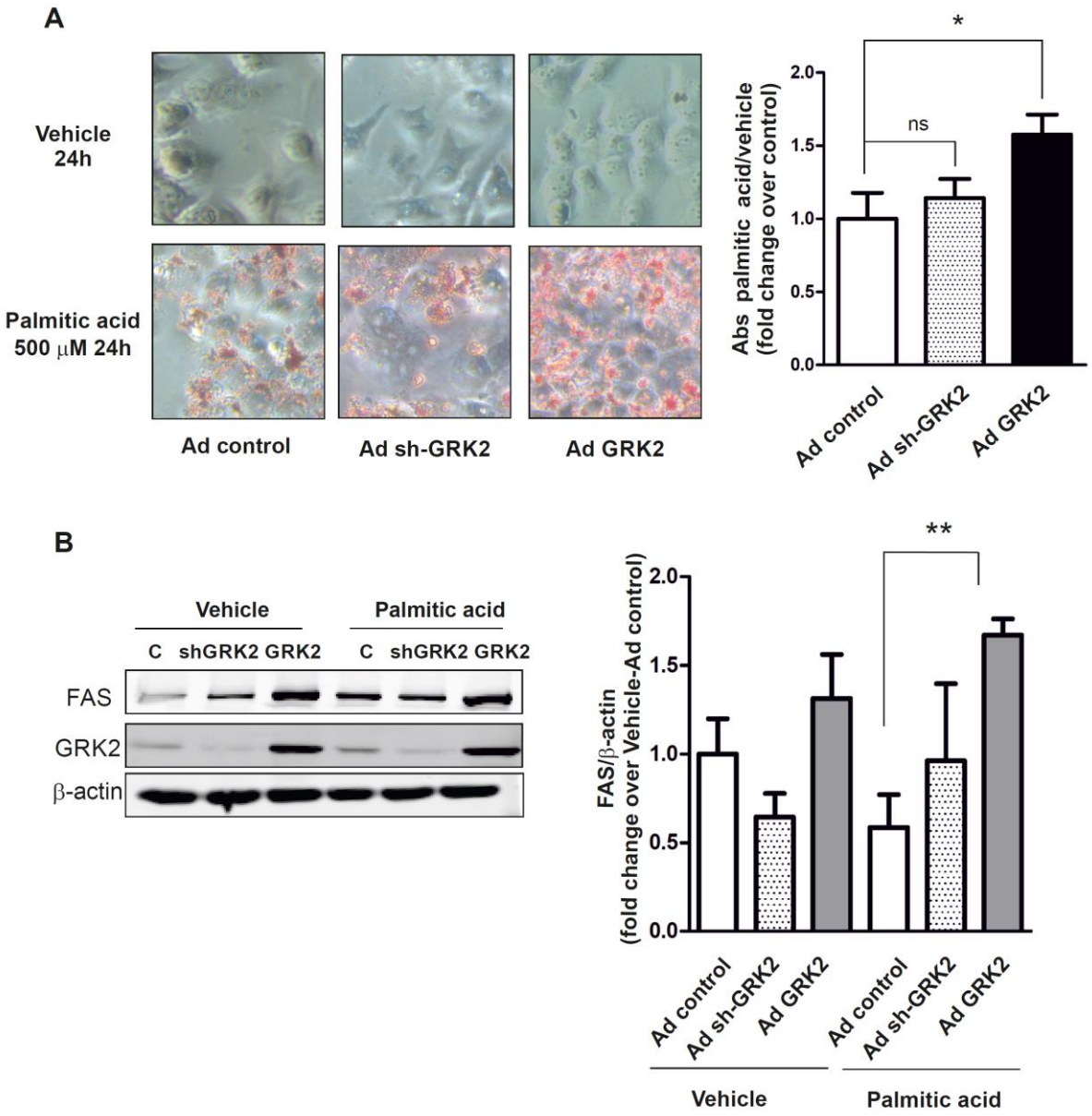

Figure 26. GRK2 overexpression increases lipid accumulation and FAS expression after palmitic acid exposure in human hepatoma cells. (A) Human hepatoma cells (Huh7) were infected with a control virus, or a GRK2-overexpressing (Ad-GRK2) or silencing (sh-GRK2) adeno-associated virus and exposed to palmitic acid for 24 hours. The stored intracellular lipid content was quantified by Oil Red O elution and the increase in absorbance over vehicle is represented together with representative pictures. **(B)** Densitometric analysis of WB from lysates of Ad-control, Ad-GRK2 and Ad-shGRK2 Huh7 cells exposed or not to palmitic acid probed against GRK2, FAS and β-actin. Representative immunoblots are shown. Data are means ± SEM of 5 independent experiments performed in triplicates (A) or 3-5 independent experiments (B). Statistical significance was analyzed by one-way ANOVA followed by Bonferroni´s post-test. *P < 0.05; **P < 0.01.

PART 2: GRK2 in health:

2.1.- Fasting as a model of physiological steatosis

In the first part of this thesis we have demonstrated the importance of maintaining GRK2 levels under a certain threshold to prevent pathological steatosis/NASH linked or not with obesity. We wanted to continue our study on this topic addressing the importance of GRK2 levels in the accumulation of lipids within the liver in a physiological context. In this regard, fasting induces weight loss with increased WAT lipolysis and FA release into the bloodstream that can reach the liver. When the hepatic FA influx exceeds its oxidative capacity, the excess FA is stored as TG thus causing hepatic steatosis (Guan et al. 2009; Nishikawa et al. 2008). This physiological response allows us to study the role of GRK2 in the fasting-induced steatosis as a model of non-obese non-pathological fatty liver.

Due to the important role of GRK2 in lipid and glucose homeostasis (Lucas et al. 2015) and in lipid deposition within the liver (demonstrated in the work compiled in this thesis), we used a model of 24-hour fasting in order to explore a possible role of GRK2 in the adaptation to metabolic stress and/or in fasting-induced hepatic steatosis.

Fasting-induced weight loss is higher in GRK2+/- mice

Weight loss was induced by 24 hours of fasting both in WT and GRK2+/- mice (Figure 27A). However, the decrease in body weight is higher in the case of GRK2+/- mice both in total gram loss and also in percentage over the initial weight (Figure 27B). This could be explained by a greater lipolytic response to fasting in the adipose tissue of GRK2+/- mice since previous results using fat pad explants from Tam-GRK2-/- mice showed increased lipolysis upon adrenergic stimulation (Vila-Bedmar et al. 2015), a process that plays an important role in fasting-induced lipolysis. In line with these results, GRK2+/- mice with food deprivation for 24 hours showed increased circulating NEFA levels compared with WT littermates, suggesting increased lipolysis in these animals. Moreover, we found increased levels of glucose in fasted GRK2+/- compared to WT mice (Table in Figure 27C). Insulin acts as a negative regulator of glucose production and lipolysis while, upon fasting, glucagon has a positive effect on both processes. We measured the levels of both insulin and glucagon after fasting but no differences were detected between WT and GRK2+/- mice (Table in Figure 27C). Together, these data suggest that the differences in glucose and NEFA levels found between genotypes cannot be explained by different circulating levels of these hormones.

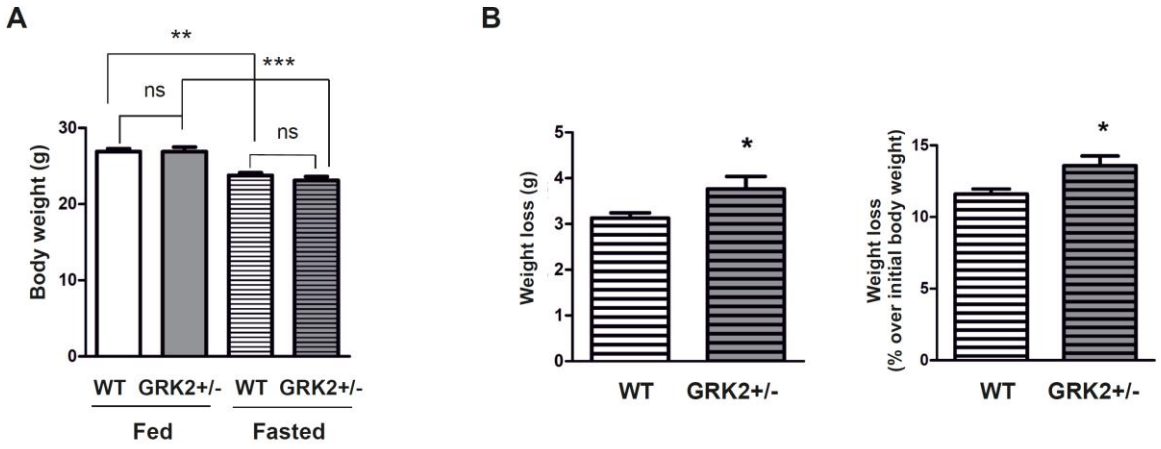

C

	WT fasted 24h	GRK2+/- fasted 24h
NEFA (mmol/L)	0.94 ± 0.02	1.11 ± 0.06 *
Glucose (mg/dL)	92.18 ± 5.3	110.3 ± 6.3 *
Insulin (µg/L)	0.33 ± 0.05	0.31 ± 0.02
Glucagon (pg/mL)	5.00 ± 0.54	7.36 ± 1.55

Figure 27. Fasting induces greater weight loss in GRK2+/- mice in parallel with increased circulating NEFA levels and higher glycemia. (A) Body weight of WT and GRK2+/- mice euthanized either in fed or fasted conditions. **(B)** Weight loss in grams and percentage over initial weight from WT or GRK2+/- mice after 24 hours of fasting. **(C)** Table with biochemical parameters of 24 hours-fasted WT and GRK2+/- mice. Data are means ± SEM of 4-5 individuals per group except for (B) and glucose and insulin measures n=10-14. Statistical significance was analyzed by unpaired t-test or one-way ANOVA followed by Bonferroni´s post-test (A). *P < 0.05; **P < 0.01; ***P < 0.005.

Fasting induces a similar accumulation of TG in the liver of WT and of GRK2+/- mice

Liver weight was significantly decreased after fasting in both WT and GRK2+/- mice, probably due to the depletion of the glycogen storage, without differences in the final liver weight between genotypes (Figure 28A). Food deprivation for 24 hours induced hepatic steatosis as shown by Oil Red O staining (Figure 28B). The quantification of hepatic TG (Figure 28C) confirmed that lipid deposition was similar in both genotypes after fasting. In sum, we have demonstrated that GRK2+/- mice did not show a different degree of liver lipid accumulation using this physiological model of steatosis as was the case in the aforementioned models of NAFLD/NASH.

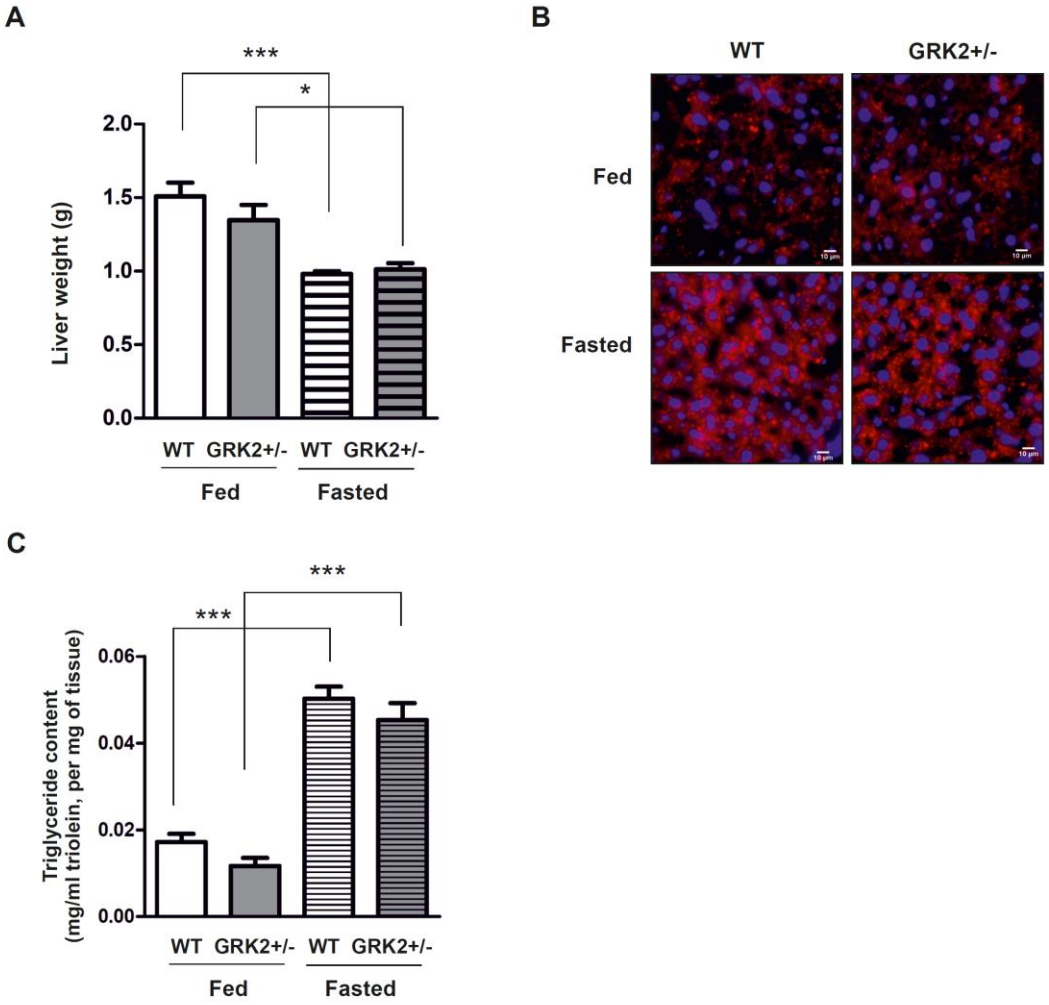

Figure 28. WT and GRK2+/- display a similar degree of fasting-induced steatosis. (A) Liver weight of WT and GRK2+/- mice either in fed or fasted conditions. **(B)** Representative pictures of Oil Red O staining of liver sections from fed or fasted WT and GRK2+/- mice (magnification x40; scale bar 10 µm). **(C)** TG content in livers of WT and GRK2+/- mice either in fed or fasted conditions expressed as equivalents triolein concentration (mg/ml) and normalized by the weight of the liver sample analyzed (mg). Data are means ± SEM of 4-5 individuals per group. Statistical significance was analyzed by one-way ANOVA followed by Bonferroni´s post-test. *P < 0.05; **P < 0.01; ***P < 0.005.

Fasting induces a decrease in GRK2 protein content specifically in the liver

Changes in GRK2 levels have been revealed to be important in several pathological conditions (Penela et al. 2006; Nogues et al. 2017; Mayor et al. 2018). Furthermore, we have shown that GRK2 levels are increased in different situations of hepatic steatosis (viz. *db/db* mice, HFD- and MCD-induced NAFLD/NASH), and that decreasing GRK2 levels confers a certain protection from excessive hepatic lipid accumulation induced by MCD or HFD feeding. However, we did not find any difference in fasting-induced steatosis between WT and GRK2+/- mice. For this reason and as part of the characterization of the fasting model, we decided to study the expression of GRK2 levels in the livers of WT and GRK2+/-

fasted mice. Surprisingly, in this model we did not find increased levels of GRK2 running in parallel with increased steatosis. On the contrary, GRK2 levels dropped upon fasting both in WT and GRK2+/- mice (Figure 29A). Moreover, this downregulation of GRK2 is already observed after 14 hours of fasting (Figure 29B) and GRK2 levels remain low after a prolonged fasting period, at least for 48 hours of food deprivation (Figure 29B). Interestingly, this decrease was not observed in eWAT, suggesting that GRK2 dowmodulation is a specific response to fasting of the hepatic tissue (Figure 29C).

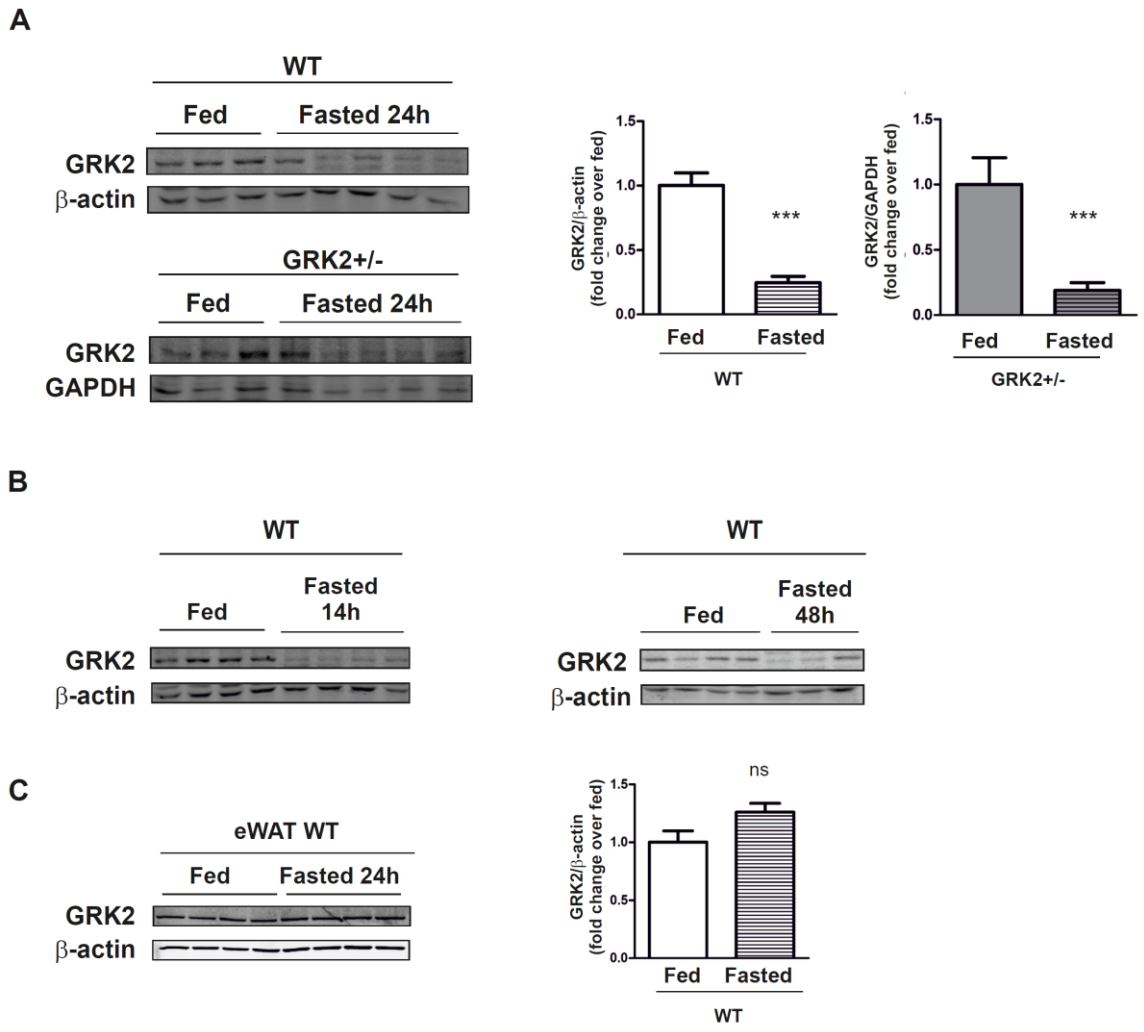

Figure 29. Hepatic GRK2 levels are decreased upon fasting both in WT and GRK2+/- mice. (A) Densitometric analysis from WB of liver lysates either fed or fasted for 24 hours using antibodies against GRK2, GAPDH or β-actin. **(B)** WT mice were fasted for 14 hours or 48 hours and analyzed as in A. **(C)** WB densitometries of eWAT lysates from mice either fed or fasted for 24 hours using GRK2 and β-actin antibodies. (Results obtained with the help of Irene Herranz) Representative blots are shown in each panel. Data are means ± SEM of 4-5 individuals per group. Statistical significance was analyzed by unpaired t-test. ***P < 0.005.

2.2.- Other responses to food deprivation: gluconeogenesis

As we have already shown, GRK2+/- mice are able to maintain higher glucose levels upon a 24h fasting compared to WT mice (See Table in Figure 27C), this observation may suggest that these mice could have an increased hepatic glucose output. Hepatic glucose output depends on glycogenolysis and gluconeogenesis and is mainly activated by the release of glucagon in the fasted state. Since we did not detect significant differences in circulating glucagon levels upon fasting between genotypes (Figure 27C), we decided to investigate whether the effects of glucagon in the liver could be modulated by GRK2 levels. In fact, this hormone acts through the GCGR that, as mentioned, has been described to be regulated by GRK2 in HEK293 (Krilov et al. 2011). For this reason, we sought to investigate the effect of GRK2 dosage in glucagon-induced glucose production using gluconeogenic substrates and on the expression of gluconeogenic genes in mouse primary hepatocytes.

GRK2 downmodulation in primary mouse hepatocytes causes an increase in glucagon-stimulated glucose production

We altered GRK2 levels in primary mouse hepatocytes with adeno-associated viruses and then treated them with glucagon in the presence of guconeogenic substrates (pyruvate and lactate). The efficiency of the silencing (shGRK2) or overexpression (ad-GRK2) was corroborated by WB and qPCR (Figures 30A and 31A). We checked the levels of β-arrestins, also implicated in GCGR desensitization, that were unaltered in sh-GRK2 and ad-GRK2 cells (Figures 30B and 31B). We quantified glucagon-induced glucose production from pyruvate and lactate in these cells and found a significantly enhanced glucose output in hepatocytes with silenced GRK2 (Figure 30C) with respect to control-infected cells (shC). This enhanced gluconeogenic response detected upon GRK2 downregulation correlated with an increased expression of the *pck1* gene that encodes for PEPCK, a key enzyme in the regulation of gluconeogenesis, in shGRK2 cells (Figure 30D). However, no differences were detected between glucagon-stimulated shGRK2 and shC hepatocytes in the expression of *ppargc1a* (PGC1-α), a master regulator of gluconeogenesis, and *g6pc*, another gluconeogenic enzyme (Figure 30D).

In contrast to these results, we did not find any difference in glucagon-stimulated glucose production between GRK2-overexpressing and GFP-overexpressing control cells (Figure 31C). Coherently, no differences were found in the expression of *ppargc1, pck1* or *g6pc* genes in glucagon-treated GRK2 and GFP-overexpressing hepatocytes (Figure 31D). These results indicate that GRK2 silencing, but not GRK2 overexpression, has a positive impact in glucagon-induced gluconeogenic responses in primary mouse hepatocytes.

In sum, our results indicate that fasting induces a decrease in GRK2 protein content specifically in the liver, which may favor glucagon responses leading to increased glucose output in this tissue.

Accordingly, GRK2+/- mice display a less pronounced hypoglycemia after 24 h of fasting compared with control mice, an effect that cannot be ascribed to differences in plasma glucagon levels. Moreover, in vitro data demonstrate that GRK2 downmodulation in hepatocytes increases glucagon-stimulated glucose production, what can help explain the role of GRK2 in the modulation of liver response to food deprivation.

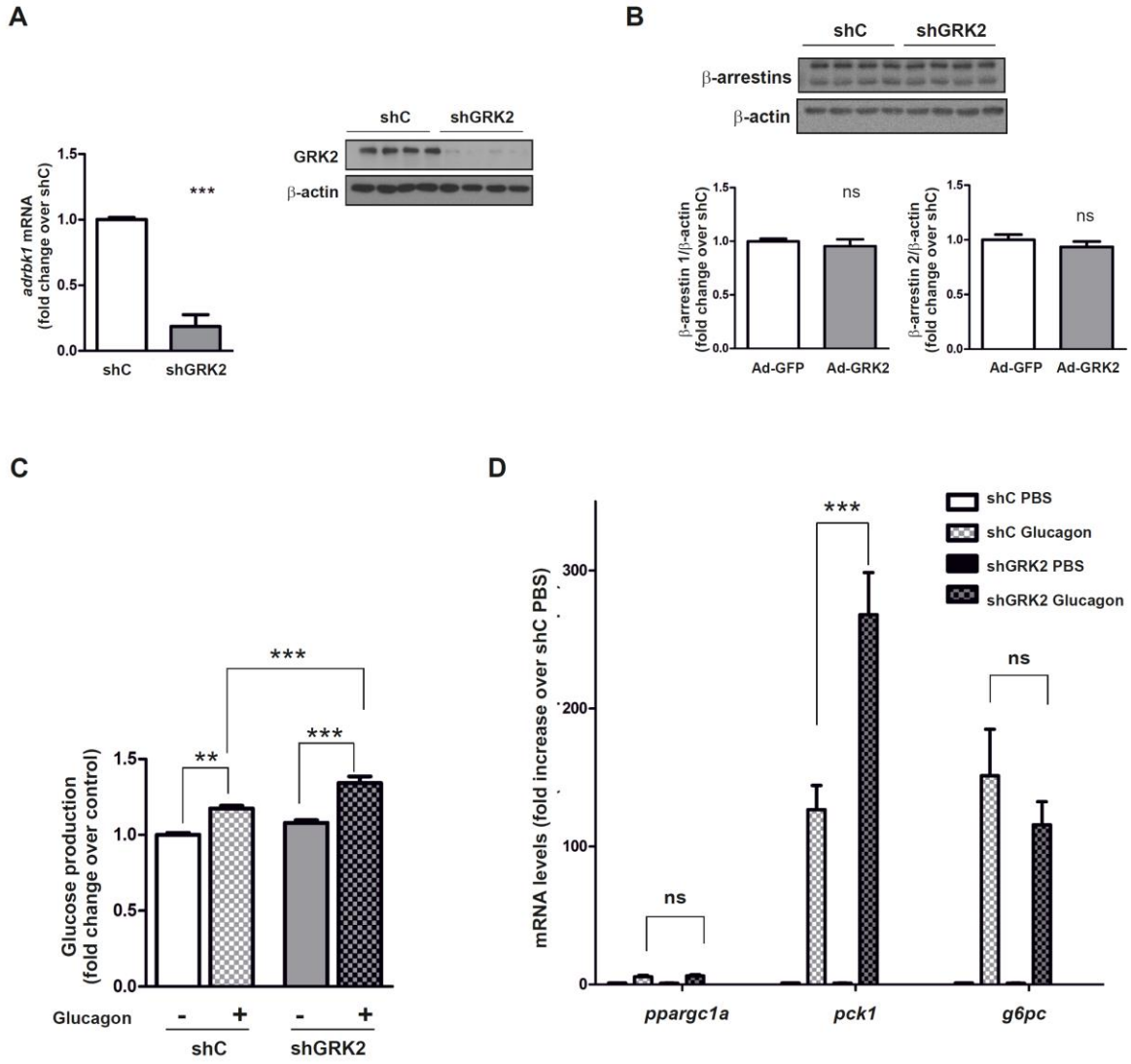

Figure 30. Silencing GRK2 in primary hepatocytes increases glucagon-induced glucose production and PEPCK (*pck1*) expression. Primary hepatocytes from C57BL6/J mice were infected with adenoviruses carrying a silencing construct for mouse GRK2 (shGRK2) or human GRK2 as a non-silencing control (shC). **(A)** qPCR of GRK2 mRNA (*adrbk1* gene normalized to *rlp13*) and WB showing GRK2 protein levels relative to β-actin. **(B)** WB densitometries of β-arrestins 1 and 2 normalized by β-actin levels. Represensative blots are shown. **(C)** Glucose production following glucagon stimulation in glucose-free DMEM supplemented with pyruvate and lactate as gluconeogenic substrates. **(C)** qPCR expression of *ppargc1a, pck1* and *g6pc* normalized to *rlp13* in shC- and shGRK2-infected hepatocytes treated with glucagon or PBS Data are means ± SEM of 3 individual experiments with triplicates. Statistical significance was analyzed by unpaired t-test (A) or one-way ANOVA followed by Bonferroni´s post-test (B,C). **P < 0.01; ***P < 0.005. (Results obtained in the Dr. P. Puigserver lab with the help of Dr. K Sharabi).

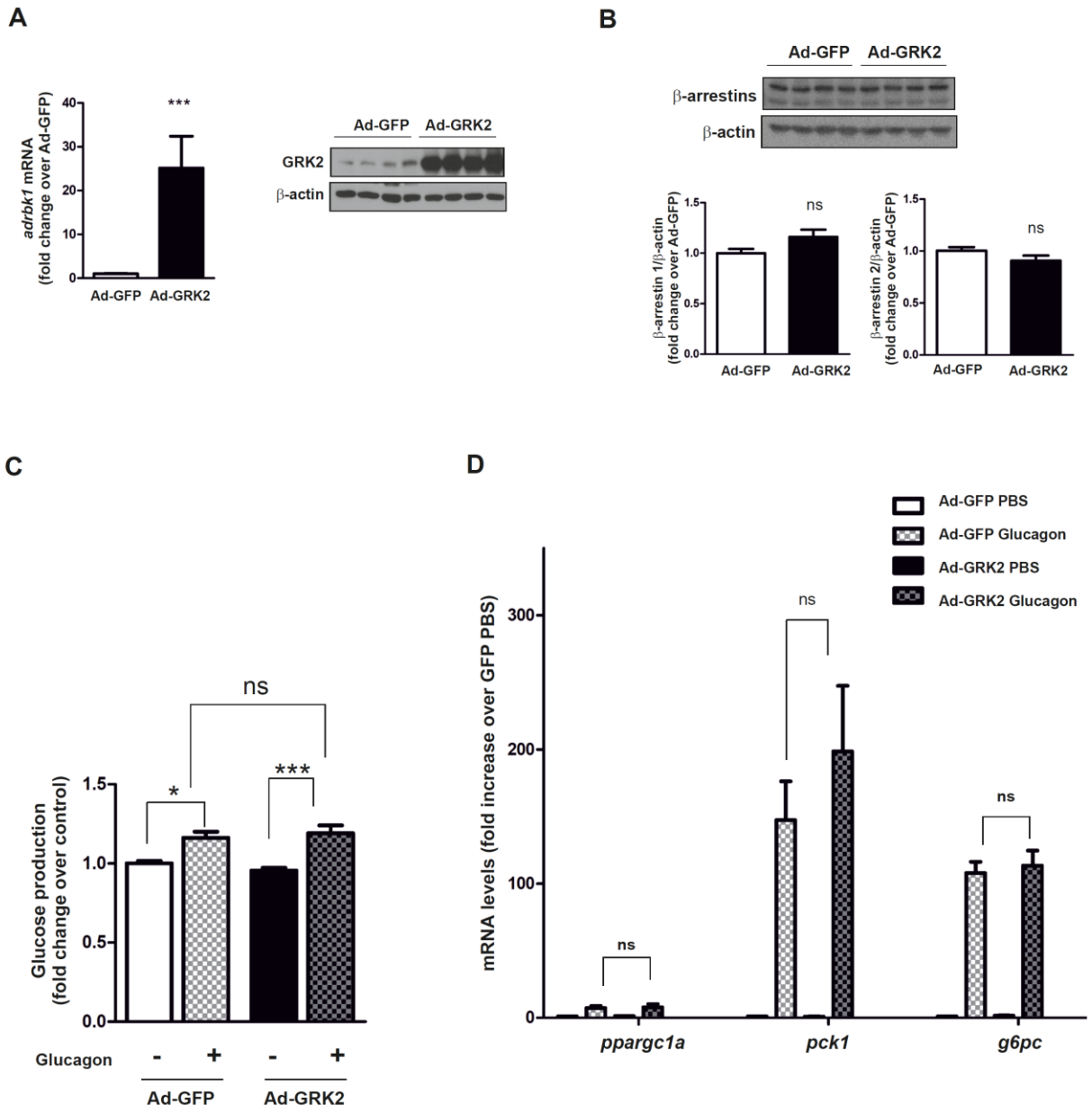

Figure 31. The production of glucose and the expression of different glucagon-induced genes are not affected by GRK2 overexpression in glucagon-stimulated primary mouse hepatocytes. Primary hepatocytes from C57BL6/J mice were infected either with an adenovirus carrying the sequence of bovine GRK2 (Ad-GRK2) or an adenovirus control (Ad-GFP). **(A)** qPCR of GRK2 mRNA (*adrbk1* gene normalized to *rlp13*) and WB showing GRK2 protein levels relative to β-actin. **(B)** WB densitometries of β-arrestins 1 and 2 normalized by β-actin levels. Represensative blots are shown. **(C)** Glucose production following glucagon stimulation in glucose-free DMEM supplemented with pyruvate and lactate as gluconeogenic substrates. **(C)** qPCR expression of *ppargc1a, pck1* and *g6pc* normalized to *rlp13* in GRK2-overexpressing and control cells. Data are means ± SEM of 3 individual experiments with triplicates. Statistical significance was analyzed by unpaired t-test (A) or one-way ANOVA followed by Bonferroni´s post-test (B,C). *P < 0.05; ***P < 0.005. (Results obtained in the Dr. P. Puigserver lab with the help of Dr. K Sharabi).

DISCUSSION

The liver plays a key role in the control of glucose and lipid metabolism and it is, at the same time, a target organ in metabolic disorders such as T2D or obesity. The excessive accumulation of fat characteristic of obesity can lead to excessive lipid deposition in the liver, the hallmark of NAFLD. Hepatic steatosis can cause (and coexist with) liver inflammation in a more pathological step during the disease progression named NASH with worse prognosis than simple steatosis (Malaguarnera et al. 2009; Cohen, Horton, and Hobbs 2011). On the other hand, hepatic steatosis also occurs during fasting as a physiological response to increased lipolysis in the adipose tissue (Lin et al. 2005). In contrast with NASH, fasting-induced fatty liver does neither lead to nor coexist with hepatic inflammation (Mustonen et al. 2013; Xu et al. 2013).

GRK2 modulates important GPCRs, many of them involved in the regulation of metabolism such as β-AR (Ruiz-Gomez and Mayor 1997) or GCGR (Krilov et al. 2011), among others. Moreover, changes in GRK2 expression and/or activity have been identified in several inflammatory, metabolic and cardiovascular diseases, suggesting that those alterations may contribute to the onset or development of these pathologies (Gurevich et al. 2012). However, the potential contribution of GRK2 to the handling of metabolic stress in pathological versus physiological conditions, and, in particular, the consequences of changes in GRK2 levels to the hepatic response to such stress have not been addressed so far.

PART 1: Role of GRK2 in disease

GRK2 exerts an important role as a negative modulator of insulin signaling (Garcia-Guerra et al. 2010; Usui et al. 2005; Ciccarelli et al. 2011). Moreover, our laboratory has described that GRK2+/- mice maintain glucose tolerance and insulin signaling in the major insulin-responsive tissues under different conditions of IR, and preserve a lean phenotype upon 12 weeks of HFD (Garcia-Guerra et al. 2010). Remarkably, GRK2 levels were increased in insulin-resistant human adipocytes and peripheral blood cells from metabolic syndrome patients, and in muscle and adipose tissue from TNFα-, aging- or HFD-induced insulin-resistant mice (Garcia-Guerra et al. 2010). However, the rise in GRK2 levels in the liver was only prompted upon HFD and not by the other IR-promoting conditions, not so directly related to hepatic steatosis. In order to study more in depth this putative correlation between hepatic GRK2 levels and liver steatosis, we set out to analyze the effects of different genetic dosages of GRK2 on the development or reversion of hepatic pathologies related to steatosis.

1.1- Influence of GRK2 downmodulation on HFD-induced phenotype

We found that, in parallel with the increase in GRK2 levels, WT mice accumulate lipids in the liver upon 12 weeks of HFD while in GRK2+/- mice this feeding barely increases liver TG content, in parallel again with unaltered GRK2 levels. Nevertheless, the maintenance of the diet for 30 weeks causes a rise in hepatic GRK2 levels both in WT and GRK2+/- mice and, interestingly, GRK2+/- mice are no longer protected from fatty liver upon this long-term HFD, displaying similar hepatic lipid accumulation compared to WT mice. Taken together, these data indicate that the expression of GRK2 in the liver is increased under HFD feeding in association with NAFLD and that this increase might play an important role in NAFLD development since keeping GRK2 levels low protects animals from the disease. The fact that GRK2+/- mice lose the protection against both steatosis and the increase in GRK2 levels upon very long-term feeding with a HFD, further stresses the link between GRK2 levels and NAFLD. These results support the hypothesis that GRK2 levels must be maintained underneath certain pathological threshold that, when surpassed, can favour lipid accumulation in the liver and trigger NAFLD. If so, decreasing GRK2 levels in mice with fatty liver (and elevated GRK2 levels) should induce the reversion of the disease. We used a tamoxifen-inducible genetic model to decrease GRK2 levels once HFD-induced obesity, IR and NAFLD were already established, and explored the effect of altering GRK2 levels on different tissues, including the liver, as well as on various metabolic parameters. This approach would allow us to assess if targeting GRK2 could be a new and feasible therapeutic strategy to tackle the metabolic syndrome and its hepatic manifestation, NAFLD.

GRK2 and insulin sensitivity

GRK2 floxed mice exhibited a pre-diabetic phenotype after eight weeks of HFD regardless of the fact that they expressed or not Cre recombinase. At that moment, tamoxifen administration induced the deletion of GRK2 only in Cre+ animals (that became Tam-GRK2-/-) and not in Cre- mice (used as controls). GRK2 depletion caused the reversion of IR and glucose intolerance, and stopped the weight gain in Tam-GRK2-/- animals even when they continued under a high fat feeding for five more weeks. Moreover, Tam-GRK2-/- recovered from the hyperglycemic and hyperinsulinemic situation that had been induced by the HFD prior to GRK2 downregulation. Thus, we have demonstrated that lowering GRK2 levels can reverse an already established insulin-resistant phenotype and prevent further body weight gain (Lucas et al. 2015; Vila-Bedmar et al. 2015)

Decreasing GRK2 levels appeared to preserve both systemic and peripheral insulin sensitivity, since insulin-targeted tissues key for glucose homeostasis exhibited augmented insulin-induced AKT phosphorylation after a HFD in animals with low levels of GRK2 compared to control mice. Enhanced GRK2 expression has been reported to impair insulin-mediated AKT stimulation and glucose uptake by interacting with IRS1 in adipocytes and myocytes (Garcia-Guerra et al. 2010), by directly

phosphorylating IRS1 at Ser 307 in cardiomyocytes (Ciccarelli et al. 2011) or by mediating endothelin-1-induced IR through the inhibition of both Gαq/11 and IRS1 pathways in 3T3-L1 adipocytes (Usui et al. 2005). Of note, HFD increases GRK2 levels in WAT, muscle and liver (Garcia-Guerra et al. 2010) what could be in part responsible for the impaired insulin signaling in these tissues upon HFD. Conversely, decreasing GRK2 levels, as in Tam-GRK2-/- mice, would preserve insulin signaling in these key tissues.

Effects of GRK2 downmodulation in the liver

The liver is a target for the lipotoxicity caused by the high fat feeding and HFD-fed control mice displayed different signs of NAFLD. However, Tam-GRK2-/- mice were protected against lipid accumulation and inflammation in the liver. Moreover, Tam-GRK2-/- mice had lower levels of PPARγ, an important transcription factor involved in lipogenesis, and of FAS, the enzyme catalyzing the last step of DNL, both of them known to be upregulated in fatty liver (Vidal-Puig et al. 1996; Inoue et al. 2005). This could indicate that Tam-GRK2-/- mice have a lower rate of DNL in the liver, a process that is increased in obesity and NAFLD contributing to the development of the disease (Paglialunga and Dehn 2016; Ferre and Foufelle 2010). On the other hand, IR and hepatic lipid accumulation can cause liver inflammation, and macrophages and Kupffer cells play a central role in the pathogenesis of NAFLD (Rivera et al. 2007). Macrophages display remarkable plasticity in their activation programs and diet-induced obesity leads to a shift from an M2-polarized state (or alternatively activated macrophages) with a beneficial role in T2D and metabolic syndrome (Gordon 2003; Odegaard et al. 2008), to an M1 pro-inflammatory state (or classically activated macrophages) that helps trigger IR (Lumeng and Saltiel 2011). Macrophages in the M1 state are responsible for most of the expression of pro-inflammatory cytokines within this tissue and thus signal for further macrophage recruitment (Weisberg et al. 2003; Olefsky and Glass 2010). Despite the overall homogeneous presence of macrophages/Kupffer cells in Tam-GRK2-/- and control mice, they were more polarized towards an M1 pro-inflammatory phenotype in control mice, indicative of greater hepatic inflammation. It is likely that the reduced liver fat deposition detected upon GRK2 reduction helps suppress tissue inflammation. Nevertheless, it should be taken into consideration that not only hepatocytes, that account for approximately the 80% of the volume of the liver, but also macrophages/Kupffer cells have lower levels of GRK2 given that the expression of the Cre recombinase is under the control of a ubiquitous promoter. Thus, we cannot disregard the possibility that decreasing GRK2 levels in macrophages themselves may also have a direct effect on the polarization, cytokine expression pattern or migration of these cells (further discussed in 1.3).

GRK2 regulation of adrenergic effects on adipose tissues

Some effects observed upon GRK2 lowering might be ascribed to increased adrenergic signaling related to the canonical function of GRK2 in β-AR phosphorylation and desensitization. However, we have shown that the improved glucose tolerance obtained upon GRK2 depletion prevails even under conditions of adrenergic shutdown as demonstrated by treating the animals with the β-blocker propranolol. These results demonstrate that GRK2 loss can influence glucose handling independently of its effects on the control of adrenergic stimulation. During obesity, the adipose tissue becomes less sensitive to catecholamines what in turn reduces lipolysis and energy expenditure (Jocken et al. 2008; Yehuda-Shnaidman et al. 2010; Horowitz and Klein 2000; Mowers et al. 2013). Noteworthy, GRK2 levels were found upregulated in numerous tissues upon high fat feeding what could be responsible of the aforementioned desensitization towards catecholamines, in addition to other mechanisms already described (Stich et al. 2002). β-ARs are the main activators of the lipolytic process in WAT and transgenic mice overexpressing β1-AR have decreased adipose stores as a result of increased lipolytic activity, and are resistant to the development of obesity (Soloveva et al. 1997). We show here that Tam-GRK2-/- have an enhancement of lipolysis as suggested by the increased NEFA release in response to fasting, what would be consistent with an increased activation of adrenergic cascades upon GRK2 decrease and could help correct the defective lipid mobilization and metabolism observed during obesity (Gaidhu et al. 2010). In agreement with this, eWAT explants from Tam-GRK2-/- mice displayed greater lipolytic response upon treatment with a β-adrenergic agonist (Vila-Bedmar et al. 2015). However, a decompensated stimulation of the adrenergic axis can also have detrimental effects. Long-term increase in circulating plasma levels of FA can stimulate *de novo* glucose synthesis and can cause lipotoxicity that would further exacerbate hepatic and skeletal muscle IR, also, β2-AR activation directly induces glycogenolysis and gluconeogenesis, which may increase plasma glucose. In fact, persistent sympatho-adrenal activation has been linked to glucose dysregulation and IR (Boyda et al. 2013). Since no IR or signs of lipotoxicity are found upon GRK2 lowering, other compensatory mechanisms and tissue-specific effects triggered by GRK2 loss must be taking place in parallel that compensate for these processes.

The positive impact of lower GRK2 levels in BAT function appears to be one such compensatory mechanism. Sympathetic stimulation is critical for key effects of BAT on energy homeostasis including thermogenesis (Collins, Yehuda-Shnaidman, and Wang 2010) and glucose utilization (Orava et al. 2011). Moreover, activation and/or increased expression of the thermogenic protein UCP1 has been suggested to ameliorate impaired glucose metabolism caused by IR (Inokuma et al. 2005). Therefore, enhanced adrenergic signaling in BAT upon decreasing GRK2 levels would not only promote thermogenesis, but also contribute to the improvement in glucose homeostasis observed in Tam-GRK2-/- mice. Interestingly, GRK2+/- mice exhibit an increase in energy expenditure, in FA oxidation in BAT and in thermogenic capacity (Vila-Bedmar et al. 2012). In this regard, the morphology of BAT in Tam-GRK2-/-

was representative of a more functional tissue and correlated with increased UCP1 levels. Furthermore, catecholamine sensitivity is decreased in the BAT of obese organisms (Marette et al. 1990) and, accordingly, the *ex vivo* treatment of BAT explants with the β-adrenergic agonist isoproterenol induced greater lipolysis in BAT from Tam-GRK2-/- than in BAT from control mice fed a HFD (Vila-Bedmar et al. 2015). Also, an improved BAT function can explain the absence of lipotoxicity in Tam-GRK2-/- mice even when they present an increased lipolytic response, since this tissue would help control the increased release of FA from WAT. These results thus suggest that BAT could have a key role in the overall phenotype in Tam-GRK2-/- mice. Of note, the principal receptor mediating catecholamine-stimulated thermogenesis (Cannon and Nedergaard 2004) and glucose uptake (Dallner et al. 2006) in brown adipocytes is the β3 subtype. Since β3-AR lacks intracytoplasmic phosphorylation sites and is resistant to agonist-induced desensitization and/or downregulation (Liggett et al. 1993), altered GRK2 levels may impact BAT adrenergic pathways through alternative mechanisms downstream and/or independent from β3-AR. In fact, GRK2 overexpression in cultured brown adipocytes blocks β3 agonist-induced lipolysis by a mechanism possibly involving ERK (Vila-Bedmar et al. 2012). Moreover, GRK2 could be influencing β-adrenergic signaling through other β-AR that can also induce adrenergic response in BAT, since it has been demonstrated that β1-AR is also key to cold- and diet-induced thermogenesis in mice and may mediate many of the SNS stimulation of adaptive thermogenesis (Ueta et al. 2012).

Integrated effects of GRK2 downmodulation on HFD-induced phenotype

Summing up, GRK2 deletion in the course of a HFD restores glucose tolerance and insulin sensitivity while it impairs further body weight gain. Moreover, it causes increased fasting-induced lipolysis in WAT and improved BAT function. As a result of all these metabolic changes and/or due to a specific effect of GRK2 in the liver, Tam-GRK2-/- mice are able to revert HFD-induced NAFLD (Figure D1).

Overall, our data demonstrate that GRK2 controls IR, obesity and NAFLD development *in vivo*. We suggest that GRK2 constitutes a signaling hub that controls and integrates metabolic functions in different tissues thanks to its ability to regulate several GPCRs involved in metabolism as well as the insulin receptor cascade, without ruling out the involvement of additional modulatory functions of this kinase (Mayor et al. 2018; Penela et al. 2010). These findings put forward GRK2 as a potential target for multiple therapeutic interventions for the treatment of the metabolic syndrome and NAFLD.

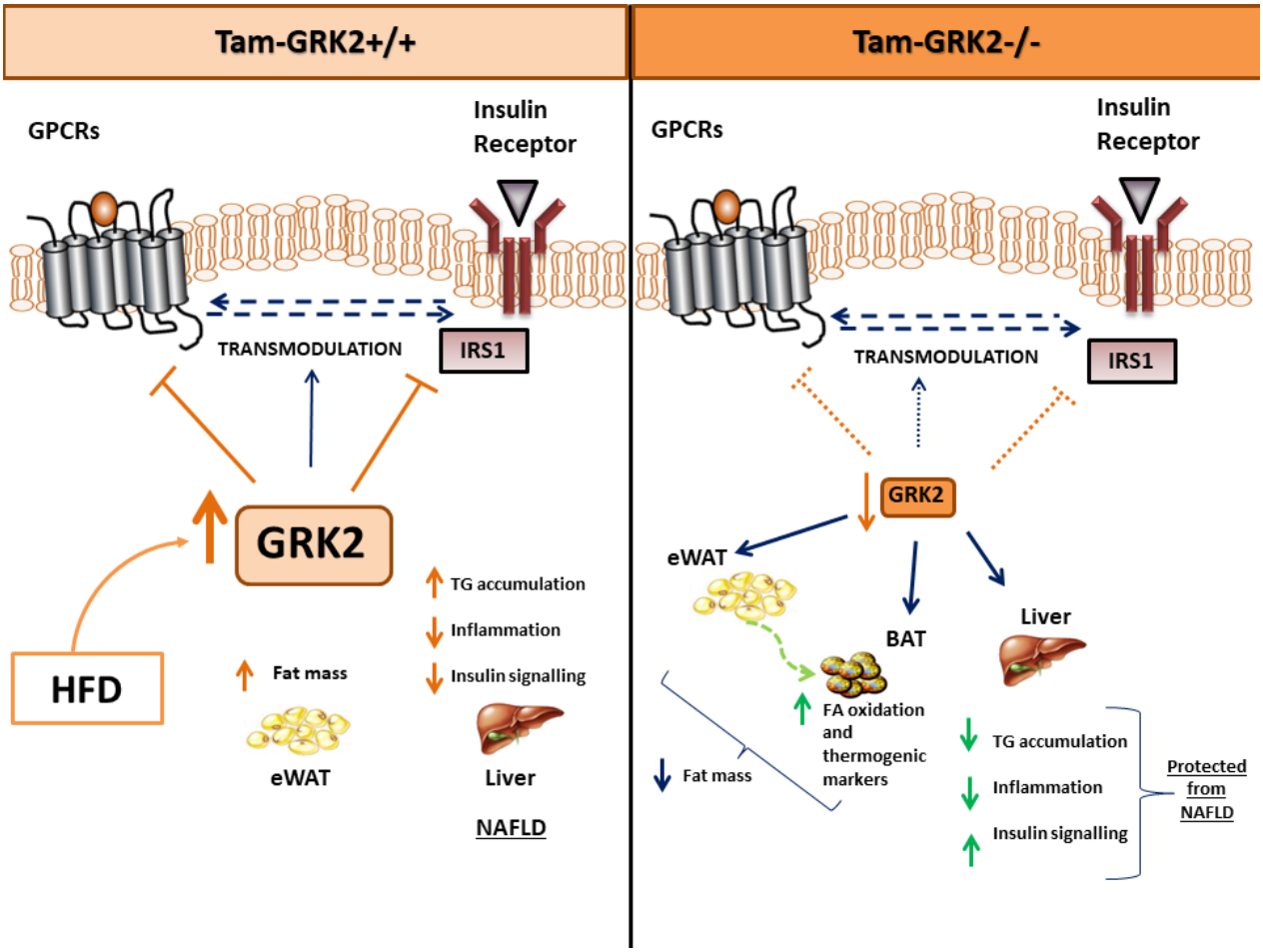

Figure D1. GRK2 depletion during the course of a HFD can reverse an already established obese and insulin resistant phenotype, potentially through the combination of its effects on different tissues. Besides its role as a GPCR kinase, GRK2 inhibits insulin signaling and may also control the GPCR-mediated transmodulation of the insulin pathway. A reduction in GRK2 abundance after obesity and IR have been established (Tam-GRK2-/-, right panel) leads to: (i) an increased adrenergic-dependent lipolytic capacity in eWAT that provides BAT with free FA. In turn, BAT displays an enhanced expression of oxidative and thermogenic markers, and consequently both tissues may contribute to the concerted protection against excessive fat mass accretion; (ii) improved insulin signaling in muscle which can underlie the enhanced insulin-induced glucose clearance; (iii) increased insulin signaling in liver associated with a decrease in TG accumulation and inflammation within this tissue

1.2- Impact of GRK2 levels in non-obese NASH

In the first part of this thesis we have shown that both GRK2+/- mice and tamoxifen-induced GRK2-depleted mice do not show hepatic steatosis after a HFD. However, this protection could just be a consequence of the preserved insulin sensitivity and lean phenotype that these mice displayed. Therefore, we set out to determine whether GRK2 has a role in the development of NAFLD in a manner autonomous from GRK2-dependent control of insulin sensitivity and body weight. For this aim, we fed WT and GRK2+/- mice with an MCD, a nutritional model in which the development of NASH is neither accompanied by increased body weight/adiposity nor by IR establishment (Reid and Eksteen 2015; Rinella and Green 2004).

Influence of GRK2 on MCD-induced steatosis and inflammation in the liver

The MCD challenge caused NASH and a rise in hepatic GRK2 levels in WT mice, as happened in HFD-fed mice, suggesting that this boost may be more closely connected to fatty liver than to the overall changes in the systemic metabolic profile of the mice. Of note, this increase takes place specifically in the hepatocytes but not in Kupffer cells. Moreover, the increase of hepatic GRK2 protein levels triggered by MCD was not observed in GRK2+/- animals, which are protected from steatosis and full-blown NASH (see below), in line with the results obtained in the 12 weeks HFD model. The data in the MCD model further strengthens the hypothesis that GRK2 elevation above a certain threshold may be linked to the development of hepatic steatosis and progression of NAFLD/NASH since lower GRK2 levels appear to protect against the induction of several major features of NASH. GRK2+/- mice were partially protected from MCD-dependent hepatic steatosis and inflammation as demonstrated, respectively, by quantification of the TG content and macrophage infiltration and TNFα expression in the liver. Moreover, the anatomopathological analysis of liver tissue samples from WT and GRK2+/- mice fed either CD or MCD established that WT-MCD mice had NASH while GRK2+/- mice were protected against full-blown NASH. These results strongly suggest that keeping hepatic GRK2 levels below a given “pathological" threshold prevents or delays the development of NASH.

The protection against inflammation was further confirmed by checking the activation of JNK1/2, members of the family of stress-activated MAPK that are involved in the pathogenesis of obesity, IR and NAFLD (Hirosumi et al. 2002). JNK activation leads to the transcription of different pro-inflammatory genes, including TNFα and to the inhibitory phosphorylation of IRS1 (Schattenberg et al. 2006). JNK1 is the most important isoform in obesity/IR and in MCD-induced NASH as demonstrated using specific knock-out mice (Schattenberg et al. 2006). Some studies suggest that its activation upon MCD feeding lasts only for a short time (Soon et al. 2010), what would explain why we could not detect a strong activation of JNK1 in the liver of WT mice upon MCD. In any case, this activation was absent in the liver of MCD-fed GRK2+/- mice. Also, the transcription factor STAT3 was phosphorylated after 4 weeks MCD in the liver of WT mice as previously described (Yamaguchi et al. 2010) while this activation was not observed in GRK2+/- animals. Activated STAT3 could be mediating pro-inflammatory effects via the induction of acute phase proteins and chemokines in the liver (Horiguchi et al. 2008) even when it has been also related with anti-inflammatory and anti-steatotic effects (Inoue et al. 2004; Wang et al. 2011). Accordingly with the activation of these two proteins, MCD-induced expression of TNFα was increased in the liver of WT compared to GRK2+/- mice. These results further confirm the existence of an inflammatory signature that is more evident in the liver of WT than in the liver of GRK2+/- mice upon an MCD.

A role for other tissues/ cell types in the phenotype observed for GRK2+/- mice after the MCD dietary intervention cannot be disregarded, as they are global hemizygous mice. However, several pieces of

evidence derived from this work allow us to assign the effect primarily to changes in the levels/function of GRK2 in the liver. First, this diet has been described to mainly affect this tissue. Also, we did not find differences between GRK2+/- and WT MCD-fed mice in global metabolic parameters such as systemic insulin sensitivity, or in circulating levels of NEFA or TG. In this regard, the fact that MCD feeding increases lipolysis in the adipose tissue has been described as the main reason for the weight loss induced by this diet (Jha et al. 2014). However, we did not find differences in circulating NEFA or body weight after the MCD between WT and GRK2+/- mice suggesting that the differences in hepatic steatosis are not due to different release of FA from the adipose tissue. Moreover, methionine restriction produces a chronic increase in SNS outflow to the adipose tissue that causes a coordinated set of changes that limits fat deposition and increases energy expenditure (Plaisance et al. 2010). Thus, based on our previous data showing that Tam-GRK2-/- mice have increased UCP1 in BAT, we cannot rule out that the BAT of GRK2+/- mice could be oxidizing more FA thus helping decrease lipid content in the liver.

Regarding other cell types within the liver, even when hepatocytes represent almost 80% of total liver volume and perform the majority of the hepatic functions, non-parenchymal liver cells, which contribute to only 6.5% of liver volume, account for circa 40% of the total number of liver cells (Kmiec 2001). Among non-parenchymal cells, Kupffer cells/macrophages are of key importance in the liver and particularly during NAFLD (Rivera et al. 2007). Notably, the MCD feeding appears to cause an increase of GRK2 expression levels in hepatocytes and not in Kupffer cells. However, the fact that Kupffer cells/macrophages are also heterozygous for GRK2 forces us to take its potential impact on the phenotype into consideration (further discussed in 1.3).

Molecular and cellular processes modified by changes in GRK2 levels

The greatest phenotypic differences in the MCD model between GRK2+/- and WT mice were found in hepatic lipid accumulation even with similar circulating levels of NEFA and TG in both genotypes. Consistently, WT and GRK2+/- animals display a differential status of signaling routes that control lipid metabolism within the liver in the face of an MCD. PPARγ promotes lipid storage in the liver and its protein levels are increased in steatotic livers (Inoue et al. 2005; Pettinelli and Videla 2011), as we observe in MCD-fed WT animals. Conversely, MCD-fed GRK2+/- mice were able to maintain intact hepatic PPARγ protein levels. Consistent with PPARγ, we found that the protein and mRNA levels of its target gene FAT/CD36, a transmembrane protein that facilitates FA influx, are more increased by the MCD in WT animals, coherently with what is described in murine fatty livers (Miquilena-Colina et al. 2011; Zhou et al. 2008). Another important source of FA in the liver is the activation of DNL, which has an important contribution to hepatic lipid accumulation in NAFLD (Paglialunga and Dehn 2016; Ferre and Foufelle 2010). However, in the MCD-induced NASH model, opposite to what happens in the human pathology, an impairment of DNL takes place when compared to control diet-fed animals (Rizki et al.

2006) in parallel with a concomitant decline in FAS levels (Rinella et al. 2008). Consistently, we found that the expression of FAS dropped in both WT mice and GRK2+/- littermates after the MCD feeding. Overall, we can conclude that upon MCD feeding, low GRK2 levels are able to impinge on lipid accumulation in the liver by mechanisms probably involving PPARγ and CD36-mediated FA influx, but, apparently not FAS, in contrast to what happens in the HFD feeding model, as well as in the human hepatocyte cell line Huh7 in which GRK2 overexpression increased FAS expression. Considering these results altogether, in the human pathology, decreasing GRK2 levels might preclude PPARγ and CD36 upregulation and either help maintain low FAS levels or have no influence on DNL, what could be a good molecular signature to prevent hepatic steatosis.

The excessive lipid accumulation caused by the MCD disturbs the function of the ER in hepatocytes, thereby generating an ER stress response that is however unable to alleviate ER stress in the context of a fatty liver. Furthermore, ER stress responses can promote lipid accumulation in hepatocytes that could trigger further ER stress, thus initiating a positive feedback loop (Baiceanu et al. 2016). As expected, WT mice present increased phosphorylation of the eiF2α transcription factor after the MCD, a well-documented mechanism to downregulate protein synthesis under stress conditions. Conversely, eiF2α is not activated in GRK2+/- animals suggesting decreased ER stress may exist in these mice in response to the MCD. Moreover, the MCD caused the inactivation of p38α MAPK and ERK in the liver of WT mice but not in GRK2+/- mice. p38 MAPK is known to be activated in response to ER stress, however, p38 MAPK inactivation has been also described to induce ER stress via regulation of Xbp1 splicing (Lee et al. 2011). On the other hand, hepatic ERK2 suppresses ER stress and hepatosteatosis *in vivo* (Kujiraoka et al. 2013) and ERK1/2 activation has been suggested to improve NASH in rats (Aghazadeh and Yazdanparast 2010). Moreover, the activation of JNK in the liver of WT mice can also be related with increased ER stress (Urano et al. 2000) compared to GRK2+/- mice, in which this activation was absent, as previously mentioned. According to these markers, GRK2+/- mice do not mount an equivalent ER stress response after the MCD as their WT littermates. This could be due to a direct effect of GRK2 levels on this process, or be a direct consequence of the less important lipid accumulation detected in the livers of GRK2+/- mice. At the molecular level, GRK2 has been described to inhibit both ERK and p38α MAPK (Jurado-Pueyo et al. 2008; Jimenez-Sainz et al. 2006) so, the decreased levels of GRK2 in the liver of GRK2+/- mice could preclude the inactivation of this kinases after the MCD. However, even when ER stress has been implicated in the pathogenesis of NAFLD, reducing ER stress using chaperones do not improve *per se* MCD-induced NASH (Henkel et al. 2012) suggesting that this process might not be the main mechanism underlying the protection against NASH observed in GRK2+/- mice.

The excess of FA in the hepatocyte is usually metabolized in the mitochondria. It is known that energy metabolism depends on mitochondrial biogenesis and dynamics including fission and fusion events, which play significant roles in maintaining mitochondrial function under stress conditions (Kowald and

Kirkwood 2011). In this regard, we found higher mRNA levels of *ppargc1a* (PGC-1α) the master regulator of mitochondrial biogenesis, and its target gene *tfam* in GRK2+/- mice compared to WT what may indicate a preserved mitochondrial biogenesis after the MCD in the liver of these mice. Also, mitochondrial fusion events have a critical role in alleviating hepatic FA accumulation (Galloway et al. 2014) and a decrease in the fusion proteins OPA 1 or mitofusin 2 has been related with NAFLD (Babbar and Sheikh 2013). Such decrease was clearly observed in the livers of WT but not of GRK2+/- mice. These findings are in line with previous data using a long-term HFD model where we found that GRK2+/- mice presented increased levels of mitochondrial fusion markers in cardiac tissue compared with their WT littermates (Lucas et al. 2016). Altogether, these results suggest that GRK2 hemizygous animals preserve mitochondrial fusion events in the face of an MCD-induced metabolic disturbance, which could be associated with increased mitochondrial biogenesis since both processes have been reported to be linked through PGC-1α (Peng et al. 2017). Particularly in the context of mitochondrial functionality, GRK2 has been described to negatively regulate FA oxidation (Sato et al. 2015) and thus MCD-induced GRK2 upregulation could decrease FA catabolism, thereby helping enhance related pathological processes. However, we did not find changes in the levels of Hadha with the MCD, a subunit of the mitochondrial trifunctional protein which catalyzes the last three steps of mitochondrial β-oxidation, as already reported (Gyamfi et al. 2009; Rizki et al. 2006). However, a functional assay would be necessary to assess if GRK2 plays a role in hepatocyte β-oxidation as is described in cardiomyocytes.

When the amount of FA exceeds the capacity of oxidation by the mitochondria they are re-esterified into TG that can be accumulated in lipid droplets. Autophagy can in turn mediate the transformation of lipid droplets into FA. In fact, pharmacological or genetic activation of autophagy decreases lipid content in hepatocytes, while the inhibition of this process increases TG accumulation (Mao et al. 2016). Accordingly, healthy hepatocytes can upregulate autophagy in response to dietary lipid challenge as a mechanism of defense against lipotoxicity (Mao et al. 2016) but, in the context of NAFLD/NASH, lipotoxicity and ER stress results in an impairment of the autophagic flux (Fukuo et al. 2014; Gonzalez-Rodriguez et al. 2014). Coherently, in MCD-fed WT mice we found markers of impaired autophagy such as an accumulation of the p62 protein and the lack of conversion of LC3 I into LC3 II while, as suggested by these markers and the phosphorylation status of AMPK and mTORC1, MCD-fed GRK2+/- mice maintained an active autophagy. Altogether, these results suggest that GRK2+/- mice do not undergo the impairment of the autophagic that takes place after four weeks of MCD feeding in WT mice. This fact may contribute to the decreased hepatic steatosis detected in GRK2 hemizygous mice. Conversely, after only two weeks of MCD feeding, these autophagy markers correlated with increased autophagy in WT mice compared with GRK2+/- mice. Based on these data, we can hypothesize that autophagy is activated earlier upon MCD in WT mice, maybe as a direct effect to try to tackle with increased lipid deposition or by a differential response to the deficit of aminoacids in this diet. However, continuous

lipid accumulation and the earlier activation of ER stress responses would exhaust this process sooner in WT mice resulting in lipotoxicity and in the impairment of autophagy detected after four weeks of MCD. On the contrary, GRK2+/- mice, probably because they have less lipotoxicity and ER stress, would either activate autophagy later, or be able to keep this protective mechanism for a longer period of time, in both cases resulting in the increased autophagy detected at the four weeks time point relative to WT mice.

We are aware that all the aforementioned processes (FA influx, mitochondrial biogenesis, mitochondrial fusion, autophagy or ER stress) can be regarded at the same time the cause or as the consequence of the protection from NASH detected in GRK2+/- mice. It is also noteworthy that all these cellular processes are not independent from one another, but rather interrelated. For example, the fact that GRK2+/- mice preserve mitochondrial fusion mechanisms could help to alleviate lipid accumulation in the liver, thus favoring the decrease in ER stress and avoiding the impairment of autophagy. Also, as accumulation of TG (and especially of derived metabolites such as DAG or ceramides) favors hepatic inflammation (Cusi 2012), the fact that GRK2+/- mice show less lipid accumulation could protect them from the associated hepatitis. Therefore, we cannot definitively conclude from our data whether GRK2 downmodulation is mainly affecting one of these features and, as a consequence, the others are also altered or, alternatively, if low GRK2 levels are affecting simultaneously all of these processes, being the protection against NASH an integrated final output.

Overall, the results obtained from the MCD model show a protective effect of decreasing GRK2 levels on the modulation of several processes that converge in the amelioration of hepatic steatosis and NASH independently of IR and excessive fat mass accretion (Figure D2).

Influence of GRK2 on plasma membrane receptor signaling

The pleiotropic effect of GRK2 on different families of membrane receptors may also affect the progression of the disease from different flanks. In the first place, even if the MCD model does not exhibit systemic IR (Rinella and Green 2004), it has been described that hepatic insulin signaling is impaired in MCD-fed mice (Schattenberg et al. 2005; Schattenberg et al. 2006; Leclercq et al. 2007). In fact, IR accelerates and, conversely, the treatment with the antidiabetic drug pioglitazone attenuates MCD-induced NASH in rats (Ota et al. 2007). Since GRK2 acts as a negative regulator of insulin signaling, it is reasonable to speculate that the augmented levels of GRK2 in hepatocytes could contribute to the pathogenesis of NASH by increasing hepatic IR. On the contrary, reduced GRK2 levels in GRK2+/- mice could also ameliorate the development of the disease via enhancing insulin signaling in the liver.

In the second place, we cannot exclude the possibility that some of the observed effects could be ascribed to the canonical role for GRK2 in GPCR desensitization. In particular, treatment with the β-adrenergic receptor antagonist propranolol enhances liver injury through induction of hepatocyte cell

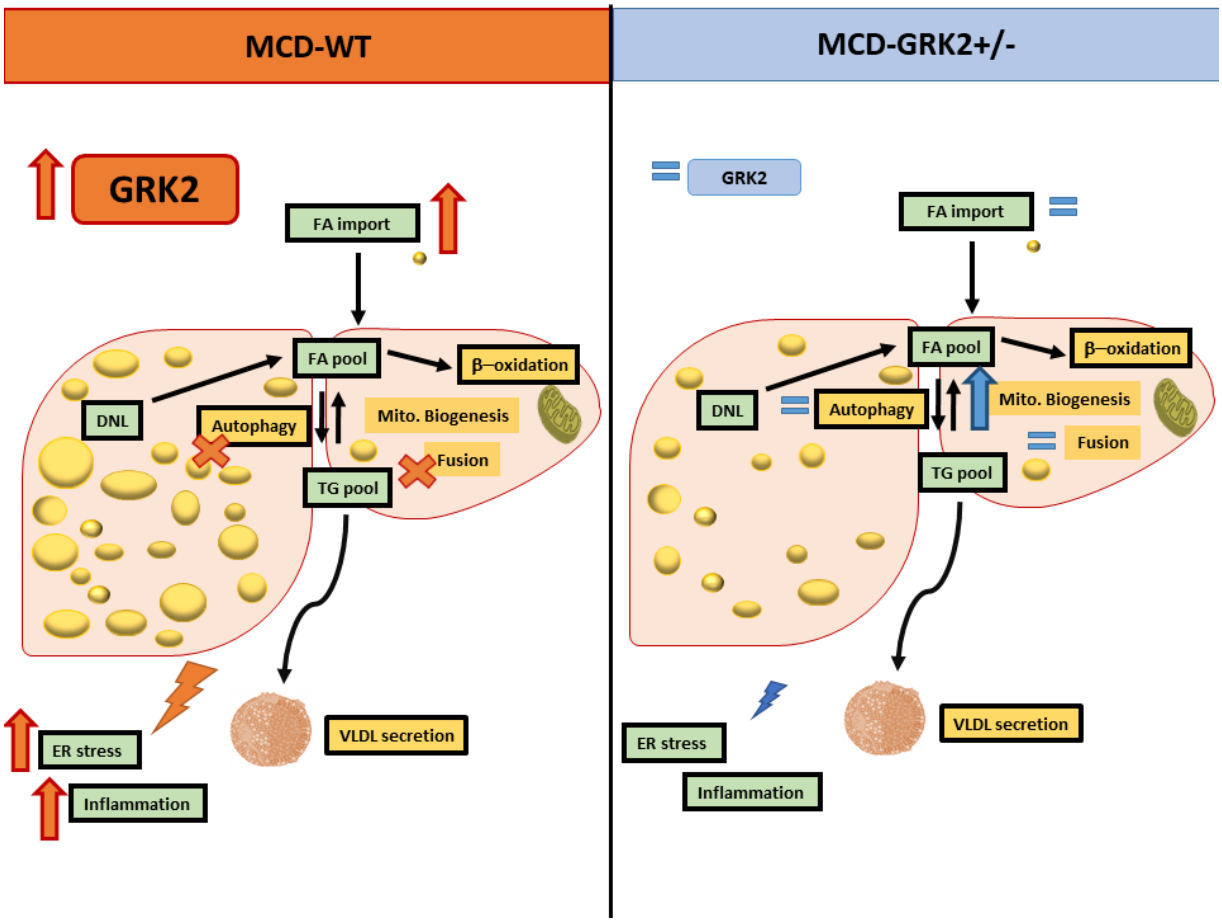

Figure D2. GRK2 contributes to the development of MCD-induced NASH in mice. MCD induced a boost in GRK2 levels in WT mice but not in GRK2+/- mice. WT mice presented increased hepatic TG content induced by the diet compared to GRK2+/- mice and displayed signs of ER stress and inflammation. WT mice had impaired autophagy and mitochondrial fusion together with increased FA influx as suggested by different markers, what could be responsible of the final phenotype observed in these mice that were diagnosed with NASH. However, GRK2+/- mice retained certain hepatic protective mechanisms after the MCD as revealed using markers of autophagy and mitochondrial fusion processes. Moreover, GRK2+/- mice had decreased FA influx and increased mitochondrial biogenesis compared to WT as suggested by mRNA levels of *cd36, ppargc1a* and *tfam* altogether leading to decreased TG accumulation and minor induction of ER stress and inflammation in the liver of MCD-fed GRK2+/- mice.

death (McKee et al. 2013). Also, β-AR stimulation enhances VLDL-TG production by the liver (Geerling et al. 2014) and mobilizes cytosolic lipases for lipid droplets breakdown in hepatocytes (Schott et al. 2017). Finally, it has been shown that the β2-AR agonist clenbuterol stimulates autophagy and autophagic flux in hepatoma cells, primary hepatocytes and *in vivo* (Wauson et al. 2014). Thus, GRK2 through the inhibition of β2-AR signaling could be affecting hepatocyte cell death, lipolysis and autophagy in a manner that would favor the progression of the hepatic disease. However, it has been reported that β-adrenergic agonist treatment induces hepatic lipid accumulation *in vitro* and *in vivo* (Ghosh et al. 2012). Since no hepatic steatosis is found upon GRK2 lowering, other mechanisms and/or tissue-specific effects triggered by GRK2 loss must also be taking place.

Furthermore, the GCGR is another GPCR that can be controlled by GRK2 (Krilov et al. 2011). Glucagon has been shown to improve fatty liver in dairy cows (Bobe et al. 2007) and a GLP1R/glucagon receptor

dual agonist effectively reduces MCD-induced NASH in mice (Valdecantos et al. 2017). In this regard, MCD caused an increase in glucagon levels to the same extent in WT and GRK2+/- mice, but we found that GRK2+/- mice had increased PGC-1α and PEPCK expression in the liver, which can be indicative of increased glucagon signaling and goes in line with the fact that these mice can elicit greater glucose production upon pyruvate administration.

In sum, GRK2 upregulation may have an effect on the development of NASH in part by desensitizing GPCR signaling together or alternatively to its influence on the insulin receptor cascade.

1.3- GRK2 levels and their influence in pathological hepatic steatosis

We have reported in this thesis that GRK2 levels are upregulated in mice with hepatic steatosis, including *db/db*, HFD- and MCD-induced fatty liver. Similarly, GRK2 levels were increased in the liver of *ob/ob* mice (Taguchi et al. 2017) and also in the liver of Sprague-Dawley rats fed a HFD (Charbonneau, Unson, and Lavoie 2007). Very importantly, we also report here that hepatic tissue obtained from patients with NAFLD and NASH express significantly higher levels of GRK2 than those without steatosis in two different cohorts of patients and that in these biopsies GRK2 levels correlated with the degree of steatosis and the NAS of these patients. These data confirm that the rise in GRK2 levels in fatty liver is an event intrinsic to the pathology and conserved between species. The fact that GRK2 levels are also increased in subjects with a BMI<25 with steatosis as well as in overweight and obese subjects compared to normal livers further confirms that GRK2 upregulation occurs in NAFLD independently of the accompanying phenotype.

Moreover, a direct link between GRK2 levels and steatosis was found in human Huh7 cells in which GRK2 upregulation was able *per se* to enhance the accumulation of intracellular TG induced by exposure to palmitic acid. This result provides a proof of concept supporting that GRK2 levels in the liver (specifically hepatocytes) directly affect lipid accumulation under steatosis-promoting conditions. Moreover, the fact that silencing the kinase does not affect lipid accumulation is in line with the idea that a "pathological threshold" exists that marks the influence of GRK2 levels on the pathology. According to this idea, increased levels of GRK2 above a certain threshold would be detrimental for the liver and favor NAFLD onset/progression. Conversely, keeping baseline levels of this kinase would prevent these harmful effects in organisms subjected to metabolic stress and fed a steatotic diet. Furthermore, we have demonstrated that GRK2-overexpressing Huh7 cells exposed to palmitic acid for 24 hours have increased expression of FAS, what can underlie the increased lipid accumulation observed in these cells when compared to control cells. This is in agreement with the results in HFD-fed tamoxifen-treated mice, were control mice have significantly higher levels of FAS than GRK2-depleted animals what suggest that elevated GRK2 may activate DNL through the upregulation of FAS, while decreased levels

of this kinase would not impact the expression of this enzyme. Of note, the fact that in Huh7 cells palmitic acid-induced lipid accumulation does not provoke an increase in GRK2 reflects that the *in vivo* environment of the hepatocytes is quite different to that existing in a cell culture system and points to some circulating hormone/cytokine/metabolite coming from other cell types or tissues as responsible for the modulation of GRK2 levels.

Role of macrophages in GRK2-mediated effects

Macrophages infiltrating adipose tissue during obesity are essential contributors to the development of this condition (Boutens and Stienstra 2016). Kupffer cells, the hepatic resident macrophages, represent the largest group of fixed macrophages in the body and account for about 20–25% of non-parenchymal cells in the liver (Dixon et al. 2013). Lipid accumulation and lipid metabolites (namely FA, ceramides and DAG) in the liver can cause the activation of inflammatory pathways in hepatocytes and inflammatory cells leading to the secretion of pro-inflammatory cytokines altogether causing IR (Petersen and Shulman 2017). Thus, inflammatory cells play an important role in metabolism and specifically Kupffer cells/macrophages are of key importance in NAFLD (Baffy 2009). GRK2 has been described to regulate different functions of macrophages. In this regard, cells producing chemokines act on chemokine receptors (mostly GPCRs), and initiate chemotactic response (Cotton and Claing 2009). GRK2 regulates cell migration and, in most immune cell types, exerts a negative regulation of chemotactic responses consistent with its canonical negative regulatory role in GPCR signaling (Packiriswamy and Parameswaran 2015). Conversely, we do not observe an increase in macrophages in the livers of HFD- or MCD- fed GRK2+/- mice, but even rather a decrease upon the MCD. This can be ascribed to the fact that regulation of chemotaxis is complex as it is both cell type- and stimulus-dependent (Lafarga, Mayor, and Penela 2012; Penela, Nogues, and Mayor 2014) and differences in the secretion of chemokines between WT and GRK2+/- hepatocytes/immune cells may exist, promoting differences in the recruitment/attraction of macrophages to the liver. In the same line, positive and negative effects of GRK2 on cytokines production and signaling have been described. For instance, GRK2+/- primary cultures of macrophages (Peregrin et al. 2006) and microglial cells (Nijboer et al. 2010) have increased LPS-induced TNFα production and GRK2 can negatively regulate LPS-induced NFκB-ERK activation in macrophages (Patial et al. 2011). Conversely, the knockdown of GRK2 in macrophages significantly inhibits NFκB proinflammatory signaling induced by TNFα (Patial et al. 2009). In conclusion, the role of GRK2 in the modulation of inflammatory responses is complex and, in our system, other cell types as hepatocytes might be playing a substantial role in the final anti-inflammatory outcome detected in GRK2 deficient mice. However, to what extent GRK2 dosage within Kupffer cells/macrophages contributes to the phenotypes described upon HFD and MCD remains an issue that deserves future investigation.

PART 2: GRK2 in physiology: adaptation to fasting

Upon fasting, the liver orchestrates the fuel redistribution in the organism to preserve glucose supply to all tissues, especially the brain, and handles the increase in plasma FA coming from WAT lipolysis. In this regard, food deprivation causes a transient physiological state of fatty liver (Lin et al. 2005), serving us as a model of this condition that is independent of obesity and that has, unlike the MCD, lipid accumulation in the absence of inflammation (Mustonen et al. 2013; Mustonen et al. 2012; Xu et al. 2013).

We observed that 24 hours of food deprivation induces more weight loss in GRK2+/- compared to WT mice. This could be ascribed to increased lipolysis (as suggested by the greater plasma FA levels detected in GRK2+/- mice) and explained by a defective desensitization of β-AR, that mediates WAT lipolysis upon fasting (Duncan et al. 2007). In this line, fat depots from Tam-GRK2-/- mice treated with the β-adrenergic agonist isopropanol had a greater lipolytic capacity than equivalent samples from control mice (Vila-Bedmar et al. 2015).

Regarding hepatic lipid accumulation, fasting induced the same extent of fat deposition in the liver in WT and in GRK2+/- mice. These results put forward that fasting-induced steatosis is induced by pathways that are different from those triggering steatosis by an increase in dietary fat supply (HFD model) or a decrease in VLDL production (MCD model). In fact, fasting induces a massive, acute hepatic lipid accumulation very different to the slow, chronic development of steatosis that occurs during NAFLD. Therefore, fasting-induced steatosis would not accurately recapitulate NAFLD. Interestingly, we have shown that fasting does not induce an increase in GRK2 hepatic levels as do HFD and MCD, but, conversely, it markedly decreases hepatic GRK2 protein both in WT and GRK2+/- mice. This could explain the fact that fasting induces a comparable degree of lipid accumulation in the liver of WT and GRK2+/- mice, since both genotypes end up having very low levels of GRK2. Moreover, these results reveal that differences must exist in the mechanisms controlling GRK2 levels in physiological *vs.* pathological steatosis. GRK2 expression is governed, depending on the tissue, cell type and condition, by transcriptional and/or post-transcriptional mechanisms at the level of protein stability (Penela, Ribas, and Mayor 2003). In this regard, GRK2 is a short-lived protein (half-life of 1 h) that undergoes poly-ubiquitination and is mainly degraded by the proteasome (Penela 2016). Thus, the decrease of GRK2 protein might be explained by the increased adrenergic input upon food deprivation, since β-AR activation has been shown to increase GRK2 ubiquitination and degradation (Penela et al. 1998). However, chronic treatment with a β-adrenergic agonist enhances GRK2 mRNA expression in the heart (Iaccarino et al. 1998). Also, growth factors seem to impact the degradation rate of this kinase paving

the way for the possibility that insulin itself could be influencing GRK2 levels (Salcedo, Mayor, and Penela 2006). In fact, chronic treatment with insulin in FL83B liver cells induced increased GRK2 protein expression (Shahid and Hussain 2007) what could explain the rise in GRK2 levels in hyperinsulinemic HFD-fed mice and the drop in fasting, but would not explain GRK2 upregulation in MCD-mice with low insulin levels. Moreover, the activation of ERK can mediate GRK2 degradation (Elorza et al. 2003). The precise mechanisms underlying the regulation of GRK2 protein levels in the liver upon fasting remain to be unveiled.

The decrease of GRK2 levels upon fasting seem to be tissue-specific (since it is not observed in WAT) and also an early but sustained response (already observed at 14h and maintained at 48h). A possible physiological explanation for this decrease could be the facilitation of glucagon signaling. Glucagon is the major hormone orchestrating glucose metabolism in the fasting state and GRK2 has been shown to desensitize the GCGR at least in HEK293 cells (Krilov et al. 2011). Accordingly, GRK2 silencing in primary hepatocytes resulted in an increased response to glucagon in terms of glucose production and *pck1* expression. However, GRK2 overexpression does not seem to have an impact on glucagon signaling. This could be explained by the implication of β-arrestins in the desensitization of the GCGR, specifically β-arrestin 2 (Zhu et al. 2017). In this regard, enhanced GCGR desensitization and internalization would probably require an upregulation of β-arrestin 2 levels in parallel with the increase in GRK2 levels. However, β-arrestins are unchanged in GRK2 overexpressing cells. Conversely, decreasing GRK2 levels impacts glucagon signaling since less kinase would imply less phosphorylated receptor and an inability to recruit arrestins, allowing increased GCGR signaling via G proteins.

GENERAL DISCUSSION: Influence of GRK2 levels in liver adaptation to physiological and pathological metabolic situations

Overall, we have herein described the critical influence of GRK2 levels in the adaptation of the liver to different metabolic stresses such as lipid overload or fasting. GRK2 levels are regulated in the different situations and such differences in dosage might interfere with glucose and lipid handling in the liver.

GRK2 levels are downmodulated upon fasting probably to increase glucagon signaling, as suggested by the results in primary hepatocytes. Interestingly, besides its role in fasting, glucagon has been described to participate in obesity and T2D and these patients present hyperglucagonemia (Knop et al. 2012) what seems to be strongly linked to NAFLD (Junker et al. 2016). Moreover, HFD induces hepatic glucagon resistance (Charbonneau, Couturier, et al. 2005) and the high levels of GRK2 found in the liver in this context could be the related to the lower amount of GCGR in the membrane of the hepatocytes (Charbonneau, Unson, and Lavoie 2007). Conversely, glucagon infusion in cows (Nafikov et al. 2006; Bobe et al. 2003; Bobe et al. 2007) or the treatment with glucagon/GLP1 dual receptor agonists in mice (Valdecantos et al. 2017) have shown to reduce NASH. Moreover, GCGR signaling is essential for the survival of hepatocytes against different pathological stimuli including MCD (Sinclair et al. 2008) and hepatocyte glucose availability is essential in challenging situations as regeneration after partial hepatectomy (Fernandez-Rojo et al. 2012; Lai, Chen, and Chen 1992). Taking all these data into account, improved glucagon signaling could also be contributing to the protection against NASH in GRK2+/- mice as suggested by the increased PEPCK expression found in MCD-fed GRK2+/- mice and in the *in vitro* results. Also, glucagon increases FA oxidation and thermogenesis what could be participating in the protection of Tam-GRK2-/- against HFD-induced excessive fat mass accretion. On the other hand, despite the fact that glucose-raising effects of glucagon are detrimental in the metabolic syndrome context, dual agonists for both GLP1R and GCGR have been shown to be effective in vivo to treat T2D and NASH (Valdecantos et al. 2017; Pocai et al. 2009). Of note, GRK2 has also been shown to translocate to the GLP1R (Jorgensen et al. 2011), and thus low levels of GRK2 could act in a similar way to these new dual agonists allowing for more GLP1 and glucagon signaling at the same time.

On the other hand, altered GRK2 dosage may also affect MAPK cascades. GRK2 phosphorylates p38α MAPK preventing its activation (Peregrin et al. 2006). p38 MAPK plays a key role in several processes including inflammation and ER stress (Nandipati, Subramanian, and Agrawal 2017) and hepatic IR (Liu et al. 2007; Pereira et al. 2016). Regarding p38 MAPK role in the immune system, decreased GRK2 levels can mediate increased LPS-induced cytokine production in macrophages and microglia through p38 MAPK activation (Peregrin et al. 2006; Nijboer et al. 2010). In contrast, p38 MAPK activation has been also described to favor M2-polarization of macrophages upon certain stimuli (Escolano et al. 2014;

Jimenez-Garcia et al. 2015), thus increased p38 MAPK signaling in GRK2+/- or Tam-GRK2-/- mice macrophages could increase polarization towards an M2 anti-inflammatory phenotype. On the subject of ER stress, even if it is counterintuitive due to the main positive role of p38 MAPK in this process, it has also been described that p38 MAPK activation reduces ER stress through stabilization of Xbp1 mRNA and promotion of its nuclear translocation (Lee et al. 2011). Moreover, p38 activation improves glycaemia in obesity (Lee et al. 2011). The interaction of p38 MAPK and GRK2 could be implicated in reduced ER stress in MCD-GRK2+/- mice and also in the improved glycemia upon HFD in mice with low levels of GRK2. Moreover, p38 MAPK also plays a role in gluconeogenesis as it regulates PGC-1α and CREB enhancing PEPCK and G6P transcription (Cao et al. 2005; Collins et al. 2006), and also activates FOXO1 (Asada et al. 2007). In this regard, GRK2 dowmodulation could be affecting PEPCK overexpression through mechanisms involving p38 MAPK. Additionally, p38 MAPK plays important roles in regulating glucose metabolism in skeletal muscle and adipose tissue. p38 MAPK enhances insulin and exercise or AMPK-induced glucose uptake by activating GLUT4 in cultured skeletal muscle cells (McGee and Hargreaves 2006; Geiger et al. 2005) and is a central player in muscle differentiation (Cuenda and Cohen 1999; Perdiguero et al. 2007). In brown adipocytes, p38 MAPK is an indispensable step in the transcription of the UCP1 gene in mice (Cao et al. 2004) and in eWAT modulates adipogenesis and also glucose uptake by GLUT4 (Cao et al. 2007). This pleiotropic role of p38 MAPK implies that some effects that we have detected in animals with low levels of GRK2 in muscle or adipose tissue can be mediated by increased p38 MAPK activity. Conversely, p38 MAPK blocks GRK2 mediated GPCR desensitization (Peregrin et al. 2006; Liu et al. 2012) further complicating the signaling hub that can be stablished between GPCR signaling, p38 MAPK and GRK2.

GRK2 can also bind and inhibit MEK resulting in decreased ERK1/2 activation (Jurado-Pueyo et al. 2008; Jimenez-Sainz et al. 2006). ERK can regulate growth, mitogenesis, and differentiation and is involved in inflammation and ER stress. Furthermore, it is also argued that the ERK1/2 plays a pivotal role in metabolic regulation. Indeed, the activity of ERK has been found to be increased in human and rodent adipose tissue in the diabetic state (Bashan et al. 2007; Bouzakri et al. 2003) and a treatment with an inhibitor of MEK improved IR and glucose intolerance in obese mice (Ozaki et al. 2016). Therefore, the positive effect of lowering GRK2 levels against IR and glucose intolerance cannot be explained through GRK2-mediated inhibition of the MEK-ERK cascade since it should have the opposite consequence. However, ERK inactivation has been related with ER stress as demonstrated in Huh7 cells in which inhibition of MEK increases ER stress in response to palmitate (Kujiraoka et al. 2013). Also, the inhibition of JNK together with the activation of ERK pathway improved MCD-induced NASH in rats (Aghazadeh and Yazdanparast 2010). Therefore, the inactivation of MEK-ERK by GRK2 could explain the decreased ER stress and/or the protection against NASH observed in MCD fed GRK2+/- mice compared with WT.

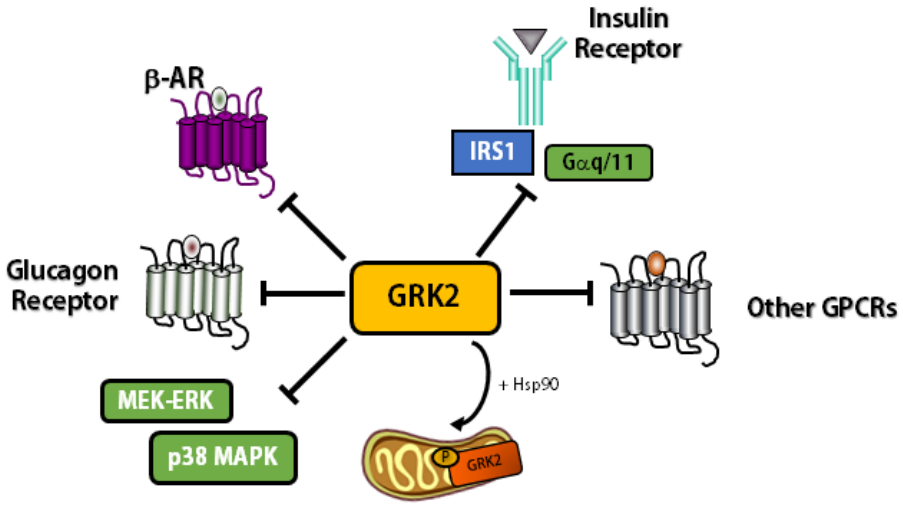

Figure D3. GRK2 establishes a signaling hub thanks to its ability to directly regulate GPCRs and other signaling partners that can lead to different phenotypic outputs depending on the levels/activity of the kinase and the cell/tissue context. GRK2 can directly regulate different GPCRs as β-AR or the GCGR and many other GPCRs including GLP-1. Moreover, GRK2 can modulate the insulin receptor cascade acting as a negative regulator of insulin signaling. Also, it directly inhibits MAPKs as p38 MAPK and the MEK-ERK pathway. Finally, GRK2 can be phosphorylated and translocated to the mitochondria where (at least in cardiomyocytes) can inhibit FA oxidation.

Summing up, a signaling node can be established around GRK2 due to its multiple functions regulating important GPCRs, the insulin receptor cascade, MAPK and others previously described or to be uncovered (Figure D3). Probably because of these multiple actions of GRK2 in metabolism, the levels of this kinase are modulated in the liver different situations.

Altogether, our results strongly suggest a causal relationship between GRK2 levels in hepatocytes and the ability of these cells to accumulate intracellular lipids, and a link between the amount of GRK2 in the liver and the degree of hepatic steatosis and NASH in mice and humans. The observations in human samples suggest that, at least at the level of the regulation of GRK2 expression, the human disease is similar to our animal models. However, the treatment of human patients with a pharmacological GRK2 inhibitor would be necessary to confirm if the reduction of GRK2 function/levels would have a positive impact in the pathology. The results in the genetically-modified mice together with the fact that the levels of GRK2 positively correlate with the degree of steatosis and the NAS of the patients in the liver biopsies encourage us to think that this inhibitor would be effective in humans. In fact, preliminary studies using GRK2 peptide inhibitors have proven useful in ameliorating parameters related to glucose homeostasis in animal models of diabetes (Anis et al. 2004), and exercise, which has a beneficial role in T2D, reduces GRK2 levels in the heart (Leosco et al. 2007). GRK2 plays different roles in several tissues (Figure D49) but a recently published work that further confirms our results also demonstrate that decreasing GRK2 expression specifically in the liver improves glucose tolerance and insulin sensitivity in *ob/ob* mice (Taguchi et al. 2017). This study encourages us to speculate that GRK2 levels in the liver are of great importance for the phenotype observed in our global GRK2+/- and GRK2 -/- mice.

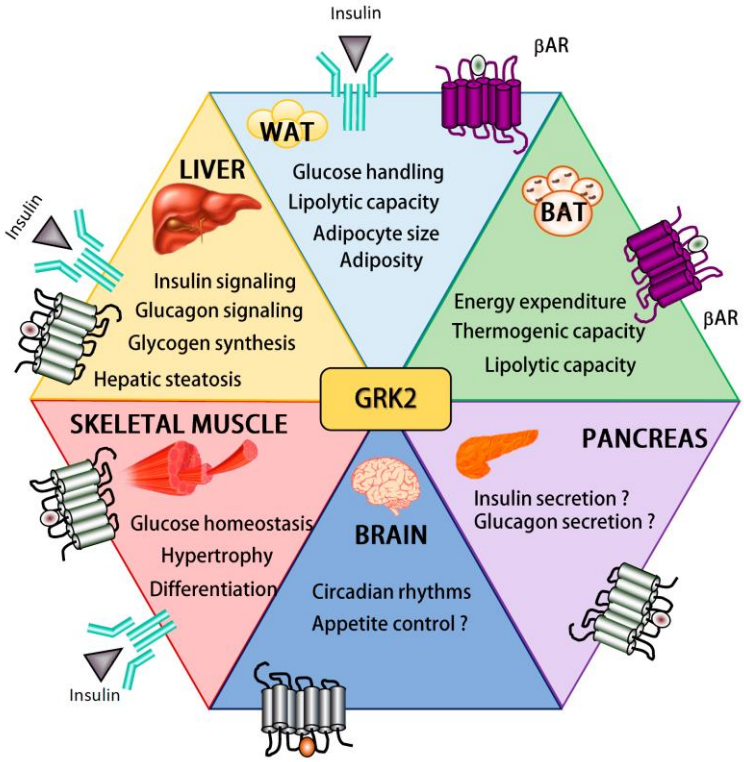

Figure D4. GRK2 as a multi-organ regulator of metabolism. GRK2 plays a central role in the orchestration of GPCR and insulin signaling in pivotal metabolic organs, and the modulation of GRK2 dosage has an important effect in glucose handling, thermogenesis, energy expenditure, metabolic flexibility, adiposity or steatosis, among others. (Adapted from Mayor et al,2018).

The fact that GRK2 reduction prevents steatosis and inflammation and ameliorates NAFLD/NASH additionally to preserving insulin sensitivity within the liver further highlights GRK2 as a potential target for the treatment of obese and non-obese NASH. Additionally, NAFLD frequently appears together with other comorbidities such as cardiovascular disease, in which GRK2 role has been extensively studied and its downmodulation has been also described to play a beneficial role (Mayor et al. 2018). In this regard, GRK2 is known to modulate GPCR and insulin responses in cardiac dysfunction (Lymperopoulos, Rengo, and Koch 2012; Schumacher et al. 2015; Mayor et al. 2018; Lucas et al. 2014), hypertension (Taguchi et al. 2012; Avendano et al. 2014) and also in cardiac hypertrophy in steatosis contexts (Lucas et al. 2016).

Therefore, targeting GRK2 could promote distinct effects in multiple tissues resulting in an improvement of the different pathological features of the metabolic syndrome not only at the systemic level but probably also through tissue-specific effects. It is tempting to suggest that selective peptidic or small molecule inhibitors of GRK2 (Homan and Tesmer 2014; Schumacher et al. 2015) and other potential GRK2 inhibitors may hold great promise for the treatment of T2D and related diseases and also of NAFLD independently of the accompanying metabolic profile.

CONCLUSSIONS/CONCLUSIONES

1. Hepatic GRK2 protein levels are upregulated in different mouse models of obesity-associated steatosis, including high-fat diet (HFD)-feeding and the *db/db* genetic model. GRK2+/- littermates are protected from HFD-induced hepatic steatosis induced by this diet and do not upregulate GRK2 in the liver.

2. Inducible genetic ablation of GRK2 in mice during a HFD feeding impairs further body weight gain, and is able to revert the already established glucose intolerance and insulin resistance. The improved glucose handling of HFD-fed tamoxifen-induced GRK2 knockout mice (Tam-GRK2-/-) is preserved under β-adrenergic blockade indicating that the effect of GRK2 on glucose homeostasis does not solely depend on β-adrenergic signaling.

3. GRK2 dowmodulation in the middle of a HFD also reverts NAFLD, enhances hepatic insulin sensitivity, and limits lipid accumulation. It also decreases inflammatory signs and molecular markers of inflammation with a decreased M1-polarization of macrophages. Furthermore, Tam-GRK2-/- mice show decreased adipose tissue weight after the HFD together with an increased lipolytic response. Moreover, Tam-GRK2-/- mice present enhanced UCP1 expression in brown adipose tissue, and this tissue displays a morphology consistent with a better thermogenic capacity.

4. A methionine and choline deficient (MCD) diet, a model of non-obese non-alcoholic steatohepatitis (NASH), induces a rise in liver GRK2 protein levels in WT mice but not GRK2+/- animals, which occurs in hepatocytes but not in Kupffer cells. GRK2 +/- mice are protected from overt non-obese NASH induced by this diet: they show reduced hepatic triglyceride accumulation, decreased expression of CD36, and less signs of inflammation in the liver. They also preserve several protective mechanisms such as enhanced autophagy and mitochondrial biogenesis and fusion, while displaying reduced markers of endoplasmic reticulum stress. Moreover, GRK2+/- mice show a preserved gluconeogenic capacity in response to a pyruvate challenge in parallel with increased PEPCK (*pck1*) mRNA expression.

5. GRK2 protein and mRNA levels are increased in human liver biopsies from simple steatosis or NASH patients compared to individuals with normal liver histology. Moreover, overexpressing GRK2 in Huh7 human hepatoma cells induces greater palmitic acid-induced steatosis and increased FAS expression thus establishing a cause-effect relationship between GRK2 levels and intracellular lipid accumulation in hepatocytes.

6. Fasting induces a degree of hepatic steatosis and a decrease in hepatic GRK2 levels that are similar in WT and in GRK2+/- mice. This downregulation of GRK2 protein levels appears to be specific of hepatic tissue. On the other hand, GRK2+/- mice lose more weight and show enhanced fasting NEFA and glucose levels compared to WT littermates. Silencing GRK2 levels in mouse primary hepatocytes increases glucagon-induced glucose production and also *pck1* mRNA expression what indicates that GRK2 is involved in regulating the response to glucagon during fasting.

7. Overall, our results point at GRK2 as a hub able to regulate different intracellular routes that control metabolic responses in vivo and consolidate this kinase as a prospective therapeutic target in diseases with a metabolic component such as IR, obesity and NAFLD.

1. Los niveles de proteicos de GRK2 están aumentados en el hígado en diferentes modelos murinos de esteatosis hepática asociada a obesidad, incluyendo el modelo de alimentación con dieta rica en grasa (HFD) y el modelo genético *db/db*. Los animales GRK2+/- están protegidos frente a la esteatosis hepática así como frente al aumento de los niveles hepáticos de GRK2 inducidos por esta dieta.

2. La reducción de GRK2 inducida por tamoxifeno (ratones Tam-GRK2-/-) en animales que están siendo alimentados con una dieta alta en grasa impide el consiguiente aumento del peso corporal y revierte la intolerancia a la glucosa y la resistencia a la insulina previamente provocadas por la dieta. Los animales Tam-GRK2-/- preservan una mejor tolerancia a la glucosa tras la dieta incluso en presencia de antagonistas β-adrenérgicos, indicando que el efecto de GRK2 sobre la homeostasis glucídica no depende únicamente de sus efectos en la señalización mediada por estos receptores.

3. La depleción de GRK2 durante la dieta alta en grasa revierte la enfermedad de hígado graso no alcohólica (NAFLD). Los ratones Tam-GRK2-/- presentan una mayor sensibilidad hepática a la insulina, menor acumulación de grasa en el hígado y menos signos de inflamación tras la dieta. Además, el peso del tejido adiposo de estos ratones es menor tras la dieta que en animales control, lo que es coherente con su mayor respuesta lipolítica frente al ayuno. Estos animales Tam-GRK2-/- expresan más UCP1 y muestran una morfología consistente con una mejor capacidad termogénica en tejido adiposo marrón después de la HFD.

4. La alimentación con dieta deficiente en metionina y colina (MCD), como modelo de esteatohepatitis no alcohólica (NASH) no relacionada con obesidad, induce un aumento en los niveles proteicos de GRK2 en el hígado en ratones silvestres (WT) pero no en animales GRK2+/-. Este incremento ocurre en los hepatocitos y no en las células de Kupffer. Los animales GRK2+/- alimentados con MCD están protegidos frente a NASH: muestran menor acumulación de triglicéridos hepáticos y menos evidencias de inflamación y estrés de retículo en el hígado. También conservan varios mecanismos de protección frente a NASH, como la autofagia, y una mayor biogénesis y fusión mitocondrial, además de mantener una mayor capacidad gluconeogénica en respuesta a piruvato en paralelo con una mayor expresión del mRNA de PEPCK (*pck1*).

5. Los niveles de proteína y mRNA de GRK2 están aumentados en biopsias hepáticas de pacientes con esteatosis simple o NASH en comparación con individuos con histología hepática normal. Además, la sobreexpresión de GRK2 en una línea de células hepáticas humanas aumenta la esteatosis por ácido palmítico y la expresión de FAS, estableciendo así una relación causa-efecto entre GRK2 y la acumulación de lípidos.

6. El ayuno induce un grado de esteatosis hepática que es similar en animales WT y GRK2 +/- y una reducción en los niveles proteicos de GRK2 en el hígado en ambos genotipos. Esta disminución parece ser específica del tejido hepático. Por otro lado, los ratones GRK2 +/- pierden más peso y muestran mayores niveles de ácidos grasos circulantes y de glucosa en ayunas en comparación con animales control. El silenciamiento de GRK2 en hepatocitos primarios de ratón aumenta la producción de glucosa y la expresión de la enzima gluconeogénica *pck1* en respuesta a glucagón.

7. Nuestros resultados consolidan a GRK2 como una posible diana terapéutica en enfermedades con un componente metabólico como la resistencia a insulina, la obesidad y la enfermedad de hígado graso.

BIBLIOGRAPHY

Aghazadeh, S., and R. Yazdanparast. 2010. 'Inhibition of JNK along with activation of ERK1/2 MAPK pathways improve steatohepatitis among the rats', *Clin Nutr*, 29: 381-5.

Akazawa, Y., S. Cazanave, J. L. Mott, N. Elmi, S. F. Bronk, S. Kohno, M. R. Charlton, and G. J. Gores. 2010. 'Palmitoleate attenuates palmitate-induced Bim and PUMA up-regulation and hepatocyte lipoapoptosis', *J Hepatol*, 52: 586-93.

Alers, S., A. S. Loffler, S. Wesselborg, and B. Stork. 2012. 'Role of AMPK-mTOR-Ulk1/2 in the regulation of autophagy: cross talk, shortcuts, and feedbacks', *Mol Cell Biol*, 32: 2-11.

Alsabeeh, N., B. Chausse, P. A. Kakimoto, A. J. Kowaltowski, and O. Shirihai. 2018. 'Cell culture models of fatty acid overload: Problems and solutions', *Biochim Biophys Acta*, 1863: 143-51.

Andersen, C. L., J. L. Jensen, and T. F. Orntoft. 2004. 'Normalization of real-time quantitative reverse transcription-PCR data: a model-based variance estimation approach to identify genes suited for normalization, applied to bladder and colon cancer data sets', *Cancer Res*, 64: 5245-50.

Anis, Y., O. Leshem, H. Reuveni, I. Wexler, R. Ben Sasson, B. Yahalom, M. Laster, I. Raz, S. Ben Sasson, E. Shafrir, and E. Ziv. 2004. 'Antidiabetic effect of novel modulating peptides of G-protein-coupled kinase in experimental models of diabetes', *Diabetologia*, 47: 1232-44.

Anstee, Q. M., and R. D. Goldin. 2006. 'Mouse models in non-alcoholic fatty liver disease and steatohepatitis research', *Int J Exp Pathol*, 87: 1-16.

Asada, S., H. Daitoku, H. Matsuzaki, T. Saito, T. Sudo, H. Mukai, S. Iwashita, K. Kako, T. Kishi, Y. Kasuya, and A. Fukamizu. 2007. 'Mitogen-activated protein kinases, Erk and p38, phosphorylate and regulate Foxo1', *Cell Signal*, 19: 519-27.

Asrih, M., and F. R. Jornayvaz. 2013. 'Inflammation as a potential link between nonalcoholic fatty liver disease and insulin resistance', *J Endocrinol*, 218: R25-36.

Avendano, M. S., E. Lucas, M. Jurado-Pueyo, S. Martinez-Revelles, R. Vila-Bedmar, F. Mayor, Jr., M. Salaices, A. M. Briones, and C. Murga. 2014. 'Increased nitric oxide bioavailability in adult GRK2 hemizygous mice protects against angiotensin II-induced hypertension', *Hypertension*, 63: 369-75.

Babbar, M., and M. S. Sheikh. 2013. 'Metabolic Stress and Disorders Related to Alterations in Mitochondrial Fission or Fusion', *Mol Cell Pharmacol*, 5: 109-33.

Bachmanov, A. A., D. R. Reed, G. K. Beauchamp, and M. G. Tordoff. 2002. 'Food intake, water intake, and drinking spout side preference of 28 mouse strains', *Behav Genet*, 32: 435-43.

Baffy, G. 2009. 'Kupffer cells in non-alcoholic fatty liver disease: the emerging view', *J Hepatol*, 51: 212-23.

Baiceanu, A., P. Mesdom, M. Lagouge, and F. Foufelle. 2016. 'Endoplasmic reticulum proteostasis in hepatic steatosis', *Nat Rev Endocrinol*, 12: 710-22.

Band, G. C., and C. T. Jones. 1980. 'Functional activation by glucagon of glucose 6-phosphatase and gluconeogenesis in the perfused liver of the fetal guinea pig', *FEBS Lett*, 119: 190-4.

Bashan, N., K. Dorfman, T. Tarnovscki, I. Harman-Boehm, I. F. Liberty, M. Bluher, S. Ovadia, T. Maymon-Zilberstein, R. Potashnik, M. Stumvoll, E. Avinoach, and A. Rudich. 2007. 'Mitogen-activated protein kinases, inhibitory-kappaB kinase, and insulin signaling in human omental versus subcutaneous adipose tissue in obesity', *Endocrinology*, 148: 2955-62.

Baumruk, F., P. Flachs, M. Horakova, D. Floryk, and J. Kopecky. 1999. 'Transgenic UCP1 in white adipocytes modulates mitochondrial membrane potential', *FEBS Lett*, 444: 206-10.

Bechmann, L. P., R. K. Gieseler, J. P. Sowa, A. Kahraman, J. Erhard, I. Wedemeyer, B. Emons, C. Jochum, T. Feldkamp, G. Gerken, and A. Canbay. 2010. 'Apoptosis is associated with CD36/fatty acid translocase upregulation in non-alcoholic steatohepatitis', *Liver Int*, 30: 850-9.

Bedossa, P., C. Poitou, N. Veyrie, J. L. Bouillot, A. Basdevant, V. Paradis, J. Tordjman, and K. Clement. 2012. 'Histopathological algorithm and scoring system for evaluation of liver lesions in morbidly obese patients', *Hepatology*, 56: 1751-9.

Begriche, K., A. Igoudjil, D. Pessayre, and B. Fromenty. 2006. 'Mitochondrial dysfunction in NASH: causes, consequences and possible means to prevent it', *Mitochondrion*, 6: 1-28.

Benveniste, R., T. M. Danoff, J. Ilekis, and H. R. Craig. 1988. 'Epidermal growth factor receptor numbers in male and female mouse primary hepatocyte cultures', *Cell Biochem Funct*, 6: 231-5.

Berk, P. D. 2008. 'Regulatable fatty acid transport mechanisms are central to the pathophysiology of obesity, fatty liver, and metabolic syndrome', *Hepatology*, 48: 1362-76.

Berlanga, A., E. Guiu-Jurado, J. A. Porras, and T. Auguet. 2014. 'Molecular pathways in non-alcoholic fatty liver disease', *Clin Exp Gastroenterol*, 7: 221-39.

Bevilacqua, S., R. Bonadonna, G. Buzzigoli, C. Boni, D. Ciociaro, F. Maccari, M. A. Giorico, and E. Ferrannini. 1987. 'Acute elevation of free fatty acid levels leads to hepatic insulin resistance in obese subjects', *Metabolism*, 36: 502-6.

Bjornsson, O. G., J. D. Sparks, C. E. Sparks, and G. F. Gibbons. 1994. 'Regulation of VLDL secretion in primary culture of rat hepatocytes: involvement of cAMP and cAMP-dependent protein kinases', *Eur J Clin Invest*, 24: 137-48.

Bobe, G., B. N. Ametaj, J. W. Young, L. L. Anderson, and D. C. Beitz. 2007. 'Exogenous glucagon effects on health and reproductive performance of lactating dairy cows with mild fatty liver', *Anim Reprod Sci*, 102: 194-207.

Bobe, G., B. N. Ametaj, J. W. Young, and D. C. Beitz. 2003. 'Effects of exogenous glucagon on lipids in lipoproteins and liver of lactating dairy cows', *J Dairy Sci*, 86: 2895-903.

Boden, G. 2005. 'Free fatty acids and insulin secretion in humans', *Curr Diab Rep*, 5: 167-70.

Boland, M. L., A. H. Chourasia, and K. F. Macleod. 2013. 'Mitochondrial dysfunction in cancer', *Front Oncol*, 3: 292.

Bologna, Z., J. P. Teoh, A. S. Bayoumi, Y. Tang, and I. M. Kim. 2017. 'Biased G Protein-Coupled Receptor Signaling: New Player in Modulating Physiology and Pathology', *Biomol Ther (Seoul)*, 25: 12-25.

Boucher, J., A. Kleinridders, and C. R. Kahn. 2014. 'Insulin receptor signaling in normal and insulin-resistant states', *Cold Spring Harb Perspect Biol*, 6.

Boutens, L., and R. Stienstra. 2016. 'Adipose tissue macrophages: going off track during obesity', *Diabetologia*, 59: 879-94.

Bouzakri, K., M. Roques, P. Gual, S. Espinosa, F. Guebre-Egziabher, J. P. Riou, M. Laville, Y. Le Marchand-Brustel, J. F. Tanti, and H. Vidal. 2003. 'Reduced activation of phosphatidylinositol-3 kinase and increased serine 636 phosphorylation of insulin receptor substrate-1 in primary culture of skeletal muscle cells from patients with type 2 diabetes', *Diabetes*, 52: 1319-25.

Boyda, H. N., R. M. Procyshyn, C. C. Pang, and A. M. Barr. 2013. 'Peripheral adrenoceptors: the impetus behind glucose dysregulation and insulin resistance', *J Neuroendocrinol*, 25: 217-28.

Brown, M. S., and J. L. Goldstein. 2008. 'Selective versus total insulin resistance: a pathogenic paradox', *Cell Metab*, 7: 95-6.

Buzzetti, E., M. Pinzani, and E. A. Tsochatzis. 2016. 'The multiple-hit pathogenesis of non-alcoholic fatty liver disease (NAFLD)', *Metabolism*, 65: 1038-48.

Caldwell, S. H., R. H. Swerdlow, E. M. Khan, J. C. Iezzoni, E. E. Hespenheide, J. K. Parks, and W. D. Parker, Jr. 1999. 'Mitochondrial abnormalities in non-alcoholic steatohepatitis', *J Hepatol*, 31: 430-4.

Cannon, B., and J. Nedergaard. 2004. 'Brown adipose tissue: function and physiological significance', *Physiol Rev*, 84: 277-359.

Cao, W., Q. F. Collins, T. C. Becker, J. Robidoux, E. G. Lupo, Jr., Y. Xiong, K. W. Daniel, L. Floering, and S. Collins. 2005. 'p38 Mitogen-activated protein kinase plays a stimulatory role in hepatic gluconeogenesis', *J Biol Chem*, 280: 42731-7.

Cao, W., K. W. Daniel, J. Robidoux, P. Puigserver, A. V. Medvedev, X. Bai, L. M. Floering, B. M. Spiegelman, and S. Collins. 2004. 'p38 mitogen-activated protein kinase is the central regulator of cyclic AMP-dependent transcription of the brown fat uncoupling protein 1 gene', *Mol Cell Biol*, 24: 3057-67.

Cao, W. H., Y. Xiong, Q. F. Collins, and H. Y. Liu. 2007. 'p38 mitogen-activated protein kinase plays a critical role in the control of energy metabolism and development of cardiovascular diseases', *Zhong Nan Da Xue Xue Bao Yi Xue Ban*, 32: 1-14.

Chan, D. C. 2006. 'Mitochondria: dynamic organelles in disease, aging, and development', *Cell*, 125: 1241-52.

Charbonneau, A., K. Couturier, M. S. Gauthier, and J. M. Lavoie. 2005. 'Evidence of hepatic glucagon resistance associated with hepatic steatosis: reversal effect of training', *Int J Sports Med*, 26: 432-41.

Charbonneau, A., A. Melancon, C. Lavoie, and J. M. Lavoie. 2005. 'Alterations in hepatic glucagon receptor density and in Gsalpha and Gialpha2 protein content with diet-induced hepatic steatosis: effects of acute exercise', *Am J Physiol Endocrinol Metab*, 289: E8-14.

Charbonneau, A., C. G. Unson, and J. M. Lavoie. 2007. 'High-fat diet-induced hepatic steatosis reduces glucagon receptor content in rat hepatocytes: potential interaction with acute exercise', *J Physiol*, 579: 255-67.

Chiang, D. J., M. T. Pritchard, and L. E. Nagy. 2011. 'Obesity, diabetes mellitus, and liver fibrosis', *Am J Physiol Gastrointest Liver Physiol*, 300: G697-702.

Ciccarelli, M., J. K. Chuprun, G. Rengo, E. Gao, Z. Wei, R. J. Peroutka, J. I. Gold, A. Gumpert, M. Chen, N. J. Otis, G. W. Dorn, 2nd, B. Trimarco, G. Iaccarino, and W. J. Koch. 2011. 'G protein-coupled receptor kinase 2 activity impairs cardiac glucose uptake and promotes insulin resistance after myocardial ischemia', *Circulation*, 123: 1953-62.

Ciccarelli, M., E. Cipolletta, and G. Iaccarino. 2012. 'GRK2 at the control shaft of cellular metabolism', *Curr Pharm Des*, 18: 121-7.

Cinti, S., G. Mitchell, G. Barbatelli, I. Murano, E. Ceresi, E. Faloia, S. Wang, M. Fortier, A. S. Greenberg, and M. S. Obin. 2005. 'Adipocyte death defines macrophage localization and function in adipose tissue of obese mice and humans', *J Lipid Res*, 46: 2347-55.

Cipolletta, E., A. Campanile, G. Santulli, E. Sanzari, D. Leosco, P. Campiglia, B. Trimarco, and G. Iaccarino. 2009. 'The G protein coupled receptor kinase 2 plays an essential role in beta-adrenergic receptor-induced insulin resistance', *Cardiovasc Res*, 84: 407-15.

Ciudad, C., M. Camici, Z. Ahmad, Y. Wang, A. A. DePaoli-Roach, and P. J. Roach. 1984. 'Control of glycogen synthase phosphorylation in isolated rat hepatocytes by epinephrine, vasopressin and glucagon', *Eur J Biochem*, 142: 511-20.

Cohen, J. C., J. D. Horton, and H. H. Hobbs. 2011. 'Human fatty liver disease: old questions and new insights', *Science*, 332: 1519-23.

Collins, Q. F., Y. Xiong, E. G. Lupo, Jr., H. Y. Liu, and W. Cao. 2006. 'p38 Mitogen-activated protein kinase mediates free fatty acid-induced gluconeogenesis in hepatocytes', *J Biol Chem*, 281: 24336-44.

Collins, S., E. Yehuda-Shnaidman, and H. Wang. 2010. 'Positive and negative control of Ucp1 gene transcription and the role of beta-adrenergic signaling networks', *Int J Obes (Lond)*, 34 Suppl 1: S28-33.

Cotton, M., and A. Claing. 2009. 'G protein-coupled receptors stimulation and the control of cell migration', *Cell Signal*, 21: 1045-53.

Cross, D. A., D. R. Alessi, P. Cohen, M. Andjelkovich, and B. A. Hemmings. 1995. 'Inhibition of glycogen synthase kinase-3 by insulin mediated by protein kinase B', *Nature*, 378: 785-9.

Cuenda, A., and P. Cohen. 1999. 'Stress-activated protein kinase-2/p38 and a rapamycin-sensitive pathway are required for C2C12 myogenesis', *J Biol Chem*, 274: 4341-6.

Cusi, K. 2012. 'Role of obesity and lipotoxicity in the development of nonalcoholic steatohepatitis: pathophysiology and clinical implications', *Gastroenterology*, 142: 711-25 e6.

Cypess, A. M., and C. R. Kahn. 2010. 'Brown fat as a therapy for obesity and diabetes', *Curr Opin Endocrinol Diabetes Obes*, 17: 143-9.

Dallner, O. S., E. Chernogubova, K. A. Brolinson, and T. Bengtsson. 2006. 'Beta3-adrenergic receptors stimulate glucose uptake in brown adipocytes by two mechanisms independently of glucose transporter 4 translocation', *Endocrinology*, 147: 5730-9.

de Almeida, I. T., H. Cortez-Pinto, G. Fidalgo, D. Rodrigues, and M. E. Camilo. 2002. 'Plasma total and free fatty acids composition in human non-alcoholic steatohepatitis', *Clin Nutr*, 21: 219-23.

DeFronzo, R. A., and D. Tripathy. 2009. 'Skeletal muscle insulin resistance is the primary defect in type 2 diabetes', *Diabetes Care*, 32 Suppl 2: S157-63.

Deter, R. L., P. Baudhuin, and C. De Duve. 1967. 'Participation of lysosomes in cellular autophagy induced in rat liver by glucagon', *J Cell Biol*, 35: C11-6.

Dixon, L. J., M. Barnes, H. Tang, M. T. Pritchard, and L. E. Nagy. 2013. 'Kupffer cells in the liver', *Compr Physiol*, 3: 785-97.

Donnelly, K. L., C. I. Smith, S. J. Schwarzenberg, J. Jessurun, M. D. Boldt, and E. J. Parks. 2005. 'Sources of fatty acids stored in liver and secreted via lipoproteins in patients with nonalcoholic fatty liver disease', *J Clin Invest*, 115: 1343-51.

Duncan, R. E., M. Ahmadian, K. Jaworski, E. Sarkadi-Nagy, and H. S. Sul. 2007. 'Regulation of lipolysis in adipocytes', *Annu Rev Nutr*, 27: 79-101.

Eaton, R. P. 1973. 'Hypolipemic action of glucagon in experimental endogenous lipemia in the rat', *J Lipid Res*, 14: 312-8.

Eckel, R. H., S. M. Grundy, and P. Z. Zimmet. 2005. 'The metabolic syndrome', *Lancet*, 365: 1415-28.

Ekstedt, M., H. Hagstrom, P. Nasr, M. Fredrikson, P. Stal, S. Kechagias, and R. Hultcrantz. 2015. 'Fibrosis stage is the strongest predictor for disease-specific mortality in NAFLD after up to 33 years of follow-up', *Hepatology*, 61: 1547-54.

Elorza, A., P. Penela, S. Sarnago, and F. Mayor, Jr. 2003. 'MAPK-dependent degradation of G protein-coupled receptor kinase 2', *J Biol Chem*, 278: 29164-73.

Erion, D. M., and G. I. Shulman. 2010. 'Diacylglycerol-mediated insulin resistance', *Nature medicine*, 16: 400-2.

Escolano, A., S. Martinez-Martinez, A. Alfranca, K. Urso, H. M. Izquierdo, M. Delgado, F. Martin, G. Sabio, D. Sancho, P. Gomez-del Arco, and J. M. Redondo. 2014. 'Specific calcineurin targeting in macrophages confers resistance to inflammation via MKP-1 and p38', *EMBO J*, 33: 1117-33.

Farah, B. L., R. A. Sinha, Y. Wu, B. K. Singh, J. Zhou, B. H. Bay, and P. M. Yen. 2014. 'beta-Adrenergic agonist and antagonist regulation of autophagy in HepG2 cells, primary mouse hepatocytes, and mouse liver', *PLoS One*, 9: e98155.

Fernandez-Rojo, M. A., C. Restall, C. Ferguson, N. Martel, S. Martin, M. Bosch, A. Kassan, G. M. Leong, S. D. Martin, S. L. McGee, G. E. Muscat, R. L. Anderson, C. Enrich, A. Pol, and R. G. Parton. 2012. 'Caveolin-1 orchestrates the balance between glucose and lipid-dependent energy metabolism: implications for liver regeneration', *Hepatology*, 55: 1574-84.

Ferre, P., and F. Foufelle. 2010. 'Hepatic steatosis: a role for de novo lipogenesis and the transcription factor SREBP-1c', *Diabetes Obes Metab*, 12 Suppl 2: 83-92.

Foster, D. W. 2012. 'Malonyl-CoA: the regulator of fatty acid synthesis and oxidation', *J Clin Invest*, 122: 1958-9.

Fukuo, Y., S. Yamashina, H. Sonoue, A. Arakawa, E. Nakadera, T. Aoyama, A. Uchiyama, K. Kon, K. Ikejima, and S. Watanabe. 2014. 'Abnormality of autophagic function and cathepsin expression in the liver from patients with non-alcoholic fatty liver disease', *Hepatol Res*, 44: 1026-36.

Gaidhu, M. P., N. M. Anthony, P. Patel, T. J. Hawke, and R. B. Ceddia. 2010. 'Dysregulation of lipolysis and lipid metabolism in visceral and subcutaneous adipocytes by high-fat diet: role of ATGL, HSL, and AMPK', *Am J Physiol Cell Physiol*, 298: C961-71.

Galloway, C. A., H. Lee, P. S. Brookes, and Y. Yoon. 2014. 'Decreasing mitochondrial fission alleviates hepatic steatosis in a murine model of nonalcoholic fatty liver disease', *Am J Physiol Gastrointest Liver Physiol*, 307: G632-41.

Gao, Z., A. Zuberi, M. J. Quon, Z. Dong, and J. Ye. 2003. 'Aspirin inhibits serine phosphorylation of insulin receptor substrate 1 in tumor necrosis factor-treated cells through targeting multiple serine kinases', *The Journal of biological chemistry*, 278: 24944-50.

Garcia-Guerra, L., I. Nieto-Vazquez, R. Vila-Bedmar, M. Jurado-Pueyo, G. Zalba, J. Diez, C. Murga, S. Fernandez-Veledo, F. Mayor, Jr., and M. Lorenzo. 2010. 'G protein-coupled receptor kinase 2 plays a relevant role in insulin resistance and obesity', *Diabetes*, 59: 2407-17.

Geerling, J. J., M. R. Boon, S. Kooijman, E. T. Parlevliet, L. M. Havekes, J. A. Romijn, I. M. Meurs, and P. C. Rensen. 2014. 'Sympathetic nervous system control of triglyceride metabolism: novel concepts derived from recent studies', *J Lipid Res*, 55: 180-9.

Geiger, P. C., D. C. Wright, D. H. Han, and J. O. Holloszy. 2005. 'Activation of p38 MAP kinase enhances sensitivity of muscle glucose transport to insulin', *Am J Physiol Endocrinol Metab*, 288: E782-8.

Ghosh, P. M., Z. J. Shu, B. Zhu, Z. Lu, Y. Ikeno, J. L. Barnes, C. K. Yeh, B. X. Zhang, M. S. Katz, and A. Kamat. 2012. 'Role of beta-adrenergic receptors in regulation of hepatic fat accumulation during aging', *J Endocrinol*, 213: 251-61.

Gonzalez-Rodriguez, A., R. Mayoral, N. Agra, M. P. Valdecantos, V. Pardo, M. E. Miquilena-Colina, J. Vargas-Castrillon, O. Lo Iacono, M. Corazzari, G. M. Fimia, M. Piacentini, J. Muntane, L. Bosca, C. Garcia-Monzon, P. Martin-Sanz, and A. M. Valverde. 2014. 'Impaired autophagic flux is associated with increased endoplasmic reticulum stress during the development of NAFLD', *Cell Death Dis*, 5: e1179.

Gordon, S. 2003. 'Alternative activation of macrophages', *Nat Rev Immunol*, 3: 23-35.

Guan, H. P., J. L. Goldstein, M. S. Brown, and G. Liang. 2009. 'Accelerated fatty acid oxidation in muscle averts fasting-induced hepatic steatosis in SJL/J mice', *J Biol Chem*, 284: 24644-52.

Gurevich, E. V., J. J. Tesmer, A. Mushegian, and V. V. Gurevich. 2012. 'G protein-coupled receptor kinases: more than just kinases and not only for GPCRs', *Pharmacol Ther*, 133: 40-69.

Gyamfi, M. A., Y. Tanaka, L. He, C. D. Klaassen, and Y. J. Wan. 2009. 'Hepatic effects of a methionine-choline-deficient diet in hepatocyte RXRalpha-null mice', *Toxicol Appl Pharmacol*, 234: 166-78.

Habegger, K. M., K. M. Heppner, N. Geary, T. J. Bartness, R. DiMarchi, and M. H. Tschop. 2010. 'The metabolic actions of glucagon revisited', *Nat Rev Endocrinol*, 6: 689-97.

Harrington, L. S., G. M. Findlay, and R. F. Lamb. 2005. 'Restraining PI3K: mTOR signalling goes back to the membrane', *Trends Biochem Sci*, 30: 35-42.

Hatting, M., C. D. J. Tavares, K. Sharabi, A. K. Rines, and P. Puigserver. 2018. 'Insulin regulation of gluconeogenesis', *Ann N Y Acad Sci*, 1411: 21-35.

Hebbard, L., and J. George. 2011. 'Animal models of nonalcoholic fatty liver disease', *Nat Rev Gastroenterol Hepatol*, 8: 35-44.

Henkel, A. S., A. M. Dewey, K. A. Anderson, S. Olivares, and R. M. Green. 2012. 'Reducing endoplasmic reticulum stress does not improve steatohepatitis in mice fed a methionine- and choline-deficient diet', *Am J Physiol Gastrointest Liver Physiol*, 303: G54-9.

Herzig, S., F. Long, U. S. Jhala, S. Hedrick, R. Quinn, A. Bauer, D. Rudolph, G. Schutz, C. Yoon, P. Puigserver, B. Spiegelman, and M. Montminy. 2001. 'CREB regulates hepatic gluconeogenesis through the coactivator PGC-1', *Nature*, 413: 179-83.

Hirosumi, J., G. Tuncman, L. Chang, C. Z. Gorgun, K. T. Uysal, K. Maeda, M. Karin, and G. S. Hotamisligil. 2002. 'A central role for JNK in obesity and insulin resistance', *Nature*, 420: 333-6.

Homan, K. T., and J. J. Tesmer. 2014. 'Molecular Basis for Small Molecule Inhibition of G Protein-Coupled Receptor Kinases', *ACS Chem Biol*.

Horiguchi, N., L. Wang, P. Mukhopadhyay, O. Park, W. I. Jeong, F. Lafdil, D. Osei-Hyiaman, A. Moh, X. Y. Fu, P. Pacher, G. Kunos, and B. Gao. 2008. 'Cell type-dependent pro- and anti-inflammatory role of signal transducer and activator of transcription 3 in alcoholic liver injury', *Gastroenterology*, 134: 1148-58.

Horowitz, J. F., and S. Klein. 2000. 'Whole body and abdominal lipolytic sensitivity to epinephrine is suppressed in upper body obese women', *Am J Physiol Endocrinol Metab*, 278: E1144-52.

Iaccarino, G., E. D. Tomhave, R. J. Lefkowitz, and W. J. Koch. 1998. 'Reciprocal in vivo regulation of myocardial G protein-coupled receptor kinase expression by beta-adrenergic receptor stimulation and blockade', *Circulation*, 98: 1783-9.

Imamura, T., P. Vollenweider, K. Egawa, M. Clodi, K. Ishibashi, N. Nakashima, S. Ugi, J. W. Adams, J. H. Brown, and J. M. Olefsky. 1999. 'G alpha-q/11 protein plays a key role in insulin-induced glucose transport in 3T3-L1 adipocytes', *Mol Cell Biol*, 19: 6765-74.

Inokuma, K., Y. Ogura-Okamatsu, C. Toda, K. Kimura, H. Yamashita, and M. Saito. 2005. 'Uncoupling protein 1 is necessary for norepinephrine-induced glucose utilization in brown adipose tissue', *Diabetes*, 54: 1385-91.

Inoue, H., W. Ogawa, M. Ozaki, S. Haga, M. Matsumoto, K. Furukawa, N. Hashimoto, Y. Kido, T. Mori, H. Sakaue, K. Teshigawara, S. Jin, H. Iguchi, R. Hiramatsu, D. LeRoith, K. Takeda, S. Akira, and M. Kasuga. 2004. 'Role of STAT-3 in regulation of hepatic gluconeogenic genes and carbohydrate metabolism in vivo', *Nat Med*, 10: 168-74.

Inoue, M., T. Ohtake, W. Motomura, N. Takahashi, Y. Hosoki, S. Miyoshi, Y. Suzuki, H. Saito, Y. Kohgo, and T. Okumura. 2005. 'Increased expression of PPARgamma in high fat diet-induced liver steatosis in mice', *Biochem Biophys Res Commun*, 336: 215-22.

Itagaki, H., K. Shimizu, S. Morikawa, K. Ogawa, and T. Ezaki. 2013. 'Morphological and functional characterization of non-alcoholic fatty liver disease induced by a methionine-choline-deficient diet in C57BL/6 mice', *Int J Clin Exp Pathol*, 6: 2683-96.

Itoh, M., H. Kato, T. Suganami, K. Konuma, Y. Marumoto, S. Terai, H. Sakugawa, S. Kanai, M. Hamaguchi, T. Fukaishi, S. Aoe, K. Akiyoshi, Y. Komohara, M. Takeya, I. Sakaida, and Y. Ogawa. 2013. 'Hepatic crown-like structure: a unique histological feature in non-alcoholic steatohepatitis in mice and humans', *PLoS One*, 8: e82163.

Jezek, P., and L. Hlavata. 2005. 'Mitochondria in homeostasis of reactive oxygen species in cell, tissues, and organism', *Int J Biochem Cell Biol*, 37: 2478-503.

Jha, P., A. Knopf, H. Koefeler, M. Mueller, C. Lackner, G. Hoefler, T. Claudel, and M. Trauner. 2014. 'Role of adipose tissue in methionine-choline-deficient model of non-alcoholic steatohepatitis (NASH)', *Biochim Biophys Acta*, 1842: 959-70.

Jimenez-Garcia, L., S. Herranz, A. Luque, and S. Hortelano. 2015. 'Critical role of p38 MAPK in IL-4-induced alternative activation of peritoneal macrophages', *Eur J Immunol*, 45: 273-86.

Jimenez-Sainz, M. C., C. Murga, A. Kavelaars, M. Jurado-Pueyo, B. F. Krakstad, C. J. Heijnen, F. Mayor, Jr., and A. M. Aragay. 2006. 'G protein-coupled receptor kinase 2 negatively regulates chemokine signaling at a level downstream from G protein subunits', *Mol Biol Cell*, 17: 25-31.

Jocken, J. W., G. H. Goossens, A. M. van Hees, K. N. Frayn, M. van Baak, J. Stegen, M. T. Pakbiers, W. H. Saris, and E. E. Blaak. 2008. 'Effect of beta-adrenergic stimulation on whole-body and abdominal subcutaneous adipose tissue lipolysis in lean and obese men', *Diabetologia*, 51: 320-7.

Joel, C. D. 1966. 'Stimulation of metabolism of rat brown adipose tissue by addition of lipolytic hormones in vitro', *J Biol Chem*, 241: 814-21.

Jorgensen, R., S. Norklit Roed, A. Heding, and C. E. Elling. 2011. 'Beta-arrestin2 as a competitor for GRK2 interaction with the GLP-1 receptor upon receptor activation', *Pharmacology*, 88: 174-81.

Junker, A. E., L. Gluud, J. J. Holst, F. K. Knop, and T. Vilsboll. 2016. 'Diabetic and nondiabetic patients with nonalcoholic fatty liver disease have an impaired incretin effect and fasting hyperglucagonaemia', *J Intern Med*, 279: 485-93.

Jurado-Pueyo, M., P. M. Campos, F. Mayor, and C. Murga. 2008. 'GRK2-dependent desensitization downstream of G proteins', *J Recept Signal Transduct Res*, 28: 59-70.

Kamagate, A., S. Qu, G. Perdomo, D. Su, D. H. Kim, S. Slusher, M. Meseck, and H. H. Dong. 2008. 'FoxO1 mediates insulin-dependent regulation of hepatic VLDL production in mice', *J Clin Invest*, 118: 2347-64.

Kane, S., H. Sano, S. C. Liu, J. M. Asara, W. S. Lane, C. C. Garner, and G. E. Lienhard. 2002. 'A method to identify serine kinase substrates. Akt phosphorylates a novel adipocyte protein with a Rab GTPase-activating protein (GAP) domain', *The Journal of biological chemistry*, 277: 22115-8.

Kawano, Y., and D. E. Cohen. 2013. 'Mechanisms of hepatic triglyceride accumulation in non-alcoholic fatty liver disease', *J Gastroenterol*, 48: 434-41.

Keller, J. S. 1979. 'Effect of glucagon on the metabolic rate in growing chicken', *Acta Physiol Pol*, 30: 409-16.

Kersten, S., J. Seydoux, J. M. Peters, F. J. Gonzalez, B. Desvergne, and W. Wahli. 1999. 'Peroxisome proliferator-activated receptor alpha mediates the adaptive response to fasting', *J Clin Invest*, 103: 1489-98.

Kim, D., W. R. Kim, H. J. Kim, and T. M. Therneau. 2013. 'Association between noninvasive fibrosis markers and mortality among adults with nonalcoholic fatty liver disease in the United States', *Hepatology*, 57: 1357-65.

Kimball, S. R., B. A. Siegfried, and L. S. Jefferson. 2004. 'Glucagon represses signaling through the mammalian target of rapamycin in rat liver by activating AMP-activated protein kinase', *J Biol Chem*, 279: 54103-9.

Klein, J., M. Fasshauer, H. H. Klein, M. Benito, and C. R. Kahn. 2002. 'Novel adipocyte lines from brown fat: a model system for the study of differentiation, energy metabolism, and insulin action', *Bioessays*, 24: 382-8.

Kleiner, D. E., E. M. Brunt, M. Van Natta, C. Behling, M. J. Contos, O. W. Cummings, L. D. Ferrell, Y. C. Liu, M. S. Torbenson, A. Unalp-Arida, M. Yeh, A. J. McCullough, A. J. Sanyal, and Network Nonalcoholic Steatohepatitis Clinical Research. 2005. 'Design and validation of a histological scoring system for nonalcoholic fatty liver disease', *Hepatology*, 41: 1313-21.

Kmiec, Z. 2001. 'Cooperation of liver cells in health and disease', *Adv Anat Embryol Cell Biol*, 161: III-XIII, 1-151.

Knop, F. K., K. Aaboe, T. Vilsboll, A. Volund, J. J. Holst, T. Krarup, and S. Madsbad. 2012. 'Impaired incretin effect and fasting hyperglucagonaemia characterizing type 2 diabetic subjects are early signs of dysmetabolism in obesity', *Diabetes Obes Metab*, 14: 500-10.

Kohjima, M., M. Enjoji, N. Higuchi, M. Kato, K. Kotoh, T. Yoshimoto, T. Fujino, M. Yada, R. Yada, N. Harada, R. Takayanagi, and M. Nakamuta. 2007. 'Re-evaluation of fatty acid metabolism-related gene expression in nonalcoholic fatty liver disease', *Int J Mol Med*, 20: 351-8.

Kondomerkos, D. J., S. A. Kalamidas, O. B. Kotoulas, and A. C. Hann. 2005. 'Glycogen autophagy in the liver and heart of newborn rats. The effects of glucagon, adrenalin or rapamycin', *Histol Histopathol*, 20: 689-96.

Koopman, R., G. Schaart, and M. K. Hesselink. 2001. 'Optimisation of oil red O staining permits combination with immunofluorescence and automated quantification of lipids', *Histochem Cell Biol*, 116: 63-8.

Kotoulas, O. B., S. A. Kalamidas, and D. J. Kondomerkos. 2006. 'Glycogen autophagy in glucose homeostasis', *Pathol Res Pract*, 202: 631-8.

Kowald, A., and T. B. Kirkwood. 2011. 'Evolution of the mitochondrial fusion-fission cycle and its role in aging', *Proc Natl Acad Sci U S A*, 108: 10237-42.

Kraegen, E. W., D. E. James, L. H. Storlien, K. M. Burleigh, and D. J. Chisholm. 1986. 'In vivo insulin resistance in individual peripheral tissues of the high fat fed rat: assessment by euglycaemic clamp plus deoxyglucose administration', *Diabetologia*, 29: 192-8.

Krilov, L., A. Nguyen, T. Miyazaki, C. G. Unson, R. Williams, N. H. Lee, S. Ceryak, and B. Bouscarel. 2011. 'Dual mode of glucagon receptor internalization: role of PKCalpha, GRKs and beta-arrestins', *Exp Cell Res*, 317: 2981-94.

Kujiraoka, T., Y. Satoh, M. Ayaori, Y. Shiraishi, Y. Arai-Nakaya, D. Hakuno, H. Yada, N. Kuwada, S. Endo, K. Isoda, and T. Adachi. 2013. 'Hepatic extracellular signal-regulated kinase 2 suppresses endoplasmic reticulum stress and protects from oxidative stress and endothelial dysfunction', *J Am Heart Assoc*, 2: e000361.

Lafarga, V., F. Mayor, Jr., and P. Penela. 2012. 'The interplay between G protein-coupled receptor kinase 2 (GRK2) and histone deacetylase 6 (HDAC6) at the crossroads of epithelial cell motility', *Cell Adh Migr*, 6: 495-501.

Lai, H. S., W. J. Chen, and K. M. Chen. 1992. 'Energy substrate for liver regeneration after partial hepatectomy in rats: effects of glucose vs fat', *JPEN J Parenter Enteral Nutr*, 16: 152-6.

Lanthier, N., O. Molendi-Coste, Y. Horsmans, N. van Rooijen, P. D. Cani, and I. A. Leclercq. 2010. 'Kupffer cell activation is a causal factor for hepatic insulin resistance', *Am J Physiol Gastrointest Liver Physiol*, 298: G107-16.

Leavens, K. F., and M. J. Birnbaum. 2011. 'Insulin signaling to hepatic lipid metabolism in health and disease', *Crit Rev Biochem Mol Biol*, 46: 200-15.

Leclercq, I. A., V. A. Lebrun, P. Starkel, and Y. J. Horsmans. 2007. 'Intrahepatic insulin resistance in a murine model of steatohepatitis: effect of PPARgamma agonist pioglitazone', *Lab Invest*, 87: 56-65.

Lee, J., C. Sun, Y. Zhou, J. Lee, D. Gokalp, H. Herrema, S. W. Park, R. J. Davis, and U. Ozcan. 2011. 'p38 MAPK-mediated regulation of Xbp1s is crucial for glucose homeostasis', *Nat Med*, 17: 1251-60.

Lee, J. Y., M. Kapur, M. Li, M. C. Choi, S. Choi, H. J. Kim, I. Kim, E. Lee, J. P. Taylor, and T. P. Yao. 2014. 'MFN1 deacetylation activates adaptive mitochondrial fusion and protects metabolically challenged mitochondria', *J Cell Sci*, 127: 4954-63.

Leinonen, E., E. Hurt-Camejo, O. Wiklund, L. M. Hulten, A. Hiukka, and M. R. Taskinen. 2003. 'Insulin resistance and adiposity correlate with acute-phase reaction and soluble cell adhesion molecules in type 2 diabetes', *Atherosclerosis*, 166: 387-94.

Leosco, D., G. Rengo, G. Iaccarino, A. Filippelli, A. Lymperopoulos, C. Zincarelli, F. Fortunato, L. Golino, M. Marchese, G. Esposito, A. Rapacciuolo, B. Rinaldi, N. Ferrara, W. J. Koch, and F. Rengo. 2007. 'Exercise training and beta-blocker treatment ameliorate age-dependent impairment of beta-adrenergic receptor signaling and enhance cardiac responsiveness to adrenergic stimulation', *Am J Physiol Heart Circ Physiol*, 293: H1596-603.

Li, J. H., D. Gautam, S. J. Han, J. M. Guettier, Y. Cui, H. Lu, C. Deng, J. O'Hare, W. Jou, O. Gavrilova, C. Buettner, and J. Wess. 2009. 'Hepatic muscarinic acetylcholine receptors are not critically involved in maintaining glucose homeostasis in mice', *Diabetes*, 58: 2776-87.

Li, S., M. S. Brown, and J. L. Goldstein. 2010. 'Bifurcation of insulin signaling pathway in rat liver: mTORC1 required for stimulation of lipogenesis, but not inhibition of gluconeogenesis', *Proc Natl Acad Sci U S A*, 107: 3441-6.

Li, Y., S. Xu, M. M. Mihaylova, B. Zheng, X. Hou, B. Jiang, O. Park, Z. Luo, E. Lefai, J. Y. Shyy, B. Gao, M. Wierzbicki, T. J. Verbeuren, R. J. Shaw, R. A. Cohen, and M. Zang. 2011. 'AMPK phosphorylates and inhibits SREBP activity to attenuate hepatic steatosis and atherosclerosis in diet-induced insulin-resistant mice', *Cell Metab*, 13: 376-88.

Liggett, S. B., N. J. Freedman, D. A. Schwinn, and R. J. Lefkowitz. 1993. 'Structural basis for receptor subtype-specific regulation revealed by a chimeric beta 3/beta 2-adrenergic receptor', *Proc Natl Acad Sci U S A*, 90: 3665-9.

Lin, C. W., H. Zhang, M. Li, X. Xiong, X. Chen, X. Chen, X. C. Dong, and X. M. Yin. 2013. 'Pharmacological promotion of autophagy alleviates steatosis and injury in alcoholic and non-alcoholic fatty liver conditions in mice', *J Hepatol*, 58: 993-9.

Lin, J., C. Handschin, and B. M. Spiegelman. 2005. 'Metabolic control through the PGC-1 family of transcription coactivators', *Cell Metab*, 1: 361-70.

Lin, X., P. Yue, Z. Chen, and G. Schonfeld. 2005. 'Hepatic triglyceride contents are genetically determined in mice: results of a strain survey', *Am J Physiol Gastrointest Liver Physiol*, 288: G1179-89.

Liu, H. Y., Q. F. Collins, Y. Xiong, F. Moukdar, E. G. Lupo, Jr., Z. Liu, and W. Cao. 2007. 'Prolonged treatment of primary hepatocytes with oleate induces insulin resistance through p38 mitogen-activated protein kinase', *J Biol Chem*, 282: 14205-12.

Liu, K., and M. J. Czaja. 2013. 'Regulation of lipid stores and metabolism by lipophagy', *Cell Death Differ*, 20: 3-11.

Liu, X., B. Ma, A. B. Malik, H. Tang, T. Yang, B. Sun, G. Wang, R. D. Minshall, Y. Li, Y. Zhao, R. D. Ye, and J. Xu. 2012. 'Bidirectional regulation of neutrophil migration by mitogen-activated protein kinases', *Nat Immunol*, 13: 457-64.

Longuet, C., E. M. Sinclair, A. Maida, L. L. Baggio, M. Maziarz, M. J. Charron, and D. J. Drucker. 2008. 'The glucagon receptor is required for the adaptive metabolic response to fasting', *Cell Metab*, 8: 359-71.

Lowell, B. B., and B. M. Spiegelman. 2000. 'Towards a molecular understanding of adaptive thermogenesis', *Nature*, 404: 652-60.

Lucas, E., M. Cruces-Sande, A. M. Briones, M. Salaices, F. Mayor, Jr., C. Murga, and R. Vila-Bedmar. 2015. 'Molecular physiopathology of obesity-related diseases: multi-organ integration by GRK2', *Arch Physiol Biochem*, 121: 163-77.

Lucas, E., M. Jurado-Pueyo, M. A. Fortuno, S. Fernandez-Veledo, R. Vila-Bedmar, L. J. Jimenez-Borreguero, J. J. Lazcano, E. Gao, J. Gomez-Ambrosi, G. Fruhbeck, W. J. Koch, J. Diez, F. Mayor, Jr., and C. Murga. 2014. 'Downregulation of G protein-coupled receptor kinase 2 levels enhances cardiac insulin sensitivity and switches on cardioprotective gene expression patterns', *Biochim Biophys Acta*, 1842: 2448-56.

Lucas, E., R. Vila-Bedmar, A. C. Arcones, M. Cruces-Sande, V. Cachofeiro, F. Mayor, Jr., and C. Murga. 2016. 'Obesity-induced cardiac lipid accumulation in adult mice is modulated by G protein-coupled receptor kinase 2 levels', *Cardiovasc Diabetol*, 15: 155.

Lumeng, C. N., and A. R. Saltiel. 2011. 'Inflammatory links between obesity and metabolic disease', *J Clin Invest*, 121: 2111-7.

Lymperopoulos, A., G. Rengo, and W. J. Koch. 2012. 'GRK2 inhibition in heart failure: something old, something new', *Curr Pharm Des*, 18: 186-91.

Malaguarnera, M., M. Di Rosa, F. Nicoletti, and L. Malaguarnera. 2009. 'Molecular mechanisms involved in NAFLD progression', *Journal of molecular medicine*, 87: 679-95.

Mao, Y., F. Yu, J. Wang, C. Guo, and X. Fan. 2016. 'Autophagy: a new target for nonalcoholic fatty liver disease therapy', *Hepat Med*, 8: 27-37.

Marette, A., A. Geloen, A. Collet, and L. J. Bukowiecki. 1990. 'Defective metabolic effects of norepinephrine and insulin in obese Zucker rat brown adipose tissue', *Am J Physiol*, 258: E320-8.

Martinez-Chantar, M. L., M. Vazquez-Chantada, M. Garnacho, M. U. Latasa, M. Varela-Rey, J. Dotor, M. Santamaria, L. A. Martinez-Cruz, L. A. Parada, S. C. Lu, and J. M. Mato. 2006. 'S-adenosylmethionine regulates cytoplasmic HuR via AMP-activated kinase', *Gastroenterology*, 131: 223-32.

Mayor, F., Jr., M. Cruces-Sande, A. C. Arcones, R. Vila-Bedmar, A. M. Briones, M. Salaices, and C. Murga. 2018. 'G protein-coupled receptor kinase 2 (GRK2) as an integrative signalling node in the regulation of cardiovascular function and metabolic homeostasis', *Cell Signal*, 41: 7.

Mayor, F., Jr., P. Penela, and A. Ruiz-Gomez. 1998. 'Role of G protein-coupled receptor kinase 2 and arrestins in beta-adrenergic receptor internalization', *Trends Cardiovasc Med*, 8: 234-40.

McArdle, M. A., O. M. Finucane, R. M. Connaughton, A. M. McMorrow, and H. M. Roche. 2013. 'Mechanisms of obesity-induced inflammation and insulin resistance: insights into the emerging role of nutritional strategies', *Frontiers in endocrinology*, 4: 52.

McCuskey, R. S., Y. Ito, G. R. Robertson, M. K. McCuskey, M. Perry, and G. C. Farrell. 2004. 'Hepatic microvascular dysfunction during evolution of dietary steatohepatitis in mice', *Hepatology*, 40: 386-93.

McGee, S. L., and M. Hargreaves. 2006. 'Exercise and skeletal muscle glucose transporter 4 expression: molecular mechanisms', *Clin Exp Pharmacol Physiol*, 33: 395-9.

McKee, C., J. Soeda, E. Asilmaz, B. Sigalla, M. Morgan, N. Sinelli, T. Roskams, and J. A. Oben. 2013. 'Propranolol, a beta-adrenoceptor antagonist, worsens liver injury in a model of non-alcoholic steatohepatitis', *Biochem Biophys Res Commun*, 437: 597-602.

Miquilena-Colina, M. E., E. Lima-Cabello, S. Sanchez-Campos, M. V. Garcia-Mediavilla, M. Fernandez-Bermejo, T. Lozano-Rodriguez, J. Vargas-Castrillon, X. Buque, B. Ochoa, P. Aspichueta, J. Gonzalez-Gallego, and C. Garcia-Monzon. 2011. 'Hepatic fatty acid translocase CD36 upregulation is associated with insulin resistance, hyperinsulinaemia and increased steatosis in non-alcoholic steatohepatitis and chronic hepatitis C', *Gut*, 60: 1394-402.

Mohan, M. L., A. Chatterjee, S. Ganapathy, S. Mukherjee, S. Srikanthan, G. P. Jolly, R. S. Anand, and S. V. N. Prasad. 2017. 'Noncanonical regulation of insulin-mediated ERK activation by phosphoinositide 3-kinase gamma', *Mol Biol Cell*, 28: 3112-22.

Mortimore, G. E., and C. E. Mondon. 1970. 'Inhibition by insulin of valine turnover in liver. Evidence for a general control of proteolysis', *J Biol Chem*, 245: 2375-83.

Mortimore, G. E., and C. M. Schworer. 1977. 'Induction of autophagy by amino-acid deprivation in perfused rat liver', *Nature*, 270: 174-6.

Mowers, J., M. Uhm, S. M. Reilly, J. Simon, D. Leto, S. H. Chiang, L. Chang, and A. R. Saltiel. 2013. 'Inflammation produces catecholamine resistance in obesity via activation of PDE3B by the protein kinases IKKepsilon and TBK1', *Elife*, 2: e01119.

Mustonen, A. M., R. Kakela, T. Halonen, V. Karja, E. Vartiainen, and P. Nieminen. 2012. 'Fatty acid mobilization in voles--model species for rapid fasting response and fatty liver', *Comp Biochem Physiol A Mol Integr Physiol*, 163: 152-60.

Mustonen, A. M., V. Karja, M. Kilpio, R. Tammi, M. Tammi, K. Rouvinen-Watt, T. Halonen, and P. Nieminen. 2013. 'Manifestations of fasting-induced fatty liver and rapid recovery from steatosis in voles fed lard or flaxseed oil lipids', *Nutrients*, 5: 4211-30.

Nafikov, R. A., B. N. Ametaj, G. Bobe, K. J. Koehler, J. W. Young, and D. C. Beitz. 2006. 'Prevention of fatty liver in transition dairy cows by subcutaneous injections of glucagon', *J Dairy Sci*, 89: 1533-45.

Nair, K. S. 1987. 'Hyperglucagonemia increases resting metabolic rate in man during insulin deficiency', *J Clin Endocrinol Metab*, 64: 896-901.

Nandipati, K. C., S. Subramanian, and D. K. Agrawal. 2017. 'Protein kinases: mechanisms and downstream targets in inflammation-mediated obesity and insulin resistance', *Mol Cell Biochem*, 426: 27-45.

Nassir, F., and J. A. Ibdah. 2014. 'Role of mitochondria in nonalcoholic fatty liver disease', *Int J Mol Sci*, 15: 8713-42.

Ng, J. M., K. Azuma, C. Kelley, R. Pencek, Z. Radikova, C. Laymon, J. Price, B. H. Goodpaster, and D. E. Kelley. 2012. 'PET imaging reveals distinctive roles for different regional adipose tissue depots in systemic glucose metabolism in nonobese humans', *Am J Physiol Endocrinol Metab*, 303: E1134-41.

Nielsen, S., and F. Karpe. 2012. 'Determinants of VLDL-triglycerides production', *Curr Opin Lipidol*, 23: 321-6.

Nijboer, C. H., C. J. Heijnen, H. L. Willemen, F. Groenendaal, G. W. Dorn, 2nd, F. van Bel, and A. Kavelaars. 2010. 'Cell-specific roles of GRK2 in onset and severity of hypoxic-ischemic brain damage in neonatal mice', *Brain Behav Immun*, 24: 420-6.

Nikolaou, N., C. J. Green, P. J. Gunn, L. Hodson, and J. W. Tomlinson. 2016. 'Optimizing human hepatocyte models for metabolic phenotype and function: effects of treatment with dimethyl sulfoxide (DMSO)', *Physiol Rep*, 4.

Nishikawa, S., K. Doi, H. Nakayama, and K. Uetsuka. 2008. 'The effect of fasting on hepatic lipid accumulation and transcriptional regulation of lipid metabolism differs between C57BL/6J and BALB/cA mice fed a high-fat diet', *Toxicol Pathol*, 36: 850-7.

Nogues, L., J. Palacios-Garcia, C. Reglero, V. Rivas, M. Neves, C. Ribas, P. Penela, and F. Mayor, Jr. 2017. 'G protein-coupled receptor kinases (GRKs) in tumorigenesis and cancer progression: GPCR regulators and signaling hubs', *Semin Cancer Biol*.

Nogues, L., C. Reglero, V. Rivas, A. Salcedo, V. Lafarga, M. Neves, P. Ramos, M. Mendiola, A. Berjon, K. Stamatakis, X. Z. Zhou, K. P. Lu, D. Hardisson, F. Mayor, Jr., and P. Penela. 2016. 'G Protein-coupled Receptor Kinase 2 (GRK2) Promotes Breast Tumorigenesis Through a HDAC6-Pin1 Axis', *EBioMedicine*, 13: 132-45.

Nonogaki, K. 2000. 'New insights into sympathetic regulation of glucose and fat metabolism', *Diabetologia*, 43: 533-49.

Oakes, N. D., G. J. Cooney, S. Camilleri, D. J. Chisholm, and E. W. Kraegen. 1997. 'Mechanisms of liver and muscle insulin resistance induced by chronic high-fat feeding', *Diabetes*, 46: 1768-74.

Odegaard, J. I., R. R. Ricardo-Gonzalez, A. Red Eagle, D. Vats, C. R. Morel, M. H. Goforth, V. Subramanian, L. Mukundan, A. W. Ferrante, and A. Chawla. 2008. 'Alternative M2 activation of Kupffer cells by PPARdelta ameliorates obesity-induced insulin resistance', *Cell Metab*, 7: 496-507.

Olefsky, J. M., and C. K. Glass. 2010. 'Macrophages, inflammation, and insulin resistance', *Annu Rev Physiol*, 72: 219-46.

Orava, J., P. Nuutila, M. E. Lidell, V. Oikonen, T. Noponen, T. Viljanen, M. Scheinin, M. Taittonen, T. Niemi, S. Enerback, and K. A. Virtanen. 2011. 'Different metabolic responses of human brown adipose tissue to activation by cold and insulin', *Cell Metab*, 14: 272-9.

Ota, T., T. Takamura, S. Kurita, N. Matsuzawa, Y. Kita, M. Uno, H. Akahori, H. Misu, M. Sakurai, Y. Zen, Y. Nakanuma, and S. Kaneko. 2007. 'Insulin resistance accelerates a dietary rat model of nonalcoholic steatohepatitis', *Gastroenterology*, 132: 282-93.

Owen, C., E. K. Lees, L. Grant, D. J. Zimmer, N. Mody, K. K. Bence, and M. Delibegovic. 2013. 'Inducible liver-specific knockdown of protein tyrosine phosphatase 1B improves glucose and lipid homeostasis in adult mice', *Diabetologia*, 56: 2286-96.

Ozaki, K. I., M. Awazu, M. Tamiya, Y. Iwasaki, A. Harada, S. Kugisaki, S. Tanimura, and M. Kohno. 2016. 'Targeting the ERK signaling pathway as a potential treatment for insulin resistance and type 2 diabetes', *Am J Physiol Endocrinol Metab*, 310: E643-E51.

Ozcan, U., Q. Cao, E. Yilmaz, A. H. Lee, N. N. Iwakoshi, E. Ozdelen, G. Tuncman, C. Gorgun, L. H. Glimcher, and G. S. Hotamisligil. 2004. 'Endoplasmic reticulum stress links obesity, insulin action, and type 2 diabetes', *Science*, 306: 457-61.

Ozcan, U., E. Yilmaz, L. Ozcan, M. Furuhashi, E. Vaillancourt, R. O. Smith, C. Z. Gorgun, and G. S. Hotamisligil. 2006. 'Chemical chaperones reduce ER stress and restore glucose homeostasis in a mouse model of type 2 diabetes', *Science*, 313: 1137-40.

Packiriswamy, N., and N. Parameswaran. 2015. 'G-protein-coupled receptor kinases in inflammation and disease', *Genes Immun*, 16: 367-77.

Paglialunga, S., and C. A. Dehn. 2016. 'Clinical assessment of hepatic de novo lipogenesis in non-alcoholic fatty liver disease', *Lipids Health Dis*, 15: 159.

Pardo, V., A. Gonzalez-Rodriguez, C. Guijas, J. Balsinde, and A. M. Valverde. 2015. 'Opposite cross-talk by oleate and palmitate on insulin signaling in hepatocytes through macrophage activation', *J Biol Chem*, 290: 11663-77.

Patial, S., J. Luo, K. J. Porter, J. L. Benovic, and N. Parameswaran. 2009. 'G-protein-coupled-receptor kinases mediate TNFalpha-induced NFkappaB signalling via direct interaction with and phosphorylation of IkappaBalpha', *Biochem J*, 425: 169-78.

Patial, S., Y. Saini, S. Parvataneni, D. M. Appledorn, G. W. Dorn, 2nd, J. J. Lapres, A. Amalfitano, P. Senagore, and N. Parameswaran. 2011. 'Myeloid-specific GPCR kinase-2 negatively regulates NF-kappaB1p105-ERK pathway and limits endotoxemic shock in mice', *J Cell Physiol*, 226: 627-37.

Penela, P. 2016. 'Chapter Three - Ubiquitination and Protein Turnover of G-Protein-Coupled Receptor Kinases in GPCR Signaling and Cellular Regulation', *Prog Mol Biol Transl Sci*, 141: 85-140.

Penela, P., M. Barradas, M. Alvarez-Dolado, A. Munoz, and F. Mayor, Jr. 2001. 'Effect of hypothyroidism on G protein-coupled receptor kinase 2 expression levels in rat liver, lung, and heart', *Endocrinology*, 142: 987-91.

Penela, P., C. Murga, C. Ribas, V. Lafarga, and F. Mayor, Jr. 2010. 'The complex G protein-coupled receptor kinase 2 (GRK2) interactome unveils new physiopathological targets', *Br J Pharmacol*, 160: 821-32.

Penela, P., C. Murga, C. Ribas, A. S. Tutor, S. Peregrin, and F. Mayor, Jr. 2006. 'Mechanisms of regulation of G protein-coupled receptor kinases (GRKs) and cardiovascular disease', *Cardiovasc Res*, 69: 46-56.

Penela, P., L. Nogues, and F. Mayor, Jr. 2014. 'Role of G protein-coupled receptor kinases in cell migration', *Curr Opin Cell Biol*, 27: 10-7.

Penela, P., C. Ribas, and F. Mayor, Jr. 2003. 'Mechanisms of regulation of the expression and function of G protein-coupled receptor kinases', *Cell Signal*, 15: 973-81.

Penela, P., A. Ruiz-Gomez, J. G. Castano, and F. Mayor, Jr. 1998. 'Degradation of the G protein-coupled receptor kinase 2 by the proteasome pathway', *J Biol Chem*, 273: 35238-44.

Peng, K., L. Yang, J. Wang, F. Ye, G. Dan, Y. Zhao, Y. Cai, Z. Cui, L. Ao, J. Liu, Z. Zou, Y. Sai, and J. Cao. 2017. 'The Interaction of Mitochondrial Biogenesis and Fission/Fusion Mediated by PGC-1alpha Regulates Rotenone-Induced Dopaminergic Neurotoxicity', *Mol Neurobiol*, 54: 3783-97.

Perdiguero, E., V. Ruiz-Bonilla, L. Gresh, L. Hui, E. Ballestar, P. Sousa-Victor, B. Baeza-Raja, M. Jardi, A. Bosch-Comas, M. Esteller, C. Caelles, A. L. Serrano, E. F. Wagner, and P. Munoz-Canoves. 2007. 'Genetic analysis of p38 MAP kinases in myogenesis: fundamental role of p38alpha in abrogating myoblast proliferation', *EMBO J*, 26: 1245-56.

Perea, A., F. Clemente, J. Martinell, M. L. Villanueva-Penacarrillo, and I. Valverde. 1995. 'Physiological effect of glucagon in human isolated adipocytes', *Horm Metab Res*, 27: 372-5.

Peregrin, S., M. Jurado-Pueyo, P. M. Campos, V. Sanz-Moreno, A. Ruiz-Gomez, P. Crespo, F. Mayor, Jr., and C. Murga. 2006. 'Phosphorylation of p38 by GRK2 at the docking groove unveils a novel mechanism for inactivating p38MAPK', *Curr Biol*, 16: 2042-7.

Pereira, S., W. Q. Yu, J. Moore, Y. Mori, E. Tsiani, and A. Giacca. 2016. 'Effect of a p38 MAPK inhibitor on FFA-induced hepatic insulin resistance in vivo', *Nutr Diabetes*, 6: e210.

Petersen, M. C., and G. I. Shulman. 2017. 'Roles of Diacylglycerols and Ceramides in Hepatic Insulin Resistance', *Trends Pharmacol Sci*, 38: 649-65.

Pettinelli, P., and L. A. Videla. 2011. 'Up-regulation of PPAR-gamma mRNA expression in the liver of obese patients: an additional reinforcing lipogenic mechanism to SREBP-1c induction', *J Clin Endocrinol Metab*, 96: 1424-30.

Plaisance, E. P., T. M. Henagan, H. Echlin, A. Boudreau, K. L. Hill, N. R. Lenard, B. E. Hasek, N. Orentreich, and T. W. Gettys. 2010. 'Role of beta-adrenergic receptors in the hyperphagic and hypermetabolic responses to dietary methionine restriction', *Am J Physiol Regul Integr Comp Physiol*, 299: R740-50.

Pocai, A., P. E. Carrington, J. R. Adams, M. Wright, G. Eiermann, L. Zhu, X. Du, A. Petrov, M. E. Lassman, G. Jiang, F. Liu, C. Miller, L. M. Tota, G. Zhou, X. Zhang, M. M. Sountis, A. Santoprete, E. Capito, G. G. Chicchi, N. Thornberry, E. Bianchi, A. Pessi, D. J. Marsh, and R. SinhaRoy. 2009. 'Glucagon-like peptide 1/glucagon receptor dual agonism reverses obesity in mice', *Diabetes*, 58: 2258-66.

Quesada, I., E. Tuduri, C. Ripoll, and A. Nadal. 2008. 'Physiology of the pancreatic alpha-cell and glucagon secretion: role in glucose homeostasis and diabetes', *J Endocrinol*, 199: 5-19.

Reid, D. T., and B. Eksteen. 2015. 'Murine models provide insight to the development of non-alcoholic fatty liver disease', *Nutr Res Rev*, 28: 133-42.

Reynisdottir, S., K. Ellerfeldt, H. Wahrenberg, H. Lithell, and P. Arner. 1994. 'Multiple lipolysis defects in the insulin resistance (metabolic) syndrome', *J Clin Invest*, 93: 2590-9.

Richieri, G. V., and A. M. Kleinfeld. 1995. 'Unbound free fatty acid levels in human serum', *J Lipid Res*, 36: 229-40.

Rinella, M. E., M. S. Elias, R. R. Smolak, T. Fu, J. Borensztajn, and R. M. Green. 2008. 'Mechanisms of hepatic steatosis in mice fed a lipogenic methionine choline-deficient diet', *J Lipid Res*, 49: 1068-76.

Rinella, M. E., and R. M. Green. 2004. 'The methionine-choline deficient dietary model of steatohepatitis does not exhibit insulin resistance', *J Hepatol*, 40: 47-51.

Ringseis, R., K. Eder, F. C. Mooren, and K. Kruger. 2015. 'Metabolic signals and innate immune activation in obesity and exercise', *Exerc Immunol Rev*, 21: 58-68.

Rivera, C. A., P. Adegboyega, N. van Rooijen, A. Tagalicud, M. Allman, and M. Wallace. 2007. 'Toll-like receptor-4 signaling and Kupffer cells play pivotal roles in the pathogenesis of non-alcoholic steatohepatitis', *J Hepatol*, 47: 571-9.

Rizki, G., L. Arnaboldi, B. Gabrielli, J. Yan, G. S. Lee, R. K. Ng, S. M. Turner, T. M. Badger, R. E. Pitas, and J. J. Maher. 2006. 'Mice fed a lipogenic methionine-choline-deficient diet develop hypermetabolism coincident with hepatic suppression of SCD-1', *J Lipid Res*, 47: 2280-90.

Roach, W. G., J. A. Chavez, C. P. Miinea, and G. E. Lienhard. 2007. 'Substrate specificity and effect on GLUT4 translocation of the Rab GTPase-activating protein Tbc1d1', *Biochem J*, 403: 353-8.

Ruderman, N. B., A. K. Saha, and E. W. Kraegen. 2003. 'Minireview: malonyl CoA, AMP-activated protein kinase, and adiposity', *Endocrinology*, 144: 5166-71.

Ruiz-Gomez, A., and F. Mayor, Jr. 1997. 'Beta-adrenergic receptor kinase (GRK2) colocalizes with beta-adrenergic receptors during agonist-induced receptor internalization', *J Biol Chem*, 272: 9601-4.

Sakamoto, K., and G. D. Holman. 2008. 'Emerging role for AS160/TBC1D4 and TBC1D1 in the regulation of GLUT4 traffic', *Am J Physiol Endocrinol Metab*, 295: E29-37.

Salcedo, A., F. Mayor, Jr., and P. Penela. 2006. 'Mdm2 is involved in the ubiquitination and degradation of G-protein-coupled receptor kinase 2', *EMBO J*, 25: 4752-62.

Salem, V., C. Izzi-Engbeaya, C. Coello, D. B. Thomas, E. S. Chambers, A. N. Comninos, A. Buckley, Z. Win, A. Al-Nahhas, E. A. Rabiner, R. N. Gunn, H. Budge, M. E. Symonds, S. R. Bloom, T. M. Tan, and W. S. Dhillo. 2016. 'Glucagon increases energy expenditure independently of brown adipose tissue activation in humans', *Diabetes Obes Metab*, 18: 72-81.

Saltiel, A. R. 2016. 'Insulin Signaling in the Control of Glucose and Lipid Homeostasis', *Handb Exp Pharmacol*, 233: 51-71.

Samuel, V. T., and G. I. Shulman. 2012. 'Mechanisms for insulin resistance: common threads and missing links', *Cell*, 148: 852-71.

———. 2016. 'The pathogenesis of insulin resistance: integrating signaling pathways and substrate flux', *J Clin Invest*, 126: 12-22.

Sanches, S. C., L. N. Ramalho, M. J. Augusto, D. M. da Silva, and F. S. Ramalho. 2015. 'Nonalcoholic Steatohepatitis: A Search for Factual Animal Models', *Biomed Res Int*, 2015: 574832.

Sanchez-Garrido, M. A., S. J. Brandt, C. Clemmensen, T. D. Muller, R. D. DiMarchi, and M. H. Tschop. 2017. 'GLP-1/glucagon receptor co-agonism for treatment of obesity', *Diabetologia*, 60: 1851-61.

Sanyal, A. J., C. Campbell-Sargent, F. Mirshahi, W. B. Rizzo, M. J. Contos, R. K. Sterling, V. A. Luketic, M. L. Shiffman, and J. N. Clore. 2001. 'Nonalcoholic steatohepatitis: association of insulin resistance and mitochondrial abnormalities', *Gastroenterology*, 120: 1183-92.

Sato, P. Y., J. K. Chuprun, J. Ibetti, A. Cannavo, K. Drosatos, J. W. Elrod, and W. J. Koch. 2015. 'GRK2 compromises cardiomyocyte mitochondrial function by diminishing fatty acid-mediated oxygen consumption and increasing superoxide levels', *J Mol Cell Cardiol*, 89: 360-4.

Schattenberg, J. M., R. Singh, Y. Wang, J. H. Lefkowitch, R. M. Rigoli, P. E. Scherer, and M. J. Czaja. 2006. 'JNK1 but not JNK2 promotes the development of steatohepatitis in mice', *Hepatology*, 43: 163-72.

Schattenberg, J. M., Y. Wang, R. Singh, R. M. Rigoli, and M. J. Czaja. 2005. 'Hepatocyte CYP2E1 overexpression and steatohepatitis lead to impaired hepatic insulin signaling', *J Biol Chem*, 280: 9887-94.

Schneider, J. L., and A. M. Cuervo. 2014. 'Liver autophagy: much more than just taking out the trash', *Nat Rev Gastroenterol Hepatol*, 11: 187-200.

Schott, M. B., K. Rasineni, S. G. Weller, R. J. Schulze, A. C. Sletten, C. A. Casey, and M. A. McNiven. 2017. 'beta-Adrenergic induction of lipolysis in hepatocytes is inhibited by ethanol exposure', *J Biol Chem*, 292: 11815-28.

Schumacher, S. M., E. Gao, W. Zhu, X. Chen, J. K. Chuprun, A. M. Feldman, G. Tesmer JJ, and W. J. Koch. 2015. 'Paroxetine-mediated GRK2 inhibition reverses cardiac dysfunction and remodeling after myocardial infarction', *Sci Transl Med*, 7: 277ra31.

Shahid, G., and T. Hussain. 2007. 'GRK2 negatively regulates glycogen synthesis in mouse liver FL83B cells', *J Biol Chem*, 282: 20612-20.

Shulman, G. I., D. L. Rothman, T. Jue, P. Stein, R. A. DeFronzo, and R. G. Shulman. 1990. 'Quantitation of muscle glycogen synthesis in normal subjects and subjects with non-insulin-dependent diabetes by 13C nuclear magnetic resonance spectroscopy', *N Engl J Med*, 322: 223-8.

Sinclair, E. M., B. Yusta, C. Streutker, L. L. Baggio, J. Koehler, M. J. Charron, and D. J. Drucker. 2008. 'Glucagon receptor signaling is essential for control of murine hepatocyte survival', *Gastroenterology*, 135: 2096-106.

Singh, R., S. Kaushik, Y. Wang, Y. Xiang, I. Novak, M. Komatsu, K. Tanaka, A. M. Cuervo, and M. J. Czaja. 2009. 'Autophagy regulates lipid metabolism', *Nature*, 458: 1131-5.

Slavin, B. G., J. M. Ong, and P. A. Kern. 1994. 'Hormonal regulation of hormone-sensitive lipase activity and mRNA levels in isolated rat adipocytes', *J Lipid Res*, 35: 1535-41.

Smith, B. W., and L. A. Adams. 2011. 'Nonalcoholic fatty liver disease and diabetes mellitus: pathogenesis and treatment', *Nat Rev Endocrinol*, 7: 456-65.

Soloveva, V., R. A. Graves, M. M. Rasenick, B. M. Spiegelman, and S. R. Ross. 1997. 'Transgenic mice overexpressing the beta 1-adrenergic receptor in adipose tissue are resistant to obesity', *Mol Endocrinol*, 11: 27-38.

Song, W. J., P. Mondal, A. Wolfe, L. C. Alonso, R. Stamateris, B. W. Ong, O. C. Lim, K. S. Yang, S. Radovick, H. J. Novaira, E. A. Farber, C. R. Farber, S. D. Turner, and M. A. Hussain. 2014. 'Glucagon regulates hepatic kisspeptin to impair insulin secretion', *Cell Metab*, 19: 667-81.

Soon, R. K., Jr., J. S. Yan, J. P. Grenert, and J. J. Maher. 2010. 'Stress signaling in the methionine-choline-deficient model of murine fatty liver disease', *Gastroenterology*, 139: 1730-9, 39 e1.

Sorriento, D., M. Ciccarelli, G. Santulli, M. Illario, B. Trimarco, and G. Iaccarino. 2014. 'Trafficking GRK2: Cellular and Metabolic consequences of GRK2 subcellular localization', *Transl Med UniSa*, 10: 3-7.

Sparks, C. E., and J. D. Sparks. 2010. 'Lipid metabolism: insights into the complexity of VLDL metabolic pathways', *Curr Opin Lipidol*, 21: 280-1.

Stich, V., F. Marion-Latard, J. Hejnova, N. Viguerie, C. Lefort, H. Suljkovicova, D. Langin, M. Lafontan, and M. Berlan. 2002. 'Hypocaloric diet reduces exercise-induced alpha 2-adrenergic antilipolytic effect and alpha 2-adrenergic receptor mRNA levels in adipose tissue of obese women', *J Clin Endocrinol Metab*, 87: 1274-81.

Storlien, L. H., D. E. James, K. M. Burleigh, D. J. Chisholm, and E. W. Kraegen. 1986. 'Fat feeding causes widespread in vivo insulin resistance, decreased energy expenditure, and obesity in rats', *Am J Physiol*, 251: E576-83.

Taguchi, K., M. Hida, M. Hasegawa, H. Narimatsu, T. Matsumoto, and T. Kobayashi. 2017. 'Suppression of GRK2 expression reduces endothelial dysfunction by restoring glucose homeostasis', *Sci Rep*, 7: 8436.

Taguchi, K., T. Matsumoto, K. Kamata, and T. Kobayashi. 2012. 'G protein-coupled receptor kinase 2, with beta-arrestin 2, impairs insulin-induced Akt/endothelial nitric oxide synthase signaling in ob/ob mouse aorta', *Diabetes*, 61: 1978-85.

Taniguchi, C. M., B. Emanuelli, and C. R. Kahn. 2006. 'Critical nodes in signalling pathways: insights into insulin action', *Nat Rev Mol Cell Biol*, 7: 85-96.

Tanti, J. F., F. Ceppo, J. Jager, and F. Berthou. 2012. 'Implication of inflammatory signaling pathways in obesity-induced insulin resistance', *Front Endocrinol (Lausanne)*, 3: 181.

Tosello-Trampont, A. C., S. G. Landes, V. Nguyen, T. I. Novobrantseva, and Y. S. Hahn. 2012. 'Kuppfer cells trigger nonalcoholic steatohepatitis development in diet-induced mouse model through tumor necrosis factor-alpha production', *J Biol Chem*, 287: 40161-72.

Ueno, T., and M. Komatsu. 2017. 'Autophagy in the liver: functions in health and disease', *Nat Rev Gastroenterol Hepatol*, 14: 170-84.

Ueta, C. B., G. W. Fernandes, L. P. Capelo, T. L. Fonseca, F. D. Maculan, C. H. Gouveia, P. C. Brum, M. A. Christoffolete, M. S. Aoki, C. L. Lancellotti, B. Kim, A. C. Bianco, and M. O. Ribeiro. 2012. 'beta(1) Adrenergic receptor is key to cold- and diet-induced thermogenesis in mice', *J Endocrinol*, 214: 359-65.

Urano, F., X. Wang, A. Bertolotti, Y. Zhang, P. Chung, H. P. Harding, and D. Ron. 2000. 'Coupling of stress in the ER to activation of JNK protein kinases by transmembrane protein kinase IRE1', *Science*, 287: 664-6.

Usui, I., T. Imamura, J. L. Babendure, H. Satoh, J. C. Lu, C. J. Hupfeld, and J. M. Olefsky. 2005. 'G protein-coupled receptor kinase 2 mediates endothelin-1-induced insulin resistance via the inhibition of both Galphaq/11 and insulin receptor substrate-1 pathways in 3T3-L1 adipocytes', *Mol Endocrinol*, 19: 2760-8.

Valdecantos, M. P., V. Pardo, L. Ruiz, L. Castro-Sanchez, B. Lanzon, E. Fernandez-Millan, C. Garcia-Monzon, A. I. Arroba, A. Gonzalez-Rodriguez, F. Escriva, C. Alvarez, F. J. Ruperez, C. Barbas, A. Konkar, J. Naylor, D. Hornigold, A. D. Santos, M. Bednarek, J. Grimsby, C. M. Rondinone, and A. M. Valverde. 2017. 'A novel glucagon-like peptide 1/glucagon receptor dual agonist improves steatohepatitis and liver regeneration in mice', *Hepatology*, 65: 950-68.

Valero, T. 2014. 'Mitochondrial biogenesis: pharmacological approaches', *Curr Pharm Des*, 20: 5507-9.

Vandesompele, J., K. De Preter, F. Pattyn, B. Poppe, N. Van Roy, A. De Paepe, and F. Speleman. 2002. 'Accurate normalization of real-time quantitative RT-PCR data by geometric averaging of multiple internal control genes', *Genome Biol*, 3: RESEARCH0034.

Ventura-Clapier, R., A. Garnier, and V. Veksler. 2008. 'Transcriptional control of mitochondrial biogenesis: the central role of PGC-1alpha', *Cardiovasc Res*, 79: 208-17.

Vidal-Puig, A., M. Jimenez-Linan, B. B. Lowell, A. Hamann, E. Hu, B. Spiegelman, J. S. Flier, and D. E. Moller. 1996. 'Regulation of PPAR gamma gene expression by nutrition and obesity in rodents', *J Clin Invest*, 97: 2553-61.

Vila-Bedmar, R., M. Cruces-Sande, E. Lucas, H. L. Willemen, C. J. Heijnen, A. Kavelaars, F. Mayor, Jr., and C. Murga. 2015. 'Reversal of diet-induced obesity and insulin resistance by inducible genetic ablation of GRK2', *Sci Signal*, 8: ra73.

Vila-Bedmar, R., L. Garcia-Guerra, I. Nieto-Vazquez, F. Mayor, Jr., M. Lorenzo, C. Murga, and S. Fernandez-Veledo. 2012. 'GRK2 contribution to the regulation of energy expenditure and brown fat function', *FASEB J*, 26: 3503-14.

Virtanen, K. A., P. Lonnroth, R. Parkkola, P. Peltoniemi, M. Asola, T. Viljanen, T. Tolvanen, J. Knuuti, T. Ronnemaa, R. Huupponen, and P. Nuutila. 2002. 'Glucose uptake and perfusion in subcutaneous and visceral adipose tissue during insulin stimulation in nonobese and obese humans', *J Clin Endocrinol Metab*, 87: 3902-10.

Wang, H., F. Lafdil, X. Kong, and B. Gao. 2011. 'Signal transducer and activator of transcription 3 in liver diseases: a novel therapeutic target', *Int J Biol Sci*, 7: 536-50.

Wang, H., M. Zhao, N. Sud, P. Christian, J. Shen, Y. Song, A. Pashaj, K. Zhang, T. Carr, and Q. Su. 2016. 'Glucagon regulates hepatic lipid metabolism via cAMP and Insig-2 signaling: implication for the pathogenesis of hypertriglyceridemia and hepatic steatosis', *Sci Rep*, 6: 32246.

Watari, K., M. Nakaya, and H. Kurose. 2014. 'Multiple functions of G protein-coupled receptor kinases', *J Mol Signal*, 9: 1.

Wauson, E. M., H. A. Dbouk, A. B. Ghosh, and M. H. Cobb. 2014. 'G protein-coupled receptors and the regulation of autophagy', *Trends Endocrinol Metab*, 25: 274-82.

Weisberg, S. P., D. McCann, M. Desai, M. Rosenbaum, R. L. Leibel, and A. W. Ferrante, Jr. 2003. 'Obesity is associated with macrophage accumulation in adipose tissue', *J Clin Invest*, 112: 1796-808.

Westergaard, N., C. L. Brand, R. H. Lewinsky, H. S. Andersen, R. D. Carr, A. Burchell, and K. Lundgren. 1999. 'Peroxyvanadium compounds inhibit glucose-6-phosphatase activity and glucagon-stimulated hepatic glucose output in the rat in vivo', *Arch Biochem Biophys*, 366: 55-60.

White, M. F. 2003. 'Insulin signaling in health and disease', *Science*, 302: 1710-1.

Wyne, K. L. 2003. 'Free fatty acids and type 2 diabetes mellitus', *Am J Med*, 115 Suppl 8A: 29S-36S.

Xu, J., A. C. Donepudi, J. E. Moscovitz, and A. L. Slitt. 2013. 'Keap1-knockdown decreases fasting-induced fatty liver via altered lipid metabolism and decreased fatty acid mobilization from adipose tissue', *PLoS One*, 8: e79841.

Yamaguchi, K., Y. Itoh, C. Yokomizo, T. Nishimura, T. Niimi, H. Fujii, T. Okanoue, and T. Yoshikawa. 2010. 'Blockade of interleukin-6 signaling enhances hepatic steatosis but improves liver injury in methionine choline-deficient diet-fed mice', *Lab Invest*, 90: 1169-78.

Yap, F., L. Craddock, and J. Yang. 2011. 'Mechanism of AMPK suppression of LXR-dependent Srebp-1c transcription', *Int J Biol Sci*, 7: 645-50.

Ye, J. 2013. 'Mechanisms of insulin resistance in obesity', *Front Med*, 7: 14-24.

Yehuda-Shnaidman, E., B. Buehrer, J. Pi, N. Kumar, and S. Collins. 2010. 'Acute stimulation of white adipocyte respiration by PKA-induced lipolysis', *Diabetes*, 59: 2474-83.

Yoon, J. C., P. Puigserver, G. Chen, J. Donovan, Z. Wu, J. Rhee, G. Adelmant, J. Stafford, C. R. Kahn, D. K. Granner, C. B. Newgard, and B. M. Spiegelman. 2001. 'Control of hepatic gluconeogenesis through the transcriptional coactivator PGC-1', *Nature*, 413: 131-8.

Younossi, Z., Q. M. Anstee, M. Marietti, T. Hardy, L. Henry, M. Eslam, J. George, and E. Bugianesi. 2018. 'Global burden of NAFLD and NASH: trends, predictions, risk factors and prevention', *Nat Rev Gastroenterol Hepatol*, 15: 11-20.

Yu, J., E. Ip, A. Dela Pena, J. Y. Hou, J. Sesha, N. Pera, P. Hall, R. Kirsch, I. Leclercq, and G. C. Farrell. 2006. 'COX-2 induction in mice with experimental nutritional steatohepatitis: Role as pro-inflammatory mediator', *Hepatology*, 43: 826-36.

Zhou, J., M. Febbraio, T. Wada, Y. Zhai, R. Kuruba, J. He, J. H. Lee, S. Khadem, S. Ren, S. Li, R. L. Silverstein, and W. Xie. 2008. 'Hepatic fatty acid transporter Cd36 is a common target of LXR, PXR, and PPARgamma in promoting steatosis', *Gastroenterology*, 134: 556-67.

Zhu, L., M. Rossi, Y. Cui, R. J. Lee, W. Sakamoto, N. A. Perry, N. M. Urs, M. G. Caron, V. V. Gurevich, G. Godlewski, G. Kunos, M. Chen, W. Chen, and J. Wess. 2017. 'Hepatic beta-arrestin 2 is essential for maintaining euglycemia', *J Clin Invest*, 127: 2941-45.

Zorzano, A., M. Liesa, and M. Palacin. 2009. 'Role of mitochondrial dynamics proteins in the pathophysiology of obesity and type 2 diabetes', *Int J Biochem Cell Biol*, 41: 1846-54.